Preparation, characterization, and biodegradation studies of novel active poly (3-hydroxybutyrate) nanocomposite films and their application in packaging fresh produce

Thesis submitted in partial fulfillment of the requirements for the degree of

DOCTOR OF PHILOSOPHY

By

SATTI VENU GOPALA KUMARI

(196107110)

Department of Chemical Engineering

Indian Institute of Technology Guwahati

Guwahati -781039, India

July 2024

Preparation, characterization, and biodegradation studies of novel active poly (3-hydroxybutyrate) nanocomposite films and their application in packaging fresh produce

- *Satti Venu Gopala Kumari.*

Department of Chemical Engineering
Indian Institute of Technology Guwahati
Assam -781039, India

CERTIFICATE

It is certified that the work described in this thesis titled **"Preparation, characterization, and biodegradation studies of novel active poly (3-hydroxybutyrate) nanocomposite films and their application in packaging fresh produce"** by **Ms. Satti Venu Gopala Kumari** for the award of degree of Doctor of Philosophy is an authentic record of the results obtained from the research work carried out under my supervision in the Department of Chemical Engineering, Indian Institute of Technology Guwahati, India, and this work has not been submitted either in whole or in part elsewhere for a degree.

Date:

(Signature of Thesis Supervisor)
Dr. G. Pugazhenthi
Professor
Department of Chemical Engineering
Indian Institute of Technology Guwahati
Guwahati-781039, Assam, India

Dedication

This Thesis is dedicated to my loving parents Shri Satti Bhaskar Reddy and Smt. Satti Sudha, whose unwavering support and love have been the cornerstones of my every success

Acknowledgments

The completion of this thesis would have not been possible without the support of various people and institutions. First and foremost, I would like to express my heartfelt thanks to my supervisor, my source of inspiration and motivation, ***Prof. G. Pugazhenthi****, Department of Chemical Engineering, IIT Guwahati. His attention to detail, unwavering commitment to help his students, and passion for research are qualities that I deeply admire and strive to emulate. His positive attitude and caring nature have been pivotal in boosting my confidence and fostering my growth as a researcher. His valuable insights through rigorous discussions, provision of funding for attending conferences, and his support in helping me utilize the available resources to the fullest potential, coupled with the freedom he granted me to think and work innovatively, have been instrumental in shaping and completing this thesis work in the best possible way. He has been there at every step of this journey, ensuring that I stayed on the right path and providing guidance to navigate challenges.* ***I consider myself truly blessed to work under his mentorship for both my MTech and PhD.***

I shall always be obliged to my doctoral committee members, ***Prof. Chandan Das****,* ***Prof. R. Prasanna Venkatesh,*** *and* ***Prof. S. Senthilkumar,*** *for their valuable insights and constructive suggestions during my progress review seminars that aided in improving the quality of my thesis work. Special thanks to* ***Prof. Kannan Pakshirajan****, Department of Biosciences and Bioengineering, IIT Guwahati, for his valuable recommendations in my thesis work and for permitting me to utilize the facilities in his lab. I would like to convey my sincere thanks and gratitude to all the faculty members and staff of the Department of Chemical Engineering, IIT Guwahati for providing the required facilities to complete my degree on time. I am also thankful to Central Instruments Facility, IIT Guwahati for providing me necessary help and support in carrying out various characterizations. I would like to extend my thankfulness to* ***Prof. Partho Sarathi Pattader****, Department of Chemical Engineering, IIT Guwahati for the*

goniometer facility. I am grateful to the ***Ministry of Human Resource Development (MHRD)*** *for the financial support during this course through fellowship. I extend my heartfelt gratitude to* ***IIT Guwahati*** *for all the beautiful memories.*

I am profoundly thankful to ***Dr. Purnima Madu****, who has not only been a senior but has also supported me like an elder sister throughout this journey. Additionally, I extend my heartfelt appreciation to my dear friend and constant,* ***Ms. Bharathi Dasari****, for standing by me during both the highs and lows of this endeavor. The love and care of these two remarkable individuals have been the source of strength in my academic and personal growth.*

I would like to thank my seniors and lab mates, Dr. Arul Manikandan, Dr. Nengneilhing Baite, Dr. Arun Sakthivel, Dr. Monisha, Dr. Kakali Priyam, Mr. Shiv Prakash, Mr. Arif, Mr. Sashwat, Mr. Raveendra, Mr. Malla Manoj, Ms. Khushboo, Mr. Vishnu Vardhan, Mr. Sashi Bushan, and Mr. Punit, especially ***Mr. Nishan*** *and* ***Mr. Sachin*** *for their friendly support in the smooth completion of my degree. I extend my thankfulness to my friends and batch mates, Mrs. Tejaswi, Mr. Nagendra Prasad, Mr. Bhargav Ram, Mr. Sai Kumar, Mr. Killi Vikas, Mr. Praveen, Ms. Avithi, and Mr. Nipu Kumar.*

My deepest gratitude to my beloved parents, ***Shri Satti Bhaskar Reddy*** *and* ***Smt. Satti Sudha*** *and my siblings,* ***Mrs. Lakshmi Saroja*** *and* ***Mr. Ayyappa Reddy****, as well as my nephews,* ***Mr. Manikanta Reddy*** *and* ***Mr. Kashish Reddy****, for their unconditional love and support. Their belief in my dreams, their understanding, and their encouragement have been my greatest strengths, guiding me through challenges and celebrating my triumphs. Above all, I bow my head to* ***Lord Shiva*** *for showering his divine blessings upon me.*

Sincerely,

Satti Venu Gopala Kumari

Abstract

The rising environmental concerns associated with non-biodegradable petrochemical-based food packaging underscore the critical need for sustainable alternatives. Poly (3-hydroxybutyrate) (PHB) is seen as a sustainable alternative to conventional plastics for food packaging owing to its renewability, high crystallinity, biocompatibility, biodegradability, and physical attributes comparable to conventional plastics. Nonetheless, PHB has certain shortcomings, including low flexibility, moderate gas barrier properties, and negligible antimicrobial and antioxidant activities for its direct application in food packaging. Loading essential oils can increase flexibility and induce antimicrobial and antioxidant activities in biopolymers but at the cost of reduced tensile strength. In contrast, nanofiller reinforcement can increase the tensile strength and barrier properties of such biopolymers. Keeping the aforementioned points in mind, this study focused on the combinational loading of essential oil and nanofillers to overcome the drawbacks associated with PHB for food packaging applications.

The process route employed for the synthesis greatly influences the morphology, structural, optical, antioxidant, and antimicrobial properties of the nanoparticles (NPs); thus, screening synthesis routes is crucial to obtain NPs with the best characteristics suitable for their use as the reinforcing agent in food packaging materials. Thus, in this work, five different chemical synthesis routes, viz., precipitation, sonication-precipitation, microwave combustion, conventional combustion, and solvothermal processes, were screened to customize the properties of MgO NPs for reinforcing in PHB. Among these methods, microwave combustion stood out, yielding MgO NPs with high specific surface area (67.32 m^2/g), smaller particle size (5-35 nm), and outstanding antimicrobial and antioxidant activities compared to other routes.

In the next step, the influence of three different essential oils, namely, grapeseed oil (GS), bergamot oil (BG), and ginger oil (GG), on the properties of PHB was studied. For this purpose,

PHB-based films with varying concentrations (1-10 wt%) of essential oils (GS, BG, and GG) were prepared by facile solution casting method, and extensive characterization was carried out. The tensile strength and elongation at break of pristine PHB films are 20.48±0.51 MPa and 0.51±0.04 %, respectively. Meanwhile, the water vapor and oxygen permeability of pristine PHB films are 1.29 $g.mm.m^{-2}.day^{-1}.atm^{-1}$ and 6.03×10^{-9} $g.m^{-1}.s^{-1}$, respectively. The best improvement (30-fold) in elongation at break is demonstrated by PHB-based films loaded with 5 wt% GS (PHB/5GS) due to good compatibility between PHB and GS. Moreover, PHB/5GS films demonstrated 33 and 1.5 % higher oxygen and water vapor barrier properties, respectively, than pristine PHB. In addition, the active constituents of GS, such as decadienal, terpenes, and phenolic compounds, endowed the PHB/5GS composite films with antimicrobial (against *Staphylococcus aureus:* 61.56±3.39 %; against *Escherichia coli:* 19.72±0.97 %) and antioxidant (53.1±4.7 %) properties. Nevertheless, the addition of GS (5 wt%) resulted in a reduction in the tensile strength (1.3-fold) and thermal stability of PHB-based films, limiting their widespread application in food packaging.

To overcome the limitations of PHB/5GS films, MgO NPs obtained via the microwave combustion route were introduced as reinforcing agents at varying loading rates (0.1-1 wt%), and the PHB/5GS/MgO composite films were fabricated by sonication-assisted solution casting route. Among the developed nanocomposite films, those loaded with 5 wt% GS and 0.7 wt% MgO NPs (PHB/5GS/0.7MgO) demonstrated 1.4-fold higher tensile strength and 30-fold higher elongation at break, along with 90 and 79 % reduction in oxygen and water vapor transmission, respectively, compared to pristine PHB. Moreover, the adverse impact of GS loading on the thermal stability of PHB-based films was partially mitigated with the reinforcement of 0.7 wt% of MgO NPs. In addition, the PHB/5GS/0.7MgO films showed hydrophobic nature, good UV-blocking properties, excellent antioxidant activity (65.25±0.98

%), and complete inhibition of *S. aureus* and *E. coli* growth. However, beyond 0.7 wt% loading of MgO NPs, a decrement in tensile, thermal, and gas barrier properties was noticed for the nanocomposite films due to agglomerate formation.

The application potential of PHB-based films of optimal composition (PHB/5GS/0.7MgO) was assessed for the storage of fresh produce, viz., white button mushrooms (*Agaricus bisporus*) and cherry tomatoes *(Solanum lycopersicum L. var. cerasiforme)*, under ambient room conditions. The shelf-life studies of the aforementioned fresh produce were conducted in four different configurations: (i) no packaging, (ii) conventional packaging, (iii) PHB packaging, and (iv) PHB/5GS/0.7MgO packaging. The results from these shelf-life studies revealed that the mushrooms and cherry tomatoes stored in PHB/5GS/0.7MgO packaging configuration experienced better preservation of quality and sensory properties compared to those in other storage groups, with their shelf-life extended to 6 and 21 days, respectively. Furthermore, it was found that the migration of MgO NPs from the nanocomposite packaging to mushrooms and cherry tomatoes was negligible.

Lastly, the biodegradability of PHB, PHB/5GS, and PHB/5GS/0.7MgO films was assessed in soil and river water environments. Extensive characterization of surface morphology, molecular weight, structural, chemical, optical, and colorimetric properties was conducted on these PHB-based films before and after degradation in soil and river water for varying durations to comprehend their biodegradation mechanism. Remarkably, all the PHB-based films showed 100 % weight loss in soil within 25 days. Whereas, the weight loss of PHB, PHB/5GS, and PHB/5GS/MgO films in river water was 26.8, 23.7, and 20.3 %, respectively, in 120 days. Thus, the findings from this thesis work demonstrated the successful development of a novel active packaging material that is not only environmentally safe but also capable of extending the shelf-life of food.

Contents

List of figures

List of tables

Abbreviations

AFM	:	Atomic force microscope
ASTM	:	American society of testing materials
ATR	:	Attenuated total reflection
BC	:	Bacterial cellulose
BET	:	Brunauer-Emmet-Teller
BG	:	Bergamot oil
BI	:	Browning index
BJH	:	Barrett-Joyner-Halenda
CB	:	Conduction band
CC	:	Conventional combustion
DPPH	:	2, 2-diphenyl-1-picrylhydrazyl hydrate
DSC	:	Differential scanning calorimetry
DTG	:	Differential thermogravimetric
EB	:	Elongation at break
FCS	:	Food contact substance
FDA	:	Food and Drug Administration
FDM	:	Fused deposition model
FESEM	:	Field emission scanning electron microscope
FETEM	:	Field emission transmission electron microscope
FTIR	:	Fourier transform infrared spectroscopy
GC-MS	:	Gas chromatography-mass spectroscopy
GG	:	Ginger oil
GPC	:	Gel permeation chromatography
GRAS	:	Generally recognized as safe
GS	:	Grapeseed oil
HDPE	:	High-density polyethylene
HRTEM	:	High-resolution transmission electron micrograph
ICP-MS	:	Inductively coupled plasma mass spectrometer
LB	:	Luria bertani
LDPE	:	Low-density polyethylene
MWC	:	Microwave combustion

NPs	:	Nanoparticles
PBAT	:	Poly (butylene adipate-co-terephthalate)
PBS	:	Polybutylene succinate
PDI	:	Polydispersity index
PET	:	Polyethylene terephthalate
PHAs	:	Polyhydroxyalkanoates
PHB	:	Poly (3-hydroxybutyrate)
PHBV	:	Poly (3-hydroxybutyrate-co-3-hydroxyvalerate)
PHBHHx	:	Poly (3-hydroxybutyrate-co-3-hydroxyhexanoate)
PL	:	Photoluminescence
PLA	:	Polylactic acid
PP	:	Polypropylene
PS	:	Polystyrene
PT	:	Precipitation
PVC	:	Polyvinyl chloride
ROS	:	Reactive oxygen species
SAED	:	Selected area electron diffraction
SPT	:	Sonication-precipitation
ST	:	Solvothermal
TA	:	Titratable acidity
TGA	:	Thermogravimetric analysis
TS	:	Tensile strength
TSS	:	Total soluble solids
VB	:	Valence band
WVTR	:	Water vapor transmission rate
XRD	:	X-ray powder diffractometer

Notations

a	:	Unit cell parameter
b	:	Unit cell parameter
c	:	Unit cell parameter

a^*	:	Redness/greenness
b^*	:	Yellowness/blueness
A	:	Constant
A_c	:	Absorbance of control sample
A_e	:	Effective surface area of the film
A_s	:	Absorbance of test sample
C_0	:	Concentration of bacterial culture in control
C_t	:	Concentration of bacterial culture in test sample
D	:	Crystallite size
D_s	:	Crystallite size calculated by Sherrer method
D_w	:	Crystallite size calculated by Williamson-Hall method
E_g	:	Band gap energy
ΔE	:	Total color difference
h	:	Planck's constant
I_a	:	Area under amorphous peaks
I_c	:	Area under crystalline peaks
L*	:	Darkness/lightness
M_i	:	Polymer sample initial weight
M_n	:	Number average molecular weight
M_{nf}	:	Number average molecular weight after degradation
M_{ni}	:	Number average molecular weight before degradation
M_t	:	Polymer sample weight during degradation
M_w	:	Weight average molecular weight
RH	:	Relative humidity
m	:	Constant
M_{eq}	:	Equivalent weight
N	:	Normality
N_t	:	Number of chain scissions per unit mass
ΔP	:	Difference in partial pressure
R_a	:	Root mean square roughness
T_m	:	Melting temperature
T_{max}	:	Thermal degradation temperature

T_{onset}	:	Temperature corresponding to 10 % weight loss
T_{600}	:	Fractional transmittance
V_s	:	Volume of test sample
V_t	:	Volume of titrate sample
W_{dry}	:	Weight of oven dried soil
W_i	:	Initial weight of cherry tomatoes
W_{sat}	:	Weight of saturated soil
W_t	:	Weight of cherry tomatoes at specific time t
x	:	Thickness
t	:	Equilibrium time
3D	:	Three dimensional

Greek symbols

α	:	Absorption coefficient
β	:	Full width at half maximum
ε	:	Microstrain
δ	:	Dislocation density
λ	:	Wavelength
θ	:	Diffraction angle
ν	:	Frequency

Chapter 1

Introduction, Literature Review and Objectives

Part of this chapter received the following scientific recognition

International Journal of Biological Macromolecules 221 (2022) 163–182

Contents lists available at ScienceDirect

International Journal of Biological Macromolecules

journal homepage: www.elsevier.com/locate/ijbiomac

Review

Recent advances and future prospects of cellulose, starch, chitosan, polylactic acid and polyhydroxyalkanoates for sustainable food packaging applications

Satti Venu Gopala Kumari [a], Kannan Pakshirajan [b], G. Pugazhenthi [a,c,*]

[a] Department of Chemical Engineering, Indian Institute of Technology Guwahati, Guwahati 781039, Assam, India
[b] Department of Biosciences and Bioengineering, Indian Institute of Technology Guwahati, Guwahati 781039, Assam, India
[c] Centre for Sustainable Polymers, Indian Institute of Technology Guwahati, Guwahati 781039, Assam, India

Kumari et al. (2022), International Journal of Biological Macromolecules, 221, 163-182

Introduction, Literature Review and Objectives

In the initial section of this chapter, a brief overview of various aspects of food packaging, such as functions, requisites, and regulations, as well as the problems associated with the use of conventional plastics, is provided. This was followed by a detailed discussion on biopolymers as sustainable alternatives to conventional plastics, including their history, potential in food packaging, and processing methods. Thereafter, the properties of biopolymers are compared with those of traditional plastics, and their advantages, drawbacks, and strategies to overcome their limitations are discussed. Following that, a thorough literature review was presented, highlighting the potential areas for future research, which formed the basis for the objectives of this thesis. Finally, the organization of the thesis is outlined.

1.1. Food packaging

Food packaging is not just about enclosing food products in a glass bottle, a metal can, or a plastic pouch; it is a coordinated system aimed at assuring the safety and quality of food products all through the supply chain. The demand for packaged food and, consequently, packaging materials is continuously increasing due to on-the-go lifestyles, changing eating habits, and increasing concerns about food wastage. The global food packaging market is valued at 3.1 trillion USD in 2023 and is expected to reach 5.32 trillion USD by 2032 (Global Market Insights, 2024). Materials with a wide range of performance characteristics, such as paper, plastic, glass, and metal, are commonly used for food packaging. At present, polyethylene terephthalate (PET), polyvinyl chloride (PVC), polystyrene (PS), polypropylene (PP), high-density polyethylene (HDPE), and low-density polyethylene (LDPE) are the commercially available plastics for packaging foodstuffs (Geyer et al., 2017).

1.1.1. Functions and requisites of food packaging

The primary functions of the food packaging system are containment; protection; preservation; and communication (Youssef et al., 2018). Good packaging should contain the product in a

form suitable and secure to transport and secure the foodstuffs from external contamination and mechanical damage. Packaging should be convenient to satisfy consumer lifestyle and effective enough to communicate brand identity and influence the buyer's decision. Various factors, such as industrial-scale preparation of food, long distribution lines, demand for prolonged shelf-life, appearance and advertising needs, environmental concerns, and regulatory aspects, influence the composition of packaging material (Ilyas et al., 2021; Zhao et al., 2020). In short, the major requisites of food packaging material are:

- Ease of processing of material
- Selective permeability to gases, moisture, and flavors as needed by the food products
- Safeguarding food against adverse effects of light
- Protection against microbial contamination of food
- Sufficient mechanical strength to handle products throughout the supply chain
- Migration limits as per regulation standards of food safety

Year after year, with the better-becoming technology, there has been more research and development introducing new purposes to food packaging systems. Various strategies, such as plasma treatment (Giannoglou et al., 2021), chemical treatment (Tzortzakis et al., 2017), edible coatings (Kowalska et al., 2021), modified atmosphere packaging (Merlo et al., 2019), and active and intelligent packaging (Roy et al., 2021a), were developed to extend the shelf-life of food or improve the sensory properties of packaging. Beyond basic barrier function against moisture and oxygen, food packaging materials can be engineered to be "active" with the incorporation of active ingredients such as antioxidants, antimicrobial agents, oxygen/ethylene scavengers, and flavor-releasing/absorbing systems (Zare et al., 2022; Majid et al., 2018). In this context, plant extracts (Chakravartula et al., 2020), essential oils (Chi et al., 2019; Li et al., 2019), and nanoparticles (NPs) with unique physiochemical and biological characteristics, viz., silver (Dairi et al., 2019), sulfur (Shankar et al., 2018), ZnO (Zare et al., 2022; Kim et al.,

2019), TiO_2 (Baek et al., 2018), and MgO (Swaroop et al., 2019), were widely investigated for loading into food packaging materials. Whereas, intelligent packaging extends the communication function of the packaging system by detecting and recording external or internal changes in products to provide food quality and safety information (Roy et al., 2021a).

1.1.2. Regulations of food packaging

Many countries have formulated regulations on food packaging materials to meet the safety of products (Ilyas et al., 2021). The U.S. Food and Drug Administration (FDA) requires that food packaging materials should adhere to Section 409 of the Federal Food, Drug, and Cosmetics Act. Accordingly, manufacturers are expected to inform the FDA in advance through the food contact notification process before introducing any new food contact substance (FCS) into the market (FDA, 2002). As per the Food Additive Directive, FDA clearance is necessary even for additives used in food packaging material that can potentially migrate into foodstuffs. Optionally, FCSs can be exempted from authorization as well as notification if the material belongs to any of the following categories: (a) considered safe by experts, (b) generally recognized as safe (GRAS), (c) common food product before 1958, and (d) non-carcinogenic compound with a dietary intake below 0.5 µg/L according to the threshold of regulation law (Werner et al., 2017; FDA 2002). In India, the Food Safety and Standards Authority of India (FSSAI), and in Europe, the European Union framework reviews and sets guidelines for food packaging materials (Ilyas et al., 2021). Although nanofillers have gained huge interest in the food packaging industry, their safety is still under doubt. Governments in Australia, New Zealand, Europe, and the US have all begun to regulate the use of nanomaterials in food packaging.

1.1.3. Problems with the use of conventional plastics

The packaging industry alone consumes more than 40 % of plastic produced worldwide, and nearly half of it is utilized for food packaging. However, as plastics used in food packaging are

primarily single-use and disposed of after a shorter service life compared to plastics used in other sectors like construction or electronics, the food packaging industry is the major producer of plastic waste (World Economic Forum, 2018). Plastic waste poses a major threat to the environment as well as to humans due to its increasing production rate and the unavailability of appropriate methods for its management and disposal (Moharir et al., 2019). 150 million tonnes of plastic waste are generated worldwide every year; of this total, 79 % is deposited in landfills and the environment, 12 % is incinerated, and only 9 % is recycled (Geyer et al., 2017). A staggering 8 million tonnes

of plastic enter oceans every year, wreaking havoc on ocean health and marine life. The majority of this plastic waste, around 70-80 % of it, is transported to oceans by rivers. Plastic pollution in rivers is as severe as that in oceans, jeopardizing fishing, tourism, and river transportation and risking the availability of drinking water. Landfilling of plastics generates toxic leachates and reduces soil fertility, while incineration releases hazardous air pollutants such as dioxins and furans, posing serious risks to human health and the environment. Moreover, recycling is often impractical for food packaging materials due to the contamination by food residues. If the current production and waste management trends of plastic persist, it is estimated that 12,000 tonnes of plastic will accumulate in landfills or the environment by 2050, thereby posing a threat to the environment (Meijer et al., 2021; Roebroek et al., 2021; Plastic Oceans Foundation, 2018). Apart from generating plastic waste, the production of conventional plastics contributes to the depletion of fossil resources. At present, more than 99 % of plastic packaging finds its origin in petrochemical industries, and about 4 % of the world's fossil resources are being used in plastic production (British Plastics Federation, 2019).

1.2. Biopolymers: sustainable alternatives to conventional plastics

Many efforts are being made to reduce the dependency on conventional petroleum-based non-biodegradable plastics for food packaging applications and avoid their deteriorating effects on

the environment. In this context, the use of biopolymers with properties derived to meet the standards of food packaging materials is considered the best solution (Manikandan et al., 2020). The concept of "biopolymer" or "bioplastic" is emphasized by two independent terms, i.e., bio-based and biodegradability. The American Society of Testing Materials (ASTM) defined the term biodegradable as "Capable of undergoing decomposition into carbon dioxide, methane, water, or biomass in which the predominant mechanism is the enzymatic action of microorganisms, that can be measured by standard tests, in a specified time, reflecting available disposal condition." Whereas the term "bio-based" is focused based on the raw material and is defined as "an organic raw material in which carbon is derived from a renewable resource via the biological process." European Bioplastics described biopolymers as "***polymeric materials which are either bio-based or biodegradable or features both properties***" (European Bioplastics, 2023). Fig. 1.1 shows the classification of biopolymers based on the source and biodegradability. Notably, biopolymers that are both bio-based and biodegradable, viz., cellulose, starch, chitosan, polylactic acid (PLA), and polyhydroxyalkanoates (PHAs), are considered sustainable alternatives to conventional plastics for food packaging applications. However, the commercial-scale application of biopolymers in the food packaging industry is limited by three main factors: production cost, processing difficulties, and performance characteristics (Youssef et al., 2018). To overcome the aforementioned drawbacks, different strategies, viz. nanotechnology, blending of biopolymers, utilizing cheaper resources as feedstock for biopolymer production, and application of biorefinery concept to harness multiple bio-based products, are being explored by the researchers (Talan et al., 2022; Geyer et al., 2017).

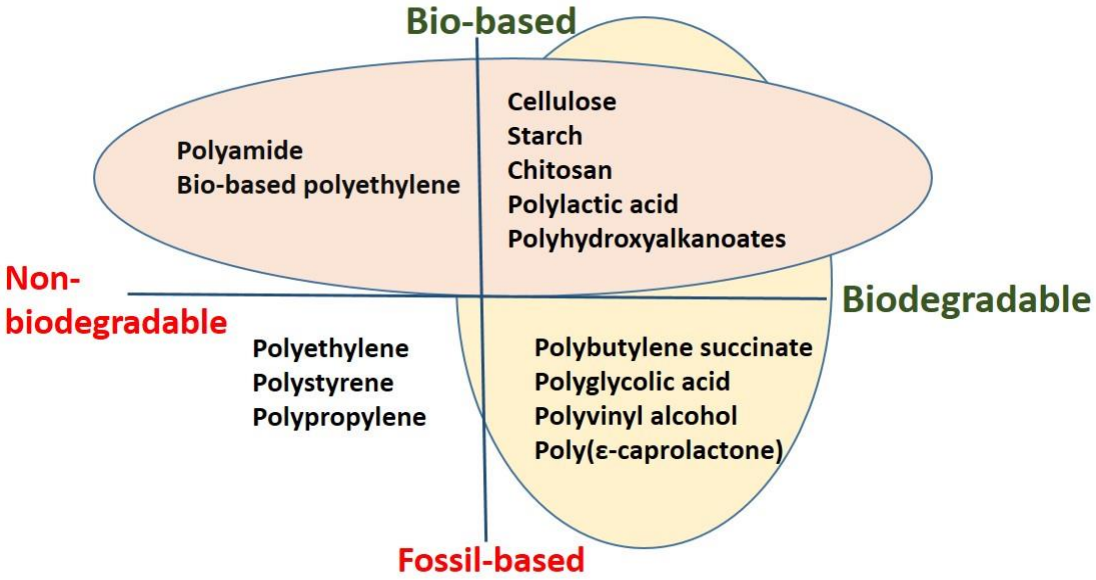

Fig. 1.1. Classification of biopolymers based on raw materials and biodegradability

1.2.1. History and potential of biopolymers in food packaging

According to statistics reported by European bioplastics, global bioplastic production amounts to 2.18 million tonnes in 2023 and is expected to hit 7.43 million tonnes by 2028. Interestingly, as shown in Fig. 1.2, packaging, especially flexible and rigid packaging, accounts for 43 percent (0.93 million tonnes) of the total bioplastic market in 2023 (European Bioplastics, 2023). NatureWorks, Novamont, Bioplast, Coca-Cola, PepsiCo, and Cereplast stand as leading companies in the bioplastic market.

PLA is the most widely used packaging material among biopolymers (Zhao et al., 2020). Nature Works is a leading manufacturer of PLA, and they introduced their first commercial product, Ingeo™, in 2003. Ingeo™ was based on dextrose of corn and was supplied to numerous retailers. For instance, Wilkinson Industries procures PLA resins from NatureWorks and manufactures plastic films and trays. In 2008, all-nature-renewable bottles were made from Ingeo™, and they were used for supplying orange juice. In the year 2010, Walmart started using NatureWorks Ingeo for packing salads, spinach, fruits, vegetables, etc. Later in 2011,

sustainable yogurt cups were launched in the German market by Danone. The first PLA-based flexible packaging was launched by Frito-Lay in 2009. The long history of the starch market begins with Novamont, a leading manufacturer of starch bioplastics. The trade name of Novamont is Mater-Bi®. Various products, such as biodegradable and compostable bags, bowls for packaging salads, compostable trays for packaging meat, etc., were launched under this trade name. Plantic Technologies Ltd. launched its product Plantic® R 1 tray based on thermoformed starch/nanoclay composite, which it sells to Cadbury® Dairy Milk™, Milk tray chocolates, and Marks & Spencer for chocolate packaging (Plantic Technologies Ltd., 2007).

Considering the PHA market, Telles is a major PHA producer till 2011. Other PHA producers are Greenbio, Metaboilx, Kaneka Biomer, Titan Biological Material Co., etc. The Greenbio, a China-based company, has a production capacity of 10,000 tonnes of PHA per year. Due to raised awareness of environmental safety, major retailers such as Walmart and Marks & Spencer developed sustainable strategies and targets for reducing plastic waste. Currently, bio-based food packaging is mostly used for products with shorter shelf life, such as fruits, vegetables, meat, fresh juices, and dairy products, that do not require high resistance to oxygen or water vapor transmission (Table 1.1) (Mangaraj et al., 2019).

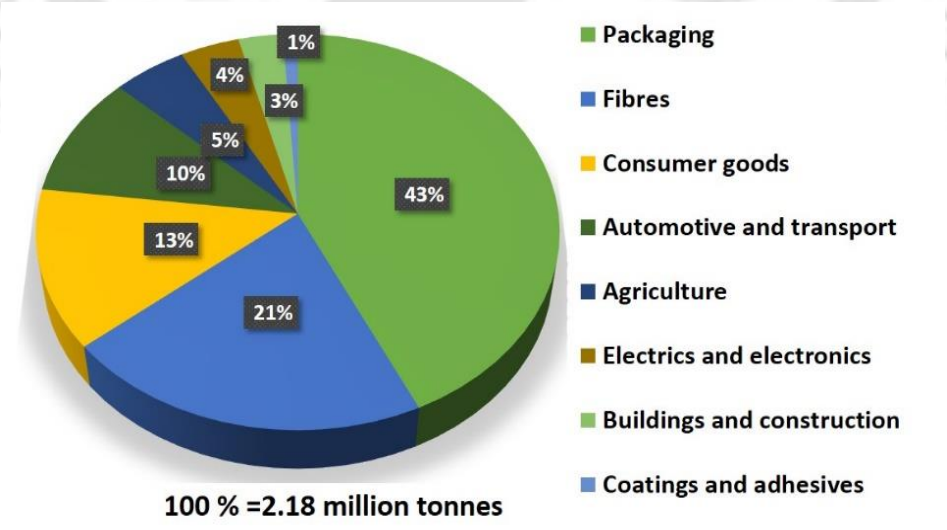

Fig. 1.2. Market segment of bioplastics for the year 2023 (European bioplastics, 2023)

Table 1.1. Commercial application of biopolymers in the food packaging industry

Biopolymer	Products	Application	Company	Country
PLA	containers and films	bakery products, dairy, meat, and confectionery	Nature Works LLC	USA
PLA	bottles	juices, and dairy drinks	Biota	USA
PLA	bags	Chips	Snyder's of Hanover	USA
PLA	jars	Yogurt	Stonyfield	USA
PLA	bowls	organic poultry	Delhaize	Belgium
PLA	films	frozen fries	Bio-Flex by McCain	Belgium
PLA	films	fruits, and vegetables	Delhaize	USA
starch-based	trays	milk chocolates	Marks & spencer	UK
starch-based	films	Peanuts	National Starch Company	UK
cellulose-based	trays	Kiwi	Walmart	US
cellulose-based	films	Sweets	Quality street	UK
cellulose-based	films	potato chips	Boulder Canyon	USA

1.2.2. Processing methods

Polymer processing can significantly affect crystallinity, molecular orientation, and hence the properties of finished products. Biopolymers can be processed into a variety of products, such as trays, cups, laminated paper, and packaging films, depending upon the processing route adapted. Different methods employed for the processing of biopolymers are listed in Table 1.2 and also schematically presented in Fig. 1.3. PLA can be processed by almost all the existing processing technologies, such as injection molding, blown film extrusion, cast film extrusion, and solution casting (Mangaraj et al., 2019). PHA's can be processed by injection molding, solution casting as well as extrusion techniques (Naser et al., 2021). The blends of thermoplastic starch with biodegradable/synthetic polymeric components such as polyvinyl alcohol and polycaprolactone have been successfully developed on an industrial scale using film blowing, injection molding, blow molding, and extrusion techniques (Peelman et al.,

2013). Solution casting and extrusion methods are used for the fabrication of chitosan films (Shankar et al., 2018; De Silva et al., 2017). Cellulose derivatives such as ethylcellulose, benzylcellulose, cellulose diacetate, and cellulose triacetate can be processed by injection molding or extrusion techniques with the addition of plasticizers or other polymers (Peelman et al., 2013). 3D printing is a cheaper and more efficient process that was introduced in 1987 at the Massachusetts Institute of Technology. In 3D printing, the final shape of the material can be predefined and controlled in 3D using AutoCAD software (Postiglione et al., 2015). However, the lack of information on user-defined biochemical and mechanical properties is a major hurdle for 3D printing to fabricate products from biopolymers. Solution casting is a facile, versatile, and low-cost methodology for the fabrication of biopolymer films, thus commonly adopted by researchers (Manikandan et al., 2020; Salari et al., 2018; Valapa et al., 2016a).

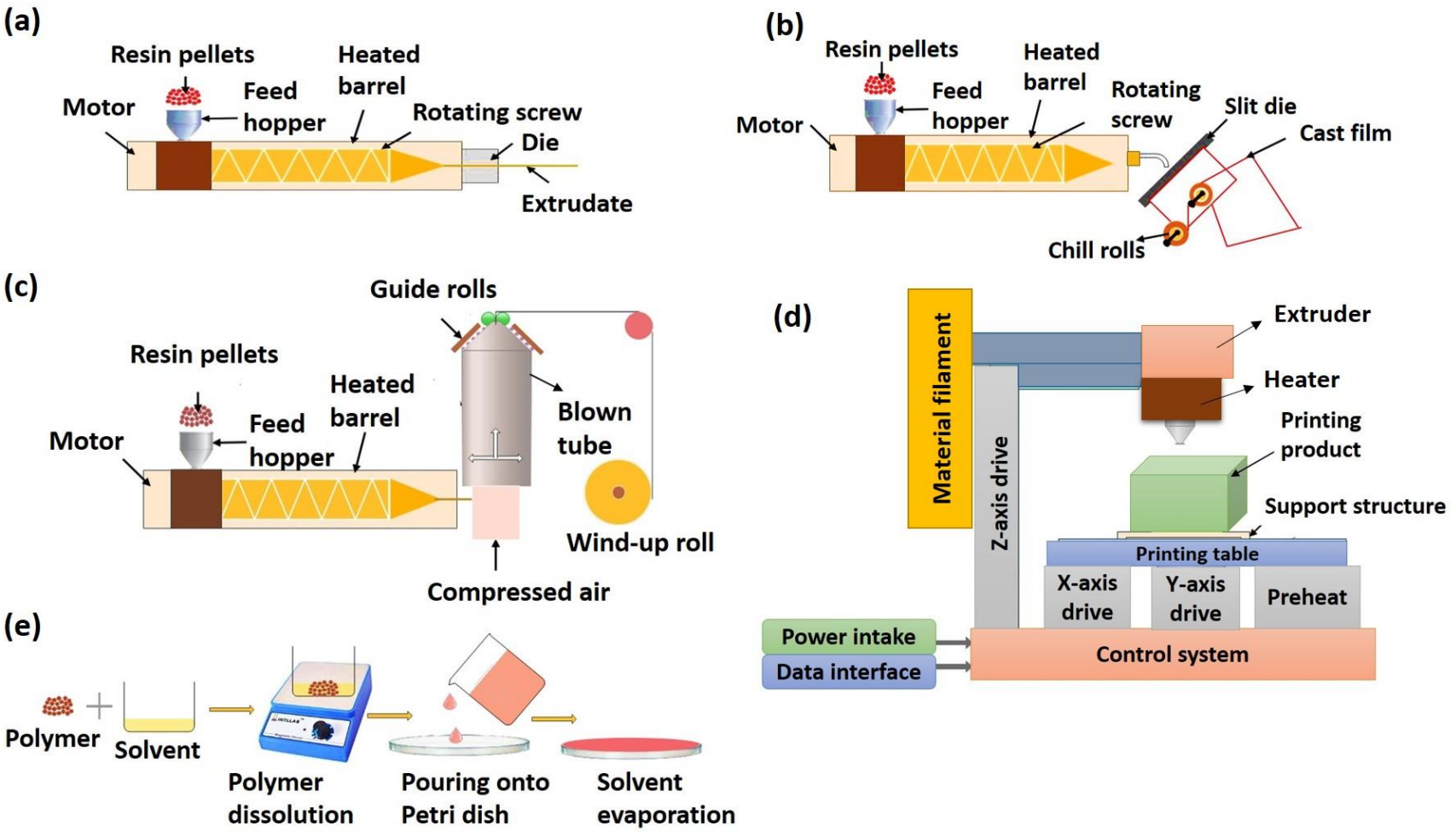

Fig. 1.3. Schematic showing (a) injection molding, (b) blown film extrusion, (c) cast film extrusion, (d) 3D printing, and (e) solution casting processes

Table 1.2. Processing methods of biopolymers

Method	Procedure and application
Injection molding	(i) This method involves forcing molten polymer under high pressure into a mold cavity through the sprue. (ii) Mainly used for thermoplastic materials.
Blown film extrusion	(i) This method involves blowing up polymer melt in a heated thermoplastic tube with compressed air to adhere to the outline of the mold and release the final product. (ii) Films formed by this method are typically 0.007-0.125 mm thick, tough, and resilient. (iii) Suitable for resin with high melt viscosity such that it is easy to pull melt from the die.
Cast film extrusion	(i) This method involves extruding polymer melt from the die onto chill rolls to form a film. (ii) Results in films with better optical properties than film blowing. (iii) Films formed are soft and stretchy.
3D printing	(i) Referred as a rapid prototyping technique. (ii) In this method, the solution gets deposited on the printing bed layer-by-layer following a pre-programmed design set to achieve the desired specification for the final material. (iii) Fused deposition model (FDM) is applied in the event of a solvent-free approach. In FDM, the polymer is typically melted at lower temperatures to avoid degradation.
Solution casting	(i)The polymer is dissolved in a suitable solvent using agitation, and then the films are obtained by evaporating the solvent. (ii) In case of polymer nanocomposites, colloidal suspension of nanomaterials is mixed with the polymer dissolved in a suitable solvent with simple shearing or stirring, followed by casting of the solution, and evaporation of solvent.

1.3. Characteristics of bio-based biodegradable biopolymers

1.3.1. Cellulose

Structurally, cellulose is a linear polymer of hydroglucose wherein glucose units are joined by β -1,4 glycosidic linkages that allow cellulose chains to tightly bind together and form inter-chain hydrogen bonds (Fig. 1.4a) (Pawar et al., 2020; Othman et al., 2014). Though cellulose has several advantages, such as high thermal resistance, UV barrier capacity, and acquired GRAS standard by the FDA, its hydrophilic nature, poor water vapor barrier properties, limited long-term stability, and poor mechanical properties due to moisture sensitivity restrict its usage in food packaging at the industrial level **(**Table 1.3) (Peelman et al., 2013). The extensive hydrogen bonding in cellulose results in insoluble microfibrils, and crystalline and amorphous structural regions that provide good tensile strength (TS) and durability to it (Shaghaleh et al., 2018). Cellulose is found in all plant materials. Cellulose can also be produced from bacteria, algae, and tunicates, hence called bacterial cellulose (BC). When compared to plant cellulose, BC possesses higher water absorptivity, crystallinity (60-90 % higher than plant cellulose), and a higher degree of polymerization (Salari et al., 2018; Shaghaleh et al., 2018; Jebel et al., 2016). The reactive functional groups in cellulose enable its chemical modification to produce a range of cellulose derivatives through carboxymethylation, etherification, hydroxypropylation, etc. Cellulose derivatives such as cellulose acetate, carboxymethylcellulose, and hydroxyethylcellulose, are considered important sources in biomaterial-based food packing owing to their flexibility, toughness, and resistivity to water. On the other hand, they are expensive for bulk use (Pawar et al., 2013). Cellulose can also be used as a reinforcement in nanocomposite films by processing into nanocrystals (Salari et al., 2018), microfibrils (Syafri et al., 2020), and nanofibrils (Yu et al., 2019). The cellulose reinforcements exhibit excellent mechanical properties, equalling glass and carbon nanofibers.

1.3.2. Starch

Starch is a semi-crystalline polymer with a hydrophilic nature. It is one of the well-studied biopolymers for food packaging applications owing to its low price, zero toxicity, high biodegradability, and easy availability. Structurally, starch is a complex branched polymer wherein D-glucose units are joined by α-(1→4) linkages, and branch points are joined by α-(1→6) linkages (Fig. 1.4b) (Wang et al., 2014). In terms of molar mass, starch comprises 10-20 % of amylose and 80-90% of amylopectin. However, the concentration of amylose and amylopectin in starch differs depending upon its source. As the content of amylose increases in starch, there is a consequent improvement in elongation and strength. Starch is not stable under heat. Its glucoside bonds begin to dissolve at 150 ℃, and starch granules collapse above 250 ℃. Poor resistance to moisture, poor thermal processability, and poor mechanical properties constrain its use in the food packaging industry**.** Plasticized starches are called thermoplastic starch. Plasticizers lower the glass transition temperature and enhance the flexibility and processability of starch (Ayana et al., 2014; Martin et al., 2001). The disadvantages of thermoplastic starch include high moisture sensitivity and poor mechanical properties, which limits its utility as a food packaging material (Table 1.3).

1.3.3. Chitosan

Chitosan is a linear cationic polysaccharide and a copolymer of β-(1 → 4)-2-acetamido-D-glucose and β-(1 → 4)-2-Amino-D-glucose units (Fig. 1.4c). The promising future for chitosan in the food packaging industry is attributable to its numerous advantages such as availability, non-toxicity, easy film-forming ability, biodegradability, selective CO_2 and O_2 permeability, good mechanical properties, antibacterial, and antifungal activity (Shankar et al., 2018; Wang et al., 2018). It has been approved as a food ingredient by the FDA (Mitelut et al., 2015). However, high sensitivity to water and low mechanical and thermal stability are major setbacks

for the industrial-scale application of chitosan (Table 1.3) (Haghighi et al., 2020; Dotto et al., 2017). Furthermore, the high water sensitivity reduces its barrier properties which may lead to complete solubilization of chitosan into foodstuffs. Blending chitosan with a hydrophobic polymer can minimize the solubility problems (Haghighi et al., 2020; Claro et al., 2016).

1.3.4. PLA

PLA belongs to the family of polyesters, usually produced by ring-opening polymerization of lactides or condensation polymerization of lactic acid (LA) monomers. The chemical structure of LA consists of L- and D- isomers that are optically active (Fig. 1.4d). The L-to D- ratio in LA influences some of the key molecular properties of PLA, such as degree of crystallinity, ease of processing, and melting temperature (Tawakkal et al., 2014). Compared to other biopolymers, PLA grabbed more attention in the packaging industry because existing technology available for conventional plastics can be used for its processing without any modification. PLA has a lower oxygen transmission rate than PET and PS, tensile strength (TS), and process stability like PS (Zhao et al., 2020). PLA starts to decompose at 300 ℃ and has thermal stability similar to PVC, but lower than PS, PP, and PET (Nilsen-Nygaard et al., 2021). Though PLA was approved by the FDA far back in the 1970s, when contemplating commercial application in the packaging industry, PLA has some setbacks, such as inherent brittleness, poor thermal processability, and water barrier properties.

1.3.5. PHAs

PHAs are polyesters produced by fermentation of sugars and lipids by bacteria. They are non-toxic, non-sticky, and insoluble in water. In addition to their biodegradable, biocompatible, and renewable nature, PHAs are known for properties such as good ultra-violet resistance, high TS, printability, grease, and oil resistance, which are suitable for application in the food packaging industry (Plackett et al., 2011). There are three main categories of PHAs: (i) PHA's with 3-5

carbon atoms such as poly (3-hydroxybutyrate) (PHB), poly (4-hydroxybutyrate), poly (3-hydroxybutyrate-co-3-hydroxyvalerate) (PHBHV); (ii) 6-14 carbon atoms like poly-3-hydroxyhexanoate; (iii) more than 14 carbon atoms called long-chain PHAs (Fig. 1.4e) (Keshavarz et al., 2010). A number of PHAs with varied characteristics can be produced by varying monomers and constitutional isomerism. Homopolymers in the PHAs family include poly (3-hydroxypropinoate), poly (3-hydroxyvalerate), poly (3-hydroxyhexanoate), and poly (3-hydroxydecanoate). PHBHV, poly (3-hydroxybutyrate-co-3-hydroxyhexanoate) (PHBHHx), poly (3-hydroxybutyrate-co-3-hydroxyoctanoate) and poly (3-hydroxybutyrate-co-3-hydroxydecanoate) are examples of some copolymers in PHA family (Chernozem et al., 2022; Naser et al., 2021). Only a few PHAs, notably, PHB, PHBHV, and PHBHHx are produced on a large scale and are commercially available (Pryadko et al., 2021). PHBHV has better flexibility, but lower crystallinity and melting point compared to PHB (Table 1.3). PHBHHx has mechanical properties equalling that of LDPE (Table 1.3). Among 100s of monomers and copolymers in the family of PHAs, PHB is the best-characterized member. PHB is a linear, isotactic, and semi-crystalline polymer. PHB is one of the most promising biopolymers for food packaging applications owing to its biodegradability, biocompatibility, and physical properties equal to those of conventional plastics (Table 1.3). It is worth mentioning that PHB has reached the commercial level of production with a wide range of applications spanning from the production of everyday items like razors and bottles to advanced biomedical products such as sutures and bone implants. Moreover, owing to its high crystallinity, PHB exhibits better gas barrier properties than other biopolymers, such as PLA, starch, chitosan, PHBHV, PHBHHx, and cellulose, which is advantageous in the context of food packaging applications (Plackett et al., 2011). Nevertheless, low elongation at break (EB), moderate barrier properties, and a high production cost are major limitations for its

commercial-scale application in the food packaging field. Recent studies revealed that utilizing cheap carbon resources as a feedstock reduces the production cost of PHB (Lee et al., 2021; Saratale et al., 2019). Several strategies, viz., the addition of NPs (Manikandan et al., 2020; Akin et al., 2018), plasticizers (Kurusu et al., 2015; Baltieri et al., 2003), essential oils (Rech et al., 2021; Mittal et al., 2023), and blending with biopolymers (Albuquerque et al., 2021; Adorna et al., 2020), were being explored to overcome the shortcomings associated with PHB use in food packaging.

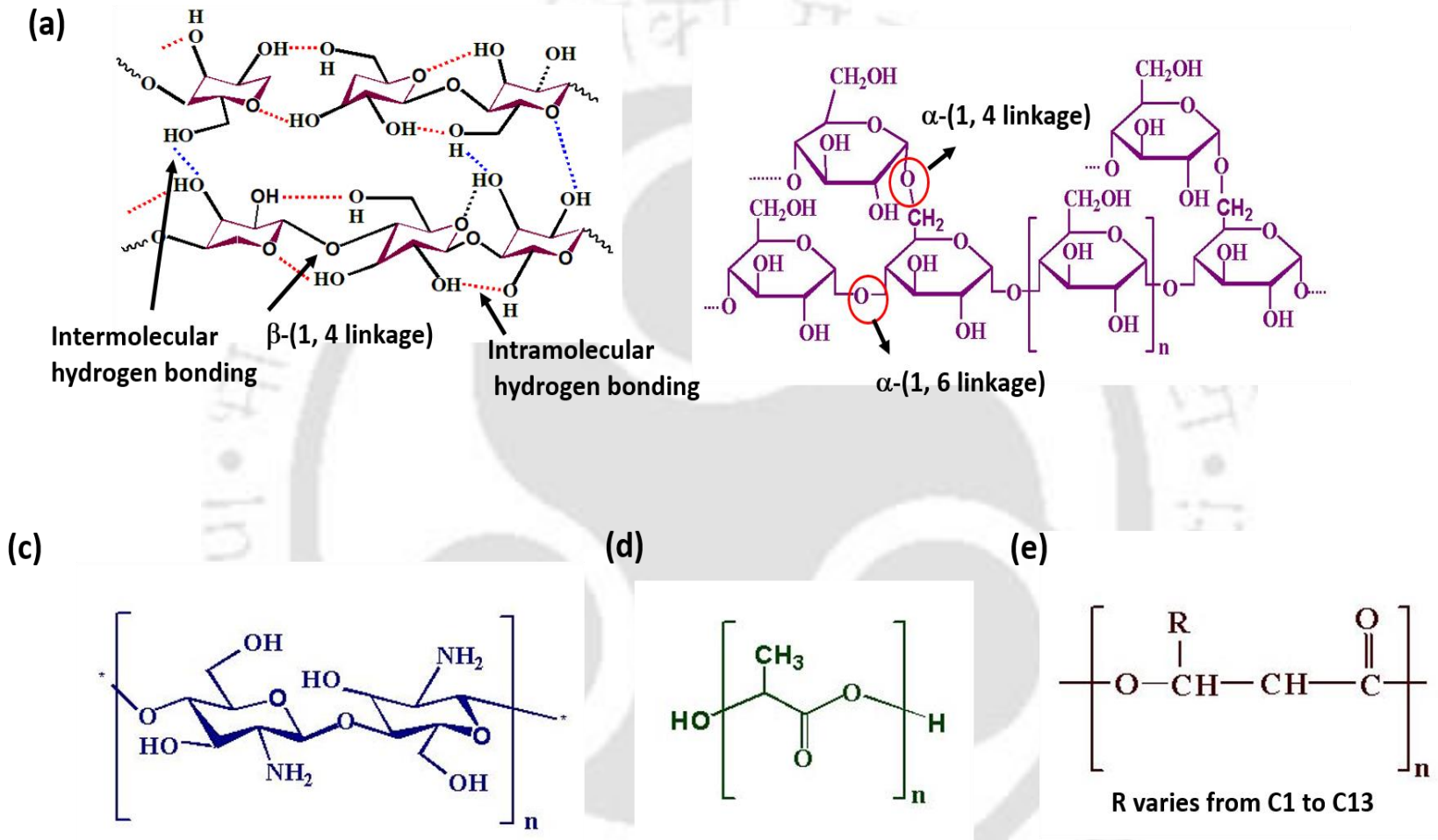

Fig. 1.4. Chemical structures of (a) cellulose (b) starch (c) chitosan (d) PLA, and (e) PHA's

Table 1.3. Characteristics of bio-based biodegradable biopolymers and conventional plastics

Polymer	Source	TS (MPa)	EB (%)	Water vapor permeability at 23 °C, 50-90 % RH (g mm m^{-2} day^{-1} atm^{-1})	Oxygen permeability at 23 °C, 0-50 % RH (ml mm m^{-2} day^{-1} atm^{-1})	Cost (USD/ kg)	References
Cellulose acetate*	plants, bacteria	17-46	3-30	3.3	0.52	2.49-4.80	Zhao et al., 2020; Dairi et al., 2019; Plackett et al., 2011
Thermoplastic starch *	plants	3-10	3	-	-	2.43-4.85	Zhao et al., 2020; Da roz et al., 2011
Chitosan*	shrimp, crab shells, and cell walls of fungi	17.02-29.39	20.27-51.56	6.90×10^{4}-10.97×10^{4}	0.28×10^{6}-24.38×10^{6}	30	Salari et al., 2018; Dotto et al., 2017
PLA*	agricultural products	28-50	7-9	5-7	15-25	3.31-3.53	Zhao et al., 2020; Swaroop et al., 2019; Plackett et al., 2011
PHB*	bacteria	20-40	0.5-6	1-5	1.5-10	6-20	Manikandan et al., 2021; Zhao et al., 2020; Plackett et al., 2011
PHBHV*	bacteria	30-38	20	1-3	5-14	6.86-20.26	Manikandan et al., 2021; Zhao et al., 2020; Plackett et al., 2011
PHBHHx*	bacteria	21	400	1.34	7.8	6.86-20.26	Naser et al., 2021; Vandewijngaarden et al., 2016

Polymer	Source	TS (MPa)	EB (%)	Water vapor permeability at 23 °C, 50-90 % RH (g mm m^{-2} day^{-1} atm^{-1})	Oxygen permeability at 23 °C, 0-50 % RH (ml mm m^{-2} day^{-1} atm^{-1})	Cost (USD/ kg)	References
HDPE	Fossil fuels	24-32	150-400	0.1-0.24	26.3-98.5	0.82-1.01	Zhao et al., 2020; Keller et al., 2017; Ortega-Toro et al., 2017
LDPE	Fossil fuels	10-12	300-500	0.5-2	50-200	0.95-1.18	Zhao et al., 2020; Ortega-Toro et al., 2017; Plackett et al., 2011
PVC	Fossil fuels	48-52	200-450	1-2	2-8	1.85-2.71	Zhao et al., 2020; Plackett et al., 2011
PP	Fossil fuels	21-27.5	100-600	0.2-0.4	50-100	0.93-1.15	Zhao et al., 2020; Ortega-Toro et al., 2017; Plackett et al., 2011
PET	Fossil fuels	55-79	15-165	0.5-2	1-5	1.15-2.12	Zhao et al., 2020; Ortega-Toro et al., 2017; Plackett et al., 2011
PS	Fossil fuels	24-60	1.6-2.5	0.8-3.9	98.5-171	2.18-3.28	Zhao et al., 2020; Keller et al., 2017

EB: elongation at break; RH: relative humidity, TS: Tensile strength; *properties vary with molecular weight, source, additives/plasticizer, and processing method used

1.4. State-of-the-art

1.4.1. Loading of plasticizers/essential oils in PHB

As discussed earlier in Section 1.3.5, low EB is one of the major drawbacks of PHB for food packaging applications. In general, plasticizers are used to improve the flexibility of polymeric materials. Nevertheless, the results of the plasticization of PHB have not been successful so far (Table 1.4). For instance, Kurusu et al. (2015) analyzed the effect of the addition of 10 wt% of industrial plasticizers, viz., tributyl citrate, triethyl citrate, and tri (ethylene glycol) bis (2-ethyl hexanoate) in PHB via the melt mixing method (Kurusu et al., 2015). However, improvement in EB from 6.8 to 7.2% was observed only in the case of PHB incorporated with tri (ethylene glycol) bis (2-ethyl hexanoate) (Kurusu et al., 2015). Another study found that the addition of 30 wt% triacetyl glycerol to PHB caused a two-fold increase in its EB, but the TS and crystallinity of composite films decreased drastically (Baltieri et al., 2003). No significant improvement in EB was noticed with the inclusion of 30 wt% of plasticizers, viz., polyadipate, dioctyl adipate, and dioctyl phthalate in PHB (Baltieri et al., 2003). Moreover, due to the rise in concerns regarding the migration of chemical plasticizers from packaging to foodstuffs and their adverse effects on human health, interest in the use of natural additives as an alternative is growing (Moeini et al., 2021).

Essential oils are bioactive compounds that, in addition to providing antimicrobial and antioxidant properties, can improve the flexibility of biopolymer films (Sharma et al., 2021; Jiang et al., 2020; Chi et al., 2019). Moreover, the FDA classified them as “Generally recognized as safe” (Atarés et al., 2016). As a result, abundantly available natural active agents, viz., essential oils derived from clove, cinnamon, rosemary, bergamot, ginger, lemongrass, and grapeseeds, have grabbed the most attention in the food packaging field (Rech et al., 2021; Sharma et al., 2021; Wang et al., 2019). However, most of these studies are limited to PLA-based composites. Fabrication of

PHB/essential oil composites is less known (Table 1.4). Rech et al. (2020) studied the influence of three different combinations of essential oils viz. citronella, melaleuca, and cinnamon on the physical and mechanical properties of PHB (Rech et al., 2021). A maximum EB value of 6.95 % was achieved using a combination of 15 wt% of citronella oil and 15 wt% of cinnamon oil in the PHB matrix; however, TS of the films decreased from 11.10 to 6.93 MPa. No significant change in EB of PHB was observed with loading of 6 wt% of canola oil in PHB (Giaquinto et al., 2017).

The aforementioned findings underscore the need to find the best essential oil suitable for improving the EB of PHB, along with antioxidant and antimicrobial properties. Qin et al. (2017) reported a significant improvement in the EB of PLA with the addition of 9 wt% bergamot oil (BG). Moreover, PLA/BG composites showed excellent inhibitory effects against foodborne bacteria such as *Bacillus subtilis* and *Escherichia coli* (Qin et al., 2017). The addition of 4 wt% of ginger oil (GG) to the PLA/poly (3-hydroxybutyrate-4-hydroxybutyrate) blend increased the EB of films from 95 to 124 %; moreover, the composite films exhibited 71.2 % antioxidant activity (Jiang et al., 2020). The addition of 1.5 % (v/v) of grapeseed oil (GS) improved the EB and antifungal properties of chitosan films (Tan et al., 2015). Several other studies reported the antimicrobial and antioxidant properties of GS (Wang et al., 2019), BG (Çakmak et al., 2020), and GG (Bonilla et al., 2018)-loaded biopolymer composite films. From the afore-discussed results, it can be inferred that the addition of essential oils, viz., GS, BG, and GG, is a promising strategy to improve flexibility and induce/enhance antioxidant and antimicrobial activity in the biopolymers. However, to the best of our knowledge, there are no reports yet on the fabrication of PHB-based composite films with the essential oils GS, BG, and GG for active food packaging applications.

Table 1.4 Literature summarizing the influence of plasticizers and essential oils loading on the properties of PHB

Polymer	Additive	Synthesis method	Additive loading (wt%)	TS (MPa)		EB (%)		Antibacterial activity	Reference
				Pristine PHB	Composite	Pristine PHB	Composite		
PHB	Tri(ethylene glycol) bis(2-ethylhexanoate)	Melt extrusion	10	24±0.3	18 ±0.4	6.8±0.1	7.2±0.5	NA	Kurusu et al., 2015
PHB	Triethyl citrate	Melt extrusion	10	24±0.3	19 ± 1.1	6.8±0.1	2.0±0.2	NA	Kurusu et al., 2015
PHB	Tributyl citrate	Melt extrusion	10	24±0.3	16 ±3.8	6.8±0.1	1.9±0.8	NA	Kurusu et al., 2015
PHB	Triacetyl glycerol	Melt extrusion	30	31.3±0.3	11.3±0.7	7.0±0.1	15.5±1.3	NA	Baltieri et al., 2003
PHB	Dioctyl phthalate	Melt extrusion	30	31.3±0.3	12.6±0.4	7.0±0.1	8.6±0.6	NA	Baltieri et al., 2003
PHB	Polyadipate	Melt extrusion	30	31.3±0.3	14.4±0.2	7.0±0.1	8.6±0.3	NA	Baltieri et al., 2003
PHB	Dioctyl adipate	Melt extrusion	30	31.3±0.3	13.1±0.7	7.0±0.1	4.3±0.1	NA	Baltieri et al., 2003
PHB	Canola oil	Solution casting	6	20.8+0.8	10.4±0.1	4.1+0.4	4±0.1	Inhibitory action observed against *E. coli*	Giaquinto et al., 2017
PHB	Citronella oil and cinnamon oil	Solution casting	30	11.1±0.12	6.9±0.3	1.82±0.47	6.9±0.9	Inhibition zone of *E. coli*: 5 ±1 mm Inhibition zone of *S. aureus*: 3 ±1.7 mm	Rech et al., 2021
PHB	Tea tree oil and cinnamon oil	Solution casting	30	11.1±0.12	3.23±0.29	1.82±0.47	3.88±0.56	Inhibition zone of *E. coli*: 3 ±1 mm Inhibition zone of *S. aureus*: 4 ±2 mm	Rech et al., 2021

EB: Elongation at break; NA: not available; PHB: poly (3-hydroxybutyrate); TS: Tensile strength

1.4.2. Loading of nanoparticles (NPs) in PHB

Nanotechnology is a promising strategy that can tailor the physical and functional characteristics of the biopolymers. Bionanocomposites consist of inorganic/organic NPs incorporated in the biopolymer matrix (Kumar et al., 2017). The improvement in the properties of bionanocomposites depends on the morphology of the nanocomposite film as well as the dimension, length, and aspect ratio of the reinforced NPs (Salaberria et al., 2014). NPs can be loaded in the biopolymer matrix by solvent intercalation or melt mixing or in situ polymerization (Kumari et al., 2020; Chakraborty et al., 2018; Valapa et al., 2016a). However, good compatibility between polymer matrix and nanofiller is essential to achieve the desired characteristics in the composite films. Uniform dispersion of nanofillers increases the interfacial area between matrix and nanofiller, which can alter the mobility and relaxation behavior of molecules, consequently improving the mechanical and thermal behavior of the composite material. Besides, nanofillers can increase the path length of gas molecules, thereby reducing the permeability of gases through the composite matrix. For materials intended for food packaging applications, higher TS and lower permeability of gases/moisture are required to ensure the quality and safety of food. The influence of loading different nanofillers on the properties of PHB is summarized in Table 1.5.

From Table 1.5, it can be observed that the addition of as low quantity (0.3-5 wt%) of various nanofillers significantly increased the TS, UV, and gas barrier properties of PHB. Nevertheless, the EB of PHB-based films was not significantly affected by the reinforcement of nanofillers. In addition, it was worth acknowledging that apart from influencing the physicochemical properties of the polymer, antibacterial properties can be induced in PHB-based films by loading them with nanofillers having antimicrobial properties, viz. MoS_2 (Maureira et al., 2023), chitin (Zaccone et al., 2022), and ZnO (Díez-Pascual et al., 2014).

Table 1.5. Literature summarizing the influence of nanofiller reinforcement on the properties of PHB

Polymer	Nanofiller	Loading (wt%)	Synthesis method	TS (MPa)		EB (%)		Remarks	Reference
				PHB	Composite	PHB	Composite		
PHB	MoS_2	1	Solution casting	12	23	0.37±0.03	0.34±0.03	Oxygen and water vapor barrier properties increased; Inhibition of growth of *Listeria monocytogenes*	Maureira et al., 2023
PHB	Multi-walled carbon nanotubes	0.3	Solution casting	19.06±1.32	19.3±1.62	0.77±0.19	0.23±0.12	Significant improvement of UV barrier property	Gupta et al., 2023
PHB	Graphene	0.3	Solution casting	19±1.32	22.9±1.15	0.77±0.19	0.20±0.01	Significant improvement of UV barrier property	Gupta et al., 2023
PHB	Chitin	5	Melt extrusion	24±2	33±4	1.2±0.1	1.7±0.4	Decrease of degree of crystallinity	Zaccone et al., 2022
PHB	ZnO	5	Solution casting	19	26	7.6	6.5	Improvement of oxygen and water vapor barrier properties; Inhibition of growth of *E. coli* and *S. aureus*	Diez-Pascual et al., 2014

EB: elongation at break; PHB: poly (3-hydroxybutyrate); TS: tensile strength

1.4.3. Combinational loading of essential oil and nanoparticles (NPs) in biopolymers

As discussed in detail in Sections 1.4.1 and 1.4.2, loading essential oils can increase EB and induce antimicrobial and antioxidant activities in biopolymers but at the cost of reduced TS. In contrast, nanofiller reinforcement can increase the TS and barrier properties of such biopolymers, but the influence on the EB is negligible. Several researchers advocated combinational loading of essential oils and nanofillers to exploit their synergistic effects on biopolymer properties (Mittal et al., 2023; Zabidi et al., 2022; Cui et al., 2020; Chi et al., 2019). For instance, combinational loading of NPs and essential oils, viz., clove oil/alkali-treated halloysite nanotubes (Boro et al., 2022), clove oil/graphene oxide nanosheets (Arfat et al., 2018), and cinnamaldehyde/carbon nanotubes (Cui et al., 2020), showed a positive synergistic influence on the TS, EB, optical, thermal, and barrier attributes of PLA. The literature on the combinational effect of NPs and essential oils on the properties of PHB is less known in the context of active food packaging (Mittal et al., 2023). Mittal et al. (2023) investigated the effect of loading clove oil and nano-silica in the PHB/polyethylene glycol blend for food packaging application; nonetheless, in comparison with pristine PHB, water vapor barrier property decreased by 3-fold for composite films, primarily due to poor interactions between hydrophilic and hydrophobic constituents (Mittal et al., 2023).

1.4.4. Synthesis and application of MgO NPs

NPs exhibit distinctive physicochemical properties compared to their bulk counterparts owing to their nano-size, high aspect ratio, surface defects, and quantum effects. Among them, MgO NPs are noted for their economical precursors, unique structural properties such as tunable porosity and high specific surface area, and exceptionally diverse morphology varying from spheres, rods, and flakes to stars and flowers (Podder et al., 2018; Pilarska et al., 2017). Besides, nanostructured MgO has high flame resistance and mechanical strength, high density of catalytically active sites, low susceptibility to hydration, and surface defects induced electro and photoluminescence

emissions (Karthik et al., 2019; Pilarska et al., 2017). These characteristics make it a versatile material suitable for the fabrication of advanced and innovative materials (El-Sawy et al., 2020; Jain et al., 2016). MgO NPs find application in diverse fields such as catalysis, paints, refractory products, superconductors, and optoelectronic devices like light-emitting diodes, lasers, and electrochemical sensors (Ismail et al., 2020; Aksay, 2019; Pilarska et al., 2017; Jain et al., 2016). Also, porous MgO NPs are extensively utilized in the sorption of heavy metal ions, phosphorus-containing compounds, toxic gases, chlorine, CO_2, and HCl (Aksay, 2019; Heo et al., 2017). In addition, conspicuous features of MgO NPs, such as nontoxicity, biocompatibility, and broad-spectrum antimicrobial action, are interesting for application in the food industry, biomedicine, and allied fields. Interestingly, MgO has a higher permissible intake allowance than other metal oxides, such as TiO_2 or ZnO (El-Sawy et al., 2020).

Despite the many advantages of MgO NPs, certain properties, viz. particle size, morphology, crystallinity, crystallite size, and surface area, are essential for a particular application. The literature on the synthesis and application of MgO NPs is summarized in Table 1.6. For instance, MgO use as coatings on medical implants usually requires high crystallinity for improved physiological stability. On the other hand, the use of MgO in photocatalysis and adsorption processes demands high specific surface area, low crystallinity, and high concentration of surface defects (Xiong et al., 2015; Khalid et al., 2013). Indeed, the more surface defects of MgO, the greater the potential of NPs to produce reactive oxygen species (ROS), resulting in increased antibacterial activity (El-Shaer et al., 2020; Ismail et al., 2015). Luminescence, an important characteristic of NPs for optoelectronic and light-harvesting applications, can also be tuned by controlling their surface defects. Concerning the effect of particle size and morphology, Bindhu et al. (2016) reported an increase in antibacterial activity with a decrease in particle size of MgO NPs (Bindhu et al., 2016). The morphology of NPs also influences their defect-induced properties,

such as antioxidant and pro-oxidant activity. Podder et al. (2018) reported a morphology-induced crossover between the antioxidant and pro-oxidant activity of MgO NPs (Podder et al., 2018). The optical bandgap of NPs plays a crucial role in optoelectronic device applications, and its porosity greatly influences CO_2 capture and photocatalytic activity (Aksay, 2019; Heo et al., 2017; Foletto et al., 2012). The extensive literature studies reveal that the synthesis methods and conditions adapted significantly impact the aforementioned characteristics of MgO NPs as well as their suitability for a given application. Thus, the interest in synthesizing MgO NPs with desirable properties is phenomenal. For the synthesis of MgO NPs, diverse approaches were reported in the literature. Among them, the chemical routes are simple and cost-effective, as these require low reaction temperatures and provide a high yield (Aksay, 2019; Pilarska et al., 2017; Jain et al., 2016). The synthesis routes for the production of MgO NPs include but are not limited to, precipitation (Rao et al., 2014), sonication-precipitation (Alavi et al., 2010), sol-gel (Wong et al., 2020), hydrothermal (Podder et al., 2018), solvothermal (Hadia et al., 2015), pulsed laser deposition (Ismail et al., 2019), conventional combustion (Selvam et al., 2011), and microwave methods (Selvam et al., 2011). Literature on MgO NPs synthesis is mainly focused on optimizing different experimental parameters involved (Ercan et al., 2018; Alavi et al., 2010; Esmaeili et al., 2009); however, a comparative evaluation of the effect of different synthesis routes on MgO characteristics is lacking. Screening synthesis routes to customize the MgO NPs with high surface area, and outstanding antimicrobial and antioxidant activities are required for their reinforcement in food packaging materials (Chinthala et al., 2021). To the best of our knowledge, comparative study on the synthesis of MgO NPs by five diverse synthesis routes, viz. precipitation (PT), sonication-precipitation (SPT), microwave combustion (MWC), conventional combustion (CC), and solvothermal (ST) processes as well as evaluation of their structural, optical absorption, photoluminescence, antioxidant, and antimicrobial characteristics is not reported yet in the

literature. Among the aforementioned routes, PT is a simple and cost-effective technique in which the cationic source is homogeneously dispersed in an alkaline medium and the obtained precipitate is calcined to get MgO (Rao et al., 2014). In the SPT method, sonication aids in deagglomerating NPs by generating strong turbulence and acoustic cavitation in the solution during the precipitation reaction (Majhi et al., 2010). Unlike the PT and SPT methods, in the ST process, the reaction proceeds in a solvent at a point above its normal boiling condition by containing the reaction mixture in an autoclave reactor (Hadia et al., 2015). On the other hand, combustion synthesis utilizes a self-sustained exothermic reaction between oxidizer and fuel (Selvam et al., 2011; Esmaeili et al., 2019). Moreover, microwave irradiation in MWC provides volumetric heating and rapid completion of the reaction. Whereas in the CC process, the reaction mixture is heated from the surface to the interior resulting in steep temperature gradients and slow reaction kinetics (Selvam et al., 2011).

Table 1.6. Literature on the synthesis and application of MgO NPs

Nanostructure	Synthesis route	Application	Remarks	Reference
MgO nanofibers	Co-precipitation	Solid state lightening	Strong photoluminescence emissions	Jain et al., 2016
MgO nanoflowers	Reflux method	Electrochemical sensor to detect 4-chlorophenol	Excellent electrochemical activity	Ahmed et al., 2018
MgO nanospheres, nanoplates and nanorods	Hydrothermal method, Wet chemical method	Food and medical fields	Morphology-induced crossover between antioxidant and pro-oxidant activity	Podder et al., 2019
MgO nanosheets	Sol-gel method	Antibacterial agent	More the structural defects of MgO, the greater the potential of NPs to produce reactive oxygen species (ROS), resulting in increased antibacterial activity	El shaer et al., 2020
Spherical shaped MgO	Co-precipitation method	Antibacterial agent	Increase in antibacterial activity with a decrease in particle size	Bindhu et al., 2016
MgO nanosheets	Reflux method	Photocatalytic applications	Presence of structural defects simulates photocatalytic activity	Mageshwari et al., 2013

1.4.5. Storage of fresh produce

Fresh produce, viz. fruits and vegetables, are on the list of top priority items not only for their calorific value but also for meeting the daily nutritional needs of consumers. Nevertheless, fruits and vegetables undergo several biological transformations due to certain factors, involving transpiration and respiration, even after harvesting. As a result, maintaining their quality across the supply chain is formidable (Liu et al., 2020). As per the statistical data reported by the Food and Agriculture Organization of the United Nations, 40-50 % of fruits and vegetables produced worldwide easily get contaminated and/or deteriorate before reaching consumers (Parsafar et al., 2023). Therefore, the quest for advanced methods to extend the shelf-life of vegetables and fruits became a key focus of contemporary research within the food industry. *Agaricus bisporus,* popularly called white button mushrooms, are rich in dietary fibers, proteins, polyphenols, minerals, vitamins, and amino acids and are currently the most extensively grown edible mushrooms worldwide (Liu et al., 2019). Nevertheless, the commercial potential of *A. bisporus* is limited due to its short shelf-life, i.e., 1-3 days at ambient conditions, owing to its high respiration rate and high susceptibility to microbial attack and browning (Liu et al., 2019; Gholami et al., 2017). Cherry tomatoes (*Solanum lycopersicum L. var. cerasiforme*), popularly called salad tomatoes, are well known for their intense color, flavor, and nutritional benefits, including vitamin E, flavonoids, phenolic acids, and antioxidant-rich carotenoids (Olawuyi et al., 2022; Sganzerla et al., 2021). Similar to other climacteric crops, these fruits undergo rapid deterioration under inappropriate storage conditions. Their deterioration is driven by factors such as ripening, dehydration, microbial attack, and postharvest diseases, which collectively affect their taste, texture, appearance, and aroma, ultimately influencing their economic value (Olawuyi et al., 2022; Sganzerla et al., 2021).

Recent research is focused on investigating several postharvest techniques, viz., cold storage (Dawadi et al., 2022; Buendía et al., 2019; Cantwell et al., 2009), treatment with chemical preservatives (Leng et al., 2020; Gharezi et al., 2012), edible coatings (Sganzerla et al., 2021; Thakur et al., 2021), active packaging (Buendía et al., 2019), and modified atmosphere packaging (Dawadi et al., 2022; D'Aquino et al., 2016) for shelf-life extension of mushrooms and cherry tomatoes. Nevertheless, storing fruits and vegetables at low temperatures can increase energy consumption and warehouse costs. The use of chemical preservatives is not preferable due to potential chemical residues and their adverse effects on human health. Modified-atmosphere packaging demands huge investment yet yields unstable effects. Concerns related to edible coatings include the complex application process and potential alteration of taste, visual appeal, and texture of the food products (Zeng et al., 2019). On the contrary, active food packaging using biopolymers could meet the customer's desire for minimally processed, fresh, and healthy food without potential risk to human health or the environment (Sharma et al., 2022; Kaewklin et al., 2018). A variety of active compounds, including nanomaterials (Kaewklin et al., 2018), natural plant extracts (Moeini et al., 2021), and essential oils (Mittal et al., 2023), are incorporated in various biopolymers for the development of active packaging materials (Riahi et al., 2023). In particular, active composite films of cellulose/wheat gluten (Guillaume et al., 2010), cellulose/chitosan/ dopamine-grafted carboxymethyl cellulose (Yu et al., 2022), chitosan/gallic acid (Liu et al., 2019) are investigated for extending the shelf-life of mushrooms. Whereas, the active composite films of chitosan/TiO_2 (Kaewklin et al., 2018), gelatine/CuO (Sooch et al., 2021), chitin/polyvinyl alcohol/β-cyclodextrin/cinnamaldehyde (Qian et al., 2022), and polylactide/poly(adipate-co-terephthalate)/tannic acid (Sharma et al., 2022) have been examined for the storage of cherry tomatoes. To the best of our knowledge, no study yet investigated the PHB-based active

packaging material for the storage and handling of white button mushrooms and cherry tomatoes.

1.4.6. Environmental fate of food packaging materials

As discussed in detail earlier in Section 1.1.3, the food packaging industry is one of the major producers of plastic waste. To reduce plastic pollution, researchers are extensively investigating bio-based biodegradable biopolymers, viz. PLA, starch, cellulose, PHB, and chitosan, as sustainable substitutes for conventional plastics in food packaging. After their useful life, even such biopolymer-based food packaging materials are prone to end up in diverse terrestrial and aquatic environments with varying physicochemical characteristics. In such environments, their biodegradation rate is influenced by conditions such as pH, temperature, humidity, microbial community, and diversity, alongside the characteristics of biopolymers, which include chemical structure, molecular weight, crystallinity, surface wettability, and polymer chains as well as the type and concentration of the additives incorporated (Emadian et al., 2016). For instance, Accinelli et al. (2012) reported a higher rate of degradation of starch-based bags in soil compared to seawater over the same time period (Accinelli et al., 2012). Syahirah et al. (2021) observed that the rate of biodegradation of PHBHV films in lake water and soil increased upon blending it with starch or cellulose (Syahirah et al., 2021). Rapisarda et al. (2022) reported a slight decline in the rate of biodegradation of polybutylene adipate-co-butylene terephthalate films with the incorporation of $CaCO_3$ NPs (Rapisarda et al., 2022). Therefore, assessing the biodegradation behavior of biopolymers and their composites in different environmental conditions is essential to comprehend their environmental impact for their safe disposal (Albright et al., 2021). However, studies on the biodegradability of PHB-based food packaging films are either limited or striving to establish their environmental safety.

1.5. Outcomes from the literature review

- The rising environmental concerns associated with non-biodegradable petrochemical-based food packaging underscore the critical need for sustainable alternatives. The detailed literature review revealed the continuing efforts by the researchers in developing environment-friendly food packaging materials.
- Though cellulose, starch, chitosan, PLA, PHBHV, PHBHHx, and PHB are all bio-based and biodegradable biopolymers, the characteristics of PHB, such as hydrophobicity, high crystallinity, excellent tensile strength (TS), and gas barrier properties make it a promising candidate for food packaging application. Interestingly, PHB resembles conventional plastics in physical properties and its gas barrier properties are better than commercially used bioplastic, PLA. Nevertheless, the drawbacks of PHB for industrial-level application in food packaging include high cost of production and low elongation at break (EB).
- The raw materials account for more than half of the production cost of PHB, with 70-80 % of it attributable to the carbon sources that are used as feedstock for the growth of microorganisms that produce PHB. However, recent studies reported that the production cost of PHB can be kept low by using inexpensive carbon substrates such as agro-industrial wastes, suggesting a substantial increase in the mass production and usage of PHB in the near future.
- Conventionally, plasticizers are used for improving the EB of polymeric materials; however, growing concerns about the migration of chemical plasticizers from packaging to foodstuffs and their adverse effects on human health are underscoring the necessity to explore natural alternatives for chemical plasticizers.
- Essential oils are abundantly available natural bioactive compounds that, in addition to providing antimicrobial and antioxidant properties, can improve the EB of biopolymer films but at the cost of reduction in TS. In contrast, nanofiller reinforcement can increase

the TS and barrier properties of such biopolymers. Thus, combinational loading of essential oil and nanofiller can be explored to overcome the shortcomings of PHB for food packaging applications.

- Among the wide range of available NPs, MgO NPs are particularly preferred for loading in food packaging materials as they not only improve TS and barrier properties but also offer UV screening and antimicrobial and antioxidant properties that aid in extending the shelf-life of food. They have higher permissible intake value than other metal oxides, and they possess interesting features such as non-toxicity, economical precursors, and crystallization-promoting ability.
- The process route employed for the synthesis greatly influences the morphology, structural, optical, antioxidant, and antimicrobial properties of the NPs; thus, screening synthesis routes is crucial to obtain MgO NPs with the best characteristics suitable for its use as the reinforcing agent in food packaging materials.
- Though nanotechnology is proven to be a stimulating route for developing advanced biopolymer-based packaging with nanofiller loading as low as ≤ 5 wt%, safety concerns should be addressed.
- Active packaging materials with antimicrobial and antioxidant properties can help maintain the safety and quality of fresh produce.
- The rate of bio-degradation of biopolymer-based materials is influenced by both environmental conditions and material characteristics.

1.6. Research gap and scope for further research

Despite the excellent potential, there is limited literature on the development of PHB-based active packaging materials with the combinational loading of NPs and essential oils. Moreover, the results in the available reports are not fulfilling, underscoring the need for further research. Essential oils, namely grapeseed oil (GS), bergamot oil (BG), and ginger oil (GG), demonstrated

remarkable improvement in EB, as well as antimicrobial and antioxidant properties of biopolymers such as chitosan and PLA; however, the influence of these essential oils on the properties of PHB remained unexplored. While it is well known that the synthesis methods of NPs significantly impact their characteristics, such as particle size, surface area, surface defects, morphology, crystallinity, antimicrobial and antioxidant properties, there is a lack of comparative evaluation of different synthesis routes on the characteristics of MgO NPs in the context of food packaging application. In addition, no study has yet investigated the application of PHB-based packaging for the storage of fresh produce, such as white button mushrooms and cherry tomatoes. Lastly, it is worth acknowledging that after their useful life, even biopolymer-based food packaging materials are prone to end up in diverse terrestrial and aquatic environments with varying physicochemical characteristics. Wherein, their biodegradation rate is influenced by environmental conditions as well as material characteristics. Therefore, assessing the biodegradation behavior of the developed biopolymer-based packaging materials in different environmental conditions is essential to comprehend their environmental impact for their safe disposal.

1.7. Aim and objectives

The aim of this project is to develop active and eco-friendly PHB-based films with combinational loading of essential oil and nanofiller for food packaging applications, evaluate the suitability of developed nanocomposite films for storing fresh produce, and assess their biodegradation in natural environmental conditions (Fig. 1.5). To fulfill this aim, the following objectives are framed.

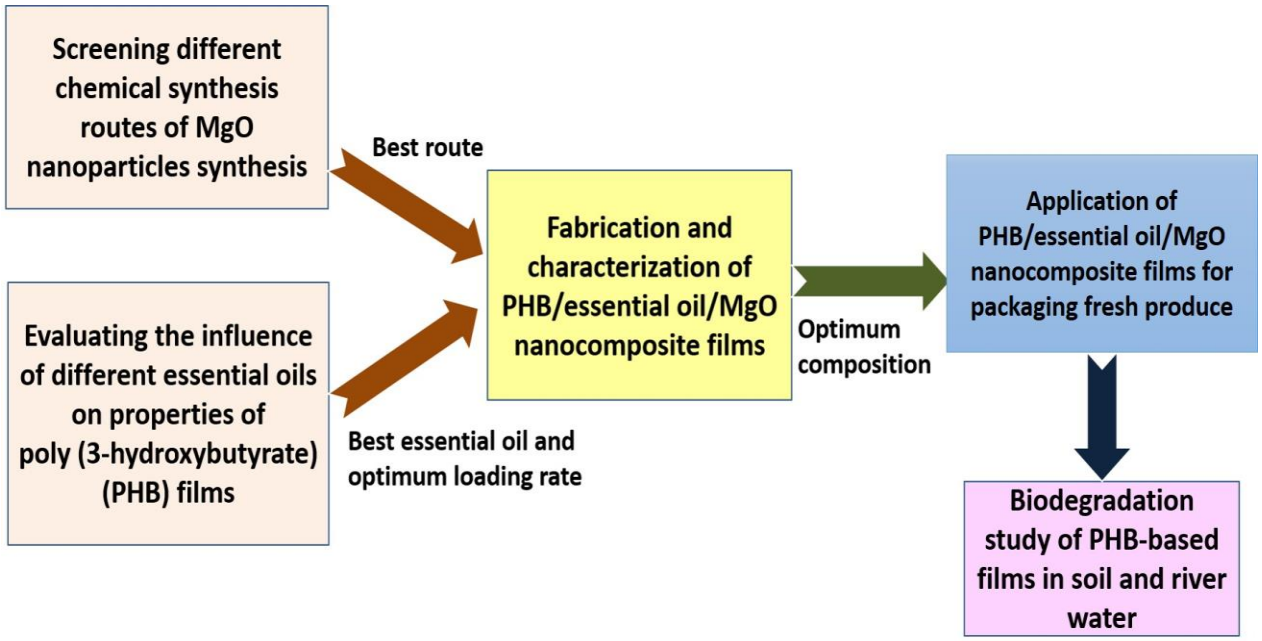

Fig. 1.5. Overall scheme and different steps involved in the present project

- **Screening different chemical synthesis routes to customize MgO NPs for reinforcement in food packaging materials**
  - Preparation of MgO NPs by precipitation (PT), sonication-precipitation (SPT), microwave combustion (MWC), conventional combustion (CC), and solvothermal methods (ST)
  - Characterization of physicochemical, morphological, optical, antimicrobial, and antioxidant properties of MgO NPs
- **Studying the influence of different essential oils on the properties of PHB-based films and subsequent finalization of the best essential oil and its optimal loading rate for further research**
  - Preparation of PHB-based films loaded with varying concentrations of essential oils, viz. grapeseed oil (GS), bergamot oil (BG), and ginger oil (GG) by solution casting route

- Characterization of PHB/essential oil composite films for the physicochemical, morphological, tensile, barrier, surface wettability, antimicrobial, and antioxidant properties
- Analysis of overall migration of components of pristine and composite films of PHB in different food simulants

❖ **Preparation of PHB-based films loaded with the essential oil (best oil at the optimum loading rate from objective 2) and MgO NPs (synthesized by the best route finalized from objective 1 at varying loading rates) and subsequent finalization of optimal composition**

- Preparation of PHB/essential oil/MgO nanocomposite films using sonication-assisted solution casting route
- Characterization of PHB/essential oil/MgO nanocomposite films for the physicochemical, morphological, tensile, barrier, surface wettability, antimicrobial, and antioxidant properties

❖ **Application of PHB/essential oil/MgO nanocomposite films of optimal composition for the storage of different fresh produce**

Part A: Shelf-life study of white button mushrooms

- Storage of mushrooms without packaging, in commercial packaging, in PHB packaging, and in PHB/essential oil/MgO nanocomposite packaging
- Analysis of quality and sensory properties of mushrooms at various stages of storage
- Measuring the leakage and transfer of MgO NPs from PHB/essential oil/MgO nanocomposite packaging to mushrooms

Part B: Shelf-life study of cherry tomatoes

- Storage of cherry tomatoes without packaging, in low-density polyethylene packaging, in PHB packaging, and in PHB/essential oil/MgO nanocomposite packaging
- Analysis of quality and sensory properties of cherry tomatoes at various stages of storage
- Measuring the leakage and transfer of MgO NPs from PHB/essential oil/MgO nanocomposite packaging to cherry tomatoes

❖ **Evaluation of biodegradation mechanism and kinetics of PHB-based films in soil and river water environments**

- Biodegradation of PHB, PHB/essential oil, and PHB/essential oil/MgO nanocomposite films in natural soil and river water environments
- Characterization of surface morphology, molecular weight, structural, chemical, and optical properties of the PHB-based films before and after degradation in soil and river water for varying durations

1.8. Organization of thesis

The present thesis work is divided into the following seven chapters

✪ **Chapter 1:** Introduction, literature review, and objectives of this project are presented in this chapter.

✪ **Chapter 2:** The focus of this chapter is screening different chemical synthesis routes to customize MgO NPs for reinforcement in food packaging materials.

✪ **Chapter 3:** This chapter details the fabrication, characterization, and optimizing composition of PHB-based films loaded with different essential oils.

- **Chapter 4:** This chapter discusses the fabrication, characterization, and optimizing composition of PHB/essential oil/MgO nanocomposite films.
- **Chapter 5:** This chapter provides a detailed assessment of the application potential of PHB/essential oil/MgO nanocomposite films of optimal composition for the storage of fresh produce.
- **Chapter 6:** This chapter elaborates on the biodegradation behavior and biodegradation mechanism of PHB-based films in natural soil and river water environments.
- **Chapter 7:** This chapter summarizes the conclusions drawn from previous chapters. Additionally, it presents recommendations for future work based on the outcomes of this thesis.

Chapter 2

Screening different chemical synthesis routes to customize MgO nanoparticles for reinforcement in food packaging materials

This chapter received the following scientific recognition

Materials Chemistry and Physics 294 (2023) 127036

Contents lists available at ScienceDirect

Materials Chemistry and Physics

journal homepage: www.elsevier.com/locate/matchemphys

Synthesis and characterization of MgO nanostructures: A comparative study on the effect of preparation route

Satti Venu Gopala Kumari [a], Kannan Pakshirajan [b], G. Pugazhenthi [a,*]

[a] Department of Chemical Engineering, Indian Institute of Technology Guwahati, Guwahati, 781039, Assam, India
[b] Department of Biosciences and Bioengineering, Indian Institute of Technology Guwahati, Guwahati, 781039, Assam, India

Kumari et al. (2023), Materials Chemistry and Physics, 294, 127036

Screening different chemical synthesis routes to customize MgO nanoparticles for reinforcement in food packaging materials

As discussed in detail in Chapter 1, the synthesis method significantly influences the morphology, structural, optical, antimicrobial, and antioxidant properties of nanoparticles (NPs). Therefore, screening various synthesis routes is crucial to obtain NPs with the optimal characteristics for their use as reinforcing agents in PHB-based films intended for food packaging applications. In this context, the current chapter elaborates on the preparation of MgO NPs by five different chemical synthesis routes, viz. precipitation (PT), sonication-precipitation (SPT), microwave combustion (MWC), conventional combustion (CC), and solvothermal (ST) processes. By analyzing the properties of the MgO NPs produced by these methods, the most effective route for the MgO NPs synthesis is identified in this chapter.

2.1. Materials and Methods

2.1.1. Materials

$Mg(NO_3)_2 \cdot 6H_2O$, NaOH, and urea were procured from Merck Specialties Pvt. Ltd., India. Acetone, methanol (99.9 %), and ethanol (99.9 %) were purchased from Finar Ltd., India. Nutrient broth was supplied by Hi-Media Laboratories Pvt. Ltd., India. 2,2-diphenyl-1-picrylhydrazyl hydrate (DPPH) was purchased from Sigma Aldrich Co. Ltd., India. All the chemicals were of analytical grade and used without further purification. Water used in all the experiments was obtained from an in-house Millipore water synthesis unit (Millipore, ELix-3, USA).

2.1.2. Synthesis of MgO NPs

In order to examine the influence of synthesis methods on the properties of MgO NPs, five simple methods were adopted in this work and their details are presented below:

2.1.2.1. Precipitation (PT) method

The synthesis conditions in this approach were adapted from the literature (Rao et al., 2013). Accordingly, 250 mL of NaOH (1 M) solution was first added dropwise into 250 mL magnesium nitrate (0.2 M) solution. After mixing the admixture for 30 min using a magnetic stirrer, the solution was filtered, and the resulting precipitate was washed multiple times with water followed by acetone to remove any remaining salts. Then, the precipitate was dried for 12 h at 100 ℃ in a hot air oven and calcined at 500 ℃ for 5 h in an air atmosphere.

2.1.2.2. Sonication-precipitation (SPT) method

In this approach, the admixture consisting of $Mg(NO_3)_2 \cdot 6H_2O$ (250 mL of 0.2 M solution) and NaOH (250 mL of 1 M solution) was prepared as described in the literature (Rao et al., 2013) and the solution was sonicated for 30 min. Subsequently, the precipitates collected after sonication were washed and calcined, following the procedure described in Section 2.1.2.1.

2.1.2.3. Microwave combustion (MWC) method

In the current approach, $Mg(NO_3)_2 \cdot 6H_2O$ (oxidizer) and urea (fuel) were subjected to microwave-induced combustion, adapting the experimental conditions from the literature (Selvam et al., 2011) with a slight modification. Accordingly, 0.85 g of $Mg(NO_3)_2 \cdot 6H_2O$ and 0.6 g of urea were separately dissolved in 10 ml of water and mixed until a clear solution was obtained. The obtained solution was then subjected to microwave irradiation in a conventional microwave oven (Samsung, model: MC28h5023AK/TL, frequency: 50 Hz) operated at 900 W for 10 min, wherein the solution initially boils, undergoes dehydration followed by decomposition and becomes solid. The resultant solid was finely ground, washed, dried, and calcined following the procedure described in Section 2.1.2.1.

2.1.2.4. Conventional combustion (CC) method

In this approach, the combustion reaction of urea (fuel) and $Mg(NO_3)_2 \cdot 6H_2O$ (oxidizer) was performed in a muffle furnace. A homogeneous solution of $Mg(NO_3)_2 \cdot 6H_2O$ and urea was prepared as described in Section 2.1.2.3. The solution was then transferred into a silica crucible and heated to 500 ℃ for 5 h in a furnace with a heating rate of 5 ℃ min^{-1} under an air atmosphere to get MgO NPs.

2.1.2.5. Solvothermal (ST) method

In this approach, the synthesis procedure and conditions as described in the literature (Hadia et al., 2015) were adopted with a slight modification. Firstly, 15 g of NaOH was dissolved in 175 mL of 50 % (v/v) ethanol/water solution, and 8.62 g of $Mg(NO_3)_2 \cdot 6H_2O$ was directly added into it and mixed for 30 min using a magnetic stirrer. The admixture was transferred into a Teflon-coated stainless steel autoclave reactor of 250 mL capacity, and the reaction was carried out for 12 h at 180 ℃. After completion of the reaction, the solution was allowed to cool to room temperature, and the precipitate formed was recovered via filtration and then washed and calcined as described in Section 2.1.2.1.

2.1.3. Antioxidant and antibacterial activities

The antioxidant activity of MgO NPs was estimated by measuring their scavenging ability against DPPH radicals (Podder et al., 2018). For this experiment, 200 µL of methanolic DPPH solution (0.1 mM) was mixed with 3 mL of MgO NPs at various concentrations (10, 50, 100, 250, and 500 µg/mL) and incubated in the dark at room temperature. After 30 min of incubation, the absorbance of the solution was measured at 517 nm using a UV-visible spectrophotometer (Perkin Elmer, Lambda 35, Switzerland), and the measured absorbance was recorded as A_s. A control experiment was carried out by dissolving 200 µL of DPPH in 3 mL of water and the absorbance measured

after incubation was recorded as A_c. Then, the DPPH radical scavenging activity was calculated using Equation (2.1) (Podder et al., 2018). All the experiments were performed in triplicate and results were expressed as mean± standard deviation.

$$\text{DPPH radical scavenging activity (\%)} = \frac{A_c - A_s}{A_c} \times 100 \qquad (2.1)$$

The antibacterial property of MgO NPs was assessed against *Staphylococcus aureus* and *Escherichia coli*. The cultures were taken in 10 mL of sterile Luria Bertani (LB) broth and added with 20 mg of MgO NPs to determine the antibacterial activity. 10% (v/v) of freshly grown respective bacterial culture was used as inoculum and the medium was incubated at 37 °C and 130 rpm in an orbital shaker. LB broth containing the bacteria but without NPs was taken as a positive control in this experiment. Following 24 h of incubation, the optical density of the culture was measured at 600 nm by UV-visible spectrophotometer (Perkin Elmer, Lambda 35, Switzerland), and percentage growth inhibition of bacteria was calculated using Equation (2.2) (Kumari et al., 2020). All the experiments were performed in triplicate and results were presented as mean± standard deviation.

$$\text{Growth Inhibition (\%)} = \frac{C_0 - C_t}{C_0} \times 100 \qquad (2.2)$$

Where C_o is the concentration of bacterial culture in control (mg/L), C_t is the concentration of bacterial culture in the test sample (mg/L) at the end of the experiment. The results obtained in this test were further analyzed statistically by carrying out one-way ANOVA followed by Tukey's Honest Significance Difference Test using Origin™ Pro 9.0 software. Tukey's test involves in pairwise comparison of means to assess if two sets of data are statistically significant.

2.1.4. Analytical Methods

The structural characteristics of both calcined and uncalcined samples synthesized through five different processes were analyzed by an X-ray powder diffractometer (Rigaku, Micromax-007HF, Japan) operated at 40 kV and 40 mA using Ni-filtered Cu Kα radiation (λ = 0.15418 nm). The analysis was done in the 2θ range of 5°- 90° with a scanning rate of 5° min^{-1}. Fourier transform infrared spectroscopy (FTIR) analysis (Shimadzu, IR Affinity-1, Japan) was performed for calcined and uncalcined samples in the wavelength range of 400 to 4000 cm^{-1} using KBr pellet route with an average of 30 scans and spectral resolution of 4 cm^{-1}. Furthermore, uncalcined samples were analyzed by Thermo Gravimetric Analyzer (Netzsch, TG 209 F1 Libra, Germany) in the temperature range of 30 °C - 700 °C with a heating rate of 5 °C min^{-1} in an air atmosphere (flow rate of 40 mL min^{-1}).

Nitrogen adsorption-desorption analysis was carried out for MgO samples at -196 °C using an automated gas sorption analyzer (Quantachrome, Autosorb-IQ-MP, USA). The samples were outgassed at 200 °C for 4 h before measurement. The pore size distribution of MgO samples synthesized via various routes was evaluated from the desorption branch of the N_2 isotherm by Barrett-Joyner-Halenda (BJH) method, and the specific surface area of the NPs was derived following Brunauer-Emmet-Teller (BET) method. Morphology of MgO samples was further analyzed by Field Emission Scanning Electron Microscope (FESEM) and Field Emission Transmission Electron Microscope (FETEM). For FESEM analysis, samples were drop cast, dried overnight, and placed on a stainless steel stub using double-sided carbon tape. The stubs were then sputtered with gold and observed under FESEM (Sigma 300, Zeiss, Germany). For observation under FETEM, the samples were drop cast on a copper grid and dried overnight. FETEM images, selected area electron diffraction (SAED) patterns, and high-resolution transmission electron

micrographs (HRTEM) were obtained using FETEM (JEOL, JEM 2100F, Japan) operated at 200 kV.

The optical properties of MgO NPs were studied by preparing samples in colloidal form using Millipore water. The absorption measurements were performed using a UV-visible spectrophotometer (Perkin Elmer, Lambda 950, USA) in the wavelength range of 190-600 nm. Millipore water without NPs was used as blank for measurement of UV-Vis absorption spectra of samples. Steady-state photoluminescence spectra (PL) were obtained using a Fluorimeter (Horiaba Scientific, FluoroMax-4, Japan) at an excitation wavelength of 385 nm.

2.2. Results and discussion

2.2.1. Thermogravimetric analysis

TGA and differential thermogravimetric analysis (DTG) of uncalcined samples obtained via various methods were performed in order to identify the calcination temperatures to get MgO NPs. The obtained results are depicted in Fig. 2.1 (a-d). The as-synthesized samples (uncalcined) through PT, SPT, and ST methods displayed a total weight loss of about 32.67 %, 32.53 %, and 32.87 %, respectively, in two stages (I, II) with a sharp endothermic peak centered at 350 °C. Whereas the sample obtained via the MWC route showed one additional stage (III) and a total weight loss of 41.7 % (see Fig. 2.1c). For all the samples, the first stage (I) of weight loss observed below 200 °C is attributed to the liberation of physically adsorbed water. The second stage (II) of weight loss observed beyond 270 °C is very close to the theoretical weight loss (30.89 %) of magnesium hydroxide decomposition and consequent formation of MgO and water as per the reaction: $Mg(OH)2 \rightarrow < MgO > + < H2O >$ (El-Shaer et al., 2020; Yousefi et al., 2017). The third additional stage (III), observed in Fig. 2.1c, is attributed to the combustion of remnants of fuel (urea) as reported in the literature (Yousefi et al., 2017; Selvam et al., 2011).

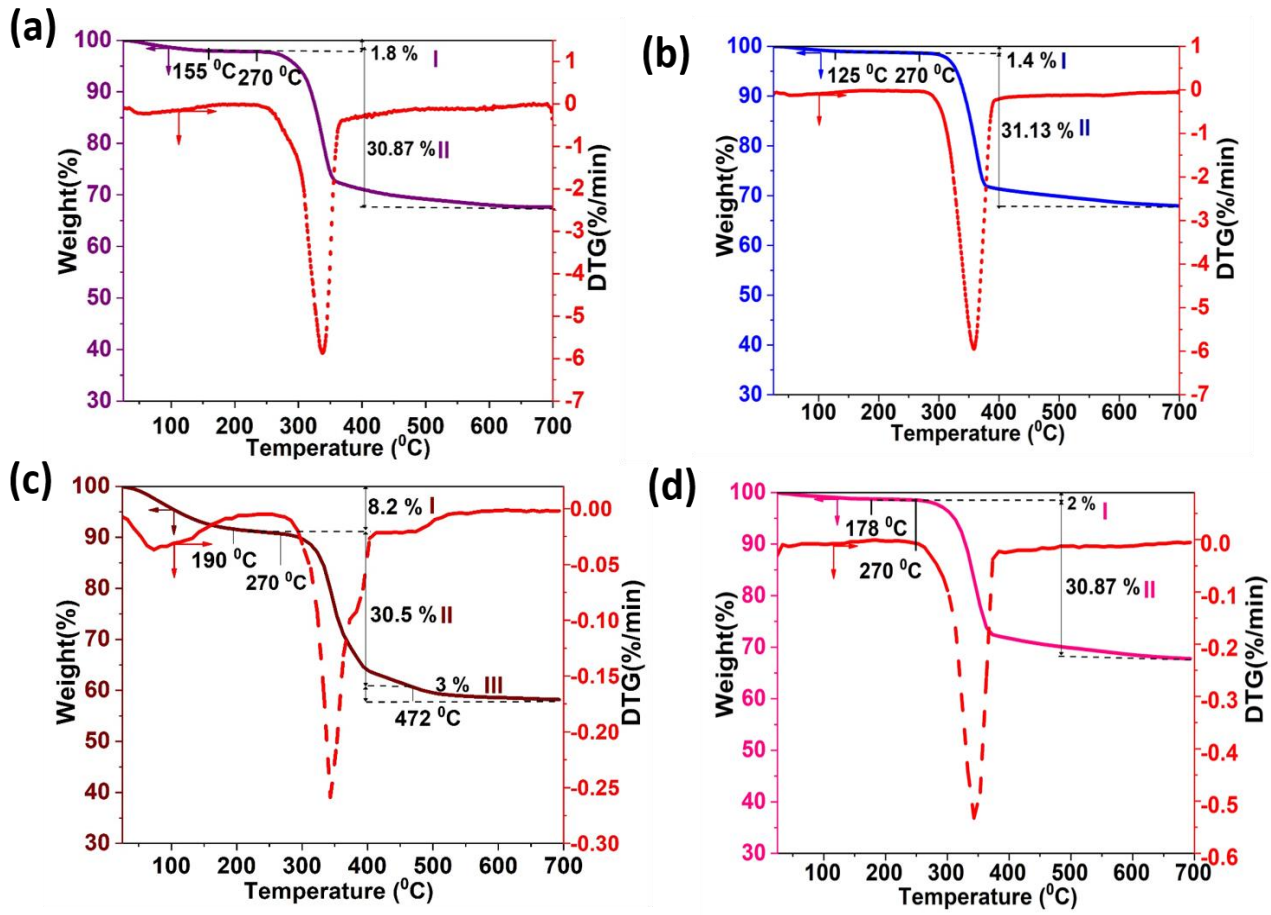

Fig. 2.1. TGA and DTG spectra of uncalcined samples synthesized via (a) PT, (b) SPT, (c) MWC, and (d) ST

2.2.2. Infrared characteristics

FTIR analysis was performed for both uncalcined and calcined samples to evaluate the changes in their chemical state during calcination. The recorded spectra, shown in Figs. 2.2a and 2.2b, are well-matched with the FTIR patterns of $Mg(OH)_2$ and MgO samples, respectively, as reported in the literature (Balakrishnan et al., 2020; Ansari et al., 2018; Hadia et al., 2015). In Fig. 2.2a, the sharp intense band detected at 3700 cm^{-1} for all the samples accounts for the –OH stretching in $Mg(OH)_2$, which is completely absent in the calcined samples (Fig. 2.2b), suggesting the complete transformation of $Mg(OH)_2$ to MgO upon calcination. Furthermore, bands observed in the 3400-

3500 cm^{-1} and 1500-1650 cm^{-1} ranges in Figs. 2.2a and 2.2b can be assigned to stretching and bending vibrations of –OH group in the surface absorbed water molecules. As evident from Fig. 2.2a and Fig. 2.2b, a decrease in the peak intensity at 3500 cm^{-1} is observed for the calcined samples when compared to the uncalcined samples, indicating a gradual reduction in the degree of binding of water molecules at the crystallite surface of samples due to transformation of $Mg(OH)_2$ to MgO (Halder and Bandyopadhyay, 2017). In Figs. 2.2a and 2.2b, two main bands can be noticed for each of $Mg(OH)_2$ and MgO samples in the range of 400-1000 cm^{-1}, in which the high-frequency bands at 878 and 850 cm^{-1} are ascribed to v_1 stretching of Mg-O, and the low-frequency stretching bands at 500 and 650 cm^{-1} are due to v_2 stretching of Mg-O (Ansari et al., 2017). Furthermore, the small peak at 2300 cm^{-1}in Fig. 2.2b and 1385 cm^{-1} in Fig. 2.2a can be assigned to the bending vibrations of surface adsorbed CO_2 (Halder and Bandyopadhyay, 2017). However, the complete transformation of $Mg(OH)_2$ to MgO is further confirmed by XRD analysis, which is discussed in the next section.

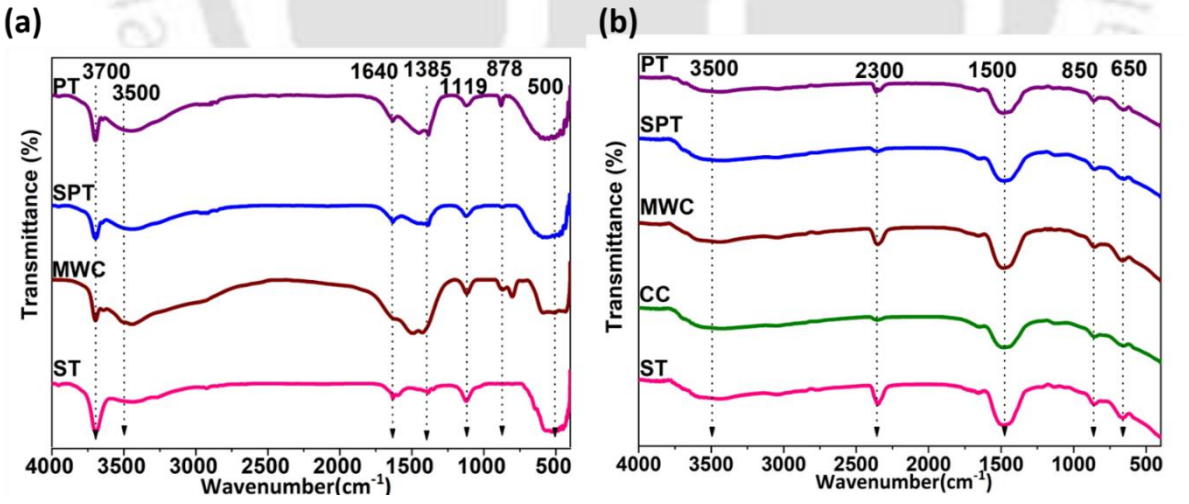

Fig. 2.2. FTIR spectra of (a) uncalcined and (b) calcined samples derived through various processes

2.2.3. Structural characteristics

XRD analysis was performed to determine the structural phases of both calcined and uncalcined samples. The XRD patterns of non-calcined samples portrayed in Fig. 2.3a aligned well with that brucite phase, hexagonal $Mg(OH)_2$ with unit cell parameters of a = 3.12 Å, b = 3.12 Å, and c = 4.75 Å, as confirmed from the standard data (JCPDS 00-001-0316). Similarly, XRD patterns of the calcined samples depicted in Fig. 2.3b, are well-matched with MgO (JCPDS 00-001-1235) of periclase phase, and cubic crystal system with a lattice parameter of a = 4.2 Å. Moreover, in Fig. 2.3b, there is no evidence of bulk remnants and no shift in peak position as compared to that of standard data (JCPDS 00-001-1235). However, there is a change in peak broadening in different samples owing to variations in the crystallite size of MgO NPs obtained via various methods. Thus, XRD patterns, together with TGA and FTIR results, confirmed the successful transformation of $Mg(OH)_2$ to MgO upon calcination.

The relative crystallinity of MgO NPs was estimated using Equation (2.3) by considering peak intensities reported for MgO in standard data (JCPDS 00-001-1235) as reference (Amani et al., 2019; Vahid and Haghighi, 2016). The intensity of peaks in Fig. 2.3b manifests that the obtained MgO NPs are in well-crystallized form, and the same can be observed from the percentage relative crystallinity reported in Table 2.1. In Fig. 2.3b, the peak corresponding to the (2 0 0) plane was most intense compared to other peaks indicating the preferential orientation of MgO NPs through the (2 0 0) plane. The d-spacing (d) corresponding to the (2 0 0) plane was calculated by Bragg's law presented in Equation (2.4). The d-spacing was obtained to be 0.21 nm for the MgO NPs synthesized through various routes, as no difference was observed in 2θ position of the (2 0 0) plane. Furthermore, the average crystallite size of MgO NPs was determined following the Debye-Scherrer method and Williamson-Hall (W-H) method with the help of Equations (2.5) and (2.6),

respectively (Sangeeta et al., 2017). Scherrer method solely assigns crystallite size to peak broadening in the diffraction pattern, whereas the W-H method supposes that peak broadening is affected by both crystallite size as well as strain in NPs. Based on the crystallite size (D) obtained in Scherrer and W-H methods, dislocation density (δ) which is the number of dislocation lines per unit volume of crystal, was calculated using Equation (2.7) (Revathi and Karthik, 2018). In general, dislocation density affects material characteristics, whereas other disruptions connect the activity of disorder (Vaizogullar, 2018).

Table 2.1. Structural characteristics of MgO NPs derived from XRD data

Synthesis Method	**$d_{(2\,0\,0)}$ (nm)**	**Scherrer method**		**Williamson-Hall method**			**Relative crystallinity (%)**
		D_s (nm)	**$\delta\times10^3$ $(nm)^{-2}$**	**D_w (nm)**	**$\delta\times10^3$ $(nm)^{-2}$**	**$\varepsilon\times10^4$**	
PT	0.21	13.35	5.61	14.49	4.77	4.42	90.70
SPT	0.21	9.00	12.34	10.44	9.17	11.12	99.06
MWC	0.21	10.43	9.19	11.26	7.88	6.25	97.06
CC	0.21	38.08	0.68	42.00	0.66	2.3	92.18
ST	0.21	10.00	10.00	13.73	5.30	1.98	97.76

$$\text{Relative crystallinity}\,(\%)=\frac{\sum\text{Peak intensities of sample}}{\sum\text{Peak intensities of reference}}\times100 \qquad (2.3)$$

$$n\lambda = 2d\sin\theta \qquad (2.4)$$

$$D_s = \frac{k\lambda}{\beta\cos\theta} \qquad (2.5)$$

$$\beta\cos\theta = \frac{k\lambda}{D_w} + 4\varepsilon\sin\theta \qquad (2.6)$$

$$\delta = \frac{1}{D^2} \qquad (2.7)$$

Where, n = 1, λ = 0.154 nm, k = 0.9. D_s and D_w are crystallite sizes calculated by the Scherrer method and W-H method, respectively, β is full width at half maximum, θ is diffraction angle, and ε is microstrain.

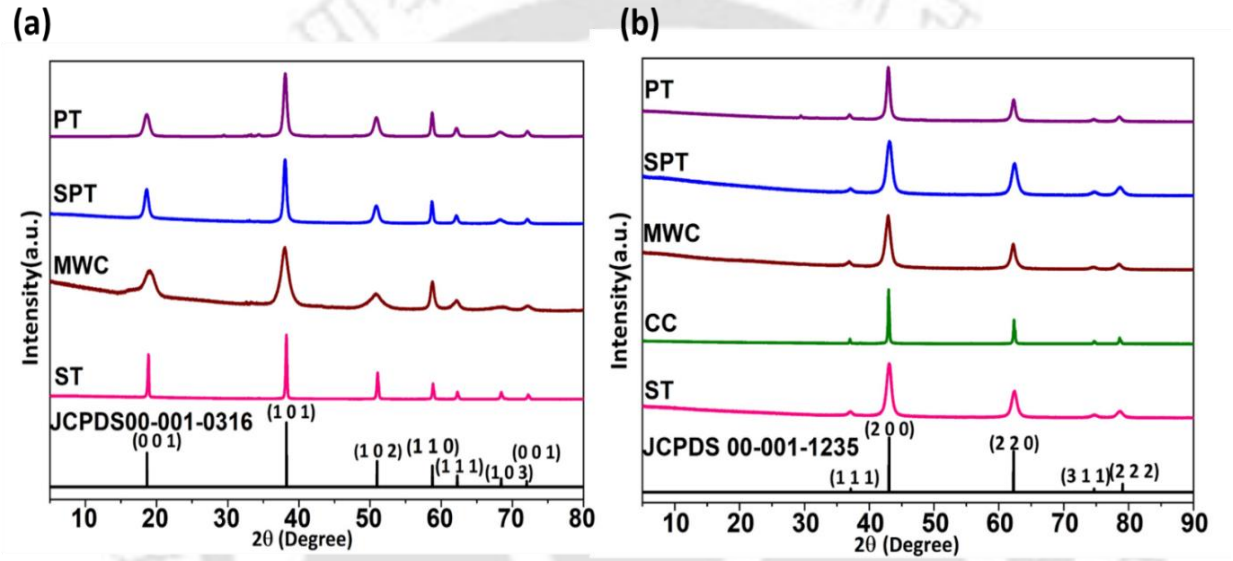

Fig. 2.3. XRD analysis of samples obtained via different synthesis routes: (a) before calcination and (b) after calcination

As reported in Table 2.1, the crystallite size of MgO NPs calculated from the Scherrer and W-H method matched well with each other. Generally, the higher the speed of nucleation and growth, the smaller will be the crystallite size (Pan et al., 2009). It can be seen from Table 2.1 that the average crystallite size of MgO NPs synthesized via SPT route is slightly smaller than the NPs obtained through PT method. This can be attributed to faster kinetics and small-scale turbulence developed during sonication that restricts the growth and agglomeration of nuclei in SPT process (Majhi et al., 2010). Likewise, though the same fuel (urea) and fuel ratio are maintained in MWC

and CC methods, a larger crystallite size was obtained in CC owing to slow reaction kinetics. As reported in Table 2.1, microstrain is found to be positive for all the MgO samples, which can be ascribed to the influence of tensile forces on crystal structures (Ercan et al., 2018). Also, high values of microstrain and dislocation density of MgO samples obtained via SPT and MWC processes suggest the existence of more lattice imperfections and structural defects in the MgO NPs (Imran and Ullar, 2018).

The specific surface area and pore characteristics of the prepared MgO NPs were evaluated using nitrogen adsorption-desorption analysis as these properties influence the performance of such NPs in many applications, such as catalysis and adsorption. The isotherm profiles and pore size distribution of MgO samples are shown in Figs. 2.4a and 2.4b, respectively, and specific surface area and pore structure data are summarized in Table 2.2. It can be seen in Fig 2.4a that all the MgO samples displayed type III isotherm with H3 type hysteresis loop as per IUPAC categorization. The H3 hysteresis is a characteristic of slit-shaped pores, with a non-uniform size and/or shape in solids consisting of aggregates (Veldurthi et al., 2012; Li et al., 2011; Selvam et al., 2011). As specific surface area varies with the size and number of particles and agglomerates, the difference in specific surface area of MgO NPs obtained via PT and SPT as well as MWC and CC is due to the decrease in particle size and reduction of agglomeration. The observed results are in good agreement with the findings in the reported literature (Alavi and Morsali, 2010; Rouhani et al., 2010).

The pore size distribution determined using the BJH method, presented in Fig. 2.4b, revealed the existence of mesopores as well as macropores for all the MgO samples. The mesopores exist among small primary nanoparticles and the macropores account for the textural pores formed due to the aggregation of small primary nanoparticles with interparticle connections. However, as

evident from Fig. 2.4b, the pore size distribution is bimodal for MgO NPs obtained via ST route and unimodal for the rest of the samples. The average pore diameter of NPs was calculated based on surface area and total pore volume using Equation (2.8). The difference in average pore diameter and total pore volume values of MgO demonstrates that the synthesis route significantly impacts the pore structure of final MgO products (Table 2.2). More importantly, the nitrogen uptake of MgO synthesized via MWC increased sharply at high relative pressure (P/P_o) compared to other samples, suggesting its highly porous nature, which is also evident from its total pore volume (0.72 cm^3 g^{-1}). Compared to other samples, the MgO sample obtained via CC exhibited very low nitrogen adsorption quantity and low total pore volume (0.05 cm^3 g^{-1}) (Ding et al., 2015).

The porous NPs with a narrow pore size distribution and high specific surface area, such as the MgO obtained through MWC in the current study, are envisaged to be useful for practical adsorption and catalysis applications (Li et al., 2012). Also, NPs with a multimodal pore size distribution, such as that MgO obtained via ST method, may find promising application in catalysis since the combination of small and large-sized mesopores could reduce transport limitation in catalysis, resulting in higher activity and controlled selectivity (Meshkani and Rezaei, 2009).

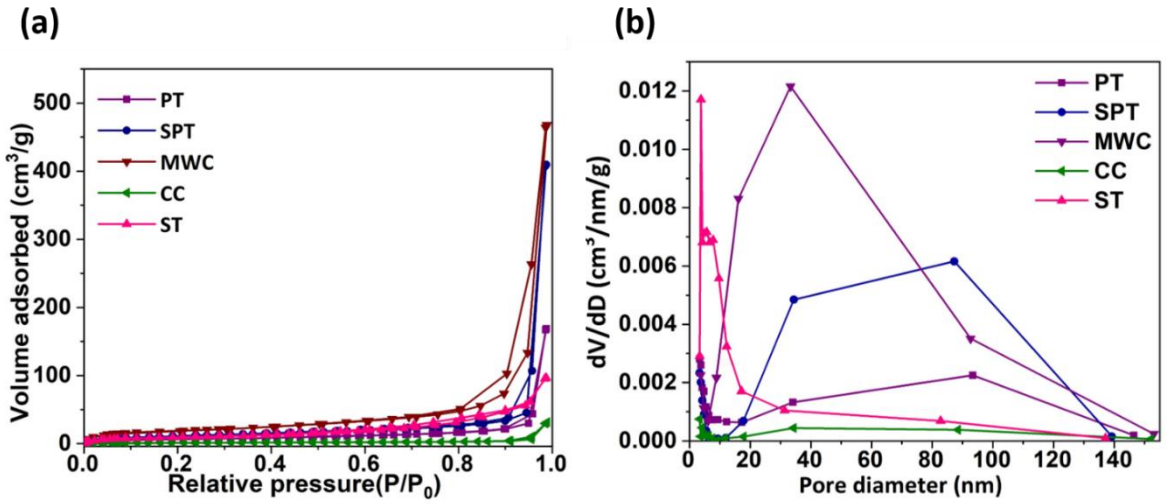

Fig. 2.4. (a) Nitrogen adsorption-desorption isotherms and (b) pore size distribution of MgO samples

$$\text{Average pore diameter} = \frac{4 \times \text{Total pore volume}}{\text{BET surface area}} \qquad (2.8)$$

Table 2.2. Structural properties of MgO NPs derived from N_2 adsorption-desorption analysis

Method	**BET surface area (m^2 g^{-1})**	**Average pore diameter (nm)**	**Total pore volume (cm^3 g^{-1})**
PT	23.14	44.94	0.26
SPT	39.70	63.47	0.63
MWC	67.32	42.78	0.72
CC	5.21	38.38	0.05
ST	35.59	16.85	0.15

2.2.4. Morphological characteristics

Morphology is a fascinating aspect of nanomaterials that plays a crucial role in antimicrobial, optoelectronic, and photocatalytic applications. The growth of materials, i.e., which facets grow and how fast they grow are governed by various factors, viz. nature of raw materials, alkalinity, the temperature of the reaction, driving force of crystallization, the energy difference between the surfaces, and the reaction kinetics (Han et al., 2020; Jamali et al., 2020). In actual, the synthesis route adopted determines the aforementioned factors, thereby affecting the morphology of the products (Han et al., 2020). Therefore, the morphology of MgO NPs obtained via different synthesis routes was confirmed by FESEM analysis. As can be seen from Fig. 2.5a and Fig. 2.5b, the MgO NPs obtained via PT, and SPT processes revealed nanoflake-like morphology with an average thickness of 11.3±2.58 nm, and 10.53± 2.79 nm, respectively. Furthermore, the high-resolution FESEM images shown in Figs. 2.5a' and 2.5b' revealed that the nanoflakes are composed of numerous nanoparticles of diameter 4-15 nm each, which is in good agreement with the crystallite size obtained by XRD analysis. Based on the XRD (Figs. 2.3a and 2.3b), FTIR (Figs. 2.2a and 2.2b), and FESEM (Figs. 2.5a' and 2.5b') analyses results, the possible growth mechanism of MgO NPs obtained via PT and SPT can be explained as follows: As shown in the Figs. 2.6a and 2.6b, firstly, numerous $Mg(OH)_2$ nanoparticles generate in solution, which after attaining the critical size during Ostwald ripening acts as building blocks for the crystallization through oriented-attachment of structurally similar surfaces at their high-energy interfaces (Ebrahimi and Yarmand, 2019). The orientation of crystallites along the crystal plane leads to the formation of nanoflake-like architectures, which transform into porous MgO nanoflakes during the calcination step. However, in the SPT method (Fig. 2.6b), sonication restricts the growth and agglomeration of nuclei during MgO synthesis.

Figs. 2.5c and 2.5c' revealed uniform nanosphere-like morphology of the MgO NPs obtained via MWC. Figs. 2.5d and 2.5d' showed that MgO NPs obtained via CC have nanoflower-like morphology that closely resembled natural marigold flowers (see inset in Fig. 2.5d'). During microwave irradiation in MWC, the fast-changing electric field may lead to the oscillation of molecules in polar media, thereby resulting in volumetric heating of the reaction mixture (Fig. 2.6c). This, in turn, led to uniform nucleation, fast reaction kinetics, explosion reaction, vigorous evolution of gases, and formation of $Mg(OH)_2$ precursor (Ercan et al., 2018; Esmaeili et al., 2009), which upon calcination transforms into fine porous MgO nanoparticles, as evident from XRD (Figs. 2.3a and 2.3b), FTIR (Figs. 2.2a and 2.2b) and BET (Fig. 2.4b) analyses. Whereas in the case of CC method, the reaction mixture is heated from the surface to the interior resulting in steep temperature gradients that spread more on the surface (Fig. 2.6d). The magnesium nitrate hexahydrate is completely combusted and transformed to MgO in the CC process, unlike in MWC which necessitates an additional calcination step. Moreover, prolonged reaction time in CC facilitated the growth of grains into the bulk phase and escape of gaseous products formed along with MgO, resulting in sheet-like structures on their surface, and thereby leading to its nanoflower morphology. The average thickness of petals (sheet-like structures) of nanoflowers obtained via CC method is 16.19 ±1.89 nm. In case of MgO NPs obtained by MWC and CC methods, the particle size observed through FESEM is consistent with that of XRD results, which revealed that the crystallite size of MgO obtained via CC method is larger than that obtained via MWC method.

Fig. 2.5e shows the nanoflower-like morphology of the MgO synthesized via ST method that closely resembled natural rose flowers (shown in the inset of Fig. 2.5e'). The high-resolution FESEM image (Fig. 2.5e') revealed that nanoflowers obtained via ST were composed of nanoflakes constructed from fine aggregated nanoparticles, similar to the results described in the

literature (Ebrahimi et al., 2019; Mollamahale et al., 2017). The average thickness of petals (nanoflakes) of nanoflowers obtained via ST method is 8.38±2.84 nm. The mechanism behind nanoflakes-assembled flower-like morphology in the MgO obtained by ST process can be deduced as follows: as shown in Fig. 2.6d, firstly, hotspots which are potential reaction points originate in solution due to heating, and these hotspots serve as driving force and generate a large number of small $Mg(OH)_2$ crystallites (Mollamahale et al., 2017). Due to the high surface energy of the initial crystallites, they aggregate to minimize their surface energy. The aggregated crystallites orient along a crystal plane which results in petal morphology. The petals then undergo random self-assembly and Ostwald ripening process giving rise to flower-like morphology. As reported in the literature (Mollamahale et al., 2017), ethanol (solvent) plays a vital role in providing a favorable environment for the nucleation and growth of nanoflowers. The high-resolution FESEM image presented in Fig. 2.5e' revealed that the nanoflakes assembled nanoflowers are primarily composed of small nanoparticles of 8-10 nm diameter, which correlates well with the crystallite size obtained by XRD analysis.

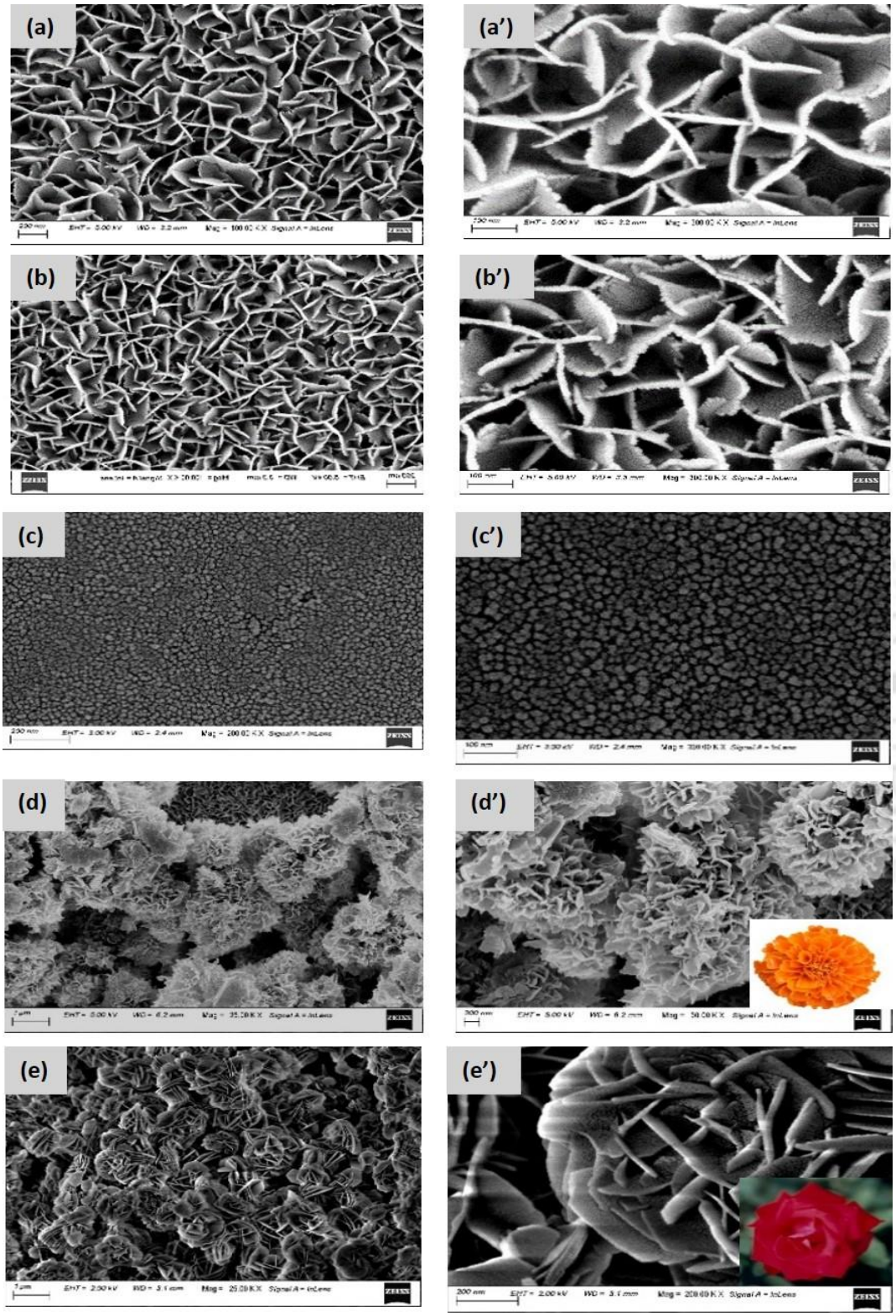

Fig. 2.5. Lower and higher magnification FESEM images of MgO NPs synthesized via PT (a, a'), SPT (b, b'), MWC (c, c'), CC (d, d'), and ST (e, e')

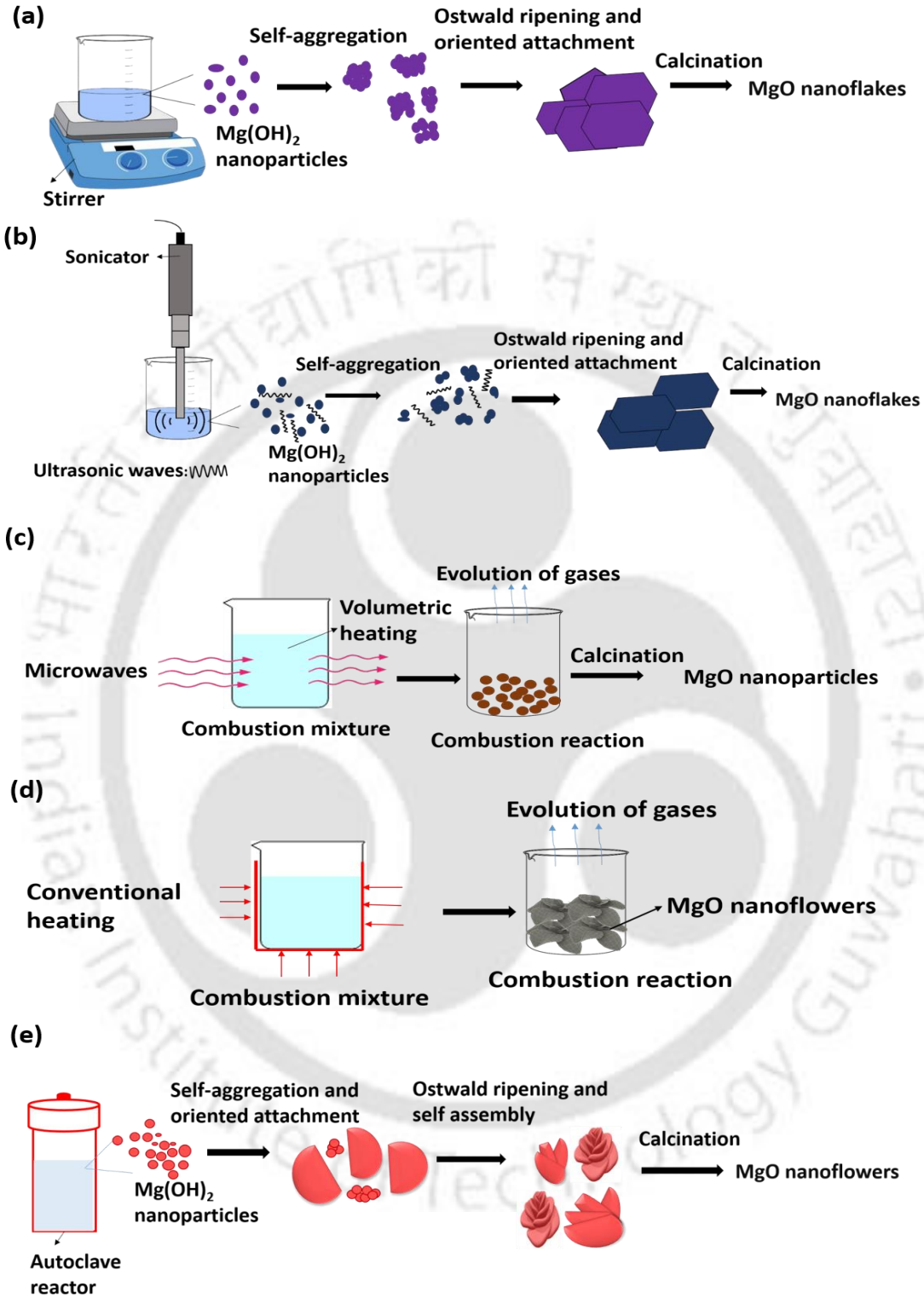

Fig. 2.6. Probable formation mechanism of MgO NPs synthesized via (a) PT, (b) SPT, (c) MWC, (d) CC, and (e) ST routes

The morphology and crystal structure of MgO NPs were further analyzed by FETEM and HRTEM. The FETEM images shown in Fig. 2.7 reconfirmed the morphology observed through FESEM analysis. The HRTEM images shown in Fig. 2.7 (a', b', c', d', and e'**)** along with Inverse Fast Fourier Transform images (presented as an inset in their corresponding images) revealed well-defined lattice fringes of d-spacing 0.21 nm corresponding to (2 0 0) plane. The obtained results are in good agreement with the XRD results, confirming the growth direction of NPs along the (2 0 0) plane for MgO NPs. Furthermore, SAED patterns shown as an inset in Fig. 2.7 (a, b, c, d, and e) can be indexed to the Face-centred cubic phase of MgO, which is also in good agreement with the XRD results. Moreover, the bright spots in the SAED pattern indicate the high crystallinity of the NPs (Ouraipryvan et al., 2009). Furthermore, the particle size distribution of MgO NPs was calculated from FETEM images depicted in Fig. 2.7 (a, b, c, d, and e). The particle sizes are in the range of 30-110 nm, 25-64 nm, 5-35 nm, 1129.68-2247.89 nm, and 661.38-1175.81 nm for MgO NPs prepared via PT, SPT, MWC, CC, and ST methods, respectively (see Fig. 2.7 (a'', b'', c'', d'', and e'')).

As 2D nanomaterials reinforced in polymers can create a tortuous path for oxygen and water vapor permeation and extend the shelf-life of food (Talukdar et al., 2021), the nanoflake-like MgO obtained via PT and SPT methods are attractive for loading in polymer matrix for food packaging applications. The nanosphere morphology with a high specific surface area yielded from MWC route is interesting for catalysis, adsorption, and antibacterial applications (Chinthala et al., 2021). The nanoflakes assembled nanoflower morphology obtained via ST route could be of great choice for water treatment (Srivastava et al., 2015) and electrochemical sensor applications (Ahmad and Mobin, 2019), as it renders high specific surface area, numerous active sites, and rapid electron and mass transport kinetics.

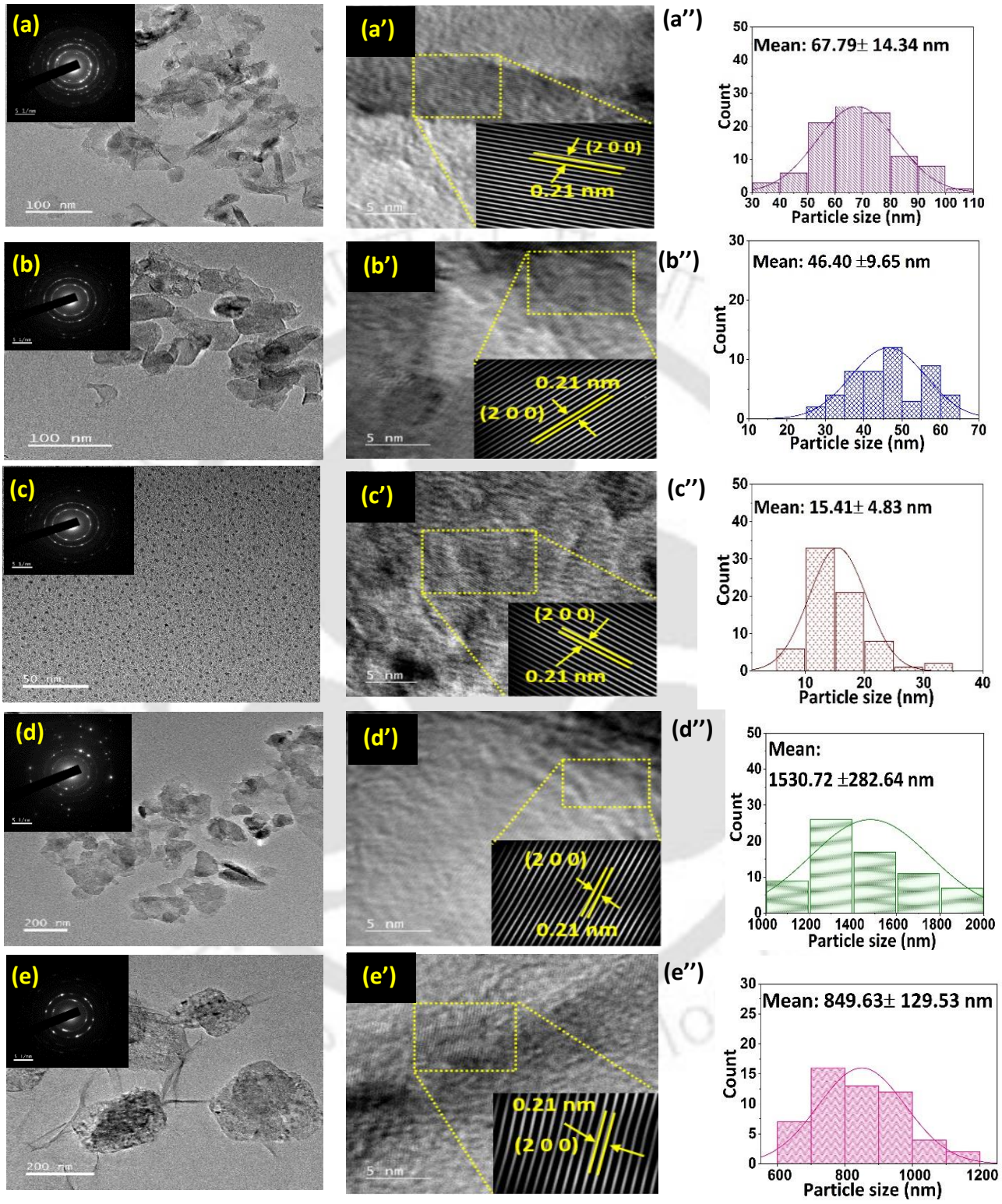

Fig. 2.7. FETEM (a, b, c, d, e), HRTEM (a', b', c', d', e'), and particle size distribution (a", b", c", d", e") of MgO NPs synthesized via PT, SP, MWC, CC, and ST methods, respectively

2.2.5. Optical characteristics

In general, optical transitions ought to occur when a photon is absorbed or emitted by the defect site. Antibacterial and antioxidant activities of metal oxides highly depend on their ability to generate reactive oxygen species (ROS). The ROS generation is influenced by the presence of structural defects such as oxygen vacancies. Therefore, the absorbance and photoluminescence (PL) characteristics were investigated to determine the presence of intrinsic point defects, particularly oxygen vacancies in synthesized MgO NPs (Verma et al., 2014). The absorption spectra of synthesized NPs depicted in Fig. 2.8a revealed that all MgO samples exhibited strong absorption in the wavelength range of 190-250 nm due to excitation of four-fold coordinated O^{2-} anions in edges and corners. From the absorption data, the optical band gap of synthesized NPs was determined using the Tauc relation given by Equation (2.9) (Pachiyappan et al., 2020).

$$(\alpha h\nu) = A(h\nu - E_g)^m \qquad (2.9)$$

Where, 'A' is a constant, α is the absorption coefficient, 'hν' is incident photon energy, E_g corresponds to bandgap energy, and m= ½ for direct transition. Fig. 2.8b shows the plot of $(\alpha h\nu)^2$ vs photon energy (hν), and the bandgap energy of NPs was calculated by extrapolating a straight line to $(\alpha h\nu)^2=0$. The estimated bandgap for MgO NPs synthesized via PT, SPT, MWC, CC, and ST are 5.96, 5.78, 5.44, 5.88, and 5.78 eV, respectively. The narrow bandgap of the MgO NPs can be attributed to the presence of oxygen vacancies developing new energy levels, resulting in a narrow bandgap as opposed to a perfect MgO surface with 6-coordinated surface anions at its surface, which has a bandgap of 7.8 eV (Verma et al., 2014). Besides that, the nanosize effect, defect density, and the short-range repulsion energy between atoms may all contribute to the narrow bandgap (Podder et al., 2018; Hadia and Mohamed, 2015). PL is an optical tool to describe surface defects (El-Shaer et al., 2020). PL emissions result from the recombination of

photogenerated charge carriers (Balakrishnan et al., 2020). The PL spectrum obtained at room temperature, which is illustrated in Fig. 2.8c displayed multiple emission peaks at 420, 444, 460, 524, and 630 nm due to defect band transition, and the observed results are in good agreement with the findings reported in the literature (El-Shaer et al., 2020; Balakrishnan et al., 2020). As MgO is a wide-gap material, surface defects resulting from the synthesis process or imperfect oxidation are considered the source of PL emission in MgO NPs. The highest PL intensity observed with MgO synthesized via MWC is likely to produce a maximum number of ROS (El-Shaer et al., 2020).

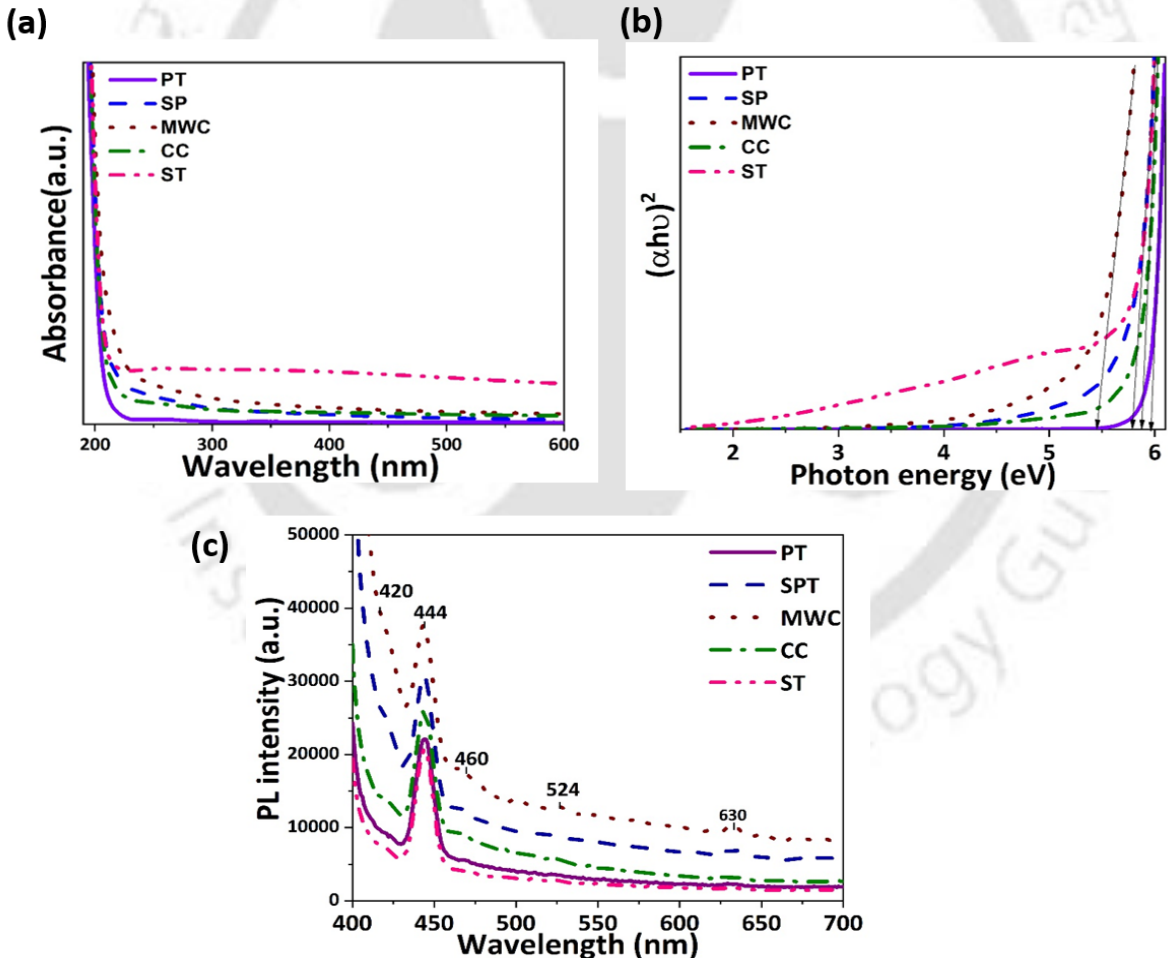

Fig. 2.8. (a) Optical absorption, (b) $(\alpha h\nu)^2$ vs $(h\nu)$, and (c) PL spectra of MgO samples obtained via different methods.

2.2.6. Antioxidant property

Lipid oxidation is a prominent cause of deterioration of a wide range of food products, next to microbial growth. To limit the extent of lipid oxidation in packaged food, packaging materials with antioxidant properties are being developed by incorporating antioxidant agents in the polymer matrix or on their surface (Gómez-Estaca et al., 2014). Therefore, to explore the antioxidant activity of the synthesized MgO NPs, its DPPH radical scavenging ability was measured at different concentrations. Fig. 2.9 shows the results along with the mechanism of antioxidant activity (Podder et al., 2018; Siripireddy et al., 2017). A monotonic increase in antioxidant activity was observed with an increase in the dosage of NPs. At 500 µg/mL concentration, MgO NPs synthesized via MWC showed 100 % scavenging of DPPH free radicals. The DPPH radical scavenging activity is probably due to the electron transfer from defect sites of MgO NPs to free radicals located at the central nitrogen atom of DPPH. Upon electron transfer, MgO becomes positively charged, whereas DPPH becomes negatively charged, leading to the formation of MgO^{+}-$DPPH^{-}$ complex. The surface area and electron transfer ability of MgO NPs are known to affect the DPPH radical scavenging activity (Podder et al., 2018; Siripireddy et al., 2017). The higher the surface area of NPs, their DPPH adsorption capacity and, therefore, DPPH radical scavenging ability are also higher. Hence, DPPH radical scavenging activity is proportional to the surface area of NPs and is highest for MgO obtained via MWC method followed by ST, SPT, PT, and CC methods, respectively. A similar observation on the antioxidant activity of MgO NPs has been reported in the literature (Podder et al., 2018).

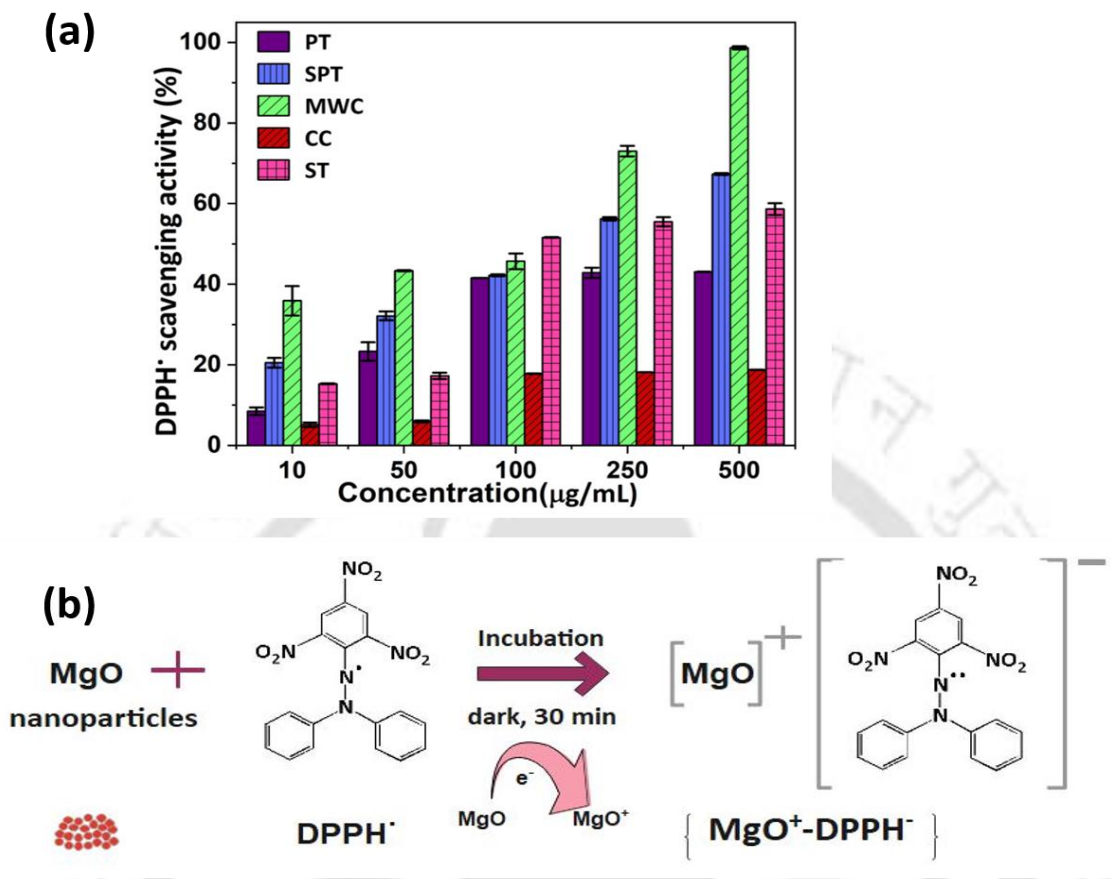

Fig. 2.9. (a) DPPH radical scavenging activity of MgO NPs at various concentrations and (b) mechanistic representation of the interaction between MgO NPs and DPPH free radical

2.2.7. Antibacterial property

Antibacterial agents are important in a variety of industries such as food, medical care, and packaging (Krishnamoorthy et al., 2012). Therefore, the development of new antibacterial agents has gained attention in parallel to combat increased outbreaks of pathogenic infections, new mutations, and multi-drug-resistant bacteria. *E. coli* belongs to the Gram-negative group of bacteria and is native to the human intestine, whereas the bacterium *S. aureus* is Gram-positive and a member of indigenous microbiota on human skin and upper respiratory tract. These bacteria

can propagate rapidly in food at room temperature (Lencova et al., 2022). Hence, the antibacterial property of the synthesized NPs was evaluated against *E. coli* and *S. aureus.*

As shown in Fig. 2.10a, maximum antibacterial activity is due to the MgO NPs obtained via MWC, followed by that due to MgO NPs synthesized via SPT, ST, PT, and CC, respectively. Moreover, *S. aureus* is more susceptible than *E. coli* to MgO NPs, which can be explained by the fact that the cell walls of Gram-positive bacteria, e.g., *S. aureus*, are devoid of outer membrane and composed of multilayers of peptidoglycan. In contrast, Gram-negative bacteria, e.g., *E. coli* are made of complex cell wall structure with a layer of peptidoglycan between the outer membrane and cytoplasmic membrane (Bindhu et al., 2016). As a result, the cell membrane of *S. aureus* can be damaged easily.

Though the antibacterial properties of MgO NPs are widely reported in the literature, the exact underlying mechanism is unclear. However, few studies (Bhattacharya et al., 2021; Rajendran et al., 2018) suggest that light radiation catalyzes redox reactions in metal oxides, generating electron and hole pairs on the conduction band (CB) and valence band (VB), respectively. The resultant electron-hole pairs could either recombine or the electrons could be readily trapped by O_2 absorbed on the MgO surface (or) dissolved O_2 to form superoxide radicals ($O_2^{\bullet-}$), while the photo-induced holes could be trapped by surface hydroxyl groups (or) H_2O on the MgO surface to form hydroxyl radicals ($OH^{\bullet}$). The superoxide radical successively ($O_2^{\bullet-}$) reacts with H^+ to produce ($HO_2^{\bullet}$) radicals, which upon subsequent collision with electrons, produce hydrogen peroxide anions (HO_2^-). These anions react with hydrogen ions to produce H_2O_2 molecules. The generated ROS (superoxide, hydrogen peroxide, and hydroxyl radical) then interact with the bacteria cells for efficient killing. As depicted in Fig. 2.10b, MgO NPs can either directly interact with bacteria leading to damage of the cell wall followed by ROS generation inside the cell, or first generate

ROS outside the cell followed by entry into the cell via damage of the cell wall. However, both mechanisms ultimately lead to cell death by disintegrating DNA, ribosomes, and proteins present inside the bacteria due to interaction with ROS. Statistical analysis of the results was carried out by one-way ANOVA using Tukey's test, which revealed a significant difference in the percentage growth inhibition of bacteria obtained in the experiments with various MgO NPs. The very high antibacterial activity of MgO NPs obtained through MWC can be attributed to its high specific surface area, small crystallite size, and ability to generate numerous ROS.

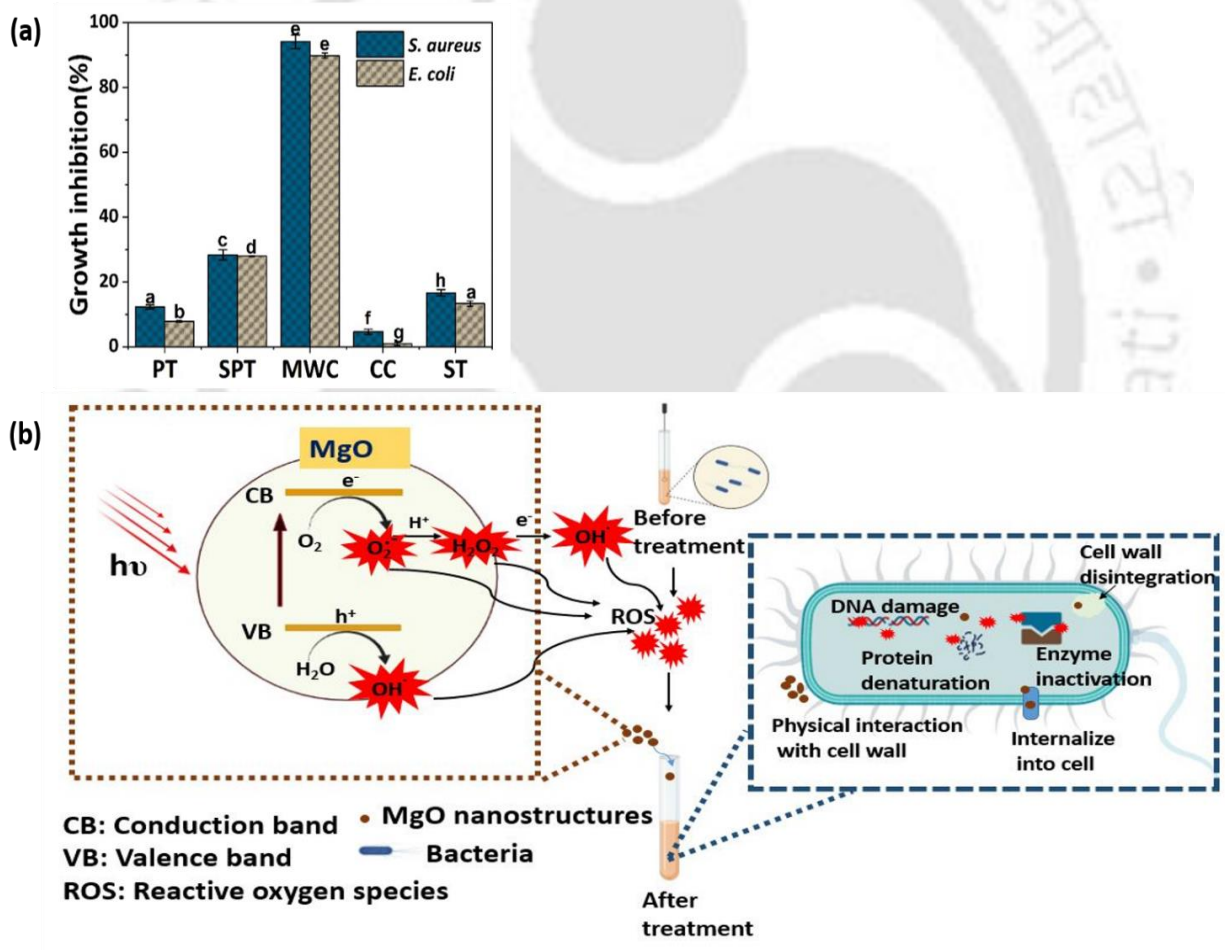

Fig. 2.10. (a) Antibacterial activity of MgO NPs against *E. coli* and *S. aureus* (bars with different alphabets indicate that difference of means is significant at 0.05 level according to one-way ANOVA followed by Tukey test), and (b) Probable mechanism of antibacterial activity of MgO NPs.

2.2.8. Comparison of characteristics of MgO nanostructures obtained via various synthesis routes

Different characteristics of MgO nanostructures obtained via various synthesis routes are presented in Table 2.3. As discussed earlier in Section 2.2.4, the diverse morphology of MgO nanostructures (nanoflakes, nanospheres, and nanoflowers) is clearly due to the difference in their formation mechanism involved in the various synthesis routes. In particular, novel rose-like morphology observed in the ST process is a result of the modification of surface energies of Mg(OH)2 crystallites during their nucleation and growth by the solvent (ethanol) (Mollamahale et al., 2017). Though the same precursors were used in the PT and SPT methods, MgO nanoflakes obtained by the SPT process revealed small crystallite, particle size, and high specific surface area compared to nanostructures obtained via PT. This can be attributed to small-scale turbulence developed during sonication that restricts the growth and agglomeration of nuclei in the SPT process (Majhi et al., 2010). Among the five routes employed for the synthesis of MgO nanostructures, CC yielded the largest crystallite size as well as particle size and the least specific surface area due to slow reaction kinetics and steep temperature gradient in the combustion reaction by conventional heating (Selvam et al., 2011). On the other hand, MgO obtained via the MWC route had the smallest crystallite size as well as particle size, and the highest specific surface area and total pore volume compared to MgO obtained via all other methods. This is due to the volumetric heating of the reaction mixture and rapid completion of the reaction offered by microwave irradiation. Besides, small particle size and high density of surface defects resulting from the synthesis route contributed to high PL emissions, narrower band gap, and excellent antimicrobial and antioxidant characteristics of the MgO obtained by the MWC route.

Table 2.3. Comparison of characteristics of MgO nanostructures obtained via various synthesis routes

Property	**PT**	**SPT**	**MWC**	**CC**	**ST**
Crystallite size calculated by Scherrer method, D_s (nm)	13.35	9.00	10.43	38.08	10.00
Relative crystallinity (%)	90.70	99.06	97.06	92.18	97.76
BET surface area (m^2 g^{-1})	23.14	39.70	67.32	5.21	35.59
Total pore volume (cm^3 g^{-1})	0.26	0.63	0.72	0.05	0.15
Morphology	nanoflakes	nanoflakes	nanospheres	nanoflowers resembling natural marigold	nanoflowers resembling natural rose
Diameter of particles calculated from FETEM images (nm)	30-110	25-64	5-35	1129.68-2247.89	661.38-1175.81
Band gap energy (eV)	5.96	5.78	5.44	5.88	5.78
$DPPH^{\cdot}$ scavenging activity (%) at 500 µg/mL concentration	43.09± 0.03	67.35±0.23	100	18.73±0.06	58.63±1.48
Growth inhibition (%) of *E. coli*	7.82±0.2	27.97±0.07	89.86±0.78	0.96±0.56	13.36±0.75
Growth inhibition (%) of *S. aureus*	12.31±0.61	28.40±1.53	94.14±2.12	4.65±0.75	16.66±1.04

CC: conventional combustion; MWC: microwave combustion; PT: precipitation; SPT: sonication-precipitation; ST: solvothermal

2.3. Summary

MgO nanostructures were successfully prepared via five different chemical synthesis routes, namely PT, SPT, MWC, CC, and ST. Structural characterization by XRD, BET, FESEM, and

FETEM analyses revealed that all the obtained nanostructures are in the cubic phase. The synthesis route has influenced crystallite size, morphology, porosity, particle size, and surface area of the obtained nanostructures. MgO nanostructures obtained via PT and SPT routes revealed nanoflakes-like morphology, whereas nanosphere-like structures were obtained via the MWC process. Nanoflowers resembling natural marigold and rose flowers are obtained through CC, and ST methods, respectively. The application of microwave irradiation (MWC) and sonication (ST) resulted in reduced particle size and increased specific surface area of MgO nanostructures compared to nanostructures obtained via CC, and PT methods. The optical characterization confirmed emission peaks that emphasize the existence of defects at surface sites. The MgO NPs obtained via the microwave combustion route have a high specific surface area, smaller particle size, narrow band gap, and outstanding antimicrobial and antioxidant activities compared to MgO NPs obtained via other routes. Thus, this chapter concluded that the MgO NPs obtained via the microwave combustion route could serve as the best reinforcing agent for food packaging materials.

Chapter 3

Preparation, characterization, and optimizing composition of the novel active poly (3-hydroxybutyrate)/essential oil composite films

This chapter received the following scientific recognition

Kumari et al. (2022), International Journal of Biological Macromolecules, 252, 126566

Preparation, characterization, and optimizing composition of the novel active poly (3-hydroxybutyrate)/essential oil composite films

The aim of this thesis work is to overcome the limitations of poly (3-hydroxybutyrate) (PHB) for food packaging applications through the combinational loading of essential oil and NPs. In Chapter 2, the optimal synthesis route for MgO NPs was identified to tailor their properties for incorporation into PHB-based films. The objective of the current chapter is to determine the best essential oil and its optimum concentration for loading in PHB to improve its elongation at break (EB). Thus, this chapter reports on the fabrication and characterization of PHB-based films with varying concentrations (1-10 wt%) of essential oils, namely grapeseed oil (GS), bergamot oil (BG), and ginger oil (GG).

3.1. Materials and methods

3.1.1. Materials

Chemical grade poly (3-hydroxybutyrate) powder (M_w=540 kg/mol) and 2,2-diphenyl-1-picrylhydrazyl hydrate (DPPH) were procured from Sigma Aldrich Co. Ltd., India. Methanol and ethanol were purchased from Finar Ltd., India. Acetic acid, sodium chloride, and activated carbon were procured from Merck Specialties Pvt. Ltd., India. Iron powder was purchased from Kalyan Industries, India. Grapeseed oil, ginger oil, and bergamot oil were purchased from All Naturals Ltd., India. Chloroform and Luria Bertani (LB) broth were purchased from Hi-Media Laboratories Pvt. Ltd., India. All the chemicals were used as received.

3.1.2. Fabrication of PHB/essential oil composite films

PHB/essential oil composite films with varying concentrations (1, 3, 5, 7, and 10 % w/w) of essential oils, namely, grapeseed oil (GS), bergamot oil (BG), and ginger oil (GG), were fabricated using the simple solution casting technique as follows: Firstly, PHB (1 g) was dissolved in

chloroform (20 mL) by continuous mixing for 2 h at 60 ℃ under reflux condition (Kumari et al., 2020). A known amount of essential oil was added to the PHB chloroform solution, and the admixture was stirred at 300 rpm for 2 h at room temperature. Subsequently, the solution was cast in glass Petri dishes and left undisturbed for solvent evaporation. The prepared PHB/essential oil composites were labeled as PHB/nX, where, X is the name of essential oil (GS, BG, and GG) and n is the wt% of essential oil with respect to the weight of polymer. PHB film without any added essential oil was employed as a control in this study and is referred to as pristine PHB.

3.1.3. Characterization

3.1.3.1. Tensile characteristics

Tensile test of pristine and composite films of PHB was performed using Electromechanical Universal Testing Machine (Zwick Roell, Z005TN, USA) following the ASTM D882-12 standard method. The dimensions of the test sample are 80 mm length, 50 mm gauge length, and 5 mm width. The thickness of the films was measured using a digital micrometer (Insize, 3109-25 S, India), and the crosshead speed for the test was maintained at 5 mm min-1. Tensile strength (TS) and elongation at break (EB) of samples were calculated from the stress-strain curve using Equations (3.1) and (3.2), respectively (Mohan et al., 2018). For each composition, five samples were tested, and the results were expressed as the mean ± standard deviation.

$$TS\,(MPa) = \frac{Maximum\ force\ to\ break\ the\ film(N)}{Initial\ cross\ sectional\ area\ of\ the\ film(m^2)} \tag{3.1}$$

$$EB(\%) = \frac{Elongation\ of\ film\ at\ the\ time\ of\ rupture\,(mm)}{Gauge\ length\ of\ film\,(mm)} \times 100 \tag{3.2}$$

3.1.3.2. Physicochemical characteristics

Fourier transform infrared (FTIR) (Shimadzu, IR Affinity-1, Japan) analysis was carried out to determine the functional groups present in the essential oils (GS, BG, and GG), pristine, and composite films of PHB. The FTIR spectra were recorded in a wavenumber range of 400 to 4000 cm^{-1} with an average of 30 scans in attenuated total reflection (ATR) mode. Furthermore, volatile constituents in essential oils (GS, BG, and GG) were identified using a gas chromatograph (Agilent Technologies, Intuvo GC, USA) equipped with a mass detector (5977B MSD) and DB-5MS column. Helium (1 mL/min) is used as the carrier gas, and 1 µL of sample is injected for analysis. Individual components in essential oils were identified based on their retention time, relative peak area, and mass fragmentation pattern using Wiley and NIST spectral libraries.

X-ray diffraction (XRD) analysis was performed for the characterization of pristine and composite films of PHB using an advanced X-ray diffractometer (Rigaku, Micromax-007HF, Japan) operated at 40 mA and 40 kV using Ni-filtered Cu-Kα radiation (λ= 0.15418 nm). The XRD spectra were obtained in the 2θ range of 5°-60° with 5° min^{-1} scan speed. The morphology of the film samples was analyzed using a Field Emission Scanning Electron Microscope (FESEM). For observation under FESEM (Sigma 300, Zeiss, Germany), films were mounted on stainless steel stubs using double-sided carbon tape and sputtered with gold. Furthermore, topographical images of pristine and composite films of PHB were obtained using an Atomic Force Microscope (AFM) (Oxford, Cypher, United Kingdom) in tapping mode with a scan angle perpendicular to the specimen surface. The obtained AFM images were analyzed using Gwyddion software version 2.60.

3.1.3.3. Optical characteristics

Transmission spectra of pristine and composite films of PHB were measured using a UV-visible spectrophotometer (Shimadzu, UV-2600, Singapore). The spectra were recorded in the

wavelength range of 200-700 nm with a 2 nm bandwidth, 50 nm min^{-1} scan rate, and $BaSO_4$ coated plate as a reference. The opacity of the films in the visible region was calculated using Equation (3.3) (Ahmed et al., 2016).

$$Opacity\ value = \frac{-\log(T_{600})}{x} \qquad (3.3)$$

Where T_{600} is fractional transmittance at 600 nm, and x is the average thickness of the film (mm). Three films were analyzed for each composition, and average values were reported.

Color properties such as L* (darkness/brightness), a* (redness/greenness), and b* (yellowness/blueness) of the pristine and composite films of PHB were obtained using a color spectrophotometer (Sensegood, India). Five samples were tested for each composition, and average values were reported. The total color difference (ΔE) between pristine and composite films of PHB was calculated using Equation (3.4) (Ahmed et al., 2016).

$$\Delta E = \sqrt{\Delta L^{*2} + \Delta a^{*2} + \Delta b^{*2}} \qquad (3.4)$$

ΔL^*, Δa*, and Δb* represent the variation between the respective colorimetric coordinates of the composite films and those of pristine PHB.

3.1.3.4. Thermal characteristics

The thermal behavior of the essential oils used in this study was analyzed using Thermogravimetric Analyzer (Netzsch, TG 209 F1 Libra, Germany) in an argon atmosphere (flow rate of 40 mL min^{-1}) at a heating rate of 10 °C/min in the temperature range of 25-600 °C. Thermogravimetric analysis (TGA) of pristine and composite films of PHB was performed using Thermogravimetric analyzer (Netzsch, STA449F3A00, Germany) in an argon atmosphere (flow rate of 60 mL min^{-1}). For TGA of films, approximately 5-8 mg of samples were placed in an alumina thermal pan of 80 µL capacity and heated in the temperature range of 25-500 °C at a

heating rate of 10 ℃/min. Differential scanning calorimetry (DSC) measurements were carried out on pristine and composite films of PHB using DSC1, Mettler Toledo, Switzerland, in the temperature range of 30-200 ℃ at a heating rate of 10 ℃/min in nitrogen atmosphere (flow rate of 40 mL min^{-1}).

3.1.3.5. Contact angle and gas barrier properties

Contact angle analysis was performed using a goniometer (Holmarc Opto-Mechatronics, HO-IAD-CAM-01B, India) and its associated software. Water droplet size (4 µL) and time (40 s) for capturing an image after releasing a water droplet on the sample (2 cm ×2 cm) were maintained constant for all the films. Three samples were tested for each composition, and average contact angle values along with the standard deviation were reported.

Water vapor transmission rate (WVTR) measurements were carried out using Permatran-W, 1/50 G, Mocon equipment (Mocon Inc., USA) following the ASTM E398 standard. Analysis was carried out on circular films of 50 cm2 at a temperature of 37.8 ℃ and atmospheric pressure. Relative humidity in the wet and dry chambers was set to 100 and 5 %, respectively. The water vapor permeability of samples was calculated using Equation (3.5) (Dhar et al., 2015).

$$Water\ vapour\ permeability = \frac{WVTR}{\triangle P} \times x \qquad (3.5)$$

Where WVTR is the water vapor transmission rate (g. m^{-2}. d^{-1}), ΔP is the difference in partial pressure across the film in the test chamber (atm), and x is the average thickness of the film (mm). The oxygen permeability values of various PHB-based films were assessed by the deoxidizer absorption method as described in the literature (Geng et al., 2023; Mao et al., 2023), with slight modifications. Firstly, 3 g of deoxidizer (a mixture of activated carbon, sodium chloride, and iron powder in 3: 2: 1 weight ratio) was filled in glass cups with an internal diameter of 50 mm. Subsequently, the individual glass cups were sealed using the test films and positioned inside a

desiccator at room temperature and atmospheric pressure, maintained at 75 % relative humidity. The change in weight of the test cups was measured every 24 h for 3 days, and the oxygen permeability values (g. m. s^{-1}) of the films were estimated by Equation (3.6). Three samples were tested for each composition and average results were reported.

$$Oxygen\ permeability = \frac{\Delta m}{t} \times \frac{x}{A_e} \qquad (3.6)$$

Wherein, Δm is the change in mass (g), t is equilibrium time (s), A is the effective surface area of the film (m^2), and x is film thickness (mm).

3.1.3.6. Antimicrobial and antioxidant activities

Staphylococcus aureus, *Listeria monocytogenes*, *Clostridia spp.*, *Escherichia coli*, and *Campylobacter jejuni* are common bacteria associated with foodborne illness (Pandey et al., 2022). Therefore, the antibacterial activity of pristine and composite films of PHB was assessed against *Escherichia coli* (Gram-negative) and *Staphylococcus aureus* (Gram-positive) bacteria. For this test, films (1 cm × 1 cm each) were taken in 10 mL of sterile LB broth and inoculated with 10 % (v/v) of the freshly grown respective bacterial culture. Thereafter, the medium was incubated at 37 °C for 24 h in an orbital shaker. Following the incubation period, the optical density of the bacterial culture in the medium was measured at 600 nm using a UV-visible spectrophotometer (Shimadzu, UV-2600, Singapore). LB broth inoculated with the respective bacterial culture but without the test samples were employed as a positive control for the test. The percentage growth inhibition of bacteria was calculated by Equation (3.7) (Kumari et al., 2020).

$$Growth\ inhibition\ (\%) = \frac{C_o - C_t}{C_o} \times 100 \qquad (3.7)$$

Where, C_o and C_t are the concentration (mg/L) of bacterial culture in the control and test solution, respectively.

DPPH radical scavenging activity was measured to assess the antioxidant activity of pristine and composite films of PHB. For this assay, films (1 cm ×1 cm each) were incubated in 10 mL of methanolic DPPH solution (0.1 mM) for 30 min in the dark at room temperature. Following the incubation period, the absorbance of the solution was measured at 517 nm using UV-visible spectrophotometer (Shimadzu, UV-2600, Singapore). Methanolic DPPH solution without the test samples was used as a control. DPPH radical scavenging activity of samples was calculated using Equation (3.8) (Garrido-Miranda et al., 2018).

$$\text{DPPH radical scavenging activity (\%)} = \frac{A_c - A_s}{A_c} \times 100 \qquad (3.8)$$

Where, A_c and A_s are the absorbance of control and test samples, respectively. The antioxidant and antimicrobial tests were performed in triplicate, and results were expressed as mean ± standard deviation.

3.1.3.7. Overall migration test

The overall migration of components of pristine and composite films of PHB into different food simulants was analyzed as per the method prescribed by Commission Regulation (EU) 2016/1416. Three food simulants, viz., distilled water, 3 % (v/v) acetic acid, and 50 % (v/v) ethanol, representing hydrophilic, acidic, and lipophilic foodstuffs, respectively, were selected based on recommendations by European food packaging regulations (European Commission, 2007). The test films (5 cm × 5 cm each) were exposed to 50 mL of food simulants and maintained at 40 ℃ for 10 days. After the exposure period, the simulant was evaporated at 105 ℃ until a constant weight was reached. Blank experiments were conducted for each simulant in the similar manner but without film samples. Thus, the overall migration of each film was expressed in milligrams per square decimetre of the surface area of the sample (Bhat et al., 2022; Requena et al., 2017).

3.1.3.8. Statistical analysis

Statistical analysis in the form of variance (ANOVA) was performed on the results of tensile, optical, oxygen transmission, and contact angle measurements, as well as antimicrobial, antioxidant, and migration experiments using Origin™ Pro 9.0 software. Furthermore, Tukey's test was employed to determine the differences at a significance level of 0.05. Moreover, the outcomes of the statistical analysis were appropriately indicated in the respective graphs and tables by asterisk/alphabet labels.

3.2. Results and discussion

3.2.1. Tensile characteristics

Tensile properties of composite films are affected by a wide array of factors, including method of preparation, nature of constituents, and their relative proportions (Atarés and Chiralt, 2016). Therefore, TS and EB of the pristine and composite films of PHB, which are crucial characteristics for their application in the food packaging field, are presented in Fig. 3.1a. Herein, TS indicates the maximum applied stress that a film can withstand while being stretched, EB is linked to the stretchability of films prior to breakage (Akhter et al., 2019). Pristine PHB film exhibited TS and EB values of 20.48±0.51 MPa and 0.51±0.04 %, respectively. A significant ($P<0.05$) reduction in TS of the composite films as compared to pristine PHB was observed at higher loadings of essential oils (GS, BG, and GG). The primary factor that could account for the TS reduction in the PHB/essential oil composites is the partial replacement of stronger polymer-polymer interactions with weaker polymer-oil interactions (Atarés and Chiralt, 2016). Interestingly, the highest EB for various composite films was achieved at 5 wt% loading of the respective essential oils (GS, BG, and GG). In particular, a 30-fold increment in EB compared to pristine PHB was demonstrated by PHB/5GS films. As shown in Fig. 3.1b, essential oils are expected to embed in free volume between adjacent polymer chains owing to their remarkably lower molecular weight compared

with macromolecules such as PHB, thus weakening the intermolecular interactions that provide strength and rigidity to the material (Pola et al., 2016). Moreover, as reported in the literature (Qin et al., 2017; Pola et al., 2016), the incorporation of essential oils increases free volume and polymer chain mobility in composite films. Nevertheless, the difference in tensile characteristics of various PHB/essential oil composites is due to the differences in the specific interactions between the polymer matrix and the oil components (Atarés and Chiralt, 2016). The best EB for composite films was observed at 5 wt% loading of the respective essential oils. A significant reduction in EB is observed for > 5 wt% loading of GS, GG, and >7 wt% loading of BG in PHB, which could be due to the saturation of essential oil content at higher loadings. Therefore, in the current study, all other characteristics of PHB composite films in the context of food packaging were evaluated at 5 wt% loading of the respective essential oils. Similar observations corresponding to an increase in EB and a decrease in TS of biopolymers with the addition of essential oils are reported in the literature (Rech et al., 2021; Qin et al., 2017; Ahmed et al., 2016). Although the TS of PHB/5GS (15.83±0.89 MPa), PHB/5BG (12.56±0.89 MPa), and PHB/5GG (10.84±0.09 MPa) were lower compared to pristine PHB (20.48±0.51 MPa), they find application in packaging food products like fruitcakes, buns, sandwich, and bread that do not require high TS (Mittal et al., 2023). Additionally, techniques such as the incorporation of nanofillers could be investigated to improve the TS of PHB/essential oil composites and broaden their application for packaging other foodstuffs (Boro et al., 2022; Arfat et al., 2018).

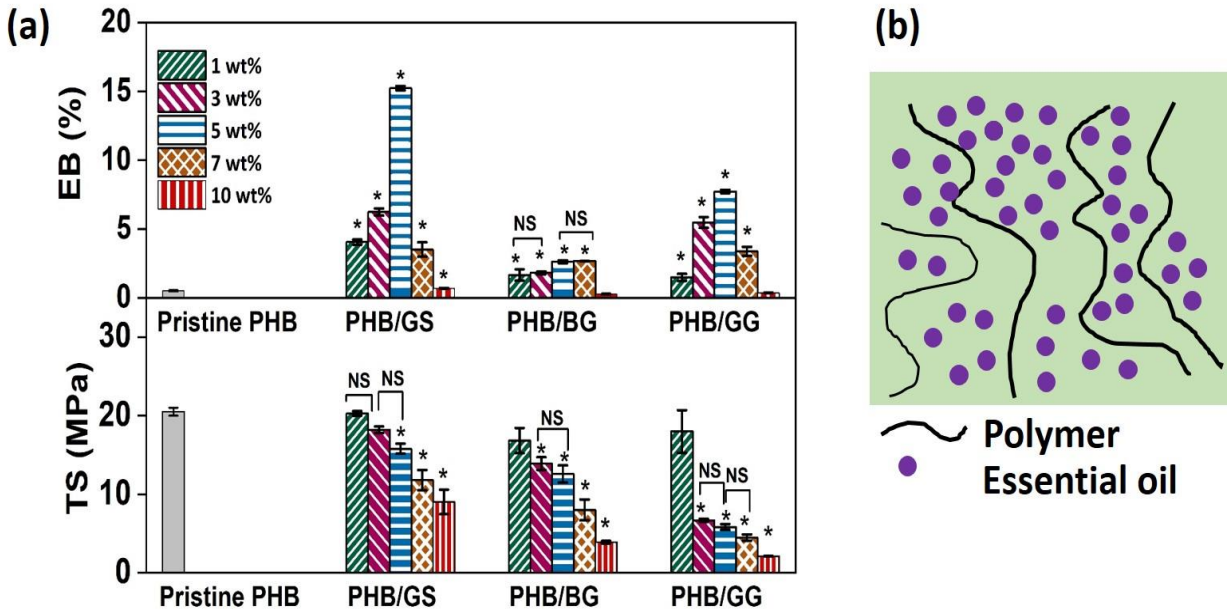

Fig. 3.1. (a) Tensile characteristics of pristine and composite films of PHB (*P <0.05: significantly different compared to control (pristine PHB); NS: not significantly different with each other) and (b) Plasticization mechanism of essential oils

3.2.2. GC-MS and FTIR analyses

Volatile constituents present in essential oils (GS, BG, and GG) were identified by GC-MS analysis and summarized in Table 3.1. The quantitative analysis revealed the prevalence of decadienal (30.18 %), ethyl hexanoate (12.50 %), nona-2, 3, -dienoic acid, ethyl ester (8.18 %), acetic acid (5.20 %) and methyl butanol (5.80 %) in GS. Limonene (39.27 %), linalool (19.44 %), branched heptadecane (7.14 %), linalyl acetate (6.13 %), and γ-terpinene (5.54 %) are major constituents of BG. Whereas, Zingiberene (20.81 %), α-curcumene (9.73 %), β-sesquiphellandrene (9.08 %), α-farnesene (8.02 %), and β-bisabolene (7.23 %) are the major constituents of GG. The aforementioned compositions of the different essential oils are in good agreement with the literature reports (Chaiwarit et al., 2018; Munda et al., 2018; Bail et al., 2008). The FTIR spectra of GS, BG, and GG are presented in Fig. 3.2a, wherein GS showed transmittance peaks at 3013, 2928, 1743, 1159, and 719 cm^{-1} that correspond to C-H stretching, asymmetric

stretching of the methyl (-CH_2) group, carbonyl group (C=O), -CH bending, and C=C bonds, respectively, similar to observations reported elsewhere (Canbay et al., 2011). In the FTIR spectrum of BG, the peaks observed at 2928 and 1740 cm^{-1} can be attributed to the C-H and C=O bonds of linalyl acetate. Whereas the peaks noticed at 896, 995, and 1370 cm^{-1} are due to the C=C of limonene (Altamimi et al., 2021). The FTIR spectrum of GG showed peaks at 2923, 1620, 1447, 1363, and 875 cm^{-1} due to asymmetric stretching of methyl (-CH_2) group, C=C stretches, C=C-C=C stretches, CH_3 group bending, and C-H bond stretching, respectively, that correspond to the zingiberene structure, the major constituent of GG (Tavares et al., 1947).

The FTIR spectra of pristine and composite films of PHB are depicted in Fig. 3.2b. PHB showed transmittance peaks at 2923, 1720, and 1049-1285 cm^{-1} which can be attributed to the C-H, C=O, and C-O-C groups, respectively (Abdelwahab et al., 2018). All the aforementioned peaks of PHB appeared in PHB essential oil composites. However, in the presence of essential oils, the C=O stretching vibration of PHB shifted from 1720 to 1723 cm^{-1}. In addition, a decrease in the peak intensity of the C-O-C group and an increase in peak intensity of the C=O group compared to pristine PHB were noticed for all the composite films. The aforementioned findings suggest that the incorporation of essential oils altered the molecular order and intermolecular interactions in the polymer matrix, which corroborated well with the tensile characteristics discussed in Section 3.2.1. Qin et al. (2017) reported similar observations in the FTIR spectra of PLA/rosemary oil, PLA/clove essential oil, and PLA/lemongrass oil composites (Qin et al., 2017).

Table 3.1. Major constituents of essential oils expressed in percentage of chromatographic area

GS		**BG**		**GG**	
Constituent	**%**	**Constituent**	**%**	**Constituent**	**%**
Decadineal	30.18	Limonene	39.27	Zingiberene	20.81
Ethyl hexanoate	12.50	Linalool	19.44	α-curcumene	9.73
Nona-2,3, -dienoic acid, ethyl ester	8.18	Branched heptadecane	7.14	β-sesquiphellandrene	9.08
Acetic acid	5.20	Linalyl acetate	6.13	α-farnesene	8.02
Methyl butanol	5.08	γ-terpinene	5.54	β-bisabolene	7.23
Hexanol	4.80	Farnesol	3.58	Geranyl acetate	6.96
Linalyl acetate	4.12	Neral	2.34	Camphene	6.69
Pentanal	3.50	Citral	1.72	Nerolidol	5.40
Branched heptadecane	3.09	α-Terpineol	1.37	β-citranellol	4.60
Hexanoic acid	3.06	α-terpinyl acetate	1.15	Geranial	4.09
Limonene	2.62	Heptyl acetate	0.89	γ-Terpinene	3.02
2-methyl butyl acetate	1.86	β-Myrcene	0.64	Nonadecane	0.50
2-heptanone	0.93				
Heptanal	0.61				
Neryl acetate	0.57				
Octanoic acid	0.50				

BG: bergamot oil; GG: ginger oil; GS: grapeseed oil

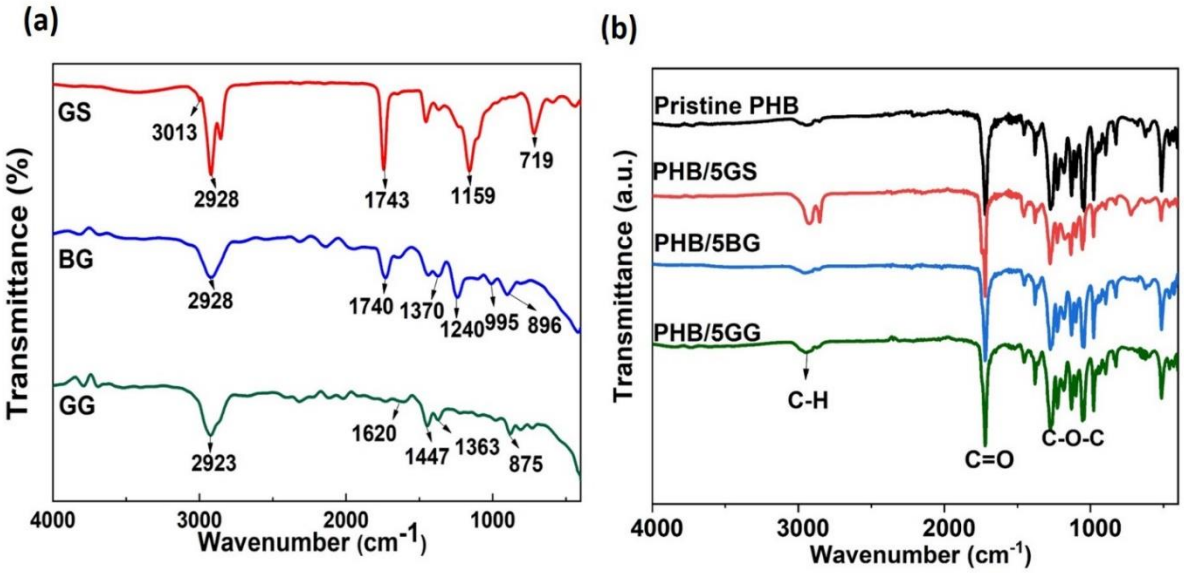

Fig. 3.2. FTIR spectra of (a) essential oils, and (b) pristine and composite films of PHB

3.2.3. XRD analysis

The XRD spectra of pristine and composite films of PHB are shown in Fig. 3.3. Sharp peaks observed in the XRD spectrum of PHB at 2θ values of 13.3° and 16.9° correspond to (0 2 0) and (1 1 0) planes of orthorhombic crystal structure. In addition, broad peaks noticed at 2θ values of 22.5°, 25.37°, 27.03°, and 44.56° can be attributed to (1 1 1), (1 2 1), (0 4 0), and (2 2 2) planes, respectively (Ankush et al., 2022; Anbukarasu et al., 2015). Moreover, the aforementioned peaks were observed for all PHB/essential oil composites, but with varying intensities. The crystallinity of the films was evaluated by dividing the area of crystalline peaks by the cumulative area of all the peaks observed in the XRD spectra (Manikandan et al., 2020). The crystallinity values of PHB, PHB/5GS, PHB/5BG, and PHB/5GG are 41.12, 53.21, 66.41, and 63.79 %, respectively. A similar observation corresponding to an increase in crystallinity with essential oil loading is reported for PLA/rosemary (Yahyaoui et al., 2016), PLA/myrtle (Yahyaoui et al., 2016), and PHB/tea tree oil/citronella composites (Rech et al., 2021). The increased crystallinity of composite films is due to increased free volume and polymer chain mobility caused by the plasticizing effect of essential oils, which facilitates the formation of packaged structures (Garcia-Garcia et al., 2020). Despite

the fact that all composite films contained the same quantity (5 wt%) of essential oil, the variations in crystallinity can be attributed to differences in the constituents and molecular structure of the essential oils employed (Arfat et al., 2018).

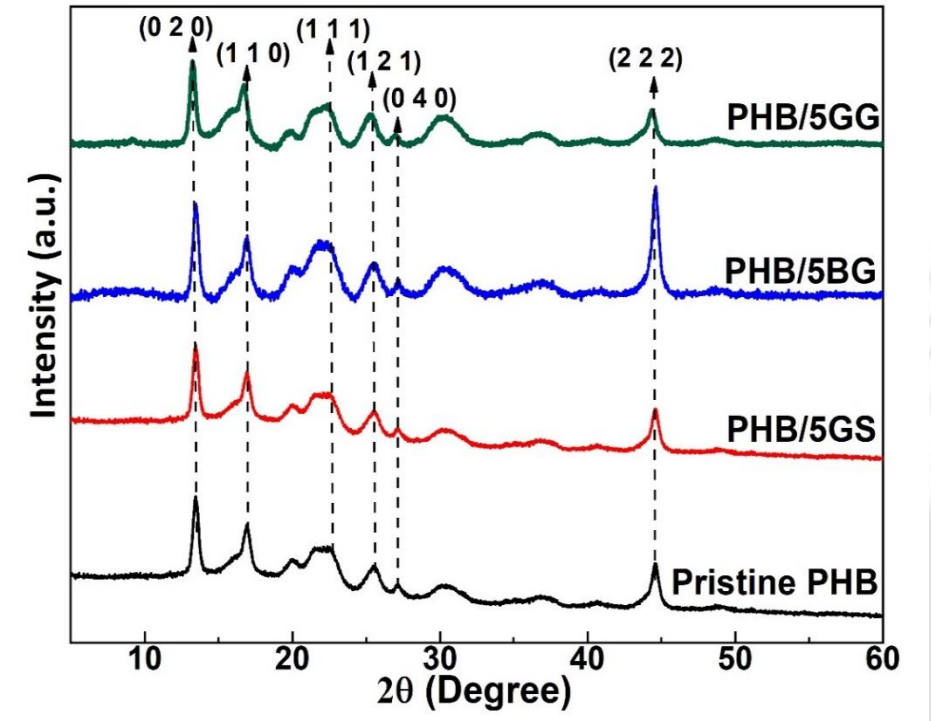

Fig. 3.3. XRD spectra of pristine and composite films of PHB

3.2.4. Morphology

The interaction between constituents of a composite material defines the internal morphological properties or microstructure of the resultant films, which directly affect their structural, barrier, mechanical, and optical properties (Haghighi et al., 2019). Therefore, good compatibility among constituents is essential to achieve desired characteristics in composite films. The morphology of the surface and cross-section of pristine PHB was relatively smooth and homogeneous without any aggregates, indicating well-assimilated polymer chains (Figs. 3.4a and 3.4a'). The surface and cross-sectional morphology of the PHB/5GS composite are compact and did not show any phase separation, implying high compatibility between PHB and GS (Figs. 3.4b and 3.4b').

Consequently, a 30-fold increase in EB is observed for PHB/5GS films. On the other hand, small aggregates were observed in FESEM images of PHB/5BG and PHB/5GG composite films (Figs. 3.4c, 3.4c', 3.4d, and 3.4d'). As stated in the literature (Ahmed et al., 2016; Khah et al., 2021), the variation in the morphology of composite films can be attributed to factors such as the polarity, viscosity, and droplet size of the essential oils, which affect the migration of oil droplets upward the film surface and evaporation rate of the solvent during the solution casting method. The topography of pristine and composite films of PHB was studied by AFM analysis, and root mean square roughness (R_a) values were obtained (Figs. 3.4 (a"-d")). The R_a of PHB, PHB/5GS, PHB/5BG, and PHB/5GG are 85±2, 113±3, 247±2, and 117±3 nm, respectively. The higher surface roughness of composite films, when compared to pristine PHB, can be attributed to the embedment of essential oil droplets in the polymer network, which could result in heterogeneous morphology (Qin et al., 2017). Moreover, the pronounced increase in roughness noticed for PHB/5BG films complemented the findings from FESEM images (Figs. 3.4 (a-d)). High roughness could result in higher friction during film processing, which is undesirable (Khah et al., 2021). A similar observation corresponding to an increase in the surface roughness of polymer films with the addition of essential oils was reported for pectin/gelatin composites with GS and virgin olive oils (Khah et al., 2021) and PLA composites with cinnamon oil (Ahmed et al., 2016).

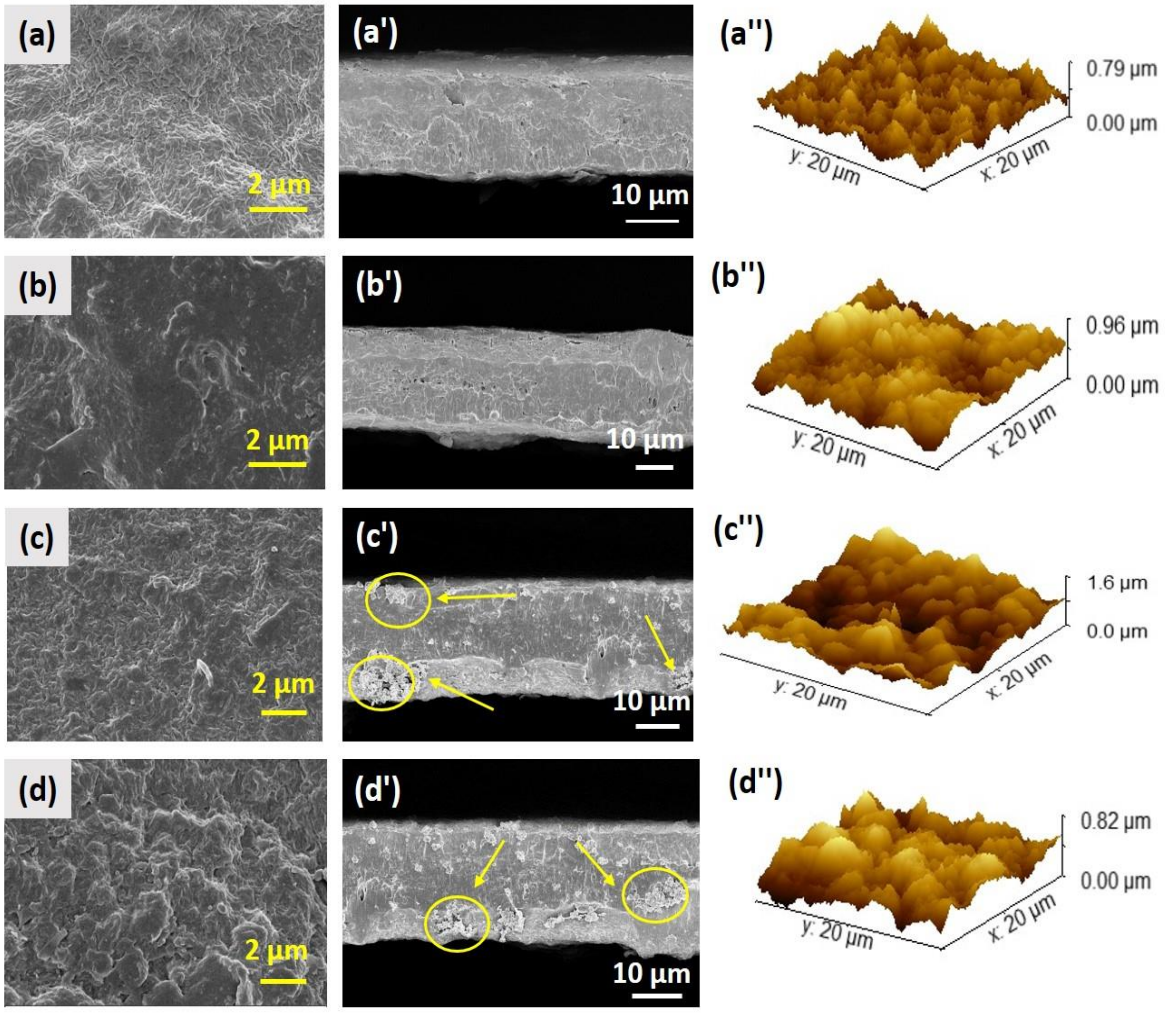

Fig. 3.4. Surface FESEM (a, b, c, and d), cross-sectional FESEM (a', b', c', and d') and AFM (a'', b'', c'', and d'') images of Pristine PHB, PHB/5GS, PHB/5BG, and PHB/5GG films, respectively.

3.2.5. Optical characteristics

Optical characteristics, namely, the opacity and color of food packaging, greatly influence its appearance and acceptance by consumers (Vianna et al., 2021). Opacity is used to gauge the transparency of films; the lower the opacity value, the higher the transparency, and vice versa (Gasti et al., 2022). Direct exposure of food to UV light may cause a series of reactions initiated by the release of singlet oxygen that result in off-flavors, discoloration, and oxidation of lipids and vitamins (Cazón et al., 2021). Therefore, to reduce the oxidative rancidity of food, packaging

material should possess UV-blocking properties. The UV-visible light transmission spectra and contact transparency of films are shown in Fig. 3.5. The colorimetric properties and opacity of the films are summarized in Table 3.2, which reveal that the PHB/essential oil composites were optically transparent with 80-95% transmittance in the visible range (400 -700 nm). No significant change ($P > 0.05$) in opacity was observed with the addition of the essential oils GS, BG, and GG to PHB (Table 3.2). Moreover, the visual inspection of films (Fig. 3.5b) well corroborated the results of spectrophotometric analysis. From Fig. 3.5a, pristine as well as composite films showed lower transparency to UV light. In particular, the increase in UV-blocking property with the addition of essential oils can be attributed to alteration in crystalline structure as well as scattering of light by oil droplets and a heterogeneous network of films (Vianna et al., 2021). Moreover, as discussed in FTIR results, essential oils constitute terpenes and other compounds with double bonds, which absorb and reflect light at different wavelengths and reduce the light transmittance (Rech et al., 2021; Ahmed et al., 2016). Considering colorimetric attributes (Table 3.2), the L^*-value (brightness) of composite films matched well with that of the pristine PHB ($P<0.05$). However, differences in values of "-a" (greenness) and "+b" (yellowness) are due to the amber color of essential oils loaded into the films.

Table 3.2. Optical properties of pristine and composite films of PHB

Film	**L***	**a***	**b***	**ΔE**	**Opacity value (A. mm^{-1})**
Pristine PHB	93.62 ± 0.21^{ab}	-2.04 ± 0.05^{b}	0.41 ± 0.09^{d}	-	0.36±0.11^{a}
PHB/5GS	92.51 ± 0.65^{b}	-1.52 ± 0.04^{a}	4.65 ± 0.66^{a}	4.46 ± 0.46^{a}	0.39±0.02^{a}
PHB/5BG	93.34 ± 1.04^{ab}	-1.57 ± 0.04^{a}	1.42 ± 0.22^{c}	1.45 ± 0.30^{b}	0.41±0.05^{a}
PHB/5GG	94.68 ± 0.36^{a}	-1.51 ± 0.07^{a}	2.65 ± 0.38^{b}	2.56 ± 0.29^{c}	0.40±0.12^{a}

Different superscript letters within the same column indicate that the difference of means is significant at 0.05 level

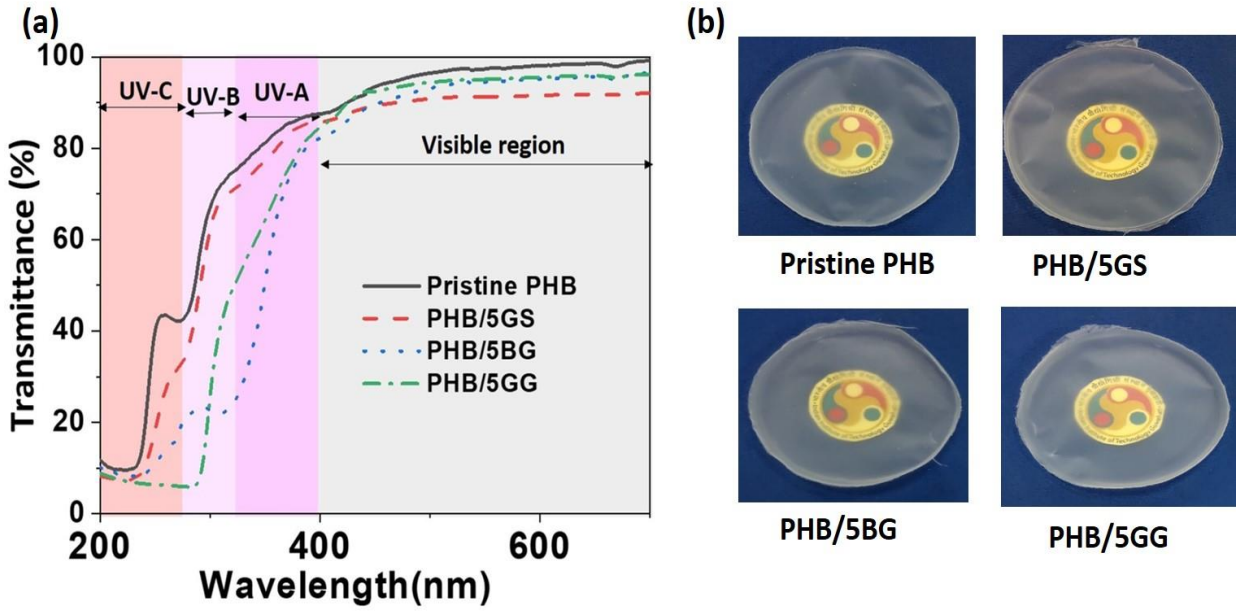

Fig. 3.5. (a) UV-visible transmittance spectra and (b) contact transparency of pristine and composite films of PHB

3.2.6. Thermal characteristics

The thermal behavior of pristine and composite films of PHB was evaluated using TGA and DSC analyses (Fig. 3.6). The maximum degradation temperature (T_{max}), which is considered one of the crucial factors for polymer composites, is determined from the maximum temperature of the peak in differential thermogravimetric (DTG) profiles (Fig. 3.6c). It can be seen from Fig. 3.6b, PHB steadily degraded in a single-step process with T_{max} centered at 287 ℃, well aligned with the literature (Ankush et al., 2022; Riaz et al., 2020). The thermal degradation of PHB occurs by a random chain scission process involving the cleavage of ester bonds to form crotonic acid (Pradhan et al., 2017). Incorporation of essential oils in the polymer matrix led to a two-step degradation process; the weight loss in the temperatures around 400, 140, and 190 ℃ for PHB/5GS, PHB/5BG, and PHB/GG can be attributed to the degradation of GS, BG, and GG, respectively (Fig. 3.6a). On the other hand, the weight loss in the temperature range of 230-320 ℃ for the composite films corresponds to the degradation of PHB. The T_{max} of PHB/5GS, PHB/5BG, and PHB/5GG are around 273, 260, and 273 ℃, respectively. The pyrolazyte residual

waste of pristine and composite films of PHB was less than 1 wt%, revealing complete thermal degradation of the samples and their inherent low environmental impact (Qin et al., 2017).

Concerning the melting behavior of PHB and PHB/essential oil composites, an unimodal endothermic peak is observed in the DSC thermographs (Fig. 3.6d), indicating the absence of heterogeneous distribution of crystals and the development of uniform crystal thickness (Valapa et al., 2015). The melting temperatures (T_m) of PHB, PHB/5GS, PHB/5BG, and PHB/5GG were found to be 178.09, 177.02, 176.36, and 175.47 °C; the values of melting enthalpy (ΔH_m) are 75.48, 92.69, 97.89, and 95.54 J. g^{-1}, respectively. The increase in enthalpy values with the incorporation of essential oil confirms the enhancement in crystallinity of composite films, as discussed earlier in Section 3.2.3 on XRD analysis. Moreover, the aforementioned observations from the DSC analysis were in good agreement with reports available in the literature on PLA/essential oil composites (Qin et al., 2017) and PHB/essential oil composites (Rech et al., 2021).

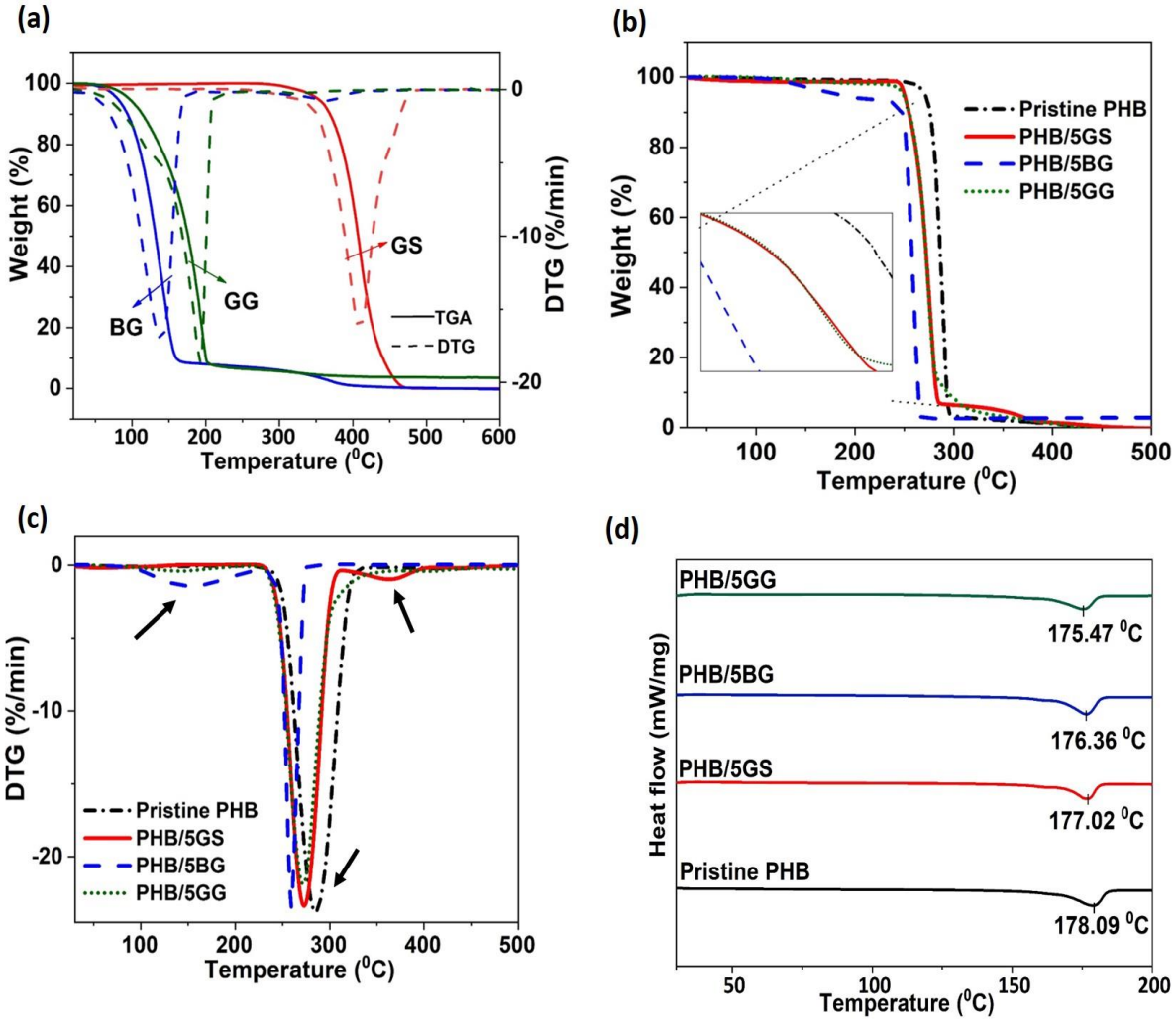

Fig. 3.6. (a) TGA and DTG profiles of different essential oils used in the study, (b) TGA, (c) DTG, and (d) DSC plots of pristine and composite films of PHB

3.2.7. Contact angle and gas barrier properties

Water contact angle is an important property for assessing the surface wettability of materials, and value over or below 65° indicates hydrophobic and hydrophilic surfaces, respectively (Zhang et al., 2022). Interestingly, pristine as well as composite films showed a water contact angle > 65°, indicating their poor affinity to water and therefore their potential use for food packaging applications (Fig. 3.7a). Furthermore, variations in the water contact angle of films were not significant (P >0.05) due to the addition of essential oils. Similar to the water contact angle, the water vapor barrier is an important characteristic of food packaging material for avoiding the

transfer of moisture from the environment to the food inside. Whereas, oxygen barrier property is crucial to restrict the oxidative degradation of food. Thus, food packaging materials should have a low water vapor and oxygen permeability to maintain the quality of food. The water vapor and oxygen permeability of PHB-based films is shown in Figs. 3.7b and 3.7c, respectively. The addition of GS, BG, and GG reduced the water vapor permeability due to the hydrophobic nature of the essential oils and the altered crystalline structure of the composite films. The gas permeability of semi-crystalline polymers is greatly influenced by the crystalline phase, which is impermeable to gases. Thus, the water vapor and oxygen barrier properties of composite films increased due to an increase in crystallinity, as discussed earlier in Section 3.2.3 (Qin et al., 2017). These observations are consistent with findings in previous literature (Boro et al., 2022; Gasti et al., 2022) which reported enhancement in gas barrier properties with the addition of essential oils to PLA.

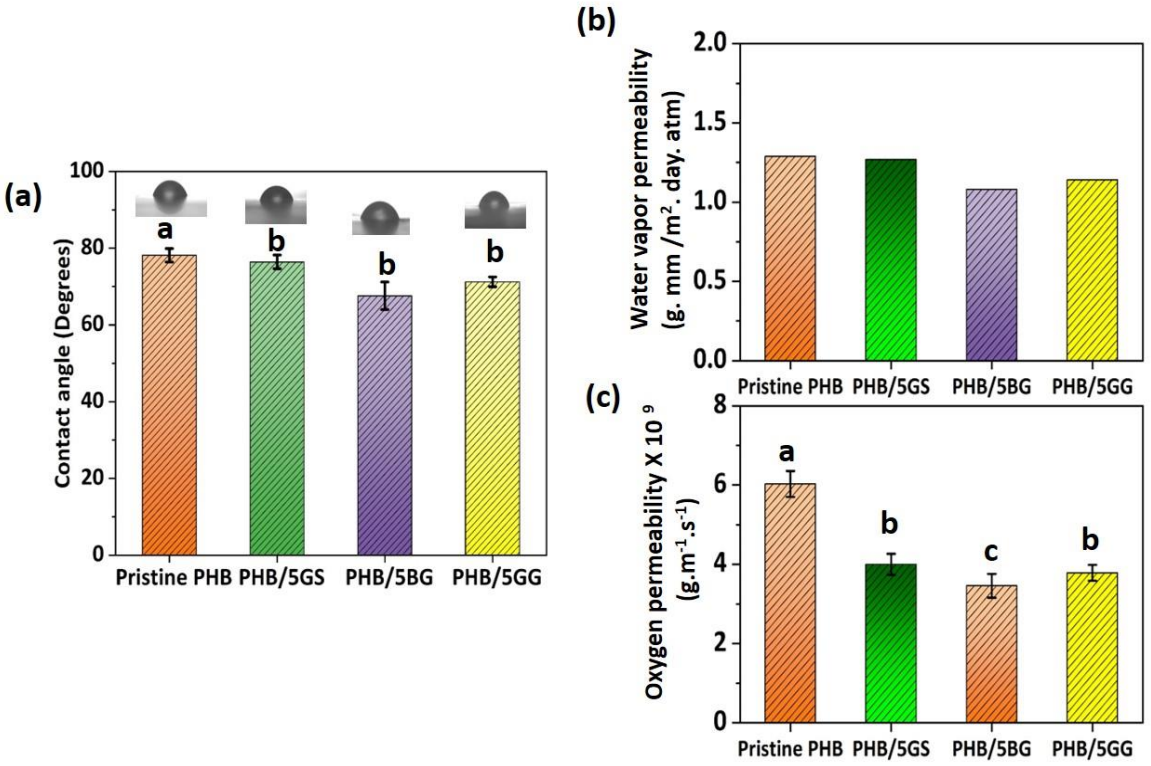

Fig. 3.7. (a) Contact angle, (b) water vapor permeability, and (c) oxygen permeability of pristine and composite films of PHB (bars with different alphabets indicate significant difference at 0.05 level)

3.2.8. Antimicrobial and antioxidant activities

The results of antibacterial tests of pristine and composite films of PHB against the foodborne bacteria (*E. coli* and *S. aureus)* are presented in Fig. 3.8a. The control film (PHB) showed negligible antibacterial activity against the test microorganisms, which is in agreement with the earlier reported studies (Abdelwahab et al., 2018). Compared with pristine PHB, the composite films exhibited very high inhibitory action against *S. aureus* due to the addition of essential oil. The antimicrobial action of essential oils depends on their constituents and bacteria i.e., Gram-positive or Gram-negative. As shown in Fig. 3.8b, the essential oils may inhibit bacterial growth by one or more of the following mechanisms: cell wall damage leading to leakage of cytoplasmic constituents, coagulation of cytoplasm, depletion of proton motive force, and disruption of membrane proteins (Varghese et al., 2020). Compared with *E. coli*, the inhibitory action of essential oil loaded films were higher in case of *S. aureus* (Fig. 3.8a). It is known that the cell

walls of Gram-positive bacteria such as *S. aureus* are made of peptidoglycan and offer minimum resistance to the penetration of essential oils (Fig. 3.8c). Contrarily, the cell walls of Gram-negative bacteria such as *E. coli* are complex, with a thin layer of peptidoglycan between the cytoplasmic membrane and outer membrane. Moreover, the lipopolysaccharides in the outer membrane of Gram-negative bacteria restrict the penetration of essential oils, which enables these bacteria to be more resistant than Gram-positive bacteria (Varghese et al., 2020; Nazzaro et al., 2013). In addition, the relatively high antimicrobial action of GG than the other essential oils is attributed to its active constituents such as zingiberene, α-curcumene, β-sesquiphellandrene, α-farnesene, and β-bisabolene (Malu et al., 2009). Similarly, the antimicrobial activity of BG is due to its major constituents, limonene, and linalyl acetate (Qin et al., 2017), whereas decadienal and phenolic compounds significantly contribute to the antimicrobial effect of GS (Garavaglia et al., 2016; Trombetta et al., 2002).

The PHB/5GS, PHB/5BG, and PHB/5GG films demonstrated more significant ($P<0.05$) DPPH radical scavenging activity than the control (PHB). The antioxidant activity of composite films is associated with the organic constituents in essential oils that contain conjugated double bonds and hydroxyl groups (mentioned earlier in Section 3.2.2), which can donate hydrogen, inhibit free radicals, and reduce oxidative stress (Amorati et al., 2013). In the current study, PHB/5GG films outperformed the other PHB composites (PHB/5BG and PHB/5GS) in antimicrobial and antioxidant action due to the presence of a large number of unsaturated components in GG. Previous studies also confirm the excellent antimicrobial and antioxidant properties of ginger oil-loaded composites (Garrido-Miranda et al., 2018; Miksusanti et al., 2013).

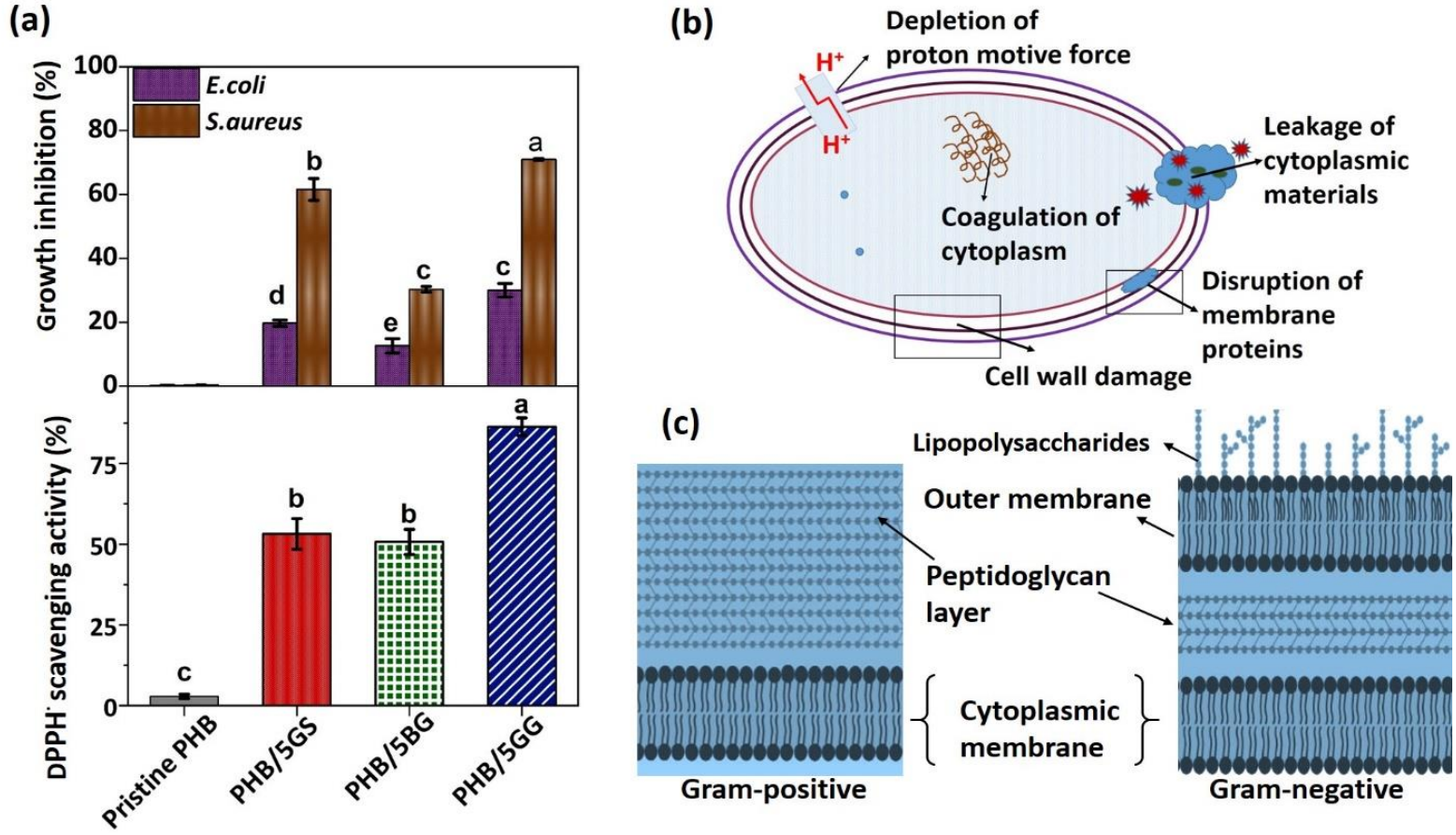

Fig. 3.8. (a) Antimicrobial and DPPH radical scavenging activities of pristine and composite films of PHB (bars with different alphabets indicate significant difference at 0.05 level), (b) Possible antibacterial mechanism of essential oils, and (c) Cell wall structure of Gram-positive and Gram-negative bacteria

3.2.9. Overall migration analysis

The overall migration limit is the maximum permitted total amount of non-volatile substances that can migrate from packaging material into the food inside. As per the 10/2011/EC regulation, the overall migration of plastic material should not exceed 10 mg of total constituents delivered per dm^2 of food contact surface (Requena et al., 2017). Nonetheless, as per regulations for active food contact materials, the active substances released should not be included in the overall migration. Moreover, overall migration due to volatile substances such as essential oils used in food packaging is not relevant as they possibly migrate along with solvents and do not contribute to total residual weight (Requena et al., 2017; Balaguer et al., 2013). This is particularly true when using aqueous solvents, as chemical evaporation occurs due to the steam drag effect. The overall migration values of PHB, PHB/5GS, PHB/5BG, and PHB/5GG in distilled water, 3% (v/v) acetic acid, and 10% (v/v) ethanol were shown in Fig. 3.9. The overall migration values of pristine and composite films of PHB were within the permissible limit (10 mg/dm^2). The migration of film components depends on various factors such as the nature of food simulants, the solubility of film components, and the interaction between polymer and additive (Bhat et al., 2022; Zheng et al., 2022).

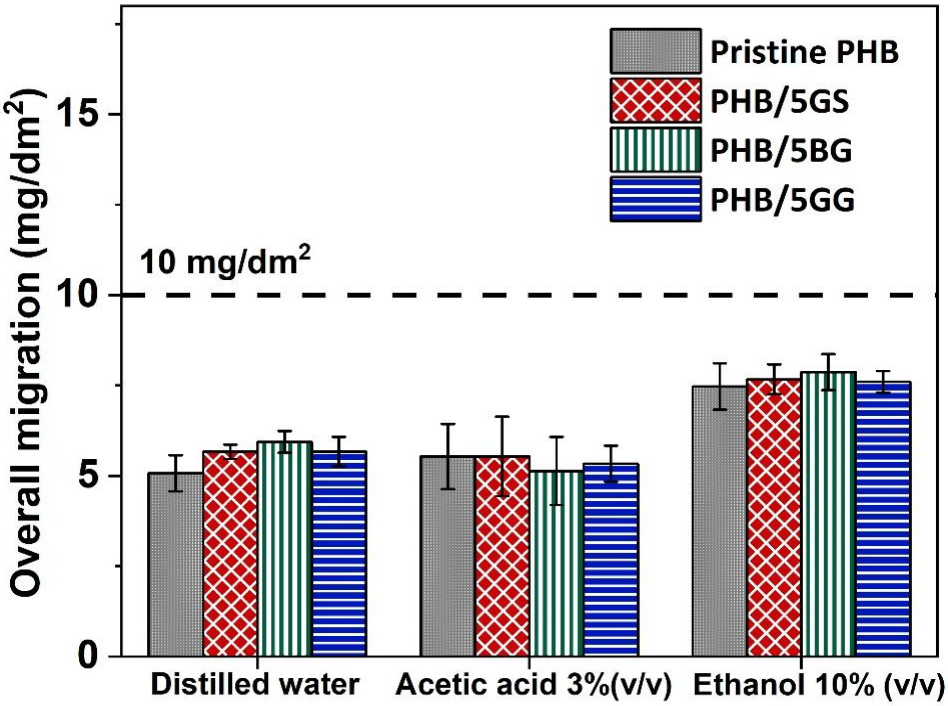

Fig. 3.9. Overall migration of components of PHB-based films into food simulants (bars with different alphabets represent significant difference at 0.05 level)

3.2.10. Contrast over prior arts

In Table 3.3, results obtained in the current study are compared with the previous literature on PHB-based composites containing different essential oils and plasticizers. Baltieri et al. (2003) achieved a maximum of 15.5±1.3 % EB by incorporating 30 wt% triacetyl glycerol in PHB (Baltieri et al., 2003). However, the composite films obtained in the aforementioned study exhibited less TS (11.3±0.7 MPa) and crystallinity than pristine PHB. In the current study, PHB-based films with a TS value of 15.8±0.8 MPa and EB of 15.2±0.2 % were obtained with loading of only 5 wt% of GS. Moreover, the tensile characteristics of PHB/5GS were better than the other PHB-based composites reported in the literature with plasticizers such as tri (ethylene glycol) bis (2-ethylhexanoate) (Kurusu et al., 2015), and dioctyl phthalate (Baltieri et al., 2003) and essential oils such as canola oil (Giaquinto et al., 2017) and combination of citronella oil and cinnamon oils

(Rech et al., 2021). Unlike plasticizer-loaded composites, PHB/5GG films demonstrated excellent antimicrobial and antioxidant activities, followed by PHB/5GS and PHB/5BG films, which could aid in extending shelf-life food by actively protecting them from microbial contamination and lipid oxidation.

Table 3.3. Comparison of various characteristics of PHB composite films containing different plasticizers and essential oils

Polymer	Additive	Additive loading (wt%)	TS (MPa)		EB (%)		Antibacterial activity	Antioxidant activity (%)	Ref
			Pristine PHB	Composite	Pristine PHB	Composite			
PHB	Dioctyl phthalate	30	31.3 ± 0.3	12.6±0.4	7.0±0.1	8.6±0.6	NA	NA	Baltieri et al., 2003
PHB	Triacetyl glycerol	30	31.3 ± 0.3	11.3±0.7	7.0±0.1	15.5±1.3	NA	NA	Baltieri et al., 2003
PHB	Tri (ethylene glycol) bis (2-ethyl hexanoate)	10	24.0 ± 0.3	18±0.4	6.8±0.1	7.2±0.5	NA	NA	Kurusu et al., 2015
PHB	Canola oil	6	20.8+0.8	10.4±0.1	4.1+0.4	4±0.1	Inhibitory action observed against *E. coli*	NA	Giaquinto et al., 2017
PHB	Citronella oil and cinnamon oil	30	11.1±0.12	6.9±0.3	1.82±0.47	6.9±0.9	Inhibition zone of *E. coli*: 5 ±1 mm; Inhibition zone of *S. aureus*: 3 ±1.7 mm	NA	Rech et al., 2021
PHB	GS	5	20.4±0.51	15.8±0.8	0.51±0.04	15.2±0.2	Growth inhibition (%) of *E. coli*: 19.7±0.9 %; Growth inhibition (%) of *S. aureus*: 61.5±3.4 %	53.1±4.7	Current study
PHB	BG	5	20.4±0.51	12.5±0.9	0.51±0.04	2.6±0.1	Growth inhibition (%) of *E. coli*: 12.6±2.2 %; Growth inhibition (%) of *S. aureus*: 30.3±0.9 %	50.7±3.9	Current study
PHB	GG	5	20.4±0.51	10.8±0.1	0.51±0.04	7.7±0.1	Growth inhibition (%) of E. coli: 29.9±2.1%; Growth inhibition (%) of S. aureus: 70.9±0.2 %	86.3±2.7	Current study

BG: Bergamot oil; EB: Elongation at break; GG: Ginger oil; GS: Grapeseed oil; NA: Not available; PHB: Poly (3-hydroxybutyrate); TS: Tensile strength

3.3. Summary

In this study, PHB composite films with varying loadings (1-10 wt%) of GS, BG, and GG were prepared by a simple solution casting technique. Volatile constituents of essential oils (GS, BG, and GG) were quantified by GC-MS analysis. The composite films with 5 wt% loading of the respective essential oil showed optimal EB but at the cost of a reduction in TS. Thus, all other characteristics of PHB composite films in the context of food packaging were evaluated at 5 wt% loading of the respective essential oils. Notably, the best improvement (30-fold) in elongation at break of PHB is achieved with 5 wt% loading of GS. FTIR characterization of the composite films revealed that the incorporation of essential oils altered the molecular order and intermolecular interactions in the PHB matrix. The composite films exhibited better gas barrier properties than pristine PHB films. A reduction in melting temperature and an increment in the crystallinity of composite films was confirmed by DSC and XRD analyses, respectively. The PHB/5GG films demonstrated excellent antioxidant and antibacterial properties, followed by PHB/5GS and PHB/5BG composites. Nevertheless, the degradation temperatures of BG and GG are close to the melting temperature of PHB, which limits their industrial-scale processing and production. Therefore, based on the results of the thermal characteristics, tensile test, and antibacterial and antioxidant assays, this chapter concluded that the PHB/5GS composite could be a great choice for packaging food products that do not require high TS, such as fruit cakes, buns, and bread. Additionally, techniques such as the incorporation of NPs could be investigated to improve the TS of PHB/5GS composite films to broaden their application for packaging other foodstuffs.

Chapter 4

Preparation, characterization, and optimizing the composition of poly (3-hydroxybutyrate)-based films loaded with grapeseed oil and MgO nanoparticles

This chapter received the following scientific recognition

International Journal of Biological Macromolecules 260 (2024) 129521

Contents lists available at ScienceDirect

International Journal of Biological Macromolecules

journal homepage: www.elsevier.com/locate/ijbiomac

Development and characterization of active poly (3-hydroxybutyrate) based composites with grapeseed oil and MgO nanoparticles for shelf-life extension of white button mushrooms (*Agaricus bisporus*)

Satti Venu Gopala Kumari [a], Kannan Pakshirajan [b], G. Pugazhenthi [a,c,*]

[a] Department of Chemical Engineering, Indian Institute of Technology Guwahati, Guwahati 781039, Assam, India
[b] Department of Biosciences and Bioengineering, Indian Institute of Technology Guwahati, Guwahati 781039, Assam, India
[c] Centre for Sustainable Polymers, Indian Institute of Technology Guwahati, Guwahati 781039, Assam, India

Kumari et al. (2024), International Journal of Biological Macromolecules, 260, 129521

Preparation, characterization, and optimizing the composition of poly (3-hydroxybutyrate)-based films loaded with grapeseed oil and MgO nanoparticles

This chapter summarizes the results of the study conducted to evaluate the effect of combinational loading of grapeseed oil (GS) and MgO nanoparticles on the properties of poly (3-hydroxybutyrate) (PHB). Based on the conclusions from Chapters 2 and 3, GS loading was fixed at 5 wt%, and MgO nanoparticles synthesized by the microwave combustion route were introduced as a reinforcing agent at varying loadings (0.1-1 wt%) in PHB via sonication-assisted solution casting route. The resulting PHB-based nanocomposite films were extensively characterized for their physicochemical, morphological, tensile, thermal, optical, water contact angle, barrier, antioxidant, and antimicrobial properties to determine the optimal composition suitable for food packaging applications.

4.1. Materials and Methods

4.1.1. Materials

Poly (3-hydroxybutyrate) powder and 2,2-diphenyl-1-picrylhydrazyl hydrate (DPPH) were supplied by Sigma Aldrich Co. Ltd., India. Methanol was purchased from Finar Ltd., India. Sodium chloride and activated carbon were procured from Merck Specialties Pvt. Ltd., India. Iron powder was purchased from Kalyan Industries, India. Chloroform and Luria Bertani (LB) broth were supplied by Hi-Media Pvt. Ltd., India. Grapeseed oil was supplied by All Naturals Ltd., India. MgO nanoparticles (MgO NPs) synthesized by microwave combustion route as per the procedure described earlier in Section 2.1.2.3 were used.

4.1.2. Fabrication and characterization of PHB-based films

PHB-based nanocomposite films with 5 % w/w of grapeseed oil (GS) and varying concentrations (0.1, 0.3, 0.5, 0.7, and 1 % w/w) of MgO NPs were developed by the sonication-assisted solution

casting technique (Boro et al., 2022; Kumari et al., 2020). At first, 1 g of PHB was dissolved in 20 mL of chloroform, 5 % w/w of GS was added to it, and the solution was mixed for 2 h at 300 rpm. Then, MgO NPs (0.1-1 wt% with respect to PHB weight) were introduced into the PHB/GS solution. The resulting solution was mixed well by magnetic stirring (300 rpm, room temperature) for 1 h, followed by ultrasonic treatment (bath sonication, power: 100 W, frequency: 40 kHz) for 45 min. Afterward, the solution was poured into Petri dishes and allowed for solvent evaporation to obtain films. In addition, PHB films without any additives (pristine PHB) and PHB-based films with 5 wt% GS loading (PHB/5GS) were prepared for comparative evaluation of their properties. The procedure involved in the fabrication of PHB/5GS/MgO nanocomposite films is illustrated in Fig. 4.1. The assessment of physicochemical, tensile, morphological, optical, gas barrier, water contact angle, antimicrobial, and antioxidant characteristics of various PHB-based films was conducted by the same procedure described earlier in Section 3.1.3. Subsequently, the data obtained was subjected to a One-way analysis of variance (ANOVA) followed by Tukey's honest significance difference test.

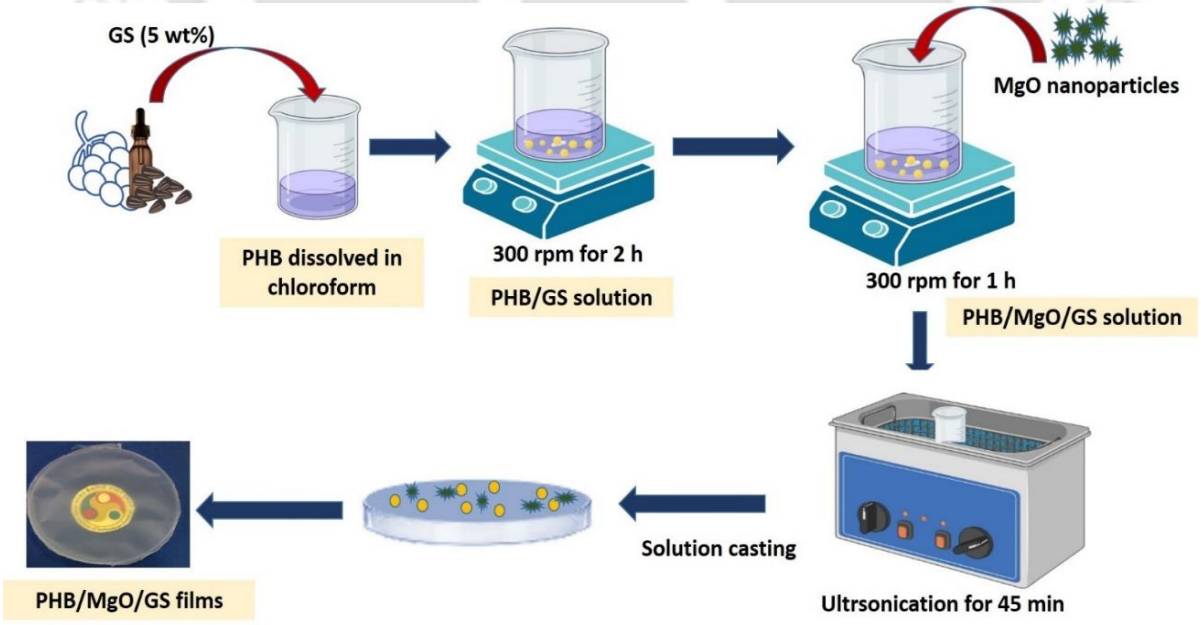

Fig. 4.1. Steps followed for the fabrication of PHB-based nanocomposite films

4.2. Results and discussion

4.2.1. Morphology

The morphology of polymer composites containing essential oils and nanofillers fabricated by the solution casting route is governed by numerous factors, viz., physicochemical properties of essential oils, the size, shape, and concentration of nanofillers, along with the distribution of these additives within the composite and the rate of evaporation of solvent during drying (Ahmed et al., 2016). Moreover, the morphology/microstructure of polymer composites directly influences their optical, barrier, mechanical, and structural attributes. Hence, the surface morphology of various PHB-based films was analyzed by FESEM (Fig. 4.2). The surface of the PHB/5GS composite showed a compact structure, similar to pristine PHB, without any voids or phase separation, indicating good compatibility between GS and PHB (Figs. 4.2a, 4.2a', 4.2b, and 4.2b'). No phase separation or aggregate formation was noticed in FESEM images of PHB/5GS/0.7MgO films (Figs. 4.2c and 4.2c'); this implies good compatibility between MgO NPs and the polymer matrix and uniform distribution of nanofiller at 0.7 wt% loading rate. On the other hand, agglomerates of MgO NPs were noticed in FESEM images (Figs. 4.2d and 4.2d') of PHB/5GS/1MgO nanocomposite due to the overcrowding effect, which occurs when filler concentration is above the optimum level. Swaroop et al. (2018) and Arumugam et al. (2022) reported analogous findings corresponding to the aggregation of nanofillers at higher loading rates in PLA/MgO and polybutylene adipate terephthalate/GS/SiO_2 nanocomposites, respectively (Arumugam et al., 2022; Swaroop and Shukla, 2018). Surface roughness is another important parameter for polymer composites, impacting their performance and processability. Hence, the topographic images of various PHB-based films were captured by AFM (please see Fig. 4.3), and root mean square roughness (R_a) values were calculated. The R_a of PHB, PHB/5GS, and PHB/5GS/MgO nanocomposites with 0.1, 0.3, 0.5, 0.7, and 1 % w/w of MgO NPs are 85±2, 113±3, 114±2, 117±2, 120±4, 135±3, and 149±3 nm, respectively. This increased trend of surface roughness is in good

agreement with results reported elsewhere for biopolymer composites loaded with essential oils and nanofillers (Khah et al., 2021; Sheikh et al., 2018).

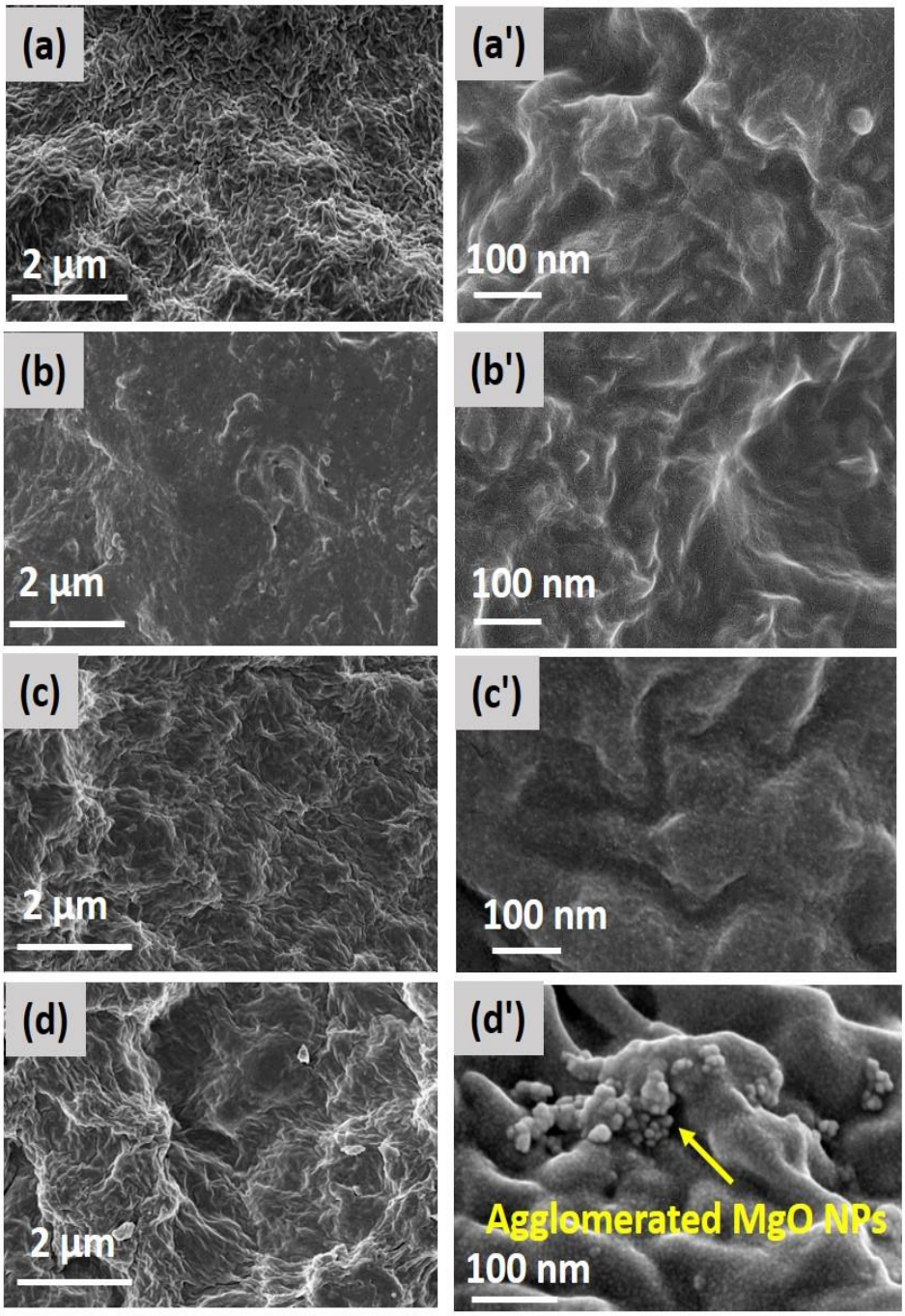

Fig. 4.2. (a, b, c, and d) lower and (a', b', c', and d') higher magnification FESEM images of pristine PHB, PHB/5GS, PHB/5GS/0.7MgO, and PHB/5GS/1MgO films, respectively

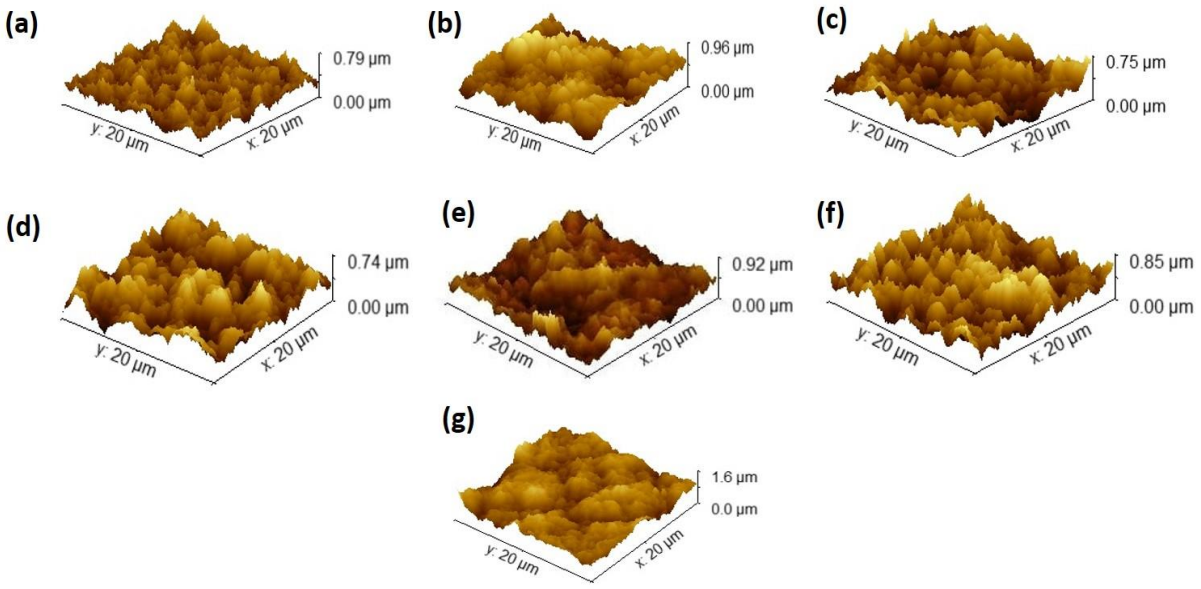

Fig. 4.3. AFM images of (a) pristine PHB, (b) PHB/5GS, and (c, d, e, f, and g) PHB/5GS/MgO nanocomposites with 0.1, 0.3, 0.5, 0.7, and 1 wt% loading of MgO NPs, respectively

4.2.2. XRD and FTIR analyses

Barrier attributes of polymer-based materials are significantly influenced by their crystal structure, so it is crucial to evaluate the structural properties of prepared composite films (Swaroop and Shukla, 2019). Figs. 4.4a and 4.4b show the XRD spectra of MgO NPs, pristine film, and composite films of PHB. The sharp and intense peaks noticed in the XRD spectrum of MgO NPs (Fig. 4.4a) at 2θ values of 37.03°, 42.94°, and 63.06° of (1 1 1), (2 0 0), and (2 2 0) planes, respectively, evidenced their highly crystalline nature. As per the JCPDS 00-001-1235 data, these peaks were indicative of the periclase phase and cubic crystal system of MgO (Amani et al., 2019). PHB was semi-crystalline in nature, and it showed diffraction peaks at 13.3°, 16.9°, 22.5°, 25.37°, 27.03°, and 44.56° for (0 2 0), (1 1 0), (1 1 1), (1 2 1), (0 4 0), and (2 2 2) planes of the orthorhombic crystal system (Manikandan et al., 2020). PHB/5GS and PHB/5GS/MgO composites showed all the aforementioned peaks of pristine PHB but at varied intensities owing to variations in their crystallinity (Fig. 4.4b). In addition, the composite films containing nanofiller showed a small diffraction peak around 63.06° corresponding to MgO, and the intensity of the aforementioned

peak consistently increased with an increase in the loading of nanofiller, similar to results reported elsewhere (Swaroop and Shukla, 2019).

The crystallinity of the PHB-based films was calculated by dividing the sum of the area under crystalline peaks by the total integrated area under all the peaks in their respective XRD spectra (Kang and Yun, 2022). It was found that the crystallinity of films increased from 41.12 % for pristine PHB to 53.21 % for PHB/5GS, accredited to the plasticizing effect of GS that increases the free volume as well as polymer chain mobility, facilitating the formation of packaged structures. Furthermore, with the introduction of 0.1, 0.3, 0.5, and 0.7 wt% of MgO NPs in the composite films, crystallinity further increased to 53.32, 55.58, 56.29, and 61.45 %, respectively. This increment is due to the nucleating effect of nanoparticles, which accelerates the rate of crystallization in polymer nanocomposites (Kim et al., 2013). Thus, it can be said that the combinational loading of GS and MgO NPs significantly improved the crystallinity of PHB-based films. A similar trend of increase in crystallinity with the loading of essential oils and nanofillers in biopolymers has been reported in the literature (Ankush et al., 2022; Yahyaoui et al., 2016). However, at higher loading (1 wt%) of MgO NPs, the crystallinity of the composite film (PHB/5GS/1MgO) dropped to 40.98 %, which could be due to chain entanglement between the matrix and filler phases that strongly restricts the crystal growth. A similar trend of drop in crystallinity at higher loading of ZnO NPs (Díez-Pascual et al., 2014) and multi-walled carbon nanotubes (Yu et al., 2014) in the PHBHV matrix is reported in the literature.

FTIR analysis was conducted for MgO NPs, GS, pristine, and composite films of PHB to assess the type of interaction between the PHB matrix and the additives. Functional group assignment for transmittance peaks observed in these FTIR spectra (Figs. 4.4c and 4.4d) is provided in Table 4.1. From Fig. 4.4d, it can be noticed that the PHB/5GS and PHB/5GS/MgO composites primarily showed transmittance peaks corresponding to PHB, with the exception of minor variations in peak intensities for the C=O and C-O-C groups and a slight shift in the C=O stretch from 1720 to 1723

cm^{-1} due to an alteration in their molecular order, and the same is discussed in detail in another Section 4.2.3. Nevertheless, the peaks associated with GS and MgO NPs were not evident in the FTIR spectra of composite films, owing to the low loading rate of these additives. Based on the aforementioned findings, it is evident that the nature of the interaction between the PHB matrix and additives (GS and MgO NPs) was physical, with no evidence of covalent bond formation or any chemical interaction. Similar findings corresponding to FTIR analysis were reported in the literature for PLA/rosemary essential oil (Qin et al., 2017), PLA/MgO (Swaroop and Shukla, 2018), and PLA/graphene/clove essential oil (Arfat et al., 2018) composites.

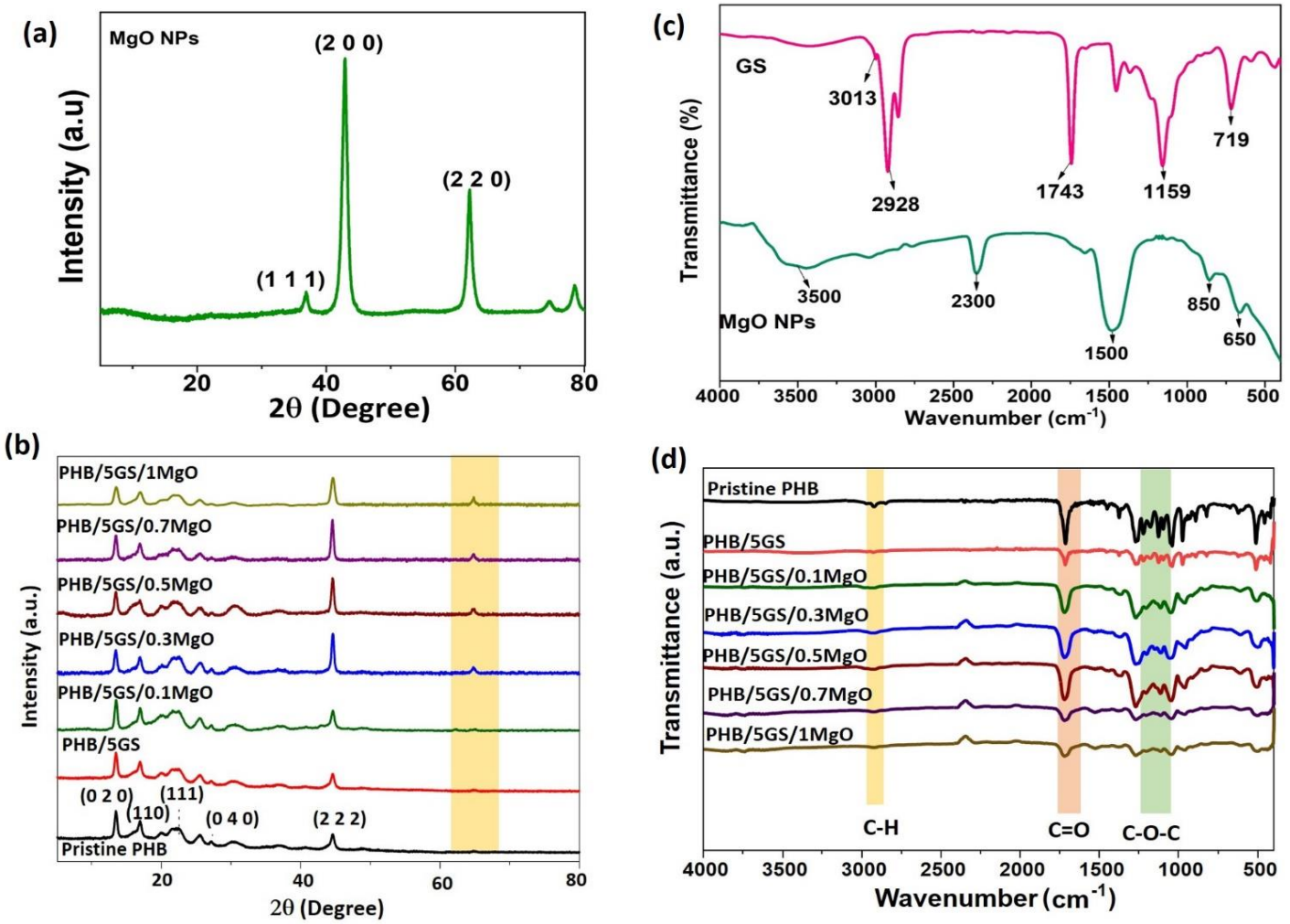

Fig. 4.4. (a and b) XRD spectra and (c and d) FTIR spectra of PHB-based films and additives

Table 4.1. Functional group assignment for transmittance peaks in the FTIR spectra

Source	Wavenumber (cm^{-1})	Peak assignment
MgO NPs	850	v_1 stretching of Mg-O
	650	v_2 stretching of Mg-O
	1500	O-H bending of surface adsorbed H_2O molecules
	2300	bending vibration of surface adsorbed CO_2
	3500	O-H stretching of surface adsorbed H_2O molecules
GS	719	C=C bond
	1159	-C-H bending
	1743	C=O group
	2928	asymmetric stretching of $–CH_2$ group
	3013	C-H stretching
PHB	1049-1285	C-O-C group
	1720	C=O group
	2928	C-H group

4.2.3. Thermal and tensile properties

The thermal stability of various PHB-based films fabricated in this study was evaluated by TGA and DTG analyses. In addition, the maximum thermal degradation temperature (T_{max}), a critical parameter for polymer composites, is estimated by DTG analysis. The T_{onset}, the temperature corresponding to 10 % weight loss, was obtained from the TGA data of the respective samples. The results obtained from TGA and DTG analyzed are presented in Figs. 4.5a, 4.5b, and Table 4.2. The pristine PHB steadily degraded in a single stage in the temperature range of 230-320 ℃, primarily due to random chain scission reactions resulting in the formation of crotonic acid (Iulianelli et al., 2017). In contrast, the degradation of GS occurred at a higher temperature, ranging from 320 to 470 ℃, surpassing the degradation range of PHB (Fig. 4.5b). However, in the composite films containing GS, the degradation occurred in two stages. Wherein, the first stage of weight loss in the temperature range of 230-320 ℃ can be accredited to the degradation of PHB

(Mittal et al., 2023). While the second stage of weight loss in the temperature range of 320-470 ℃ can be attributed to the degradation of GS (Fig. 4.5b). In comparison with pristine PHB, the decrease in thermal stability of PHB/5GS films (shift of T_{onset} from 273 to 252 ℃ and T_{max} from 287 to 272 ℃) was due to the plasticizing effect of GS, which increases the free volume between polymer chains and facilitates the release of volatiles. An analogous study by Mittal et al. (2023) also noted a decrease in the thermal stability of PHB-based films with the loading of clove essential oil (Mittal et al., 2023).

It is noteworthy that the adverse impact of GS loading on the thermal stability of PHB was partially mitigated with the introduction of MgO NPs as a reinforcing agent; both T_{max} and T_{onset} of PHB/5GS/0.7MgO are approximately 11 ℃ higher than the corresponding values for PHB/5GS. This could be due to the homogeneous distribution of MgO NPs at 0.7 wt% loading, as discussed in the previous Section 4.2.1 on FESEM results, which delayed the release of volatile components in the composite films. A similar trend of increase in thermal stability of PHB-based films with reinforcement of metal oxide nanoparticles such as TiO_2 (Iulianelli et al., 2017) and ZnO (Silva et al., 2022) is reported in the literature. However, at 1 wt% loading of MgO NPs, a remarkable decrease in thermal stability was noticed for composite (PHB/5GS/1MgO) films due to the agglomeration of nanoparticles, as disclosed earlier in Fig. 4.2d'.

The melting behavior of various PHB-based films was analyzed by DSC (Fig. 4.5c); melting temperature (T_m) and melting enthalpy values derived from this characterization are presented in Table 4.2. All the DSC thermographs showed unimodal endothermic peaks, indicating the development of uniform crystal thickness and the absence of heterogeneous crystal distribution (Valapa et al., 2015). The T_m of PHB/5GS/MgO nanocomposites (up to 0.7 wt% loading of MgO) was slightly higher than the T_m of pristine PHB, which may be a result of the nanoparticles promoting the formation of larger lamellar thickness and well-organized crystals within the spherulites of composite material. Nevertheless, the increasing trend observed in melting enthalpy

(ΔH_m) values (Table 4.2) confirmed the increase in crystallinity of composite films discussed earlier in Section 4.2.2 on the XRD results.

Table 4.2. Thermal properties of various PHB-based films based on TGA and DSC analyses

Sample	**T_{onset} (°C)**	**T_{max} (°C)**	**T_m (°C)**	**ΔH_m (J. g^{-1})**
Pristine PHB	273.8±2.0^{a}	287.2±1.3^{a}	178.0±0.9^{d}	75.5±1.3^{d}
PHB/5GS	252.7±1.1^{e}	272.4±2.1^{e}	177.1±0.5^{d}	92.2±0.4^{c}
PHB/5GS/0.1MgO	255.5±1.4^{de}	275.1±1.3^{d}	178.4±0.5^{cd}	92.4±0.7^{c}
PHB/5GS/0.3MgO	256.3±0.5^{d}	276.6±0.6^{d}	178.9±1.8^{c}	93.6±2.7^{c}
PHB/5GS/0.5MgO	260.5±0.5^{c}	279.3±1.4^{c}	180.2±0.8^{b}	95.1±0.7^{b}
PHB/5GS/0.7MgO	263.2±1.5^{b}	283.7±0.6^{b}	182.5±0.5^{a}	97.3±0.6^{a}
PHB/5GS/1MgO	252.5±2.1^{f}	276.7±1.5^{d}	180.4±1.9^{b}	71.1±1.2^{e}

Distinct superscript letters within the same column indicate a significant difference in means at a 0.05 level

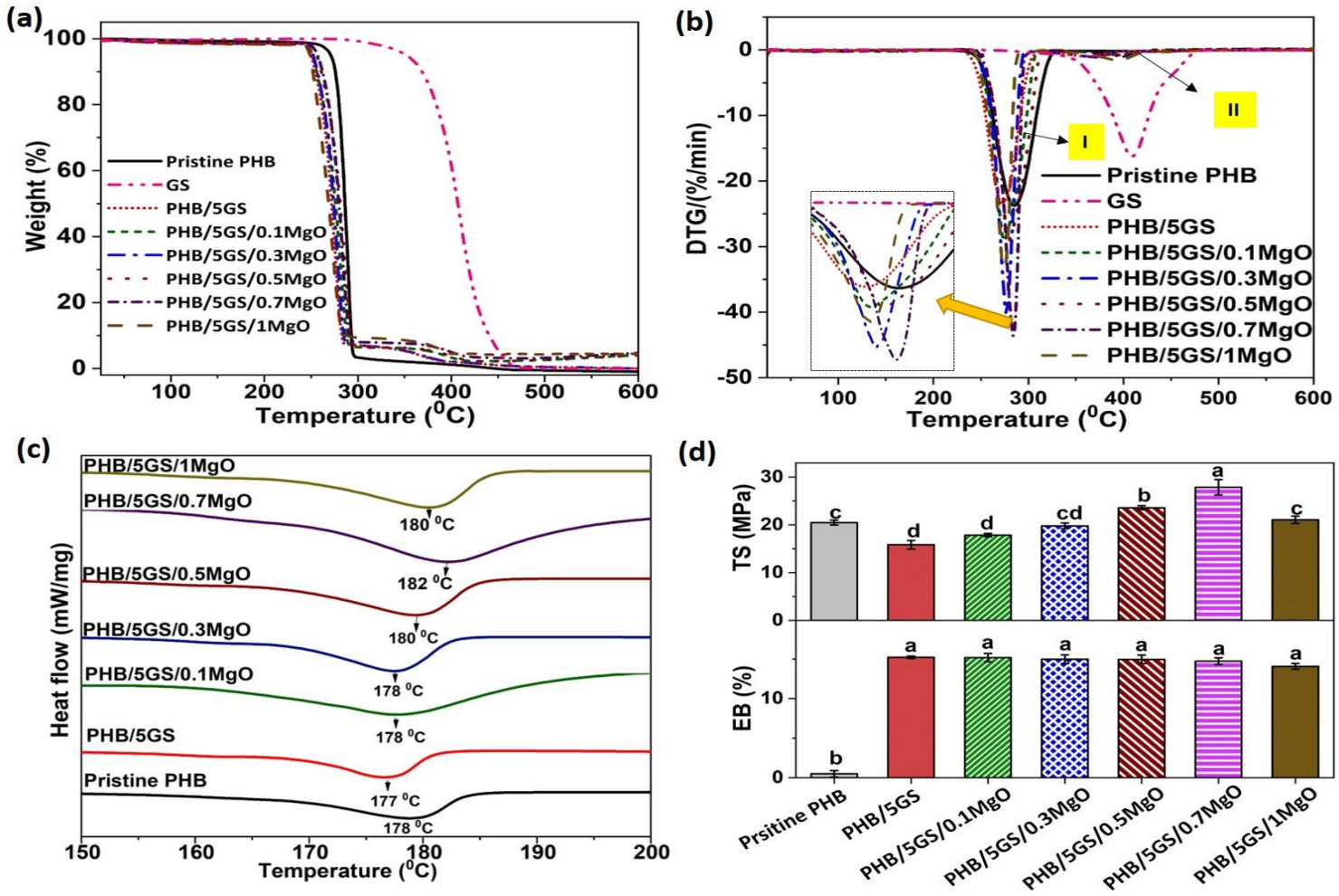

Fig. 4.5. (a) TGA, (b) DTG, and (c) DSC profiles and (d) tensile properties of pristine and composite films of PHB (distinct alphabets above the bars indicate significantly different values, $P < 0.05$)

Tensile strength (TS) and elongation at break (EB) are two important attributes of food packaging materials that disclose their maximum tolerance to tensile stress and stretching capacity before fracturing, respectively. The tensile properties of pristine PHB, PHB/5GS, and PHB/5GS/MgO nanocomposites are shown in Fig. 4.5d. Pristine PHB film exhibited an EB of 0.51±0.04 % and a TS of 20.48±0.51 MPa. The PHB/5GS films showed a remarkable 30-fold increase in EB (15.2±0.2%) in comparison to pristine PHB due to the embedment of GS droplets between adjacent polymer chains, which increases free volume and polymer chain mobility in the composite films. As expected, only GS (5 wt%) loading showed a negative effect on the TS of PHB, reducing it to 15.8±0.8 MPa. As reported in the literature (Rech et al., 2021; Ahmed et al., 2016), the decrease in TS of PHB/5GS films compared to TS of pristine PHB could be due to the weakening of intermolecular interactions in the polymer matrix with the addition of essential oil. Interestingly, when both MgO NPs (0.1-0.7 wt%) and GS (5 wt%) were loaded into PHB, the resulting composite films displayed greater tensile strength than PHB/5GS films, all while maintaining their flexibility. In particular, the PHB/5GS/0.7MgO films exhibited a TS and EB values of 27.89±1.62 MPa and 14.74±0.42 %, which are approximately 1.4 and 30-fold higher than the TS and EB values of pristine PHB, respectively. The TS enhancement in composite films containing nanofiller can be attributed to efficient load distribution between MgO NPs and polymer matrix that reduces the risk of localized failure and boosts the material's overall strength. However, at higher loadings of MgO NPs (1 wt%), the TS of composite films decreased due to the formation of agglomerates (mentioned earlier in Section 4.2.1) that weakens the stress transference between the polymer matrix and nanofiller (Manikandan et al., 2020). From the aforementioned findings, it can be inferred that the combinational loading of GS and MgO NPs in PHB demonstrated a positive synergetic influence on the TS and EB of the resulting composites. Similar observations corresponding to tensile properties were reported for PLA/clove essential

oil/alkali-treated halloysite nanotube composites (Boro et al., 2022) and PLA/citronella essential oil/montmorillonite nanoclay composites (Ferreira et al., 2023).

4.2.4. UV-visible light transmittance and color

Direct exposure of food to UV light can initiate a chain of reactions triggered by the release of singlet oxygen, leading to undesirable effects such as off-flavors, discoloration, and oxidation of vitamins and lipids in food (Narayanan et al., 2017). Thus, packaging materials must possess UV-blocking properties to maintain the safety and quality of food products. Packaging of items like fruits and bakery goods necessitates a high level of transparency to visible light, allowing consumers to easily see the products inside. Conversely, the packaging of light-sensitive food products should have low transparency to visible light (Alghamdi et al., 2022). Hence, the UV-visible transmittance spectra of various PHB-based films prepared in this study were analyzed and presented in Fig. 4.6a. The opacity and color characteristics of PHB-based films, which are pivotal factors influencing their physical appeal and consumer acceptance, are presented in Table 4.3.

Pristine as well as composite films of PHB showed greater than 85 % transmission of visible light. The inclusion of GS alone did not have a substantial impact on the opacity of films. Whereas, the addition of MgO NPs as reinforcement resulted in a significant ($P < 0.05$) rise in opacity values (Table 4.3), which can also be observed in contact transparency images (Fig. 4.6b). It is worth noting that the composite films demonstrated lower transparency to UV light than pristine PHB. Herein, the scattering of light by oil droplets and interfaces between crystallites as well as absorbance of UV light by MgO NPs, terpenes, and other double-bonded constituents in GS contributed to a reduction in UV light transmission (Vianna et al., 2021; Swaroop and Shukla, 2019). In comparison with pristine PHB, "-a*" and "+b*" values of PHB/5GS significantly ($P < 0.05$) changed due to the amber color of GS. Compared to PHB/5GS films, the increment in lightness (L*) and decrease in yellowness (+b*) values of PHB/5GS/MgO films, particularly at higher loadings of the nanofiller, are due to the whitening effect of MgO NPs. Similar to the

current study, the loading of ZnO NPs showed a whitening effect on PLA-based films (Arfat et al., 2017).

Table 4.3. Colorimetric coordinates and opacity values of various PHB-based films

Film	L*	a*	b*	ΔE	Opacity value (A. mm^{-1})
PHB	93.62 ± 0.21^{ad}	-2.04 ± 0.05^{b}	0.41 ± 0.09^{d}	-	0.36 ± 0.11^{f}
PHB/5GS	92.51 ± 0.65^{ac}	-1.52 ± 0.04^{a}	4.65 ± 0.66^{a}	4.46 ± 0.46^{a}	0.39 ± 0.02^{f}
PHB/5GS/0.1MgO	92.50 ± 0.21^{c}	-1.52 ± 0.10^{a}	2.76 ± 0.04^{b}	4.38 ± 0.03^{a}	0.41 ± 0.02^{de}
PHB/5GS/0.3MgO	92.42 ± 0.1^{c}	-1.51 ± 0.03^{a}	2.44 ± 0.05^{b}	4.23 ± 0.05^{a}	0.45 ± 0.01^{d}
PHB/5GS/0.5MgO	93.05 ± 0.5^{b}	-1.61 ± 0.03^{a}	2.27 ± 0.04^{b}	4.12 ± 0.04^{a}	0.57 ± 0.02^{bc}
PHB/5GS/0.7MgO	93.04 ± 0.2^{b}	-1.57 ± 0.05^{a}	2.27 ± 0.02^{b}	4.08 ± 0.05^{a}	0.62 ± 0.01^{b}
PHB/5GS/1MgO	93.36 ± 0.3^{bd}	-1.63 ± 0.04^{a}	1.56 ± 0.08^{c}	3.85 ± 0.07^{b}	0.65 ± 0.01^{ab}

Distinct superscript letters within the same column indicate a significant difference in means at a 0.05 level.

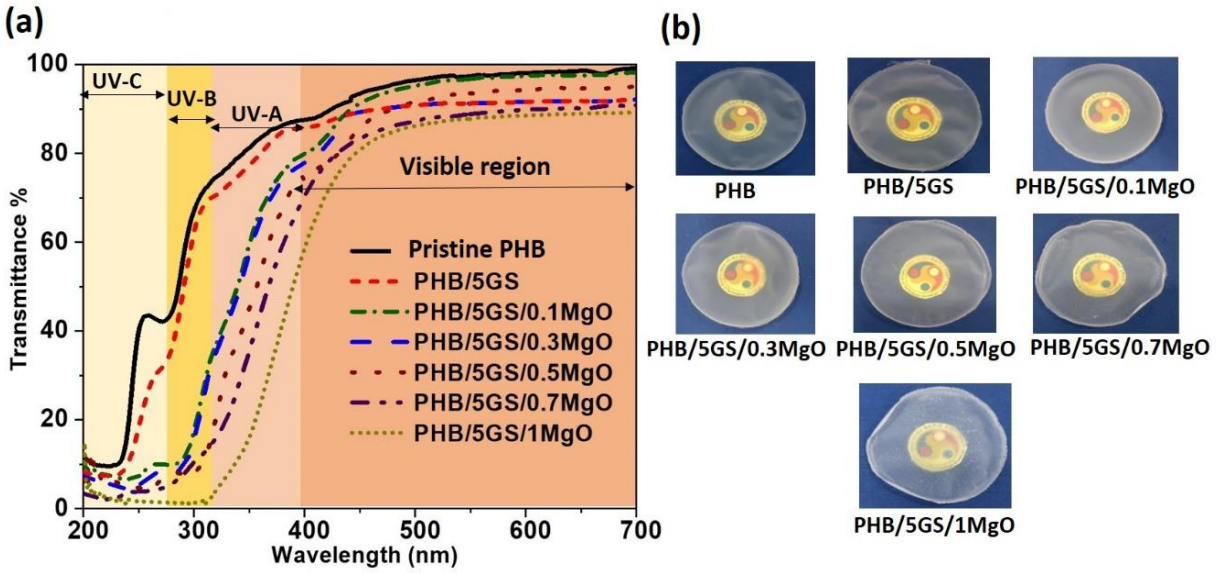

Fig. 4.6. (a) UV-visible light transmittance spectra and (b) contact transparency images of various PHB-based films prepared in this study

4.2.5. Water contact angle and barrier properties

The water contact angle was measured for various PHB-based films to assess their hydrophobic or hydrophilic character (Fig. 4.7a). Pristine as well as composite films of PHB exhibited a water contact angle greater than 65°, which indicates their hydrophobic nature and suitability for food packaging applications (Zhang et al., 2022). In comparison with pristine PHB, no significant ($P > 0.05$) change in water contact angle is observed for PHB/5GS and PHB/5GS/MgO composites up to 0.5 wt% loading of the nanofiller. In contrast, a significant ($P < 0.05$) increase in water contact angle is noticed for PHB/5GS/0.7MgO and PHB/5GS/1MgO composite films. This increment could be attributed to a pronounced increase in surface roughness from 85±2 nm for pristine PHB to 135±3, and 149±3 nm for the respective samples. Moreover, these findings are in good agreement with the results reported in the literature (Zou et al., 2016). The permeation of oxygen and water vapor through packaging materials impacts food texture, flavors, and susceptibility to degradation by oxidation and microbial growth (Fernández-Menéndez et al., 2020). In general, packaging materials need high oxygen and water vapor barrier properties to uphold the quality of food inside (Manikandan et al., 2020).

The water vapor and oxygen permeability of pristine PHB are 1.29 $g.mm.m^{-2}.day^{-1}.atm^{-1}$ and 6.03×10^{-9} $g.m^{-1}.s^{-1}$, respectively. Loading of GS and MgO NPs reduced the permeation of oxygen and water vapor through PHB-based composites (Fig. 4.7b). In comparison with pristine PHB, 79 and 90 % increments in water vapor and oxygen barrier properties are observed for the PHB/5GS/0.7MgO composite. A schematic depicting the influence of essential oils and MgO NPs loading on the gas barrier properties of composites is presented in Fig. 4.7c. The permeability of gases through semi-crystalline polymers is considerably affected by their crystalline phase, which is impermeable to gases (Qin et al., 2017). Besides, the reinforcement of nanofillers can increase the path length of gas molecules, leading to a decrease in gas permeability through composite films (Manikandan et al., 2020). Thus, the enhancement in gas barrier properties of composite

films can be attributed to an increase in crystallinity with the addition of GS and MgO NPs (discussed earlier in Section 4.2.2) and the creation of a tortuous path for gas molecules with the uniform distribution of nanofiller. However, as shown in Fig. 4.7c, at 1 wt% loading of MgO NPs, the gas barrier properties of composite (PHB/5GS/1MgO) films decreased due to a reduction in crystallinity and agglomeration of NPs. It is worth mentioning that the PHB/5GS/0.7MgO composite films developed in this study showed better water vapor barrier properties than PHB/graphene (Manikandan et al., 2020) and PHB/polyethylene glycol/clove essential oil/nano-silica composites (Mittal et al., 2023) reported in the literature.

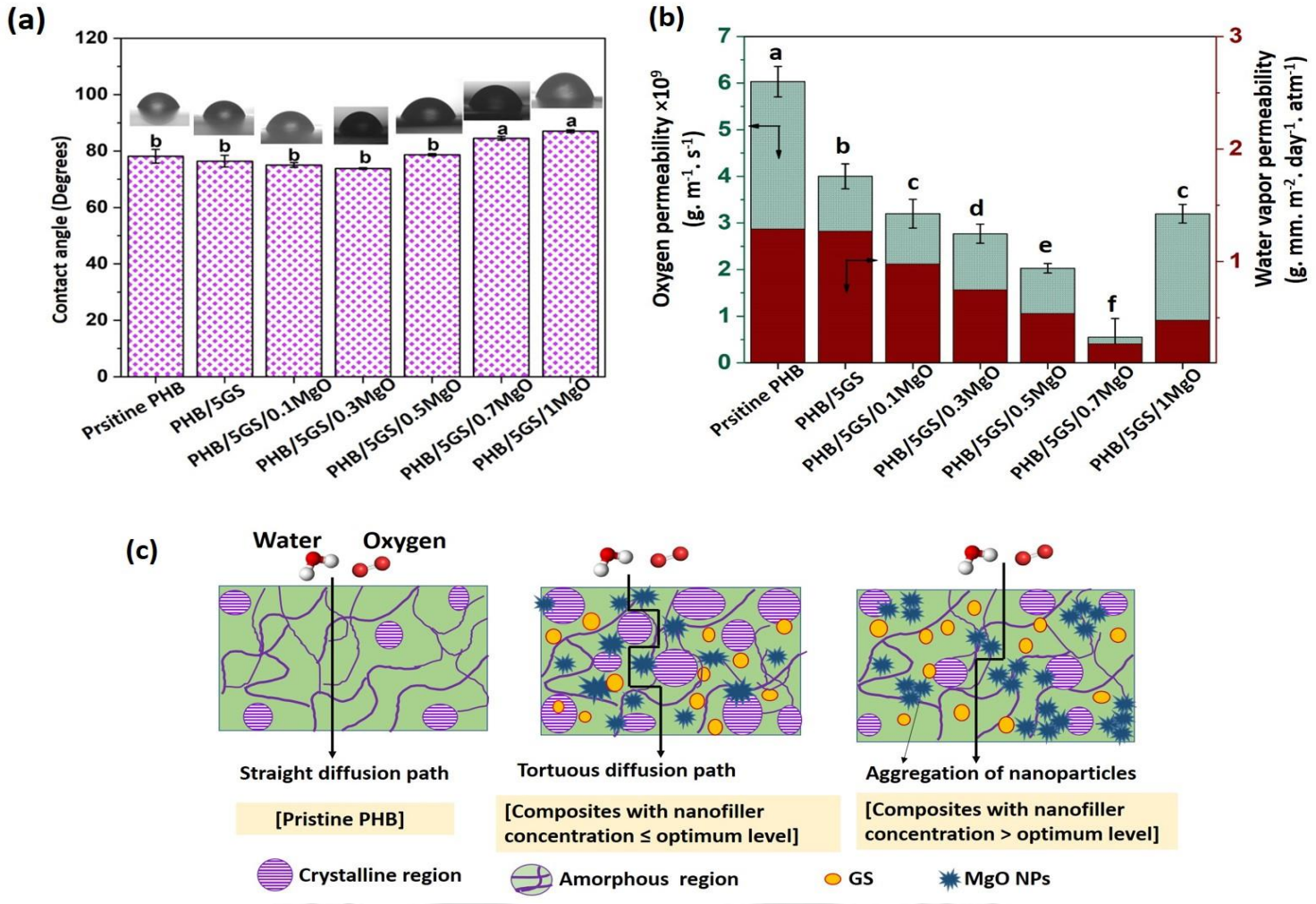

Fig. 4.7. (a) Water contact angle and (b) oxygen and water vapor permeability of various PHB-based films (distinct alphabets above the bars indicate significantly different values, $P < 0.05$), and (c) schematic depicting gas barrier mechanism

4.2.6. Antioxidant and antibacterial activities

The antioxidant property of packaging material holds a crucial role in the shelf-life extension of food by preventing/reducing oxidative deterioration, which otherwise leads to unwanted effects like discoloration, rancidity, and off-flavors in food (Gómez-Estaca et al., 2014). The results of the DPPH radical scavenging assay of various PHB-based films are presented in Fig. 4.8a. Pristine PHB showed a DPPH radical scavenging activity of 2.81±0.70 %, indicating its negligible antioxidant action. Loading of GS induced antioxidant functionality into PHB-based films, and this antioxidant capability was further enhanced with the introduction of MgO NPs, particularly at higher loading rates (Fig. 4.8a). Herein, MgO NPs play a crucial role by transferring electrons from their defect sites to free radicals at the central nitrogen atom of DPPH (Podder et al., 2018; Siripireddy et al., 2017). At the same time, the organic constituents of GS, characterized by conjugated double bonds and hydroxyl groups, contribute by donating electrons and hydrogen atoms (Amorati et al., 2013). This dual mechanism of action effectively reduces oxidative stress, providing a more potent antioxidant effect when both MgO NPs and GS are loaded in the composite films.

Microbial contamination is the primary cause of food spoilage; therefore, the ability to inhibit the proliferation of pathogenic bacteria and prevent bacterial spoilage of food is a desirable functional attribute for food packaging materials. The outcomes of the antibacterial evaluation of pristine and composite films of PHB against *E. coli* and *S. aureus* are depicted in Fig. 4.8b. As expected, pristine PHB showed negligible inhibitory action against the microorganisms tested (Abdelwahab et al., 2018). With the addition of 5 wt% GS, the composite films (PHB/5GS) were endowed with 19.7±0.9 and 61.5±3.4 % inhibitory action against *E. coli* and *S. aureus*, respectively. The antimicrobial activity of GS is attributable to its active constituents, such as decadienal, terpenes, and phenolic compounds (Garavaglia et al., 2016; Trombetta et

al., 2002). Remarkably, the PHB/5GS/0.7MgO and PHB/5GS/1MgO composite films demonstrated complete inhibition of *E. coli* and *S. aureus* growth owing to the synergistic antibacterial action of GS and MgO NPs (Fig. 4.8b). As per the existing literature (Bhattacharya et al., 2021; Varghese et al., 2020; Rajendran et al., 2018; Trombetta et al., 2002), the possible mechanism behind the antibacterial action of composite films loaded with both GS and MgO NPs could be as follows: MgO nanostructures generate reactive oxygen species (ROS) through a photocatalytic process catalyzed by light radiation. The MgO NPs either directly interact with bacteria and lead to cell wall damage followed by ROS generation inside the cell, or first generate ROS outside the cell, followed by entry into the cell via damage to the cell wall. As shown in Fig. 4.8c, in either case, when the MgO NPs, ROS, and GS oil enter the cell, they inhibit bacterial growth by one or more of the following actions: disruption of membrane proteins, enzyme inactivation, depletion of proton motive force, DNA damage, protein denaturation, and leakage of cytoplasmic constituents. Overall, the composite films demonstrated to be more effective against Gram-positive bacteria (*S. aureus*) than Gram-negative bacteria (*E. coli*), owing to the difference in the cell wall structure of these two types of bacteria (Varghese et al., 2020; Nazzaro et al., 2013). Similar observations corresponding to antimicrobial and antioxidant activity were reported in the literature for the combinational loading of rosemary essential oil and ZnO NPs in sodium caseinate (Alizadeh-Sani et al., 1906) and tea tree essential oil and ZnS NPs in a carrageenan/agar blend (Roy and Rhim, 2021b).

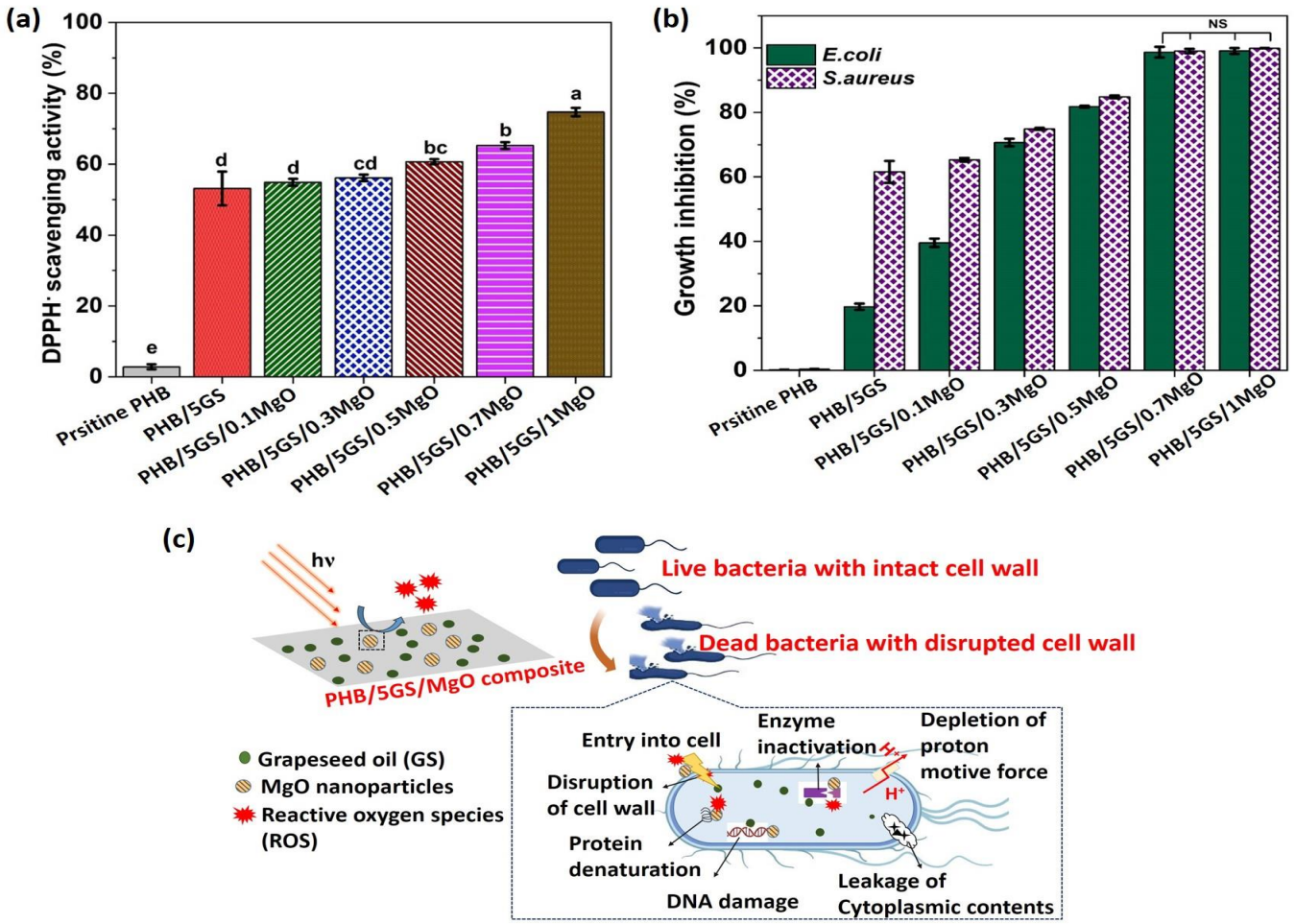

Fig. 4.8. (a) DPPH radical scavenging and (b) antimicrobial activities of pristine and composite films of PHB (distinct alphabets above the bars indicate significantly different values, $P < 0.05$; NS: not significantly different), and (c) possible mechanism of antibacterial action of PHB/5GS/MgO composite films

4.2.7. Contrast over prior arts

There are limited studies on the combinational loading of essential oil and NPs in PHB for food packaging applications. Mittal et al. (2023) developed PHB-based active packaging films incorporating polyethylene glycol as a plasticizer, silica nanoparticles as a reinforcing agent, and clove essential oil as a bioactive agent (Mittal et al., 2023). Wherein, the authors observed that at optimal loading of additives, i.e., 10 wt% polyethylene glycol, 30 wt% clove essential oil, and 1 wt% silica NPs, the TS and EB of the PHB-based films are 17.3 MPa and 10 %, respectively. Nonetheless, in comparison with pristine PHB, water vapor barrier property decreased by 3-fold for these composite films, primarily due to poor interactions between hydrophilic and hydrophobic constituents. In the current study, the PHB-based films with a TS of 27.89 MPa and EB of 14.7 % were obtained with the loading of only GS (5 wt%) and MgO NPs (0.7 wt%) without any additional plasticizer. Moreover, the resulting composite films showed 79 and 90 % higher water vapor and oxygen barrier properties, respectively compared to pristine PHB films.

4.3. Summary

In this work, PHB-based composite films with a 5 wt% loading of GS and varying concentrations (0.1-1 wt.%) of MgO NPs were successfully developed using the sonication-assisted solution casting technique. The combinational loading of GS and MgO NPs improved the crystallinity, TS, EB, and gas barrier characteristics of composite films up to the optimum concentration (0.7 wt%) of nanofiller. The PHB/5GS/0.7MgO films demonstrated 90 and 79 % improvement in oxygen and water vapor barrier properties, respectively, compared to pristine PHB. Moreover, the adverse impact of GS loading on the thermal stability of PHB-based films was partially mitigated with the reinforcement of MgO NPs. In addition, the PHB/5GS/0.7MgO films exhibited good UV-blocking properties, excellent antioxidant activity

(65.25±0.98 %), and complete inhibition of *S. aureus* and *E. coli* growth. Based on the results obtained in this study, it is concluded that PHB/5GS/0.7MgO films could be a great choice for active food packaging applications.

Chapter 5

Application of poly (3-hydroxybutyrate)/grapeseed oil/MgO nanocomposite films for packaging fresh produce

Part of this chapter received the following scientific recognition

Sustainable Chemistry and Pharmacy 41 (2024) 101681

Contents lists available at ScienceDirect

Sustainable Chemistry and Pharmacy

journal homepage: www.elsevier.com/locate/scp

Application of active and environment-friendly poly (3-hydroxybutyrate)/grapeseed oil/MgO nanocomposite packaging for prolonging the shelf-life of cherry tomatoes (*Solanum lycopersicum L. var. cerasiforme*)

Satti Venu Gopala Kumari [a], Kannan Pakshirajan [b], G. Pugazhenthi [a, c, *]

[a] Department of Chemical Engineering, Indian Institute of Technology Guwahati, Guwahati, 781039, Assam, India
[b] Department of Biosciences and Bioengineering, Indian Institute of Technology Guwahati, Guwahati, 781039, Assam, India
[c] Centre for Sustainable Polymers, Indian Institute of Technology Guwahati, Guwahati, 781039, Assam, India

Kumari et al. (2024), Sustainable Chemistry and Pharmacy, 41, 101681

Application of poly (3-hydroxybutyrate)/grapeseed oil/MgO nanocomposite films for packaging fresh produce

Building on the findings from Chapter 4, which revealed that poly (3-hydroxybutyrate) films loaded with 5 wt% grapeseed oil and 0.7 wt% MgO nanoparticles (PHB/5GS/0.7MgO) have optimal characteristics for active food packaging applications, this chapter reports the effectiveness of these nanocomposite films for packaging fresh produce. This chapter is divided into two parts, each discussing the packaging and storage of different types of fresh produce: white button mushrooms (Agaricus bisporus) and cherry tomatoes (Solanum lycopersicum var. cerasiforme).

Part A: Shelf-life studies of white button mushrooms *(Agaricus bisporus)*

5.1. Materials

H_2O_2 and HNO_3 were purchased from Finar Ltd., India. Fresh white button mushrooms (*Agaricus bisporus*) of 30-50 mm cap size (without any pretreatment and absence of damage), polyvinyl chloride films, and polystyrene trays were procured from the local market in Guwahati, Assam, India. Millipore water from the in-house production unit (Millipore, ELix-3, USA) was used for all the experiments.

5.2. Storage of white button mushrooms

Conventionally mushrooms are packaged in rigid plastic trays made of polyethylene terephthalate (PET) or polystyrene (PS) wrapped with polyvinyl chloride (PVC) or other stretchable films (Gholami et al., 2017). Therefore, in this study, storage of white button mushrooms was tested in four different configurations: (i) control (no packaging), (ii) PVC (PS tray sealed with stretchable PVC film), (iii) PHB (PS tray sealed with PHB film), and (iv) PHB/5GS/0.7MgO (PS tray sealed with PHB/5GS/0.7MgO film) at room temperature (~ 25

°C) for 6 days (Fig. 5.1). 12 replicates were included for each storage configuration, and parameters such as weight loss, visual appearance, pH, color, firmness, total soluble solids (TSS), and organoleptic properties were evaluated every 2 days. Furthermore, the extent of migration of MgO NPs from PHB/5GS/0.7MgO films to mushrooms after 6 days of storage at ambient room conditions was evaluated. All the analyses were performed in triplicate and the results were averaged.

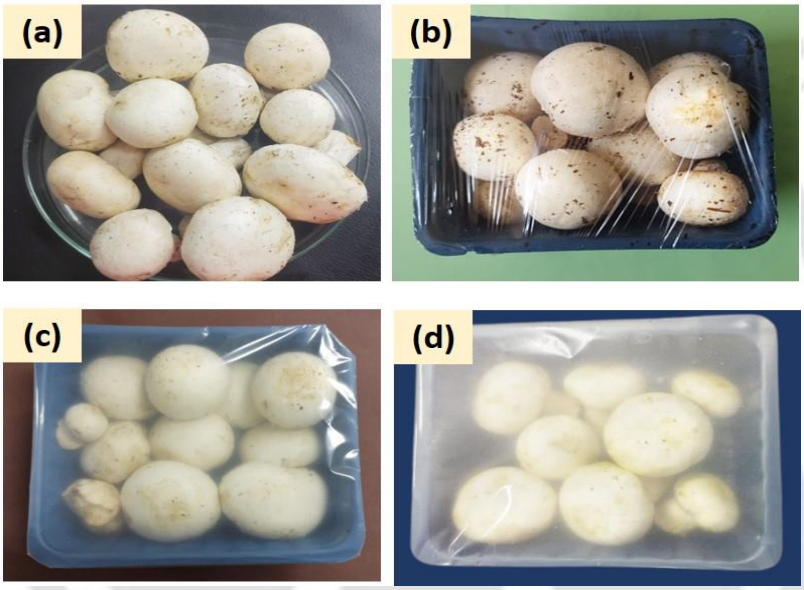

Fig. 5.1. Images depicting storage of white button mushrooms in (a) control, (b) PVC, (c) PHB, and (d) PHB/5GS/0.7MgO configurations

5.2.1. Physicochemical attributes

The weight of mushrooms in different sample groups was measured every 2 days using a digital weighing balance, and the percentage loss of weight relative to the initial weight was calculated. The firmness of mushroom caps was assessed using an ACUCAL penetrometer (ACSY3, India) equipped with an 8 mm diameter cylindrical plunger. Color coordinates (L^*, a*, and b^*) of mushroom caps were measured using a color spectrophotometer (Sensegood, India), and the

percentage browning index (BI) of mushrooms was calculated using Equation (5.1) (Cheng et al., 2019).

$$BI\,(\%) = \left(\frac{y - 0.31}{0.172}\right) \times 100 \qquad (5.1)$$

Where, $y = \frac{1.75L^* + a^*}{a^* - 3.012b^* + 5.645L^*}$

30 g of mushrooms were homogenized in 100 mL of Millipore water, and the resulting juice was filtered using a muslin cloth. Thereafter, the pH and TSS of the filtrate were measured using a pH meter (EUTECH pH meter, India) and a refractometer (ERMA portable refractometer, Brix range: 0-32 %, Japan), respectively.

5.2.2. Organoleptic attributes

The sensory evaluation of mushrooms was conducted by a panel of 5 trained members from the Indian Institute of Technology Guwahati. The panelists were asked to evaluate mushrooms based on four aspects: texture, color, aroma, and overall acceptability, using a Hedonic scale of 9-1 (Lyn et al., 2020; Jafri et al., 2013). Wherein, the scores 9, 8, 7, 6, 5, 4, 3, 2, and 1 correspond to the following levels of preference: extremely like, very much like, moderately like, slightly like, neither like nor dislike, slightly dislike, moderately dislike, very much dislike, and extremely dislike, respectively.

5.2.3. Evaluation of MgO NPs migration

To evaluate the transfer of MgO NPs from the PHB/5GS/0.7MgO packaging configuration to mushrooms packed inside, the concentration of Mg metal in the mushrooms was measured before and after storing for 6 days in PS trays sealed with PHB/5GS/0.7MgO films (Fig. 5.1d). For the analysis, 100 mg of dried mushroom samples were digested with 1 mL of H_2O_2 and 9

mL of HNO_3 in an Ethos Easy advanced microwave digestor. Subsequently, the concentration of Mg metal in the digested samples was determined by an Inductively coupled plasma mass spectrometer (ICPMS) (Agilent, 7850 ICP-MS, USA). For comparison purposes, the concentration of Mg metal in non-packaged mushrooms was measured after 6 days of their storage at ambient room conditions.

5.2.4. Statistical analysis

To determine whether there are significant differences among the means, the data of weight loss, pH, L*, BI, firmness, TSS, and Mg metal concentration of mushrooms, were subjected to statistical analysis. For this purpose, One-way analysis of variance (ANOVA) followed by Tukey's Honest Significance Difference test with a significance level (P) set at 0.05 was performed using Origin™ Pro 9.0 software. All the aforementioned parameters were reported as mean±standard deviation. Moreover, the outcomes of the statistical analysis were appropriately indicated in the respective graphs by asterisk/alphabet labels.

5.3. Results and discussion

5.3.1. Physicochemical properties

The effect of different storage configurations on weight loss, firmness, L*, BI, and TSS of mushrooms is presented in Fig. 5.2. Furthermore, the visual appearance of mushrooms during the different storage stages is displayed in Fig. 5.3. Weight loss is one of the primary factors in mushrooms degradation, causing detrimental effects such as tissue shrinkage. As per the existing literature (Gholami et al., 2017), weight loss greater than 5 % is considered unacceptable for the marketing of mushrooms. In all the storage configurations tested in this study, the weight loss of mushrooms continuously increased with time (Fig. 5.2a). A maximum of 49.1±1.65 % weight loss in 6 days was observed for the mushrooms stored in the control group, owing to the fact that the thin epidermal structure of mushrooms cannot prevent their

quick superficial dehydration and high transpiration (Liu et al., 2019). Consequently, serious surface wrinkling and shrinkage with an increase in storage duration were noticed for mushrooms stored in the control group (Fig. 5.3). Based on weight loss measurements, the mushrooms stored in the control group were found to be unacceptable at 2 days of storage, whereas the mushrooms stored in the PVC and PHB packaging groups were unacceptable at 4 days of storage. In contrast, the PHB/5GS/0.7MgO films improved the storage conditions of the mushrooms maintaining their weight loss below 5 % even on day 6. The possible reason for the result is lower water vapor permeability through PHB/5GS/0.7MgO (0.27 g. mm.m^{-2} day^{-1} atm^{-1}) than PHB (1.29 g. mm.m^{-2} day^{-1} atm^{-1}) and PVC (1.62 g. mm.m^{-2} day^{-1} atm^{-1}) films (Gholami et al., 2017). Texture is another critical factor that impacts consumer satisfaction with mushrooms. The texture quality of mushrooms can be assessed by measuring their firmness; a higher firmness indicates a better texture quality of mushrooms (Liu et al., 2019; Gholami et al., 2017). It can be seen from Fig. 5.2b that the mushrooms stored in the PHB/5GS/0.7MgO packaging configuration were significantly ($P < 0.05$) firmer than mushrooms stored in other configurations such as control, PVC, and PHB for the same storage duration. As reported in the literature (Yu et al., 2022), weight loss due to dehydration and transpiration, cell wall degradation, and chemical changes in intracellular components by microbial attack contribute to the reduction in the firmness of mushrooms. Therefore, the lowest reduction (from 14.8±0.39 N on day 0 to 13.89±0.20 N on day 6) of firmness for mushrooms stored in the PHB/5GS/0.7MgO packaging configuration can be attributed to their low WVTR and excellent antimicrobial and antioxidant activities.

The browning of mushrooms, which is often caused by enzyme oxidation, aging, and microbial growth, is a major post-harvest burden for their commercialization, as it not only reduces their nutritional value and shortens shelf-life but also influences customer acceptance (Liu et al.,

2019). Hence, L^* and BI are considered two crucial parameters for evaluating the freshness of mushrooms. As per the literature (Gholami et al., 2017), the quality of mushrooms is considered good if $L^* > 86$ and fair if $80 < L^* < 85$. Compared to mushrooms stored in the control group, a notable increase in BI and a decrease in L* were noticed for mushrooms stored in PVC and PHB packaging configurations from the 4th day of storage (Figs. 5.2c and 5.2d). This is due to dew condensation and the high-humidity internal environment in these packages, resulting in rapid microbial growth and the appearance of dark spots on the mushroom surface, which can be seen in Fig. 5.3. In contrast, even though PHB/5GS/0.7MgO showed higher water vapor barrier property than PVC and PHB packages, the mushrooms still maintained an acceptable visual appearance with a low browning degree and fair quality (L* > 86) at day 6 owing to the excellent antioxidant and antibacterial activities of the PHB/5GS/0.7MgO films that prevent bacterial attack and enzymatic decomposition of the mushrooms (Qu et al., 2020). Yu et al. (2022) observed a similar outcome concerning slowing down the browning of mushrooms stored in antimicrobial packaging based on chitosan and carboxymethyl cellulose for 6 days at ambient conditions (Yu et al., 2022).

TSS indicates the amount of total soluble sugars that influence the taste, texture, and overall quality of mushrooms. A pronounced increase in TSS with storage time was observed for the mushrooms stored in control, PVC, and PHB configurations (Fig. 5.2e). This could be due to the high respiration rate, moisture loss, senescence, and solubilization of cell wall polysaccharides and hemicellulose present in mushrooms stored in these groups, as akin to results reported in the literature (Han et al., 2015). During 6 days of storage, no significant variation in TSS was observed for the mushrooms stored in PHB/5GS/0.7MgO packaging configuration. According to existing literature (Gholami et al., 2023; Plețoianu and Nour, 2022), this can be attributed to reduced moisture losses, lower senescence, and low respiration

of mushrooms in this group owing to changes in the internal environment in the packaging. The pH of fresh mushrooms was in the range of 6.59-6.67. As reported in Fig. 5.2f, in control, PVC, and PHB storage configurations, the slight reduction in pH of mushrooms with increasing storage duration was possibly due to the growth of microorganisms and the production of organic acids, as reported by other authors (Lyn et al., 2020; Oliveira et al., 2012).

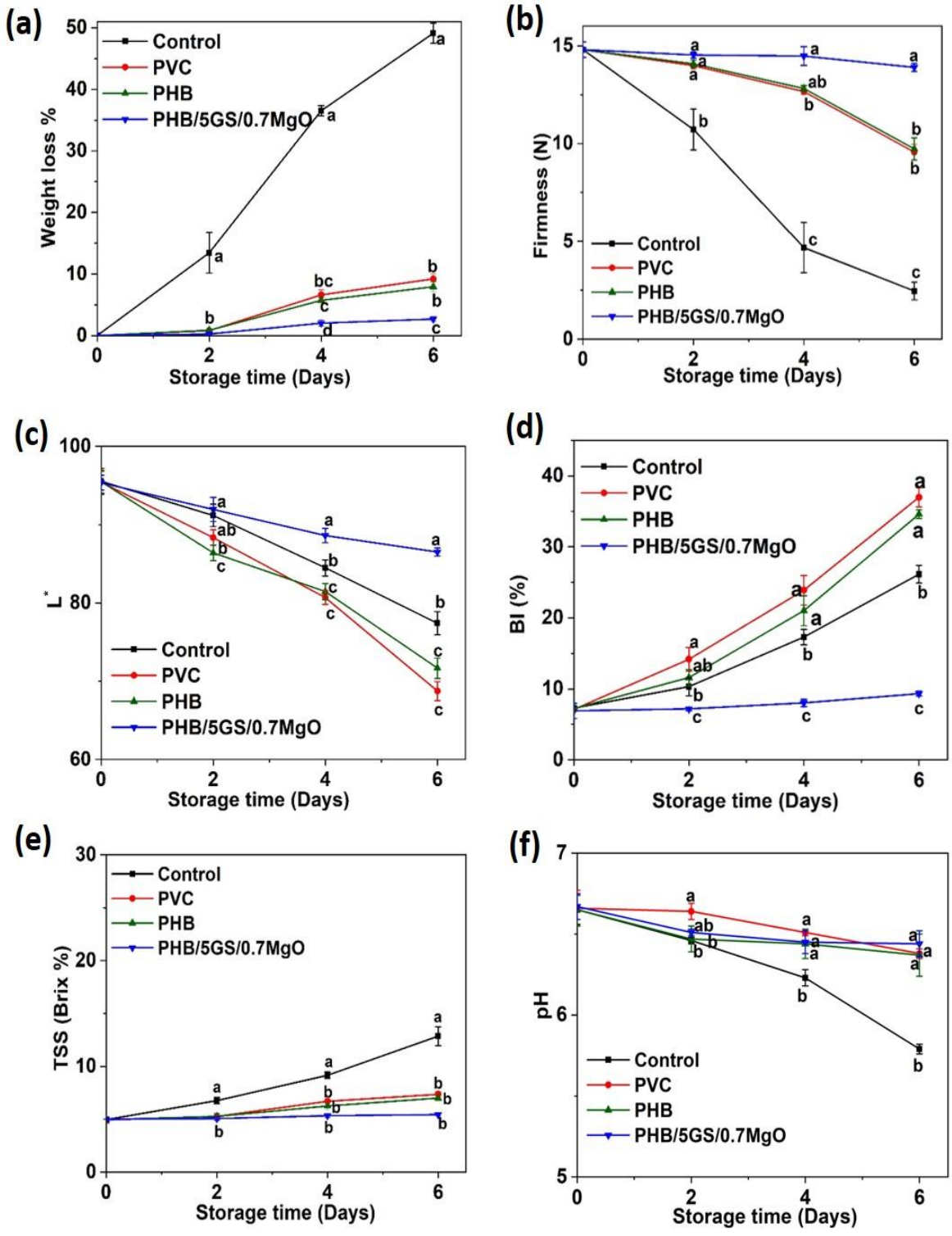

Fig. 5.2. Effect of different storage configurations on (a) weight loss, (b) firmness, (c) L*, (d) BI, (e) TSS, and (f) pH of mushrooms (distinct alphabets denote statistically significant ($P < 0.05$) variations among data associated with different storage

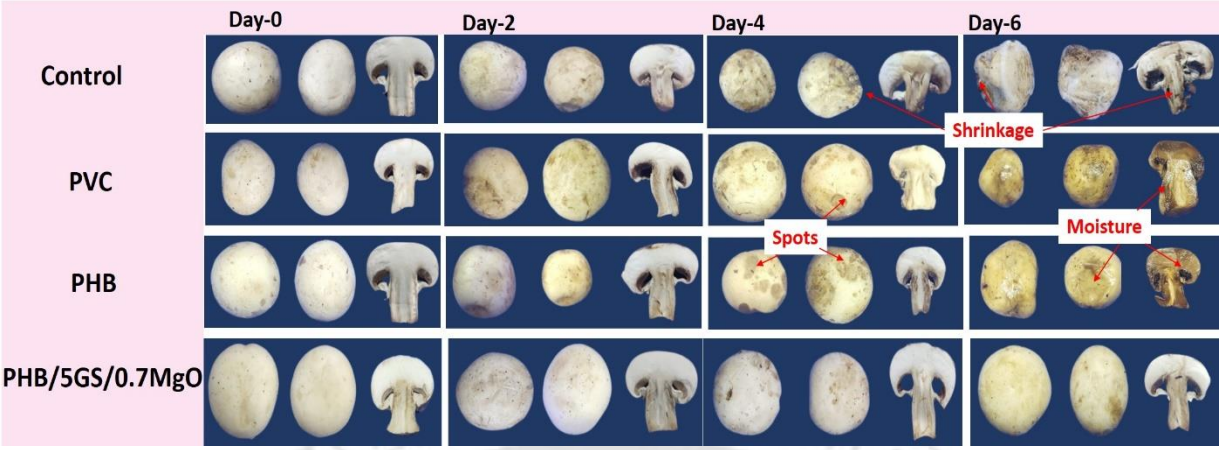

Fig. 5.3. Effect of various storage configurations on the physical appearance of mushrooms

5.3.2. Sensory attributes

Fig. 5.4 shows the sensory scores based on a hedonic scale (1-9) for the texture, color, aroma, and overall acceptability of mushrooms stored in various configurations. In this sensory analysis, a score of 5 was considered a threshold value, and any value below that was deemed unsatisfactory by the consumers. On day 0, fresh mushrooms scored 8.8 out of 9 based on their color acceptance (Fig. 5.4a). Interestingly, the mushrooms stored in the PHB/5GS/0.7MgO configuration maintained a color acceptance score above 5 even after 6 days of storage. In contrast, the mushrooms stored in control, PHB, and PVC configurations exhibited color acceptance scores below 5 by day 4. Regarding texture, the panels' acceptance score for fresh mushrooms was 8.6 on day 0, while it was 8 on day 6 for mushrooms stored in PHB/5GS/0.7MgO configuration (Fig. 5.4b). However, throughout their course of storage, mushrooms stored in the PHB/5GS/0.7MgO configuration scored the highest acceptance score for texture compared to all the other samples. Nonetheless, the acceptance scores for texture dropped below 5 for mushrooms in the control group on day 2 as well as for those stored in the PHB and PVC configurations on day 4. The acceptance scores for aroma and overall acceptability of mushrooms followed a similar trend as the acceptance scores for texture

discussed above (Figs. 5.4c and 5.4d). Hence, mushrooms stored in PHB/5GS/0.7MgO configurations ended up scoring the highest score for overall acceptance, color, aroma, and texture compared to all other samples during their 6 days of storage at ambient room conditions.

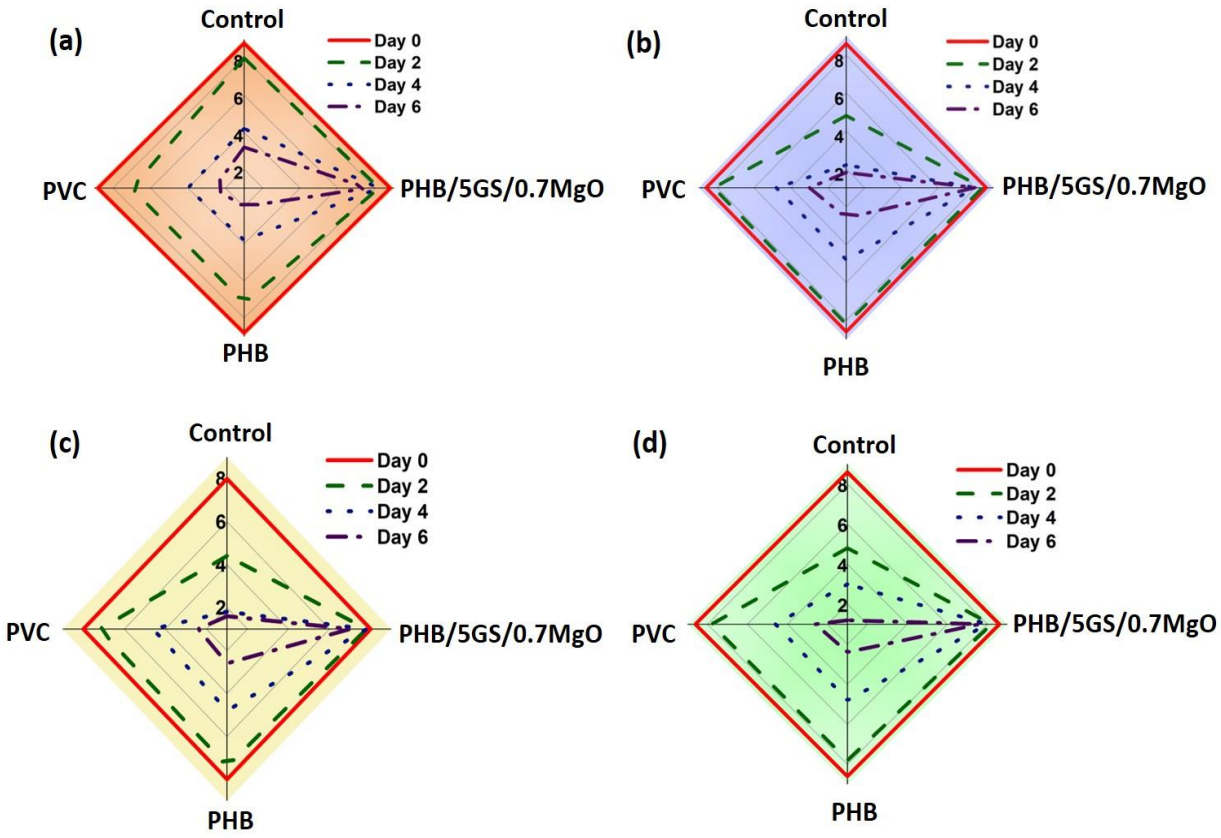

Fig. 5.4. Sensory scores for (a) color, (b) texture, (c) aroma, and (d) overall acceptability of mushrooms stored in various configurations

5.3.3. Migration of MgO NPs from nanocomposite films to mushrooms

The increasing popularity of nanotechnology in the development of novel active food packaging materials is accompanied by worries regarding the potential leaching of NPs from packaging to foodstuffs. In the event that the NPs migrate from packaging to food, they enter the human body upon consumption of food and potentially lead to health problems (Heydari-Majd et al., 2019). So, it is crucial to develop nanocomposite packaging materials with zero or

low possibility of NP transfer to food. In general, mushrooms bio-accumulate essential minerals such as Na, Fe, Mg, Ca, Zn, and K from the environment during their growth (Mallikarjuna et al., 2012). The concentration of Mg metal in fresh mushrooms (day 0) was found to be 25.32±1.5 mg/100 g of dry weight. Whereas, the concentration of Mg metal in mushrooms after 6 days of storage in unpackaged and packaged (PS tray sealed with PHB/5GS/0.7MgO films) conditions was 25.33±0.4 and 25.32±2.40 mg/100 g of dry weight, respectively. Statistical analysis confirmed that the concentration of Mg metal in mushrooms packaged using nanocomposite films was not significantly ($P > 0.05$) different from concentration of Mg in fresh (day 0) and unpackaged (day 6) mushrooms. Thus, the developed nanocomposite films can be considered safe for the packaging of mushrooms.

5.3.4. Contrast over prior arts

In Table 5.1, the impact of PHB/5GS/0.7MgO nanocomposites on the shelf-life of mushrooms was compared with various polymer-based active packaging and edible coating storage methods reported in the literature. From Table 5.1, it is evident that irrespective of storage technique, the mushrooms stored at lower temperatures had a higher shelf-life than mushrooms stored at ambient conditions due to the reduction in the biochemical reaction rates. However, the cold storage of mushrooms raises warehouse and energy consumption costs (Mohebbi et al., 2012). Among the studies performed at ambient conditions, the PHB/5GS/0.7MgO endowed a greater shelf-life for mushrooms than cellulose paper coated with wheat gluten (Guillaume et al., 2010) and apple peel powder/carboxymethyl cellulose/tartaric acid/glycerol monostearate composite coating (Thakur et al., 2021). Though the shelf-life of mushrooms was the same (6 days) with chitosan/dopamine-grafted carboxymethyl cellulose bag and PHB/5GS/0.7MgO packaging configurations, the latter showed better tensile properties, which is important for the protection of food products during handling and transportation. As

previously mentioned in Section 5.2, conventionally, mushrooms are packaged in rigid PS or PET trays sealed with stretchable materials such as PVC. The focus of the current study was restricted to the substitution of the non-renewable and non-biodegradable PVC films utilized in mushroom packaging with an active PHB/5GS/0.7MgO composite. Hence, future research endeavors should aim to substitute PS or PET trays with environmentally friendly materials, thus further advancing the sustainability of mushroom packaging.

Table 5.1. Comparison of literature on the shelf-life studies of mushrooms employing active packaging and edible coatings

Food product	Storage technique	Storage conditions	Shelf-life (days)	Reference
White button mushrooms	Commercial PS tray sealed with PHB/5GS/0.7MgO films	Ambient conditions (~ 25 °C)	6	Current study
White button mushrooms	Glass jar sealed with cellulose paper coated with wheat gluten	Modified atmosphere, 20 °C and 80 % RH	3	Guillaume et al., 2010
White button mushrooms	Coated with solution of apple peel powder, carboxy methyl cellulose, tartaric acid, and glycerol monostearate and stored in LDPE bags	Ambient conditions (~ 24 °C)	5	Thakur et al., 2021
White button mushrooms	Paper bag composed of chitosan and dopamine-grafted carboxymethyl cellulose	Ambient conditions (~ 25 °C)	6	Yu et al., 2022
White button mushrooms	Coating with aloe vera and gum tragacanth	10 °C	10	Mohebbi et al., 2012
White button mushrooms	Plastic box sealed with gallic acid grafted chitosan films	4 ± 1 °C	12	Liu et al., 2019
Oyster mushrooms	Pouches made of polyethylene coated with gelatine and pomegranate peel powder composite	Modified atmosphere and 4 ± 1 °C	11	Lyn et al., 2020
White button mushrooms	Coated with tragacanth gum incorporated with *Satureja khuzistanica* essential oil and stored in HDPE containers	4 ± 1 °C and 95 % RH	16	Nasiri et al., 2018

GS: Grapeseed oil; HDPE: High-density polyethylene; LDPE: Low-density polyethylene; PHB: Poly (3-hydroxybutyrate); PVC: Polyvinyl chloride; PS: Polystyrene; RH: Relative humidity

Part B: Shelf-life studies of cherry tomatoes (*Solanum lycopersicum var. cerasiforme*)

5.4. Materials

Low-density polyethylene pouches were purchased from Sun's Rider Enterprise, India. Cherry tomatoes *(Solanum lycopersicum var. cerasiforme)* with good physical appearance, with no pre-treatment and no visual signs of contamination were procured from a local market in Guwahati, Assam. India. H_2O_2 and HNO_3 were supplied by Finar Ltd., India.

5.5. Storage of cherry tomatoes (*Solanum lycopersicum var. cerasiforme*)

The conventional packaging method for cherry tomatoes involves the use of environmentally detrimental petroleum-based non-biodegradable plastics such as LDPE, PVC, and polypropylene (García-García et al., 2013). Therefore, in the current study, storage of cherry tomatoes was tested in the following four configurations: (i) control (no packaging), (ii) LDPE packaging, (iii) PHB packaging, and (iv) PHB/5GS/0.7MgO packaging at ambient room conditions (~25 ℃) for 23 days. Prior to packaging, the cherry tomatoes were rinsed with tap water and dried gently with clean tissue paper. Then, as shown in Fig. 5.5, the packaging pouches (12 cm× 9 cm) each accommodating 8 cherry tomatoes were prepared by heat sealing under an air atmosphere, similar to the study reported in the literature (Kaewklin et al., 2018). The average thickness of LDPE, PHB, and PHB/5GS/0.7MgO films used for packaging cherry tomatoes is 0.03 mm. The characteristics such as visual appearance, weight loss, TSS, firmness, titratable acidity (TA), color, pH, ripening index, and organoleptic properties of the cherry tomatoes were evaluated every 3 days for 23 days. In addition, the migration of MgO NPs from the nanocomposite packaging to cherry tomatoes was assessed after 23 days of their storage in nanocomposite packaging. All the aforementioned analyses were conducted in triplicate, and the results were reported as mean values accompanied by their corresponding standard deviations.

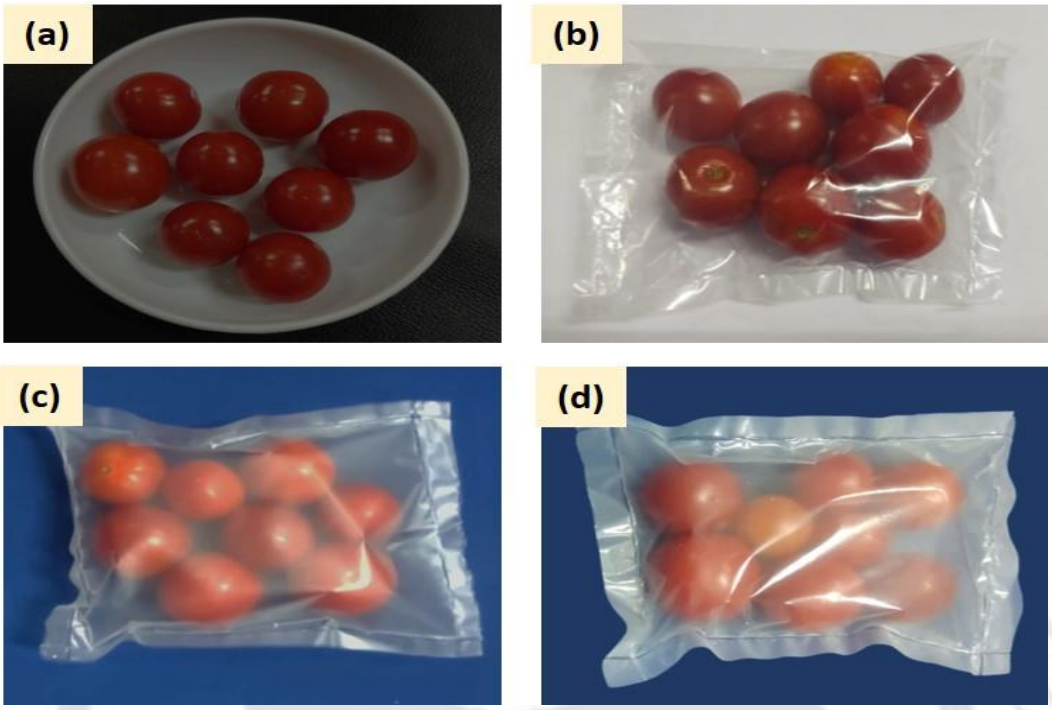

Fig. 5.5. Images showing the storage of cherry tomatoes in (a) control, (b) LDPE packaging, (c) PHB packaging, and (d) PHB/5GS/0.7MgO packaging

5.5.1. Physicochemical properties

5.5.1.1. Weight loss

The weight of cherry tomatoes in each of the storage configurations was measured every 3 days by a digital weighing balance (accuracy: ±0.1 mg). Thereafter, the percentage loss of weight of the samples was determined using Equation (5.2) (Aragüez et al., 2020).

$$Weight\,loss(\%) = \frac{W_i - W_t}{W_i} \times 100 \qquad (5.2)$$

Wherein, W_i refers to initial weight (g) and W_t refers to weight (g) at a specific time of storage.

5.5.1.2. Firmness and color

The firmness of cherry tomatoes at various stages of storage was determined using a penetrometer (ACUCAL penetrometer, ACSY3, India). This test was characterized by measuring the force (N) required for penetration of an 8 mm diameter stainless steel probe to a

depth of 10 mm into the samples. Five samples were measured from each of the storage configurations at a specific time, and average results were presented.

The color parameters, namely L* (dark/light), a* (red/green), and b* (yellow/blue), of cherry tomatoes were determined using the Sensegood™ color spectrophotometer, India. As recommended in the literature (Yun et al., 2015; García-García et al., 2013), the maturity of cherry tomatoes was assessed by a*/b* values.

5.5.1.3. Titratable acidity (TA) and pH

Firstly, cherry tomatoes were homogenized, and the resulting juice underwent filtration with the use of muslin cloth. Subsequently, a known volume of the juice was titrated against 0.1 N NaOH, employing phenolphthalein indicator. Herein, the appearance of a light pink color was considered the endpoint for the test, and the TA of the samples was determined using Equation (5.3) (Gharezi and Gharezi, 2012).

$$TA(\%) = \frac{V_t}{V_s} \times N \times M_{eq} \times 100 \qquad (5.3)$$

Herein, M_{eq} is the equivalent weight of citric acid, N is the normality of NaOH, and V_t and V_s are the volume (mL) of titrate and test samples, respectively. The pH of homogenized cherry tomatoes was assessed by a pH meter (EUTECH, India).

5.5.1.4. Total soluble solids (TSS) and ripening index

The TSS of homogenized cherry tomatoes was measured using a portable refractometer (ERMA, India). Furthermore, the ripening index of the cherry tomatoes was calculated using Equation (5.4) (Qubbaj and Daraghmah, 2023).

$$Ripening\ index = \frac{TSS}{TA} \qquad (5.4)$$

Herein, TSS denotes total soluble solids in Brix % and TA refers to titratable acidity in percentage.

5.5.2. Organoleptic properties

The analysis of the organoleptic properties of the cherry tomatoes was conducted by a panel of five trained members from the Indian Institute of Technology Guwahati. Each judge was instructed to rate the cherry tomatoes for aroma, color, texture, taste, and overall acceptability using a Hedonic scale ranging from 1 to 9 representing extreme dislike to extreme like conditions, as detailed earlier in Section 5.2.2.

5.5.3. Assessment of migration of MgO NPs to cherry tomatoes

To assess the migration of MgO NPs from the nanocomposite packaging to cherry tomatoes, the concentration of Mg metal in the cherry tomatoes was measured before and after storing them for 23 days in the PHB/5GS/0.7MgO pouches. For comparative analysis, the concentration of Mg metal in non-packaged cherry tomatoes was measured after 23 days of their storage at ambient room conditions. For this assessment, 100 mg of dried cherry tomato samples were digested with 9 mL of HNO_3 and 1 mL of H_2O_2 in a microwave digestor (Ethos Easy, USA). Thereafter, Mg metal concentration in the digested samples was measured using Agilent, 7850 ICP-MS, Inductively coupled plasma mass spectrometer, USA.

5.5.4. Statistical analysis

The results from the shelf-life study of cherry tomatoes, such as firmness, weight loss, TSS, color, TA, pH, ripening index, and Mg concentration, were subjected to statistical analysis to assess the statistical significance of the difference between mean values. The evaluations were carried out in Origin™ Pro 9.0 software by one-way analysis of variance (ANOVA) and Tukey's Honest Significance Difference Test with a significance level (P) fixed at 0.05. The results of the

statistical analysis were indicated in their respective figures using alphabet labels, and the corresponding explanations are provided in the captions of the figures.

5.6. Results and discussion

5.6.1. Weight loss and visual appearance

Reduction in weight stands as a pivotal factor and induces shriveling and wilting in agricultural products such as cherry tomatoes, leading to the deterioration of their quality and a subsequent decrease in their commercial value (Kumar et al., 2020). Water is the major constituent of cherry tomatoes, and it plays a crucial role in maintaining their cell turgor in both the growth and postharvest stages, safeguarding their texture and appearance (Yun et al., 2015). The influence of different storage configurations on the weight loss of cherry tomatoes is depicted in Fig. 5.6. In addition, the visual appearance of the cherry tomatoes across various stages of storage is shown in Fig. 5.7. Microbial contamination of cherry tomatoes in this study was examined by visual changes in the form of dark spots, bruises or any unwanted color changes due to bacterial growth and proliferation. Similarly, in case of fungal contamination, the appearance of fungal spores or mycelia was followed (Rizwana et al., 2021; Tournas et al., 2005). However, the precise determination of contamination bacteria or fungi is still necessary to ascertain their role in affecting the physical and other attributes of cherry tomatoes.

As expected, regardless of the type of storage configuration, an increase in the weight loss of cherry tomatoes was noticed with an increase in the storage duration (Fig. 5.6). As mentioned in the literature (Gharezi and Gharezi, 2012), the primary factor for weight loss in cherry tomatoes is the loss of water molecules during their transpiration and respiration processes. Furthermore, respiration contributes to weight reduction as each absorbed oxygen molecule is converted into a carbon dioxide molecule which then gets released into the atmosphere, resulting in the depletion of a carbon atom from the fruit. Notably, the highest weight loss of 38.60±1.60 % in

23 days was noticed for cherry tomatoes in the control configuration due to absence of any packaging material as a barrier for moisture loss, resulting in serious shriveling and a loss of freshness, as can be seen from Fig. 5.7. On day 15 of storage, juice leakage and microbial growth were observed for cherry tomatoes stored in LDPE and PHB packages (Fig. 5.7). In contrast, cherry tomatoes packaged in PHB/5GS/0.7MgO pouches showed no signs of putridity, microbial growth, or juice leakage and maintained glossy appearance for 21 days. Nevertheless, microbial growth was observed in the cherry tomatoes stored in the PHB/5GS/0.7MgO packaging on day 23 (Fig. 5.7). Hence, considering the results of visual appearance and the absence of microbial contamination, the use of PHB/5GS/0.7MgO packaging is deemed effective in extending the shelf-life of cherry tomatoes up to 21 days. Moreover, PHB/5GS/0.7MgO packaging provided more favorable storage conditions for cherry tomatoes in comparison to LDPE and PHB packages, resulting in minimal weight loss of cherry tomatoes, measuring 4.45± 0.06 % on day 21 (Fig. 5.6). The lower water vapor permeability through PHB/5GS/0.7MgO (0.27 g. mm.m^{-2} day^{-1} atm^{-1}) films than the LDPE (0.41 g. mm.m^{-2} day^{-1} atm^{-1}) and PHB (1.29 g. mm.m^{-2} day^{-1} atm^{-1}) films could be one potential factor contributing to the aforementioned observation (Paulsen et al., 2022). Similar findings corresponding to the better retention of the weight of cherry tomatoes using chitosan/alginate/TiO_2 (Perera et al., 2022) and β-cyclodextrin/cinnamaldehyde/chitin/polyvinyl alcohol (Qian et al., 2022) active packaging were reported in the literature.

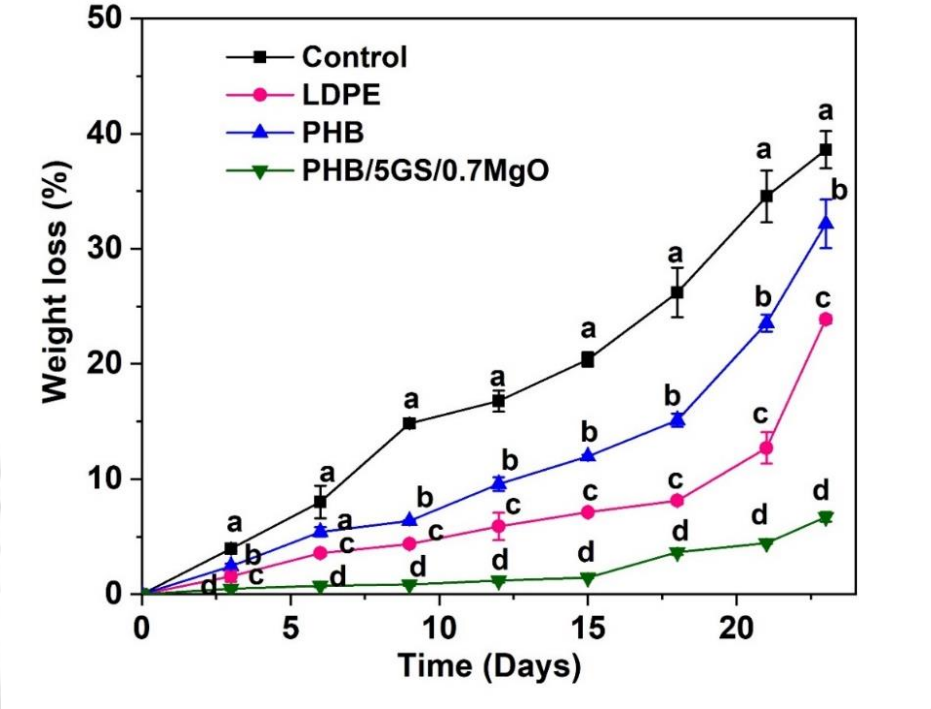

Fig. 5.6. Influence of different storage configurations on the weight loss of cherry tomatoes (Distinct letters indicate statistically significant ($P < 0.05$) differences in data among various configurations at same storage time)

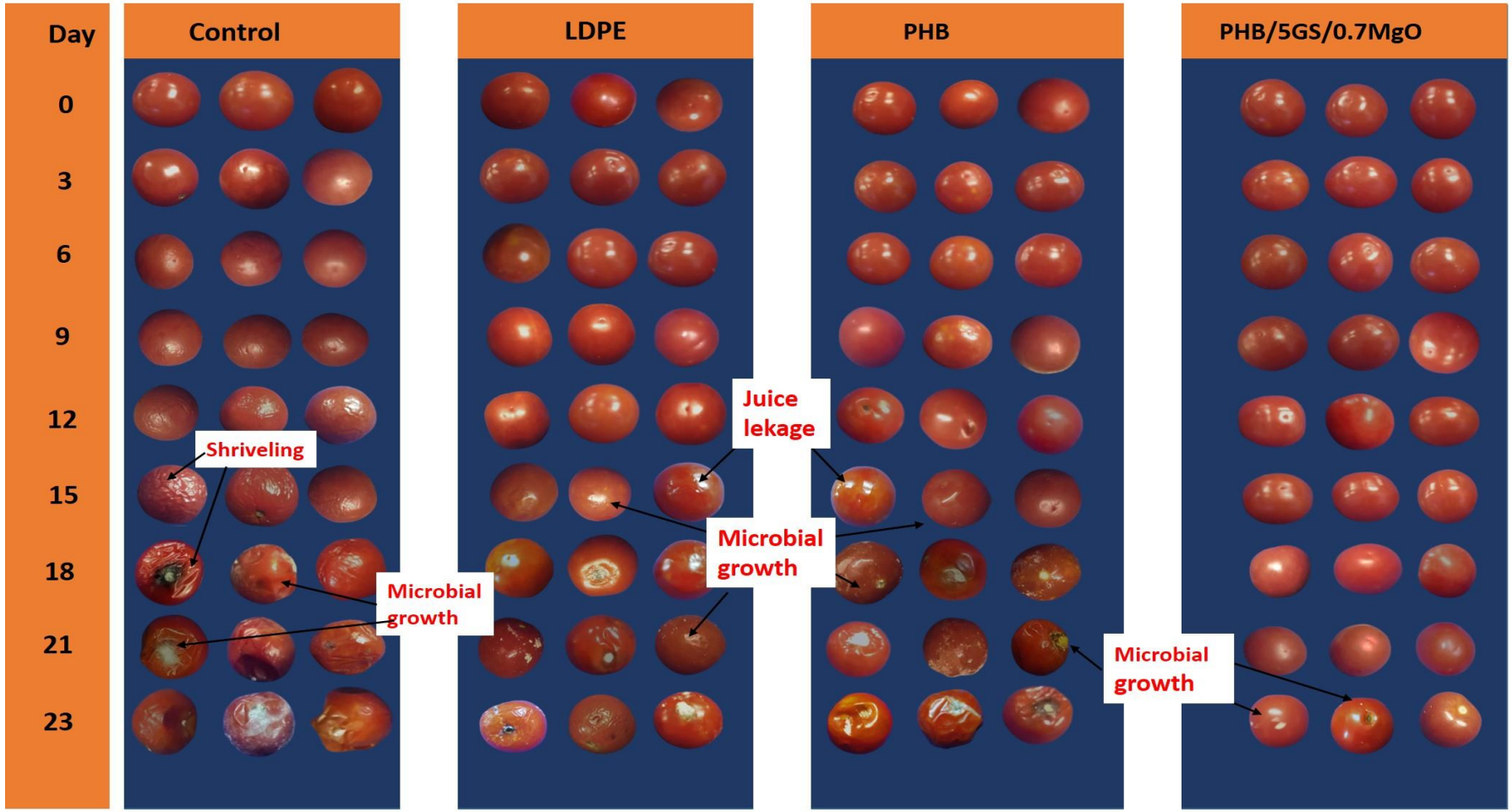

Fig. 5.7. Influence of different storage configurations on the visual appearance of cherry tomatoes

5.6.2. Firmness

Firmness serves as a reliable indicator of the texture quality and mouthfeel of fruits and vegetables, and generally, a higher firmness of cherry tomatoes indicates better texture quality, and vice versa (Yun et al., 2015). The influence of various storage configurations on the firmness of cherry tomatoes is presented in Fig. 5.8. The results revealed a drastic reduction in the firmness of cherry tomatoes stored in control, LDPE, and PHB packaging configurations with an increase in storage duration (Fig. 5.8). By the end of the storage period (day 23), the cherry tomatoes in the aforementioned storage configurations were completely rotten, with almost a 94 % reduction in firmness compared to fresh samples. The decrease in fruit firmness is a result of various factors, including weight loss through transpiration and respiration, as well as the deterioration of cell wall composition, cell structure, and intracellular materials due to microbial activity and/or the action of cell wall-degrading enzymes like glucanases, polygalacturonase, and pectin-methylesterase (Sganzerla et al., 2021; Kumar et al., 2020),. Contrarily, cherry tomatoes stored in PHB/5GS/0.7MgO packaging displayed markedly greater firmness in comparison to those in other storage configurations at the same time point. The minimal decrease in firmness (from 19.89±0.12 N on day 0 to 15.77±0.37 and 14.94±0.27 N on days 21 and 23, respectively) of cherry tomatoes packaged using PHB/5GS/0.7MgO films is due to the effective water vapor barrier, antioxidant, and antimicrobial characteristics of the nanocomposite material. A similar protective effect of such active packaging materials against the softening of cherry tomatoes has been reported in the literature (Aragüez et al., 2020; Buendía et al., 2019).

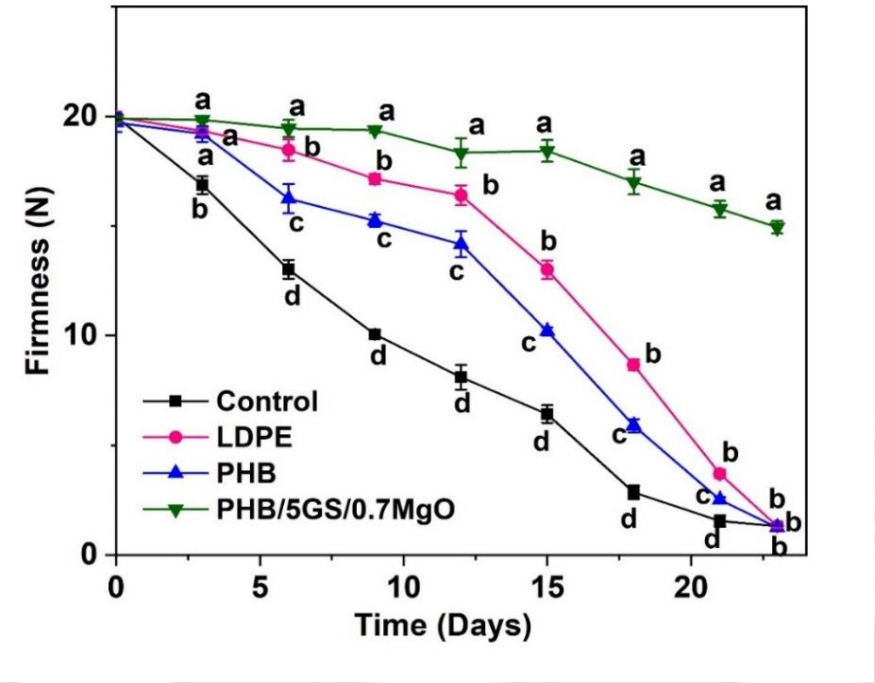

Fig. 5.8. Influence of different storage configurations on the firmness of cherry tomatoes (Distinct letters indicate statistically significant ($P < 0.05$) differences in data among various configurations at same storage time)

5.6.3. Total soluble solids (TSS)

TSS, encompassing sugar content and soluble minerals in fruits and vegetables, has a pronounced impact on the flavor and texture of these agricultural products. Therefore, TSS is widely acknowledged as a vital indicator of the quality of fruits and vegetables (Sharma et al., 2022). As per the literature (Aragüez et al., 2020), the market requirement for the TSS of cherry tomatoes ranges from 5.5 to 9.5 Brix %. In general, the TSS of fruits rises as they ripen and undergo deterioration due to the breakdown of polysaccharides into simple sugars. Hence, if the TSS value of the fruit sample was close to that of fresh ones, it implies better retention of their quality. The influence of various storage configurations on the TSS of cherry tomatoes is shown in Fig. 5.9. The TSS of fresh cherry tomatoes was around 5.8 Brix %. It can be seen from Fig. 5.9 that a pronounced increase in TSS values over the storage duration is evident in

the case of cherry tomatoes stored in the control group, followed by those in PHB and LDPE packages, respectively. As mentioned in the literature (Aragüez et al., 2020; García-García et al., 2013), the increase in TSS is attributed to moisture loss and the breakdown of polysaccharides into simple sugars in cherry tomatoes over time. Based on the TSS results, cherry tomatoes in the control group were unacceptable on day 12, whereas those in the LDPE and PHB packages were unacceptable on day 18 and day 15, respectively. In contrast, cherry tomatoes stored in PHB/5GS/0.7MgO packaging maintained their TSS levels close to those of fresh samples and remained within the acceptable market requirements throughout the storage period tested (Fig. 5.9). This could be due to minimal moisture loss, reduced deterioration due to the antioxidant and antimicrobial properties of the active films, and a lower respiration rate in the cherry tomatoes resulting from alterations in the internal packaging environment, facilitated by the excellent oxygen and water vapor barrier properties of the films. The antioxidant activity of the packaging material prevents the oxidative degradation of bioactive constituents, such as vitamins, carotenoids, and polyphenols present in cherry tomatoes, thereby prolonging their shelf-life. Moreover, due to its antimicrobial activity, the PHB-based nanocomposite prevented the spoilage of cherry tomatoes by inhibiting the growth of contaminating microorganisms. Hence, both antioxidant and antimicrobial activities of the nanocomposite (PHB/5GS/0.7MgO) packaging material aided in prolonging the shelf-life of cherry tomatoes (Sganzerla et al., 2021). The composition of GS (please see Table 3.1) reveals the presence of bioactive constituents, particularly the decadienal, terpenes, and phenolic compounds, present in the GS which contributes to its antioxidant and antimicrobial properties (Garavaglia et al., 2016; Trombetta et al., 2002). Both these properties of GS aided in maintaining TSS and extending the shelf-life of cherry tomatoes packed inside the PHB-based nanocomposite material. Aragüez et al. (2020) and Kumar et al. (2020) reported comparable results, demonstrating the diminished change in the TSS of cherry tomatoes packaged with

triticale/$KMnO_4$ and pectin/$Mg(OH)_2$ composite films, respectively (Aragüez et al., 2020; Kumar et al., 2020).

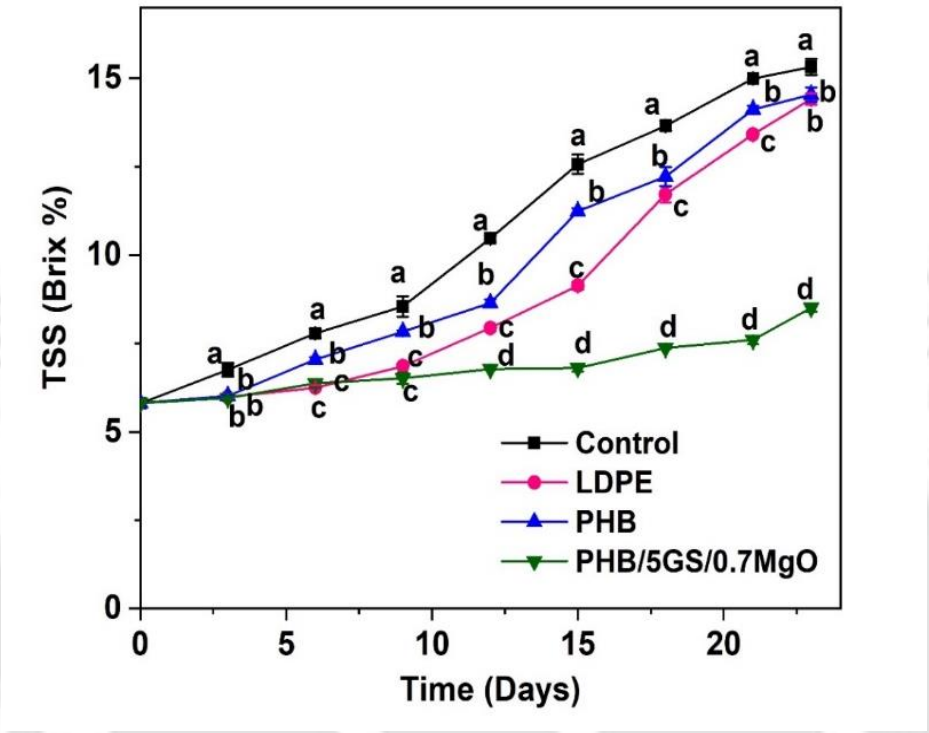

Fig. 5.9. Influence of different storage configurations on the TSS of cherry tomatoes (Distinct letters indicate statistically significant ($P < 0.05$) differences in data among various configurations at same storage time)

5.6.4. Titratable acidity (TA), pH, and ripening index

The characteristic sweet-sour flavor of cherry tomatoes is the result of complex interplay among its constituents, such as sugars, organic acids, amino acids, and salts (Riahi et al., 2023). Figs. 5.10a and 5.10b show the influence of different storage configurations on TA and pH, the two factors characterizing the acidity of cherry tomatoes. The acceptable pH range for cherry tomatoes in the market is 4-4.5 (Riahi et al., 2023; Aragüez et al., 2020). The pH and TA of fresh cherry tomatoes used in this study were around 4.23 and 0.74, respectively. A notable decline in TA with an increase in the storage duration was observed in the case of cherry

tomatoes stored in control, PHB, and LPDE storage configurations (Fig. 5.10a). As mentioned in the literature (Buendía et al., 2019; Liu et al., 2017), the probable reason for the declining trend in TA is the maturation of fruits and the utilization of organic acids as substrates for respiration. Additionally, certain volatile compounds could be produced during the conversion of organic acids into energy, impacting the aroma and sensory perception of cherry tomatoes (Sganzerla et al., 2021), which is discussed further in Section 5.6.6. The results of pH (Fig. 5.10b), corroborated well with the results of TA. Based on pH values, cherry tomatoes stored in the control group were unacceptable on day 15, and those in the LDPE and PHB packages were unacceptable on day 18. In contrast, as noted earlier in Sections 5.6.1-5.6.3, PHB/5GS/0.7MgO packaging offered better storage conditions extending the shelf-life of cherry tomatoes, maintaining their pH within the acceptable limit throughout the storage period tested. The influence of various storage configurations on the ripening index of cherry tomatoes is shown in Fig. 5.10c. The ripening index of fresh (day 0) cherry tomatoes was measured at 7.8±0.11. As can be seen from Fig. 5.10c, the ripening index of cherry tomatoes increased with an increase in storage duration across all configurations. However, the rate of variation was relatively more pronounced for cherry tomatoes stored in the control group and less prominent for those in PHB/5GS/0.7MgO packaging. As per the literature (Fagundes et al., 2015), this could be due to the gradual decrease in oxygen (O_2) levels and increase in carbon dioxide (CO_2) levels inside the PHB/5GS/0.7MgO packaging over time, attributed to the respiration process of cherry tomatoes and the high gas barrier properties of the packaging material. This change in gas composition within the packaging over time leads to a reduction in the rate of both respiration and ripening of cherry tomatoes packed inside.

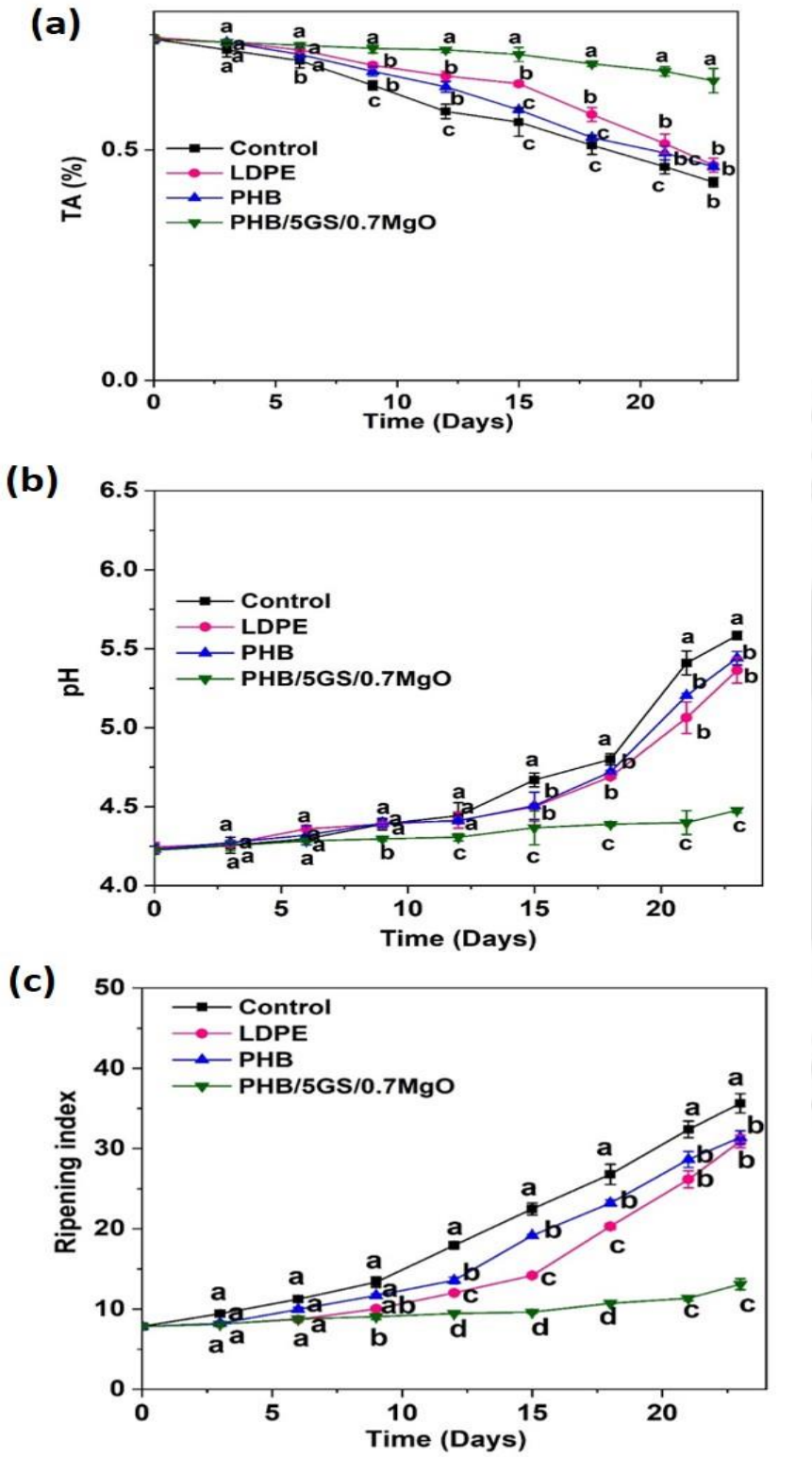

Fig. 5.10. Influence of different storage configurations on (a) TA and (b) pH and (c) ripening index of cherry tomatoes (Distinct letters indicate statistically significant ($P < 0.05$) differences in data among various configurations at same storage time)

5.6.5. Color

Color of fruits and vegetables plays a crucial role in influencing consumers' choices when purchasing such highly perishable items. Fig. 5.11 shows the influence of various storage configurations on the color parameters (L*, a*, b*, and a*/b*) of cherry tomatoes. The fresh cherry tomatoes (day 0) used in this study exhibited L*, a*, and b* around 33, 18, and 17, respectively. A gradual decrease in L* (lightness) and b* (yellowness) values, along with an increase in a* (redness) values, was noted as the storage duration increased for cherry tomatoes across all the configurations (Figs. 5.11a, 5.11b and 5.11c). However, the rate of color variation was relatively more pronounced for cherry tomatoes stored in the control group and less prominent for those in PHB/5GS/0.7MgO packaging. As per the literature (Boonsiriwit et al., 2020; Buendía et al., 2019), the alteration in the color of cherry tomatoes with increasing storage duration is attributed to the degradation of lycopene and the accumulation of pigments such as carotenoids, flavonoids, and anthocyanins in the tomato skin. As per the United States Department of Agriculture (USDA) recommendation (Yun et al., 2015), cherry tomatoes are considered attractive and acceptable for marketing when their a*/b* values fall within the range of 0.95 to 1.21. Based on the a*/b* results obtained in this study, cherry tomatoes stored in the control, LDPE, and PHB storage groups were unacceptable on the 18^{th} day (Fig. 5.11d). Whereas, cherry tomatoes stored in the PHB/5GS/0.7MgO packaging maintained a*/b* values within the acceptable range throughout the storage period tested. This is mainly due to the antioxidant properties of the films, which effectively protect the lycopene in cherry tomatoes from degradation during their storage (Buendía et al., 2019). Similar findings on the color retention of cherry tomatoes stored in active packaging were reported in the literature (Perera et al., 2022; García-García et al., 2013).

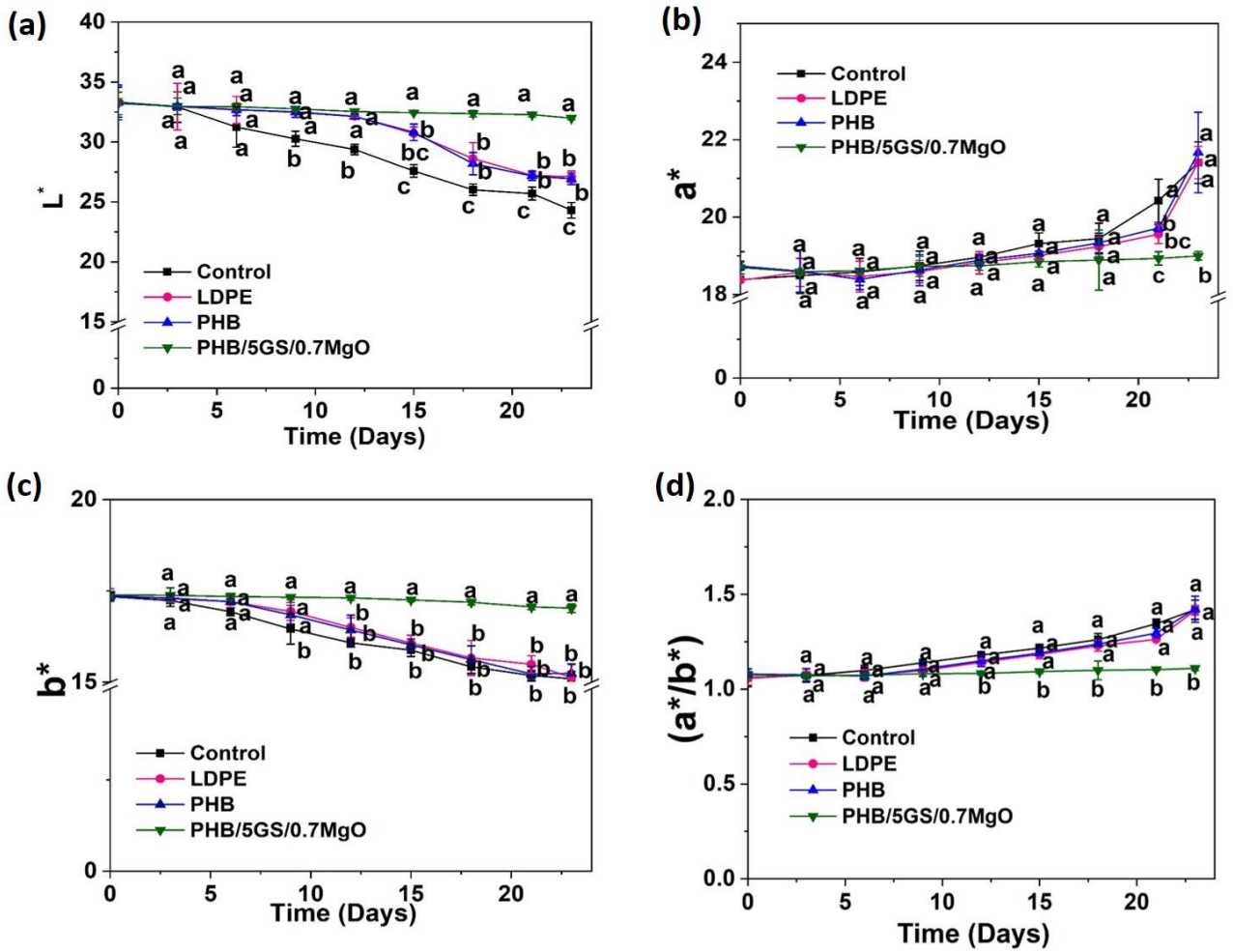

Fig. 5.11. Influence of different storage configurations on (a) L*, (b) a*, (c) b* and (a*/b*) values of cherry tomatoes (Distinct letters indicate statistically significant ($P < 0.05$) differences in data among various configurations at same storage time)

5.6.6. Organoleptic properties

The sensory scores assessing the texture, color, aroma, taste, and overall acceptability of the cherry tomatoes in various storage groups are presented in Fig. 5.12. For this analysis, a minimum sensory score of 5 was set for this study, and any score below this value was regarded as unacceptable by the consumers. On day 0, fresh cherry tomatoes received scores of 9 and 8.6 for color and aroma, respectively (Figs. 5.12a and 5.12b). However, the sensory scores for the color of cherry tomatoes in control, LDPE, and PHB storage configurations dropped below 5 by day 18. Whereas, the sensory score for aroma dropped below 5 on day 18 in the case of cherry tomatoes in the control group, and for those in the LDPE and PHB storage groups, the score was below 5 on day 21. On the other hand, cherry tomatoes stored in PHB/5GS/0.7MgO packaging maintained sensory scores for both color and aroma above 5 throughout the storage period tested.

Concerning texture, the sensory score for cherry tomatoes was 9 on day 0; however, it dropped below 5 by day 15 for the cherry tomatoes in the control group and by day 21 for those in the LDPE and PHB packaging groups (Fig. 5.12c). Contrarily, the sensory score for the texture of cherry tomatoes was above 5 throughout their 23 days of storage in PHB/5GS/0.7MgO packaging. The score for overall acceptability dropped below 5 by day 15 for the cherry tomatoes in the control group and by day 18 for those in the LDPE and PHB packaging groups (Fig. 5.12d). The score for overall acceptability of cherry tomatoes in PHB/5GS/0.7MgO packaging was 7.8 on day 21; nevertheless, it dropped to 4.6 on day 23 due to visual signs of microbial growth.

In case of the taste of cherry tomatoes, the scores continually decreased with an increase in the storage duration; nevertheless, the decline was comparatively less in the case of cherry tomatoes packaged using PHB/5GS/0.7MgO films (Fig. 5.12e). Nonetheless, it is worth

mentioning that when the sensory score for the overall acceptability dropped below 5, the samples were considered unsuitable for consumption and were assigned a least score of 1 for their taste. In short, the PHB/5GS/0.7MgO packaging outperformed the other storage configurations tested in this study in preserving the organoleptic properties of cherry tomatoes and extending the shelf-life of cherry tomatoes for up to 21 days.

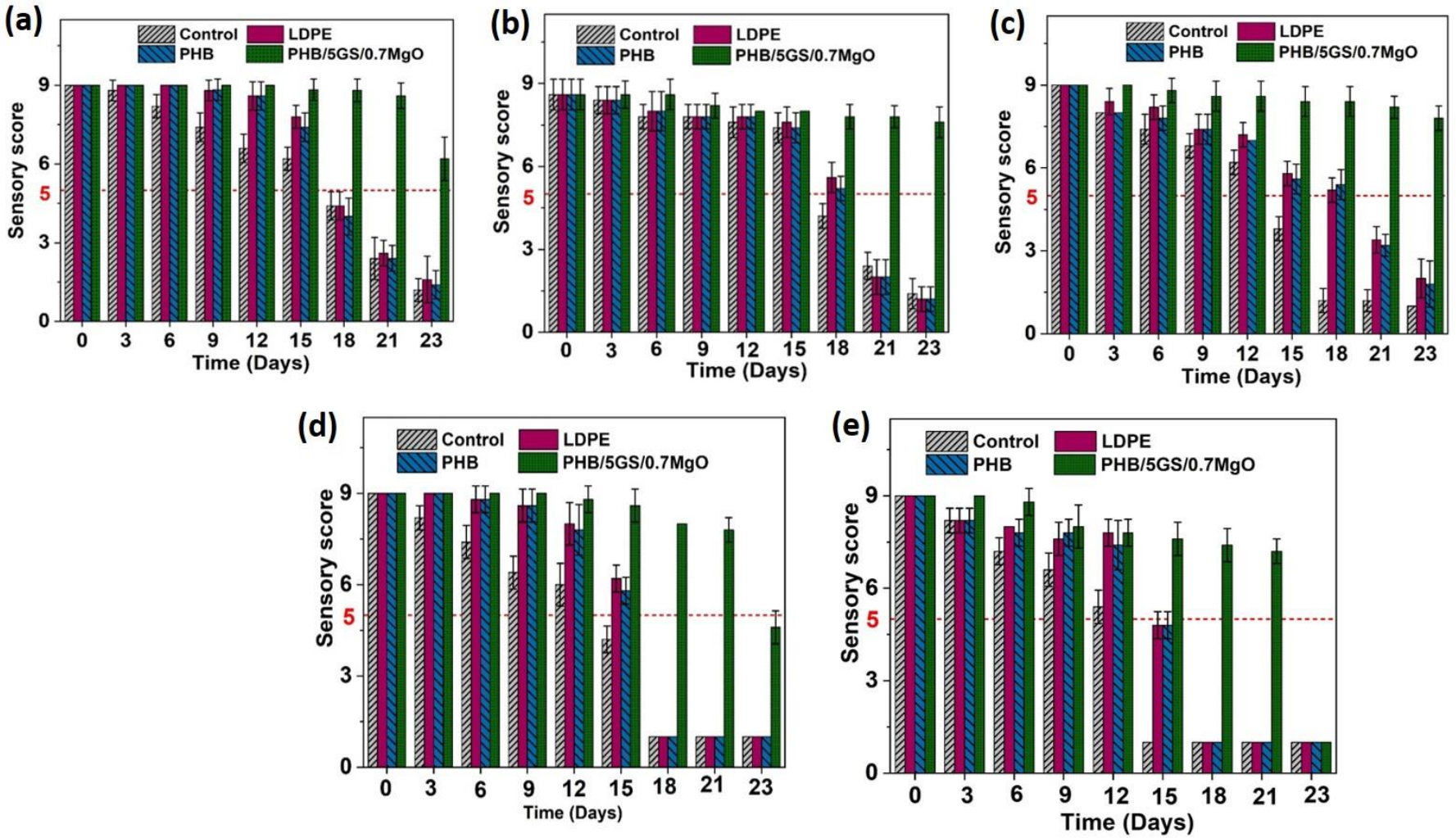

Fig. 5.12. Sensory scores for (a) color, (b) aroma, (c) texture, (d) overall acceptability, and (d) taste of cherry tomatoes in various storage configurations

5.6.7. Migration of MgO NPs from PHB/5GS/0.7MgO films to cherry tomatoes

Cherry tomatoes are a good source of several minerals, such as Cu, Ca, Zn, Mg, and Fe. They absorb these minerals from soil, fertilizers, and irrigation water during their growth (Bonemann et al., 2021). To assess the extent of migration of MgO NPs, the concentration of Mg metal ions was measured in the cherry tomatoes before (day 0) and after (day 23) their storage in PHB/5GS/0.7MgO packaging. For comparison purposes, the amount of Mg in the cherry tomatoes stored for 23 days without any packaging was also determined. The concentration of Mg in the fresh (day 0) cherry tomatoes used in the current study was 128.5±13.5 mg/100 g of dry weight, which agreed with the results reported elsewhere (Ali et al., 2021). After 23 days of storage under unpackaged and packaged conditions (utilizing PHB/5GS/0.7MgO pouches), the metal concentration (Mg) in cherry tomatoes was determined to be 130±13 and 129.5±17.5 mg/100 g of dry weight, respectively. Nevertheless, the statistical analysis demonstrated no significant ($P > 0.05$) difference in Mg concentration between cherry tomatoes packaged with PHB/5GS/0.7MgO films and the fresh (day 0) or unpackaged (day 23) samples. Thus, the bio-nanocomposite films developed in this study are deemed safe for the packaging of cherry tomatoes.

5.6.8. Contrast over prior arts

In Table 5.2, the influence of PHB/5GS/0.7MgO active packaging on the shelf-life of cherry tomatoes is compared with the performance of various active packaging and coating technologies reported in the literature. Notably, PHB/5GS/0.7MgO packaging provided a higher shelf-life for cherry tomatoes than the other active packaging methods utilizing polylactide/poly(adipate-co-terephthalate)/tannic acid (Sharma et al., 2022), triticale/$KMnO_4$ (Aragüez et al., 2020), gelatine/CuO (Sooch and Mann, 2021), cassava starch/cassava bark/grape stalk composite (Engel et al., 2022), chitosan/TiO_2 (Kaewklin et al., 2018), and

chitin/polyvinyl alcohol/β-cyclodextrin/cinnamaldehyde (Qian et al., 2022) composites. The shelf-life of cherry tomatoes stored in polyethylene terephthalate trays sealed with LDPE/potassium permanganate impregnated halloysite nanotube composite films is the same as that achieved using PHB/5GS/0.7MgO packaging developed in this study. Compared to the bionanocomposite packaging material developed in this study, the former materials raise environmental concerns due to the non-renewable and non-biodegradable nature of the plastic materials employed. Additionally, the active coatings using carboxymethyl cellulose/blackberry anthocyanin and okra leaf polysaccharide/carboxymethyl cellulose/cinnamon essential oil composites endowed a shorter shelf-life for cherry tomatoes than the PHB/5GS/0.7MgO packaging (Olawuyi and Lee, 2022; Sganzerla et al., 2021). Moreover, these coatings negatively impacted the visual appearance and texture of cherry tomatoes, which could be deterrent for the consumers to purchase such products. Therefore, given the outstanding performance of the environmentally-friendly PHB/5GS/0.7MgO packaging material developed in this study, its application in the storage of other food products, including cut fruits and meat can be further explored.

Table 5.2. Summary of literature on the storage of cherry tomatoes employing active packaging and coating technologies

Storage material	Storage conditions	Shelf-life (days)	Reference
Pouches prepared using PHB/5GS/0.7MgO films	Ambient conditions (~ 25 ℃)	21	This work
Placed in polyethylene terephthalate tray and sealed using LDPE/potassium permanganate impregnated halloysite nanotube composite films	20 ℃	21	Joung et al., 2021
Packaged with polylactide/poly (adipate-co-terephthalate)/tannic acid composite films	25 ℃ and 50 % RH	20	Sharma et al., 2022
Placed in a commercial plastic box and sealed with triticale/$KMnO_4$ composite films	23±2 ℃	20	Aragüez et al., 2020
Wrapped with gelatine/CuO nanocomposite films	40±3 ℃	18	Sooch and Mann, 2021
Placed on foam made of cassava starch/cassava bark/grape stalk composite and sealed with polyvinyl chloride films	17±2 ℃ and 64±8 % RH	15	Engel et al., 2022
Pouches prepared using chitosan/TiO_2 nanocomposite films	20 ℃ and 85 % RH	14	Kaewklin et al., 2018
Wrapped using chitin/polyvinyl alcohol/β-cyclodextrin/cinnamaldehyde composite films	Room temperature	10	Qian et al., 2022
Coated with carboxymethyl cellulose/blackberry anthocyanin composite	6 ℃	15	Sganzerla et al., 2021
Coated with okra leaf polysaccharide/carboxymethyl cellulose/cinnamon essential oil composite	30 ℃	14	Olawuyi and Lee, 2022

GS: Grapeseed oil; LDPE: Low-density polyethylene; PHB: Poly (3-hydroxybutyrate); RH: Relative humidity

5.7. Summary

In this chapter, the effectiveness of active PHB/5GS/0.7MgO nanocomposite films was assessed for the storage of two different types of fresh produce, viz., white button mushrooms and cherry tomatoes, at ambient room conditions. Furthermore, the performance of the nanocomposite packaging was compared with other storage configurations, viz., without packaging, conventional packaging, and PHB packaging. The results from the shelf-life study of white button mushrooms revealed that the mushrooms stored in the PHB/5GS/0.7MgO packaging configuration exhibited superior quality preservation over 6 days compared to the other storage groups. This was evident through minimal weight loss (2.6±0.40 % on day 6) and browning (6.89±1.05 % on day 0 to 9.3±0.32% on day 6), as well as better retention of firmness (from 14.8±0.39 N on day 0 to 13.89±0.20 N on day 6) and organoleptic properties for the mushrooms stored in the PHB/5GS/0.7MgO packaging group. Likewise, the results from the shelf-life study of cherry tomatoes clearly showed that the cherry tomatoes stored in PHB/5GS/0.7MgO packaging experienced better preservation of quality than those in other storage groups, with no signs of surface wrinkling, shrinkage, microbial growth, or juice leakage till day 21 of their storage. This was confirmed by minimal weight loss (4.45±0.06% on day 21), minimal change in titratable acidity (0.74±0.01% on day 0 to 0.67±0.01% on day 21), and better retention of firmness (19.89±0.12 N on day 0 to 15.77±0.37 N on day 21), pH, color, and organoleptic attributes for the cherry tomatoes stored in this packaging group. Moreover, the migration of MgO NPs from the PHB/5GS/0.7MgO packaging to white button mushrooms and cherry tomatoes was found to be negligible. Thus, it can be concluded that the PHB/5GS/0.7MgO films present a promising environmentally friendly option for packaging fresh produce.

Chapter 6

Key insights into mechanism and kinetics of biodegradation of poly (3-hydroxybutyrate)-based nanocomposite films in natural soil and river water environments

This chapter received the following scientific recognition

Bioresource Technology 409 (2024) 131238

Contents lists available at ScienceDirect

Bioresource Technology

journal homepage: www.elsevier.com/locate/biortech

Key insights into mechanism and kinetics of biodegradation of poly (3-hydroxybutyrate)-based nanocomposite films in natural soil and river water environments

Satti Venu Gopala Kumari [a], Kannan Pakshirajan [b], G. Pugazhenthi [a,c,*]

[a] Department of Chemical Engineering, Indian Institute of Technology Guwahati, Guwahati 781039, Assam, India
[b] Departmentof Biosciences and Bioengineering, Indian Institute of Technology Guwahati, Guwahati 781039, Assam, India
[c] Centre for Sustainable Polymers, Indian Institute of Technology Guwahati, Guwahati 781039, Assam, India

Kumari et al. (2024), Bioresource Technology, 409, 131238

Key insights into mechanism and kinetics of biodegradation of poly (3-hydroxybutyrate)-based nanocomposite films in natural soil and river water environments

Assessing the biodegradation behavior of food packaging materials in different environmental conditions is essential to comprehend their environmental impact for their safe disposal. Therefore, this chapter examines the biodegradation behavior and mechanisms of PHB-based films loaded with 5 wt% grapeseed oil (GS) and 0.7 wt% MgO nanoparticles (MgO NPs), identified as the optimal composition for active food packaging applications in Chapter 4, under natural soil and river water environments. For comparative purposes, the biodegradability of pristine PHB films and PHB-based films loaded only with 5 wt% GS (PHB/5GS) is also assessed and reported in this chapter.

6.1. Materials

Sulphuric acid and potassium permanganate were procured from Merck Specialties Pvt. Ltd., India. HPLC-grade chloroform was purchased from Hi-Media Pvt. Ltd., India. The water utilized in the experiments was sourced from the Millipore water synthesis system (Millipore, Elix-3, USA).

6.2. Biodegradation of PHB-based films in soil environment

The biodegradation of pristine PHB, PHB/5GS, and PHB/5GS/0.7MgO films in soil environment was studied using the garden soil collected locally from the Indian Institute of Technology Guwahati campus, Assam, India. Prior to the experiment, the soil was sieved using a 2 mm size sieve to remove stones and plant residues (Briassoulis et al., 2019). The soil pH was determined by employing a pH meter (EUTECH, India) in a mixture of the soil and Millipore water at a 1:2.5 (w/v) ratio (Pischedda et al., 2019). The C/N ratio of the soil was measured using CHNSO analyzer (Elementar, Vario macro cube, Germany). The bulk density of soil was determined by dividing the oven-dried soil weight (g) by soil volume (cm^3). The

organic content of the soil was assessed by combusting oven-dried soil in a muffle furnace at 600 ℃ for 5 h, and measuring weight loss (Nowak et al., 2011). The sand, silt, and clay composition of soil was determined using the sedimentation method described in the literature (Zimmermann et al., 2020). The moisture content of the soil was calculated by the gravimetric method (Karamanlioglu et al., 2014). The water-holding capacity of the soil was determined as per the following procedure described in the literature (Palai et al., 2021): firstly, a known quantity of soil was saturated with Millipore water, and its weight (W_{sat}) was recorded. The same soil was then dried in a hot air oven at 105 ℃ until its weight (W_{dry}) was constant. Thereafter, the water-holding capacity of the soil was determined using Equation (6.1).

$$Water\ holding\ capacity\,(\%) = \left(1 - \frac{W_{dry}}{W_{sat}}\right) \times 100 \qquad (6.1)$$

The soil degradation study was carried out at 25 ℃ and 80 % relative humidity in the laboratory. For this study, 10 pre-weighed film samples (25 mm×25 mm×0.03 mm) of different composition (PHB, PHB/5GS, and PHB/5GS/0.7MgO) were utilized. Each film sample was placed at a depth of 10 cm in a 2.5 L glass jar filled with soil (Palai et al., 2021; Al Hosni et al., 2019). Millipore water was added at regular intervals to maintain the moisture content of the soil at 50 % of its water-holding capacity (Pischedda et al., 2019). On days 3, 5, 7, 10, 13, 15, 17, 21, 23, and 25, a sample was retrieved from each test corresponding to PHB, PHB/5GS, and PHB/5GS/0.7MgO films by sieving the soil in the respective glass jars using a 2 mm opening size sieve. The retrieved samples were washed with Millipore water several times, and dried in a hot air oven until a constant weight was achieved. Subsequently, the percentage weight loss of samples was calculated using Equation (6.2) (Sarasa et al., 2009).

$$Weight\ loss\ (\%) = \left(1 - \frac{M_f}{M_i}\right) \times 100 \qquad (6.2)$$

Wherein M_i refers to the polymer sample's initial weight (g), and M_f denotes the polymer sample's weight (g) during the degradation period. The soil degradation tests were performed in triplicate, and results were reported as mean±standard deviation.

6.3. Biodegradation of PHB-based films in river water environment

The river water degradation study was conducted using surface water collected from the Brahmaputra river in March 2023 in Guwahati, Assam, India. The collected river water was stored in a refrigerator (~ 4 °C) until its use. The pH and total dissolved solids (TDS) of the river water were measured using a pH meter (Eutech, pH 700, India) and a TDS meter (Eutech, CON 2700, India), respectively. For the measurement of chemical oxygen demand (COD) of the river water, 3.50 mL of sulfuric acid, 2.50 mL of river water, and 1.50 mL of potassium permanganate were taken into COD vials, and the admixture was refluxed in a thermoreactor at 150 °C for 2 h. Thereafter, the absorbance of samples was noted at 600 nm using a UV visible spectrophotometer (Antech UV 7000, Ireland), and the COD was estimated from the calibration curve (Purnima et al., 2023).

For the biodegradation test, 12 pre-weighed samples (25 mm×25 mm×0.03 mm) of different (PHB, PHB/5GS, and PHB/5GS/0.7MgO) composition were utilized. Each film sample was placed in a 250 mL Erlenmeyer flask containing 125 mL of river water. These flasks were then incubated in an orbital shaker maintained at 200 rpm and 25 °C temperature. Polymer samples (PHB, PHB/5GS, and PHB/5GS/0.7MgO) were retrieved every 10 days during the study by filtering river water in the respective flasks using the Whatman filter paper of grade 1. The retrieved samples were washed several times with Millipore water and dried in a hot air oven until constant weight was achieved. Thereafter, the percentage weight loss of the respective polymer samples was determined as described earlier in Section 6.2 by using Equation (6.2). The biodegradation tests of the various PHB-based films in river water were performed in triplicate, and results were reported as mean±standard deviation.

6.4. Characterization of PHB-based films

The PHB, PHB/5GS, and PHB/5GS/0.7MgO films that were subjected to soil and river water degradation experiments were analyzed for their molecular weight, structural, chemical, morphological, and optical properties. The results were compared with those of the intact PHB-based film.

6.4.1. X-ray diffraction (XRD) analysis

The structural properties of the PHB-based samples were characterized using a powder X-ray diffractometer (Rigaku, Micromax-007HF, Japan). The XRD profiles were obtained in the 2θ range of 5-80° with a scanning rate of 5° min^{-1} at room temperature. Furthermore, the percentage crystallinity of the samples was determined using Equation (6.3) (Valapa et al., 2016b).

$$Crystallinity(\%)=\frac{\sum I_c}{\sum I_a+\sum I_c}\times 100 \qquad (6.3)$$

Where I_c and I_a refer to the area under crystalline and amorphous peaks in the XRD spectra, respectively.

6.4.2. Field emission scanning electron microscopy (FESEM)

The surface morphology of the PHB-based films was assessed using a Field emission scanning electron microscope (Zeiss, Sigma 300, Germany). The samples were affixed onto a stainless steel stub using double-sided carbon tape and then coated with a fine layer of gold to facilitate observation under FESEM.

6.4.3. Fourier transform infrared spectroscopy (FTIR)

The functional group analysis of the PHB-based samples was conducted using Fourier transform infrared spectroscopy (Shimadzu, IR Affinity-1, Japan). The FTIR spectrum of each sample was acquired in the wavenumber range of 400-4000 cm^{-1} following 30 consecutive

scans at a resolution of 4 cm^{-1} in attenuated total reflection (ATR) mode. Thereafter, the carbonyl index of the samples was calculated using Equation (6.4) (Phua et al., 2012).

$$Carbonyl\ index = \frac{I_{1720-1751}}{I_{2923-2928}} \quad (6.4)$$

Herein, $I_{2923\text{-}2928}$ and $I_{1720\text{-}1751}$ represent the intensity of transmittance peaks corresponding to C-H and C=O groups in the FTIR spectra, respectively.

6.4.4. Optical properties

The color parameters viz., b* (yellowness-blueness), a*(redness-greenness), and L* (darkness-lightness) of the PHB-based samples were measured using a color spectrophotometer (Sensegood, India). Furthermore, the percentage transmittance of light through various PHB-based samples was recorded in the wavelength range of 200-700 nm using a UV-visible spectrophotometer (Shimadzu, UV-2600, Singapore) with $BaSO_4$ coated plate as a reference. Then, the opacity values (A. mm^{-1}) of the respective samples were calculated using Equation (6.5) (Gupta et al., 2023).

$$Opacity\ value = \frac{-\log(T_{600})}{x} \quad (6.5)$$

Herein, T_{600} denotes fractional transmittance at 600 nm, and x refers to the thickness (mm) of the PHB-based samples.

6.4.5. Gel permeation chromatography (GPC)

The parameters, viz. weight average molecular weight (M_w), number average molecular weight (M_n), and polydispersity index (PDI=M_w/M_n) of the various PHB-based samples were measured by using high-temperature gel permeation chromatography (Agilent, G7820A, USA). The GPC system was equipped with 300 × 7.5 mm PLgel 10 μm MIXED-B column, and a refractive index detector. Prior to the analysis, the polymer samples were dissolved in

HPLC-grade chloroform and passed through a 0.2 µm syringe filter. Polystyrene was utilized as a calibration standard and tetrahydrofuran (3 mL.min^{-1}) was employed as the mobile phase for this analysis. Furthermore, the number of chain scissions per unit mass (N_t) of the samples was calculated using Equation (6.6) (Phua et al., 2012).

$$N_t = \frac{1}{M_{nf}} - \frac{1}{M_{ni}} \qquad (6.6)$$

Wherein, M_{ni} and M_{nf} are the number average molecular weight (kDa) of the samples before and after degradation in soil/river water, respectively.

6.4.6. Statistical analysis

To assess potential differences among the means, the results of percentage weight loss, and rate of weight loss, as well as the data on crystallinity, opacity, carbonyl index, color coordinates, molecular weight, and number of chain scissions per unit mass were subjected to statistical analysis. The evaluations were conducted using Origin™ Pro 9.0 software, employing one-way analysis of variance (ANOVA) and Tukey's Honest Significance Difference Test, with a significance level (P) set at 0.05. The results of the statistical analysis were marked in the corresponding tables and figures using alphabet labels.

6.5. Results and Discussion

6.5.1. Characterization of soil and river water

The biodegradation behavior of polymeric materials could be greatly influenced by the properties of the biodegradation environment (Emadian et al., 2016). Hence, the properties of soil and river water used in the biodegradation of PHB-based films in this work are presented in Table 6.1. These characteristics were in close agreement with the results reported elsewhere for soil (Palai et al., 2021; Pischedda et al., 2019) and river water (Rahman et al., 2021; Ahipathy and Puttaiah, 2006).

Table 6.1. Properties of soil and river water

Sample	Parameter	Value
Soil	pH	6.7±0.5
	Moisture content	19.3±0.69 %
	Water holding capacity	43.3±1.2 %
	Bulk density	1.3 $g.cm^{-3}$
	C/N ratio	7
	Organic content	5
	Composition	Sand: 51 %, silt: 29 %, and clay: 20 %
River water	pH	6.9±1.3
	Total dissolved solids	70.38±5.23 mg. L^{-1}
	Chemical oxygen demand	31.58±1.37 mg. L^{-1}
	Biological oxygen demand	2.7 mg. L^{-1} (Pollution control board Assam, 2023)
	Turbidity	15.23±2.49 NTU

6.5.2. Biodegradation of PHB-based films in soil and river water

Measurement of weight loss is one of the most widely adopted methods for evaluating the extent of degradation in polymeric materials (Zamir et al., 2022; Doh et al., 2020). Thus, the percentage weight loss of PHB, PHB/5GS, and PHB/5GS/0.7MgO films assessed as a function of incubation time in soil and river water is presented in Figs. 6.1a and 6.1b, respectively. The values of the weight loss rate and weight loss percentage of various PHB-based samples at the end of the experimental period are summarized in Table 6.2. The biodegradation of polyesters such as PHB in the natural environment is a complex process and is influenced by environmental conditions as well as material properties (Suzuki et al., 2021). Several studies in the literature (Suzuki et al., 2021; Bikiaris et al., 2013; Sridewi et al., 2006) reported that the

microorganisms present in the soil or river water cannot directly assimilate the high molecular weight water-insoluble polymers into their cells. Consequently, the microorganisms secrete extracellular enzymes particularly esterases to depolymerize the polymers. As depicted in Fig. 6.1c, the polymer biodegradation involves the following steps: (a) absorption of water by the polymer from the surrounding medium (soil moisture/river water), thereby enhancing their bioavailability to degrading microbes and enzymes, (b) attachment of microbes and enzymes on the polymer surface, (c) depolymerization or cleavage of molecular chains by enzymatic/non-enzymatic hydrolysis, (d) formation of low molecular weight compounds such as oligomers and monomers, and their solubilization into the surrounding medium, and (e) assimilation of these low molecular weight compounds by the microorganisms, (f) formation of biomass, CO_2, H_2O, or other metabolic end products.

From Figs. 6.1a and 6.1b, it can be observed that the percentage weight loss of PHB, PHB/5GS, and PHB/5GS/0.7MgO films was significant with an increase in the degradation time in the soil and river water. Though the weight loss profiles of PHB/5GS and PHB/5GS/0.7MgO films are similar to that of neat PHB, their rate of weight loss followed the order: PHB > PHB/5GS > PHB/5GS/0.7MgO. The observed trend could be due to the influence of the material characteristics, viz. crystallinity, antimicrobial activity, hydrophobicity/hydrophilicity, and the barrier effect of MgO NPs. For instance, as reported earlier in previous chapters, the water contact angle of these samples was measured at 78.2±2.4°, 78.4±2.1°, and 84.5±0.6°. The crystallinity values of PHB, PHB/5GS, and PHB/5GS/0.7MgO films are 41, 53, and 61 %, respectively. Furthermore, the PHB/5GS and PHB/5GS/0.7MgO films exhibited excellent antimicrobial properties, in contrast to neat PHB films, which exhibited negligible antimicrobial activity. Hence, the higher crystallinity, higher hydrophobicity, and antimicrobial activity of the composite films led to a reduction in water penetration, suppressed microbial growth, and offered resistance to microbial enzyme attack, thereby resulting in their slower

rate of biodegradation and thus the low rate of weight loss compared to neat PHB. Moreover, inorganic materials such as MgO NPs cannot undergo degradation by microbial enzymes; consequently, their presence reduces the available area for enzymatic hydrolysis in PHB/5GS/0.7MgO films, thereby lowering their rate of weight loss (Bikiaris, 2013). Phua et al. (2012) and Mirabolghasemi et al. (2021) reported analogous findings corresponding to a decrease in the rate of weight loss of biopolymers such as PBS and PLA with the incorporation of inorganic nanofillers (Mirabolghasemi et al., 2021; Phua et al., 2012). A detailed discussion on the influence of crystallinity on the biodegradation of PHB-based films is provided later in Section 6.5.5 of this work. While the exact rate of degradation of GS is not known, existing literature (Hassiotis et al., 2010; Oliveira et al., 2024) suggests that it gradually leaches from the polymer matrix into soil/river water, and then gets assimilated by the microorganisms present.

It is worth mentioning that, starting from day 17, the variation in the rate of weight loss of various PHB-based films in soil is found to be statistically insignificant ($P > 0.05$) (Table 6.2). By day 25, all the PHB-based samples showed complete (100 %) weight loss in the soil (Fig. 6.1a). In contrast, following 120 days of incubation in river water, the weight loss of PHB, PHB/5GS, and PHB/5GS/0.7MgO films was only 26.8±1.3, 23.7±1.1, and 20.3±1.5 %, respectively (Fig. 6.1b). A similar observation corresponding to a slower rate of weight loss of starch-based biopolymer bags in lake water (1.6 % in 90 days) compared to soil (37 % in 90 days) was reported earlier in the literature (Accinelli et al., 2012). The varied rate of weight loss of PHB-based films in soil and river water could be due to the impact of parameters including, but not limited to, microbial population, microbial diversity, and nutrient content in the respective degradation environments (Ahsan et al., 2023). In addition, the presence of heavy metal contaminants such as arsenic, zinc, lead, manganese, and iron that are commonly

reported in the Brahmaputra river water could inhibit the microbial activity for efficient degradation of PHB-based film (Nath et al., 2018).

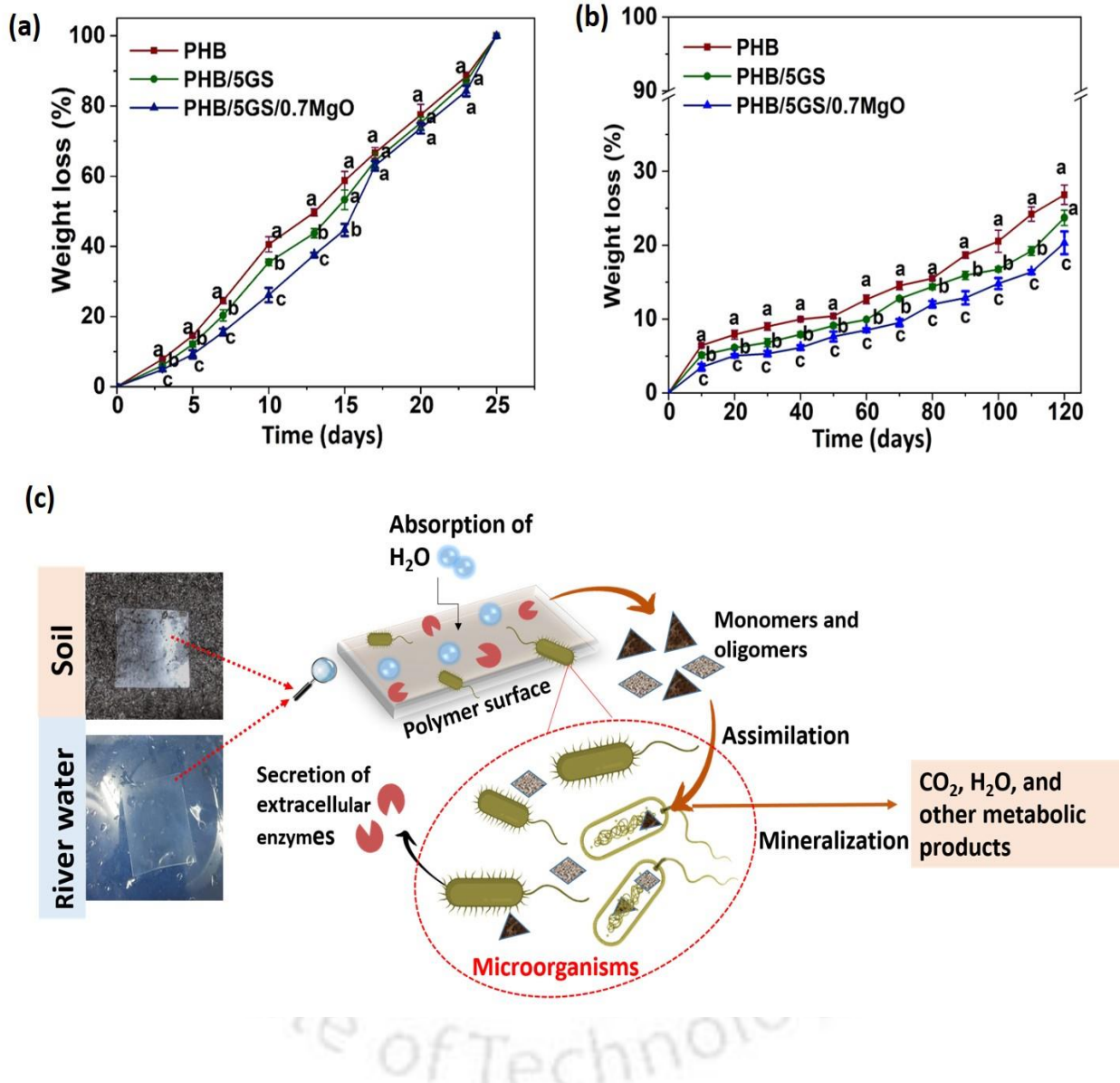

Fig. 6.1. Percentage weight loss of PHB, PHB/5GS, and PHB/5GS/0.7MgO films as a function of incubation time in (a) soil and (b) river water (distinct alphabets indicate significant ($P < 0.05$) variations among data pertaining to same time point), and (c) probable mechanism involved in the biodegradation of biopolymers

Table 6.2. Values of weight loss rate and weight loss percentage of various PHB-based samples

Samples	**In soil at 25 days**		**In river water at 120 days**	
	Rate of weight loss (mg.day^{-1})	**Weight loss (%)**	**Rate of weight loss (mg.day^{-1})**	**Weight loss (%)**
PHB	1.57±0.26^{a}	100^{a}	0.12±0.02^{a}	26.85±1.34^{a}
PHB/5GS	1.57±0.24^{a}	100^{a}	0.07±0.01^{b}	23.70±1.02^{b}
PHB/5GS/0.7MgO	1.57±0.25^{a}	100^{a}	0.02±0.01^{c}	20.32±1.51^{c}

Distinct superscript letters within a column signify statistically significant differences in means at the 0.05 significance level

6.5.3. Physical appearance and optical properties

To evaluate the physical changes occurring during the degradation process, the PHB, PHB/5GS, and PHB/5GS/0.7MgO films were visually examined both before and after degradation in soil and river water for different time duration (Fig. 6.2). Before degradation (day 0), the PHB-based films exhibited a compact surface and excellent transparency. However, following degradation in the soil, noticeable changes occurred in the physical appearance of these films, including the emergence of surface irregularities and cavities, increased roughness, the acquisition of a yellow hue, and a decrease in transparency (Fig. 6.2a). Moreover, the extent of these changes increased with an increase in their degradation time in the soil. In particular, after 23 days of degradation in the soil, the physical structure of PHB, PHB/5GS, as well as PHB/5GS/0.7MgO films was completely distorted, characterized by numerous cavities (Fig. 6.2a). In contrast, even after 100 days of degradation in river water, the structural integrity of the PHB-based films remained intact, with no cavities or breakage discernible to the naked eye (Fig. 6.2b). However, upon extending their incubation period to 110 days in the river water, the breakage of films became apparent, as indicated by the arrows in Fig. 6.2b. Furthermore, akin to their behavior in soil environment, the PHB-based films showed a decrease in transparency and an increase in yellow color with an increase in degradation time in the river water. The changes observed in the surface morphology of the PHB-based films during degradation in soil and river water environments were further confirmed through FESEM analysis, as presented in Section 6.5.4. of this work.

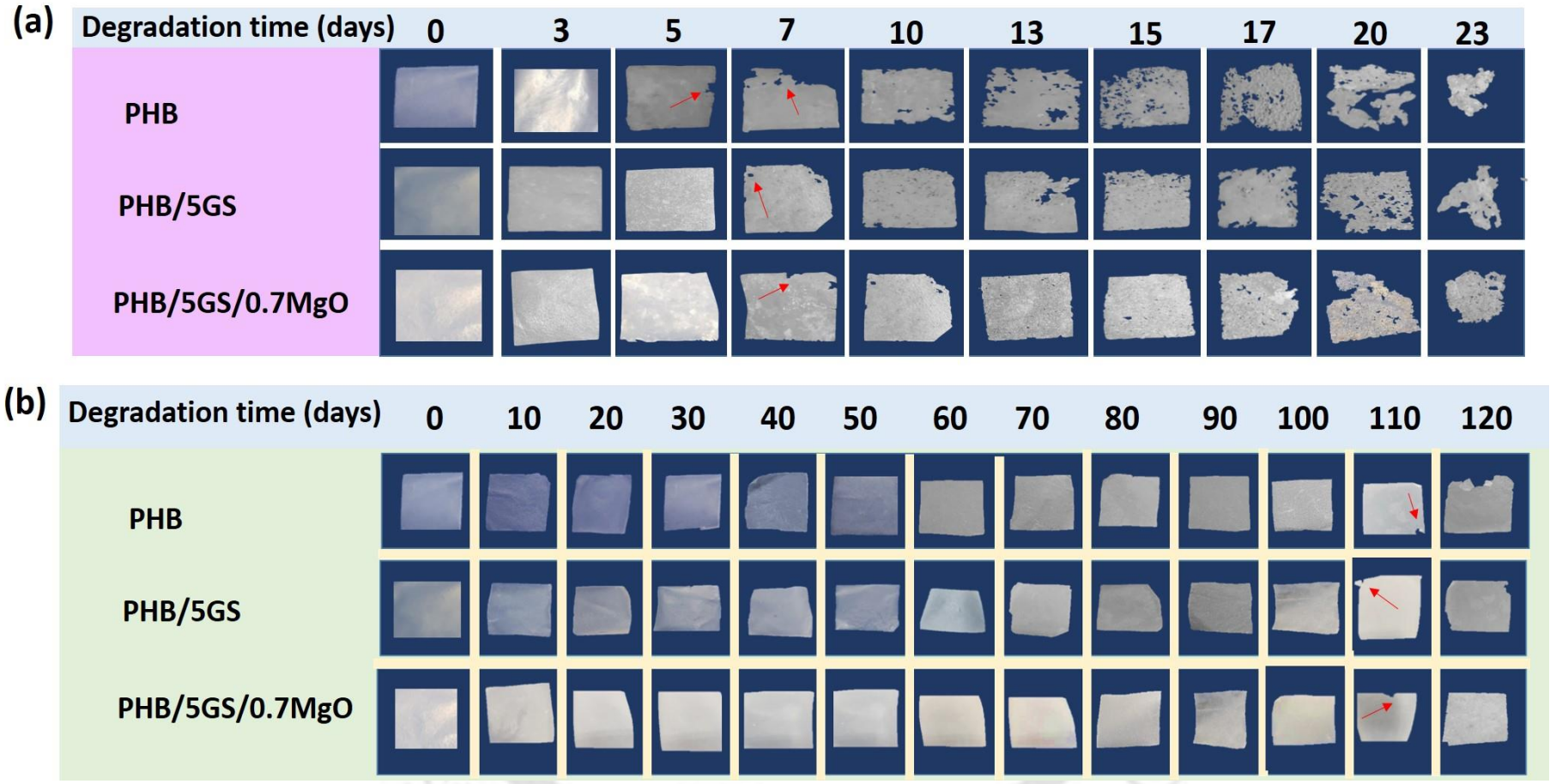

Fig. 6.2. Images showing the physical appearance of various PHB-based films during their degradation in (a) soil and (b) river water

The variations in the color of PHB, PHB/5GS, and PHB/5GS/0.7MgO films due to their biodegradation in soil and river water were quantified by the measurement of color coordinates, namely L*, a*, and b* (Figs. 6.3 and 6.4). The Figs. 6.3a, 6.3b, and 6.3c reveal a gradual decrement in "+L^*" and "-a*" values and an increment in "+b*" values for various PHB-based films with an increase in the incubation time in the soil. From the aforementioned observations, it can be inferred that prolonged degradation time in soil resulted in more dark and yellow color of the PHB-based materials, likely due to factors such as microbial activity, changes in the material's refractive index due to water absorption, and the breakdown of polymer chains into smaller fragments, which can affect light absorption and scattering. Arrieta et al. (2014) and Martucci et al. (2015) reported analogous findings on the color changes of PLA/PHB blend films and PLA/gelatine blend films, respectively, during their biodegradation (Martucci and Ruseckaite, 2015; Arrieta et al., 2014). Although the variation in yellow color was less pronounced during their degradation in river water as compared to their degradation in soil, a reduction in "+L^*" and "-a^*" values and an increment of "+b^*" values were observed for the PHB, PHB/5GS, and PHB/5GS/0.7MgO films during their prolonged degradation in the river water (Figs. 6.4a, 6.4b, and 6.4c). For instance, the L^*, a^*, and b^* values of neat PHB films prior to their degradation in river water were 93.6±0.2, -2±0.1, and 0.41±0.1, respectively. Following their degradation in river water over 120 days, these parameters were changed to 85.8±0.3, -1.1±0.1, and 6.3±0.1, respectively. Furthermore, the variation in the transparency of PHB, PHB/5GS, and PHB/5GS/0.7MgO films as a result of their degradation in soil and river water was quantified by the opacity values (Figs. 6.3d and 6.4d). Herein, a high opacity value indicates lower transparency of the films, and vice versa. From Figs. 6.3d and 6.4d, it can be seen that the opacity values of the various PHB-based films increased with an increase in degradation time in soil and river water. For instance, prior to biodegradation experiments, the

opacity values of PHB, PHB/5GS, and PHB/5GS/0.7MgO films are 0.36±0.11, 0.39±0.02, and 0.62±0.01, respectively, and after 20 days of degradation in soil, the opacity values of these films increased to 0.86±0.08, 0.8±0.07, and 0.84±0.05, respectively. Whereas, following 120 days of degradation in river water, the opacity values of PHB, PHB/5GS, and PHB/5GS/0.7MgO films were found to be 0.73±0.03, 0.76±0.04, and 0.76±0.05, respectively. This increase in opacity could primarily be attributed to the increased crystallinity of these PHB-based films during degradation processes, as discussed in Section 6.5.5 of this work. Increased crystallinity results in greater light scattering within the films, leading to higher opacity (Valapa et al., 2016b).

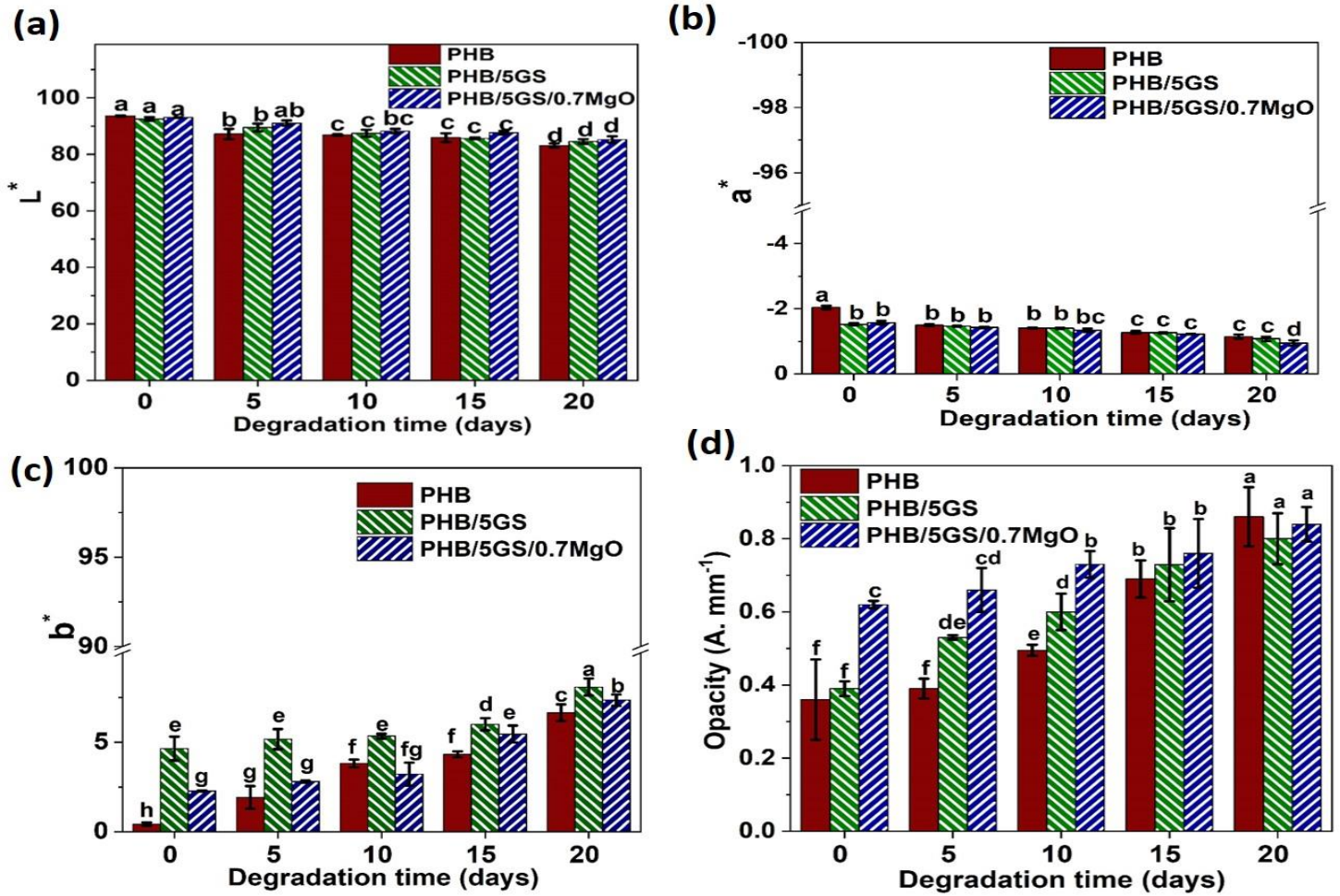

Fig. 6.3. (a) L*, (b) a*, (c) b*, and (d) opacity values of PHB-based films before and after degradation in soil (distinct alphabets above the bars signify statistically significant differences in means at the $P < 0.05$ level)

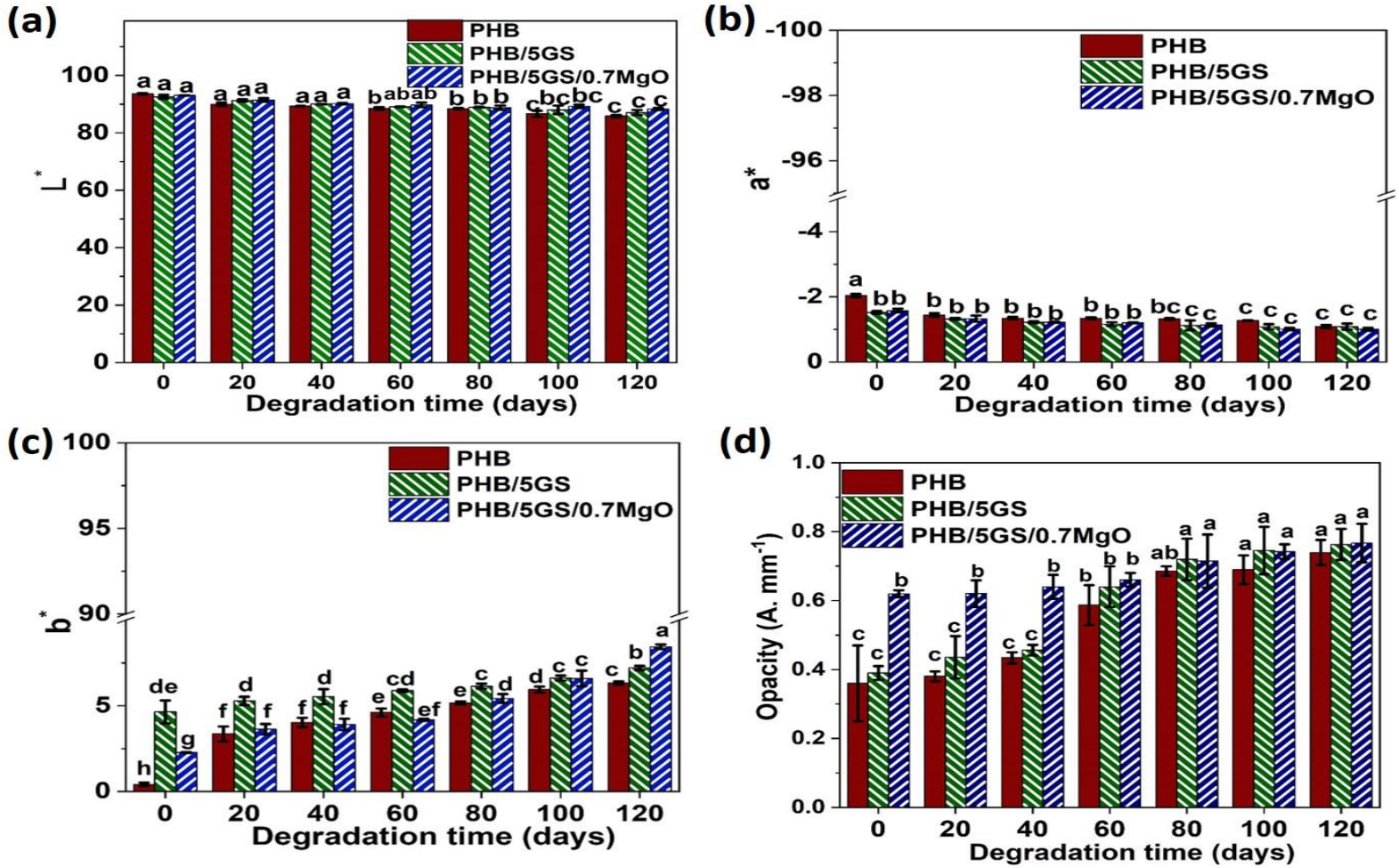

Fig. 6.4. (a) L*, (b) a*, (c) b*, and (d) opacity values of PHB-based films before and after degradation in river water (distinct alphabets above the bars signify statistically significant differences in means at the $P < 0.05$ level)

6.5.4. FESEM analysis

The changes in the surface morphology of PHB, PHB/5GS, and PHB/5GS/0.7MgO during their degradation in soil and river water were assessed through FESEM analysis (Fig. 6.5). It can be seen from the FESEM images (Fig. 6.5), that prior to their degradation (day 0), all three types of PHB-based films exhibited compact surface morphology, without any pores or cracks. After 5 days of degradation in soil, the surface of PHB, PHB/5GS, and PHB/5GS/0.7MgO films became rough and irregular, with the formation of small pores, as indicated by arrows in the respective FESEM images (Fig. 6.5a). Beyond 10 and 15 days of degradation time, both the surface roughness and the density of pores increased in these film samples. Further prolongation of the degradation time of the PHB, PHB/5GS, and PHB/5GS/0.7MgO films in the soil to 20 days resulted in significant surface erosion, accompanied by considerable enlargement of pores. As discussed earlier in Section 6.5.2, these disruptions in the surface morphology are attributed to the disintegration of the PHB-based films due to water absorption followed by hydrolysis and microbial enzyme-mediated de-esterification reactions during their degradation. Zamir et al. (2022) and Maran et al. (2013) reported similar findings regarding the increase in surface irregularities and pore formation in PLA/starch nanocrystal composite films and cassava starch films, respectively, with an increase in their degradation time in soil (Maran et al., 2013; Zamir et al., 2022). Besides in this study, at the same degradation time, the degree of surface damage was more pronounced in PHB films, followed by PHB/5GS and PHB/5GS/0.7MgO films, which aligned well with the percentage weight loss results presented earlier in Fig. 6.1a.

In the case of the river water degradation study, the surface of various PHB-based films became rough after only 20-40 days, likely due to erosion. Furthermore, after 60 days of degradation, small pores were noticed in the FESEM images of PHB, PHB/5GS, and PHB/5GS/0.7MgO

films (Fig. 6.5b). Similar to results obtained in the soil degradation study, the surface disruption, density, and size of pores in the various PHB-based films increased with an increase in degradation time in the river water. Following 120 days of degradation in river water, a highly porous morphology was observed for all the PHB-based samples. Similar findings on surface disruptions have been reported by Kadoya et al. (2023) in poly (lactate-co-3-hydroxybutyrate) films due to their biodegradation in river water (Kadoya et al., 2023). Furthermore, FESEM images shown in Fig. 6.5b, reveal that the extent of morphological damage in the PHB-based films followed the order: PHB > PHB/5GS > PHB/5GS/0.7MgO. The observed trend is also consistent with the percentage of weight loss of the PHB-based films presented earlier in Fig. 6.1b.

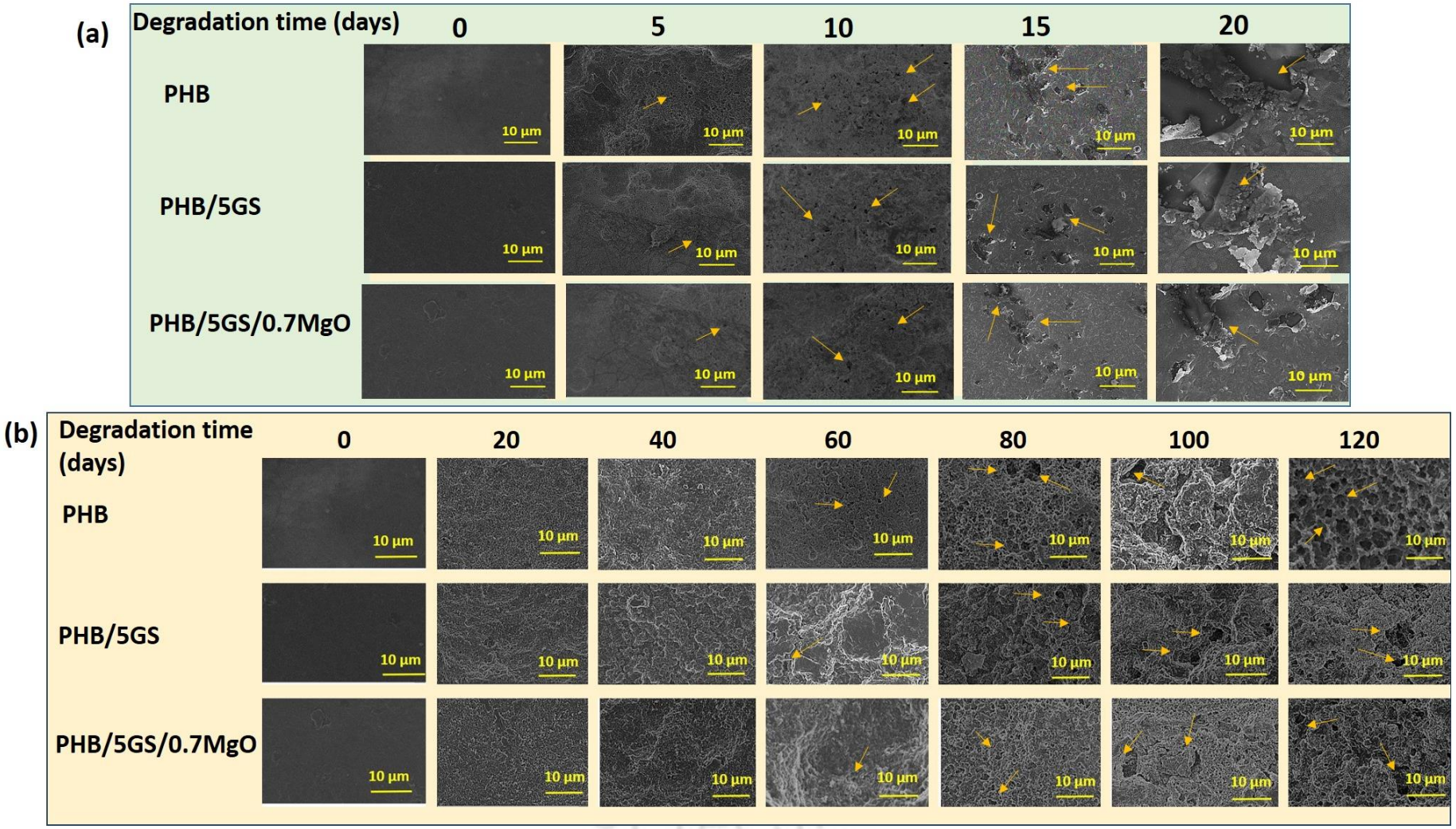

Fig. 6.5. FESEM images of the various PHB-based films before and after degradation in (a) soil and (b) river water

6.5.5. XRD analysis

To evaluate the changes in the structural properties of PHB, PHB/5GS, and PHB/5GS/0.7MgO films during their biodegradation in soil and river water, their XRD spectra were recorded and are shown in Figs. 6.6 (a-f). In addition, the crystallinity values of these samples were calculated and presented in Figs. 6.6g and 6.6h. Prior to their biodegradation (day 0), neat PHB films exhibited distinct diffraction peaks at 13.3°, 16.9°, 22.5°, 25.37°, 27.03°, and 44.56° corresponding to (0 2 0), (1 1 0), (1 1 1), (1 2 1), (0 4 0), and (2 2 2) planes of the orthorhombic crystal structure, (Gupta et al., 2023). All these peaks were evident in the XRD profiles of the composite films; however, the intensities of the peaks varied due to differences in crystallinity. In addition, PHB/5GS/0.7MgO films showed a small diffraction peak at 63.06° corresponding to MgO NPs (Figs. 6.6e and 6.6f) (Amani et al., 2019). The crystallinity values of PHB, PHB/5GS, and PHB/5GS/0.7MgO films prior to degradation (day 0) are 41.12, 53.21, and 61.45 %, respectively. It is worth mentioning that the rate of degradation of these PHB-based samples followed an inverse correlation with their respective crystallinity values, and PHB showed a maximum degradation rate followed by PHB/5GS and PHB/5GS/0.7MgO (please see Fig. 6.1). A similar trend on the low rate of biodegradation of bio-polymeric composites due to high crystallinity has been reported in the literature (Jin et al., 2019; Fukushima et al., 2010). As depicted in Fig. 6.7, the higher degradation rate of neat PHB films can be attributed to the presence of relatively higher proportions of amorphous regions compared to the composite films. These amorphous regions, characterized by loosely packed molecules, facilitate the penetration of water molecules and degrading enzymes into the polymer matrix, thereby accelerating the polymer hydrolysis and degradation processes (Vasile et al., 2018; Bikiaris et al., 2013; Iwata et al., 1999). Furthermore, as discussed earlier in Section 6.5.2, the reinforcement of MgO NPs not only increases the crystallinity and hydrophobicity of

PHB/5GS/0.7MgO films but also reduces the available surface area for enzymatic action. All of the aforementioned factors likely contributed to the lower degradation rate of PHB/5GS/0.7MgO films compared to PHB/5GS and PHB films.

The XRD spectra of PHB, PHB/5GS, and PHB/5GS/0.7MgO samples, obtained during their biodegradation in soil and river water (Figs. 6.6 (a-f)), revealed all the diffraction peaks that were even present in the samples prior to their degradation. However, during their biodegradation in soil and river water, the intensity of the crystalline peaks increased with time as compared with the peaks due to amorphous regions present in the samples (Figs. 6.6g and 6.6h). In particular, after 20 days of degradation in soil, the crystallinity of PHB, PHB/5GS, and PHB/5GS/0.7MgO samples increased to 59, 68, and 74 %, respectively. Likewise, following 120 days of degradation in river water, the crystallinity values of PHB, PHB/5GS, and PHB/5GS/0.7MgO samples are 52, 59, and 66 %, respectively. These findings confirm that the degradation of PHB, PHB/5GS, and PHB/5GS/0.7MgO samples occurred at a greater rate in amorphous regions than in the crystalline regions, as depicted in Fig. 6.7. A similar trend of increase in crystallinity with an increase in degradation time in natural environmental conditions is reported for starch films (Barragán et al., 2016), poly (butylene adipate-co-terephthalate) films (Palsikowski et al., 2018), and PLA/poly (butylene adipate-co-terephthalate) blend (Palsikowski et al., 2018) films.

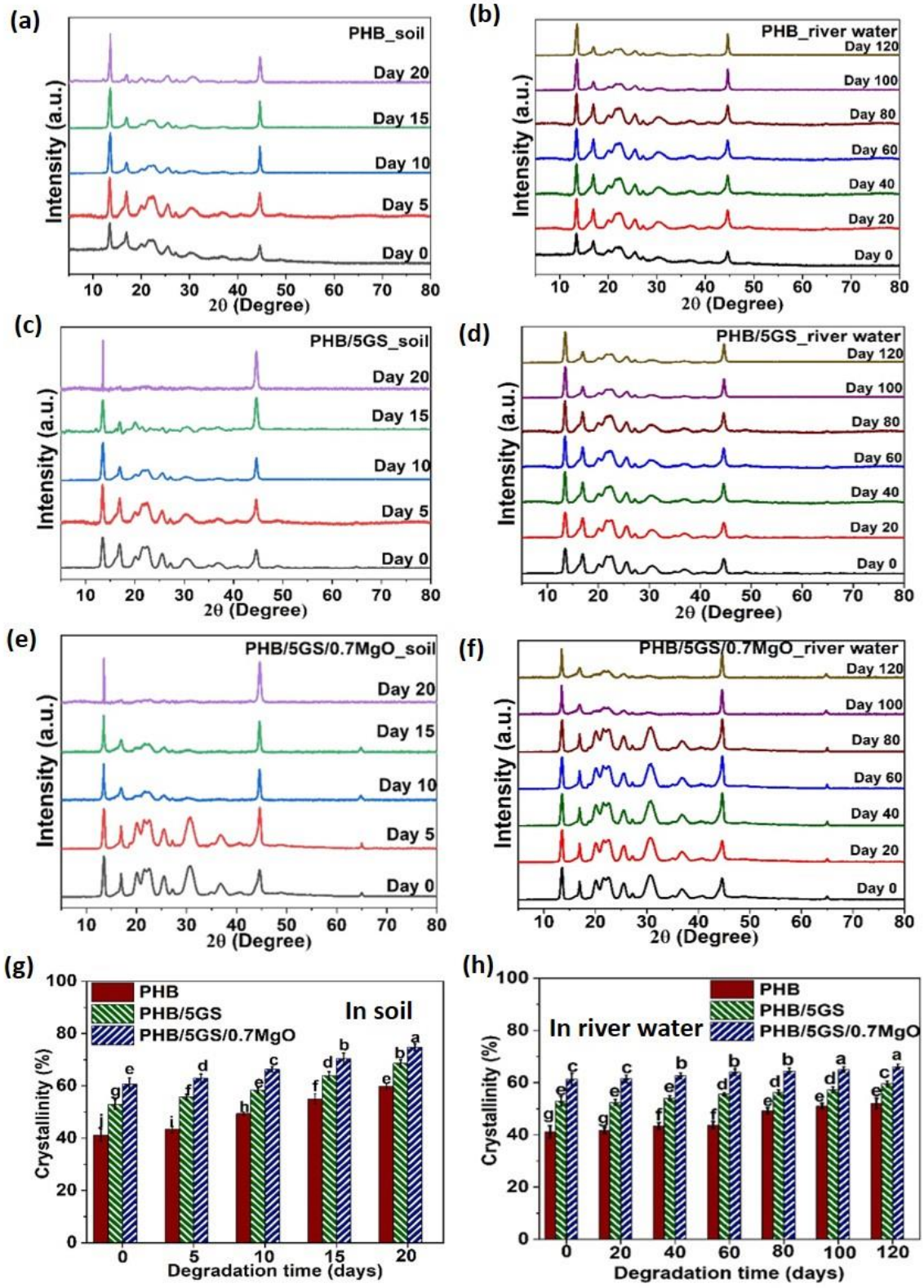

Fig. 6.6. (a-f) XRD spectra, and (g and h) crystallinity values of PHB-based films before and after degradation in soil and river water (distinct alphabets above the bars signify statistically significant differences in means at the $P < 0.05$ level)

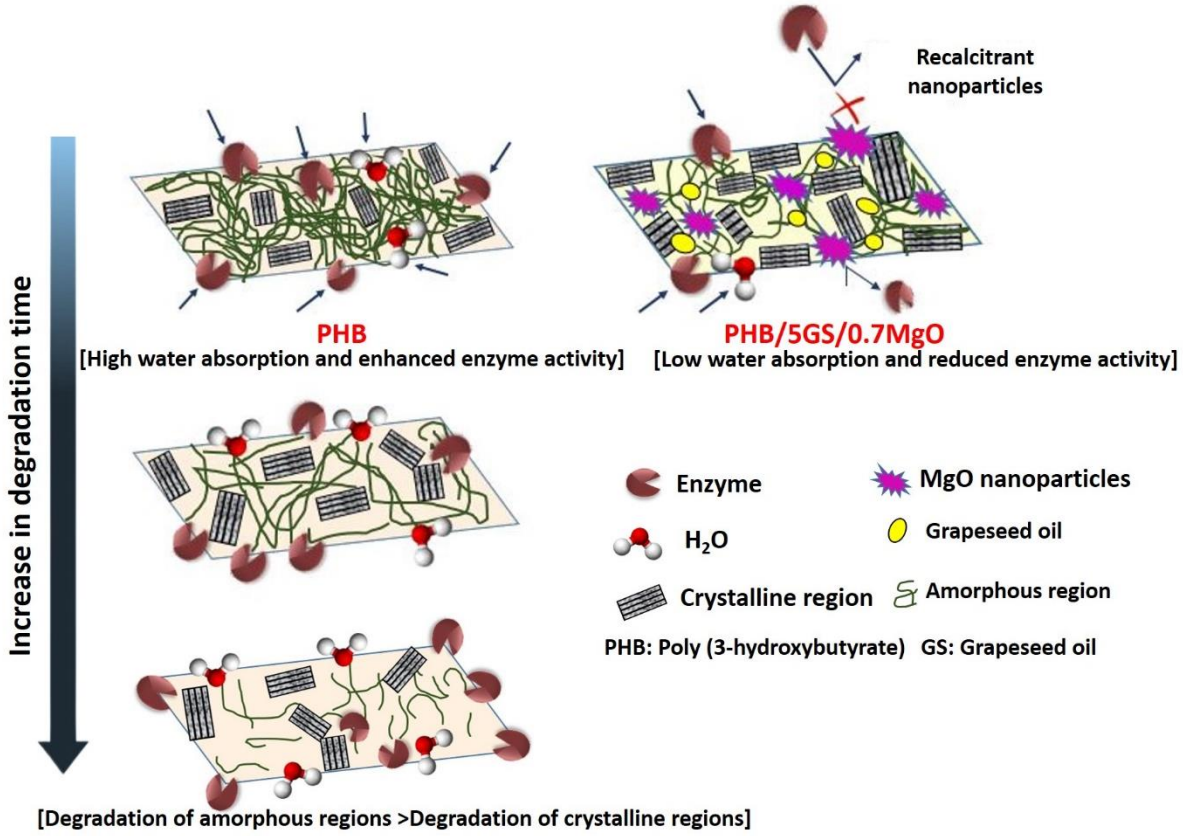

Fig. 6.7. Schematic depicting the influence of crystallinity and presence of MgO nanoparticles on the biodegradation of PHB-based films

6.5.6. FTIR analysis

FTIR spectra were recorded for PHB, PHB/5GS, and PHB/5GS/0.7MgO films, both before and after degradation in soil and river water, to monitor potential changes in the chemical structure of these materials during the biodegradation process (Figs. 6.8 (a-f)). Prior to their degradation (day 0), the transmittance peaks corresponding to the C-H and C-O-C groups present in the pristine and composite PHB films are observed at 2928 and 1049-1285 cm^{-1}, respectively. Whereas, the transmittance peak due to the carbonyl (C=O) stretch of the ester group was observed around 1720 cm^{-1} for PHB and 1723 cm^{-1} for PHB/5GS and

PHB/5GS/0.7MgO films (Manikandan et al., 2020). Nonetheless, the peaks corresponding to GS and MgO NPs were not evident in the FTIR spectra of the composite films, likely due to the presence of these additives in low amounts. After degradation in soil and river water for different lengths of time, no new peaks were noticed in the FTIR spectra of PHB, PHB/5GS, and PHB/5GS/0.7MgO samples. Nevertheless, a slight shift of transmittance peak position to higher wavenumbers and a decrease in the intensity of the transmittance peak corresponding to the C=O group were noticed with an increase in degradation time in soil and river water. From the aforementioned observations, it can be inferred that the degradation of the PHB-based films proceeded through chain scission and cleavage of carbonyl bonds in the molecular chains, resulting in the formation of oligomers and monomers (Salomez et al., 2019; Lv et al., 2018). Furthermore, to quantify these observations, the carbonyl index of the PHB-based samples was calculated as a function of degradation time (Figs. 6.8g and 6.8h). The carbonyl index of PHB, PHB/5GS, and PHB/5GS/0.7MgO samples before degradation is 5.19±0.15, 5.56±0.15, and 5.54±0.19, respectively. From Figs. 6.8g and 6.8h, a gradual decrease in the carbonyl index is observed with an increase in their degradation time in soil and river water (Salomez et al., 2019). In particular, after 20 days of degradation in soil, the carbonyl index of PHB, PHB/5GS, and PHB/5GS/0.7MgO films reduced to 1.88±0.34, 2.62±0.19, and 2.78±0.19, respectively. Similarly, for the samples degraded using river water, the carbonyl index was reduced to 4.43±0.06, 4.81±0.06, and 4.91±0.02, respectively at the end of 120 days. Herein, a more pronounced decrease in the carbonyl index of samples treated using the soil compared to those treated using river water is attributed to the high degradation efficiency of the film in soil, as noted earlier in Section 6.5.2. A similar decreasing trend in carbonyl index due to degradation in natural environmental conditions is reported in the literature for PLA/starch films (Lv et al., 2018) and PLA/poly (butylene succinate-co-adipate) blend films (Palai et al., 2021).

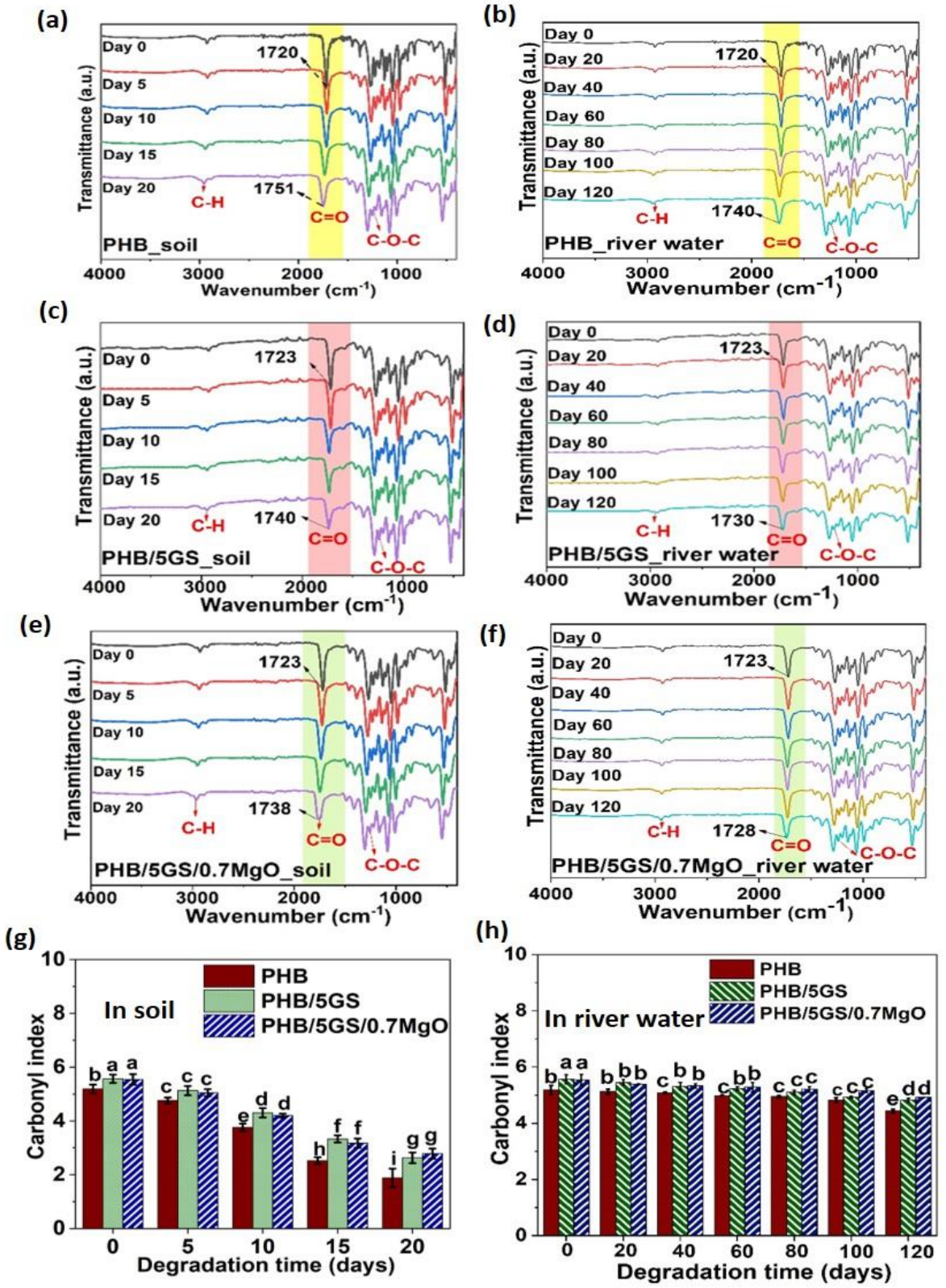

Fig. 6.8. (a-f) FTIR spectra, and (g and h) carbonyl index of PHB-based films before and after degradation in soil and river water (distinct alphabets above the bars signify statistically significant differences in means at the $P < 0.05$ level)

6.5.7. Gel permeation chromatography (GPC)

Assessment of the molecular weight of polymers during their biodegradation can provide valuable insights into the biodegradation phenomenon (Palai et al., 2021; Phua et al., 2012). Thus, the number average molecular weight (M_n) and weight average molecular weight (M_w) of PHB, PHB/5GS, and PHB/5GS/0.7MgO samples were measured before as well as after degradation in soil and river water for different time intervals (Figs. 6.9 and 6.10). Before degradation, the M_w of PHB, PHB/5GS, and PHB/5GS/0.7MgO films were 538, 492, and 447 kDa, respectively, whereas the M_n of the corresponding samples was 303, 268, and 241 kDa. It can be seen in Figs. 6.9 and 6.10 that, a gradual reduction in both M_w and M_n occurred in the various PHB-based samples along with their incubation time in soil and river water. In particular, after 20 days of treatment using soil, the M_w values of PHB, PHB/5GS, and PHB/5GS/0.7MgO samples reduced by 53, 52, and 51 %, respectively, whereas the M_n values dropped by 63, 61, and 60 %, respectively. Contrarily, following 120 days of incubation in river water, the M_w decreased by only 24, 22, and 21 %, while the M_n decreased by only 27, 25, and 23 %, respectively, for PHB, PHB/5GS, and PHB/5GS/0.7MgO samples. Notably, these observations were in good agreement with the percentage weight loss results presented in Section 6.5.2. Moreover, as depicted in Fig. 6.1c, the biodegradation of biopolymers proceeded via depolymerization or cleavage of ester bonds in molecular chains. The decrease in molecular weight further confirms the chain scissions in the PHB-based films due to enzymatic/non-enzymatic hydrolysis, which led to the formation of low molecular weight compounds, such as oligomers and monomers. A similar degradation mechanism involving the reduction in molecular weight due to biodegradation of PLA/thermoplastic starch blend films (Palai et al., 2021), PLA/poly (butylene succinate-co-adipate) blend films (Palai et al., 2021)

and poly (butylene adipate-co-terephthalate) films (Palsikowski et al., 2018) has been reported in the literature.

The extent of chain scission of PHB, PHB/5GS, and PHB/5GS/0.7MgO samples during degradation was further quantified by calculating N_t, the average number of random chain scissions per unit mass (Phua et al., 2012). From Figs. 6.9c and 6.10c, it can be seen that the number of chain scissions in the various PHB-based samples increased with an increase in the incubation time in soil and river water. Interestingly, the number of chain scissions was found to be the highest in the case of PHB, followed by PHB/5GS and PHB/5GS/0.7MgO at various time points of degradation. Moreover, the results of N_t corroborated well with the results of the carbonyl index presented in Section 6.5.6, which revealed that the decrease in the carbonyl index of these samples during their degradation followed the order: PHB>PHB/5GS>PHB/5GS/0.7MgO. Furthermore, the polydispersity index (PDI), which serves as a measure of the molecular weight distribution of polymers, is evaluated for various PHB-based samples before and after degradation (Figs. 6.9d and 6.10d). The PDI of PHB, PHB/5GS, and PHB/5GS/0.7MgO films before degradation are found to be 1.70, 1.83, and 1.85, respectively. Notably, following 20 days of soil treatment, the PDI of these films increased to 2.25, 2.26, and 2.28, respectively. Whereas, after 120 days of incubation in river water, the PDI of PHB, PHB/5GS, and PHB/5GS/0.7MgO samples are 1.86, 1.89, and 1.90, respectively. This increment in PDI signifies the broadening of molecular weight distribution due to the breakdown of polymer chains into smaller fragments during degradation. Phua et al. (2012) reported analogous findings, indicating an increase in both PDI and N_t of poly (butylene succinate) with an increase in incubation time in soil (Phua et al., 2012).

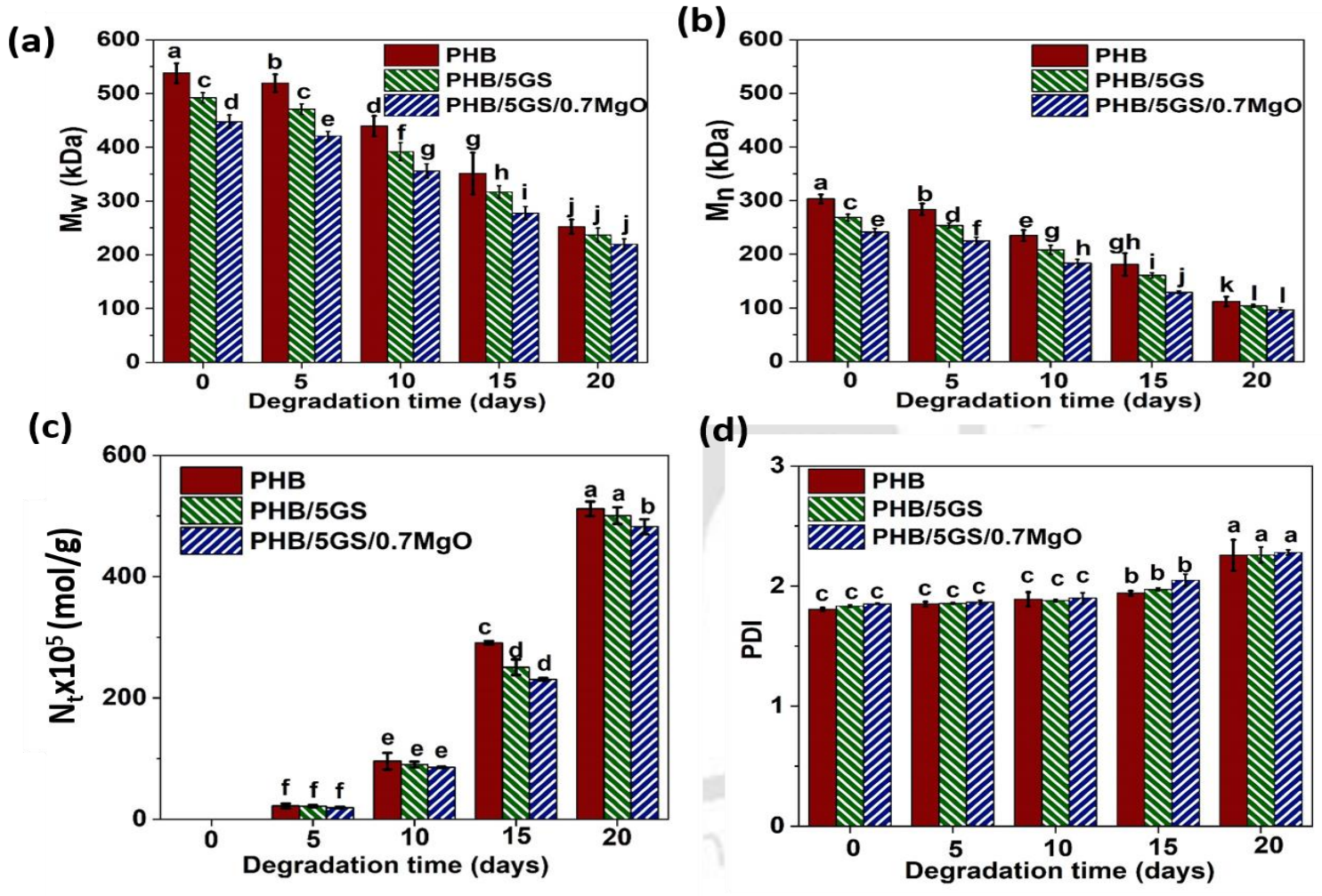

Fig. 6.9. (a) M_w, (b) M_n, (c) N_t, and (d) PDI of various PHB-based films before and after degradation in soil (distinct alphabets above the bars signify statistically significant differences in means at the $P < 0.05$ level)

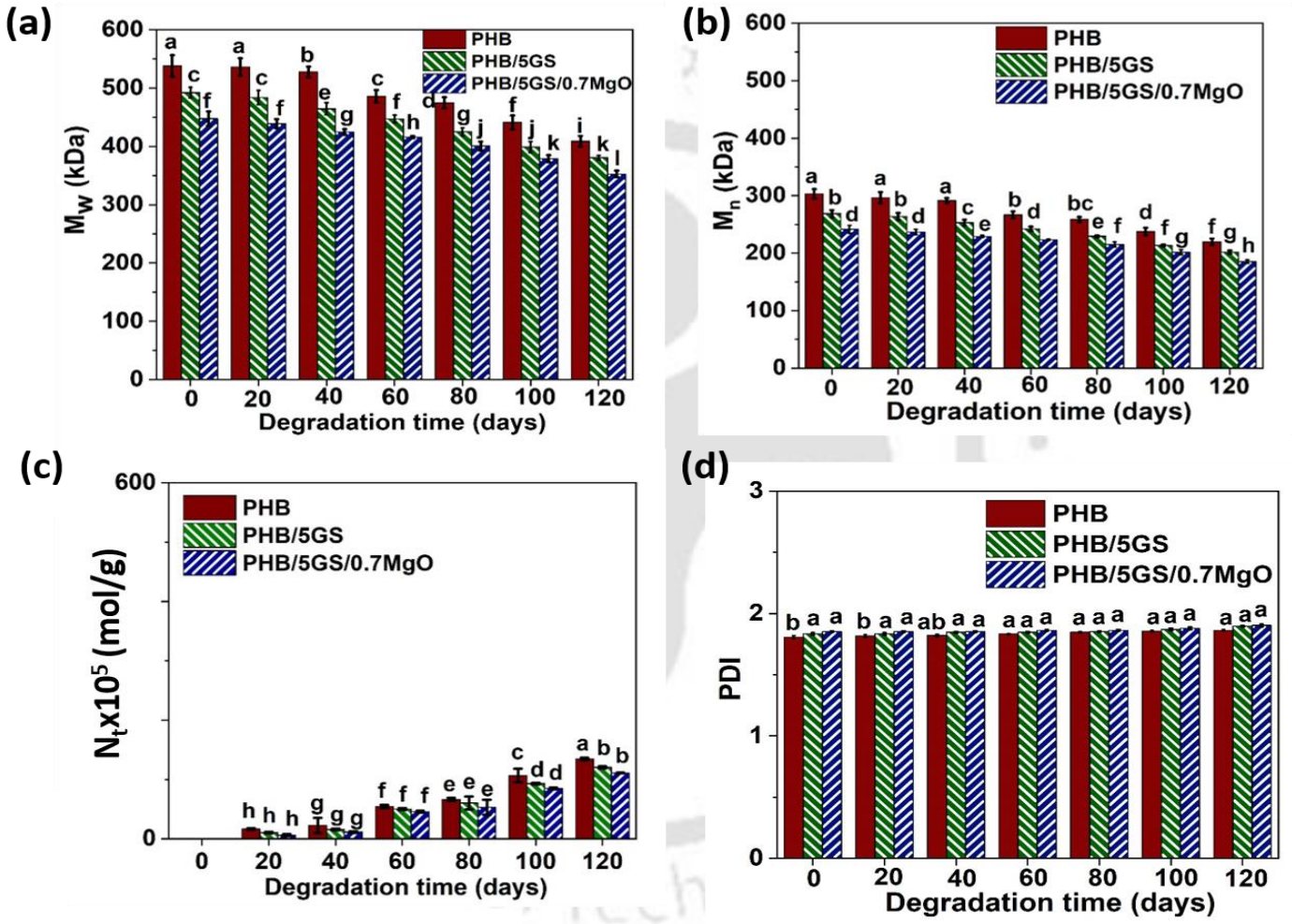

Fig. 6.10. (a) M_w, (b) M_n, (c) N_t, and (d) PDI of various PHB-based films before and after degradation in river water (distinct alphabets above the bars signify statistically significant differences in means at the $P < 0.05$ level

6.5.8. Comparison of biodegradability of PHB-based films with other biopolymer-based packaging materials

Table 6.3 compares the percentage weight loss of PHB, PHB/5GS, and PHB/5GS/0.7MgO films due to biodegradation with that of other biopolymer-based packaging materials reported in the literature. The current study revealed that the addition of GS and MgO NPs slightly reduced the initial rate of weight loss of PHB-based films in soil. However, over prolonged degradation period, the difference in percentage weight loss between the neat and nanocomposite films was not significant. These findings align well with previous studies, which observed no significant impact of graphene loading on the percentage weight loss of PHB-based films (Manikandan et al., 2020) and cinnamon essential oil incorporation on the percentage weight loss of chitosan/sodium alginate/starch blend films (He et al., 2021) over extended degradation periods in soil. Notably, the rate of weight loss of PHB/5GS/0.7MgO films in soil due to biodegradation is comparable to that reported for PHB/graphene nanocomposite films (Manikandan et al., 2020) and even superior to that reported for PBS/montmorillonite (Phua et al., 2012), PLA/carbon nanotubes (Norazlina et al., 2019), and alginate/cellulose nanocrystals (Doh et al., 2020) nanocomposite films. However, it is worth mentioning that numerous factors, including but not limited to the molecular structure of the polymer, molecular weight of the polymer, percentage loading of additives, sample dimensions, and environmental conditions, influence the rate of degradation of bionanocomposite films. The current study revealed a higher degradation efficiency of PHB/5GS/0.7MgO films in soil compared to river water, which agree well with the findings in the literature (Accinelli et al., 2012). As discussed in detail in Section 6.5.2. of this work, microbial population, microbial diversity, and nutrient content in degradation environments significantly influence the rate of biodegradation of bionanocomposite films.

Table 6.3. Summary of literature regarding the biodegradability of biopolymer-based packaging materials

Material	Type of environment	Experimental conditions	Experimental period (days)	Weight loss (%)	Reference
PHB PHB/5GS PHB/5GS/0.7MgO	Soil	Films (25 mm×25mm×0.03 mm) incubated at 10 cm depth; moisture:19 %; 25 ℃	25	100 100 100	This work
PHB PHB/5GS PHB/5GS/0.7MgO	River water	Films (25 mm×25mm×0.03 mm) incubated in 125 mL of river water on an orbital shaker; 25 ℃	120	26.8±1.3 23.7±1.1 20.3±1.5	This work
PHB PHB/graphene	Soil	Films (130mm×12mm×3mm) incubated at 10-15 cm depth, 80 % RH; 28 ℃	30	100 100	Manikandan et al., 2020
PBS PBS/montmorillonite	Soil	Dumbell-shaped films; 60-70 % RH, 30 ℃	180	9 5	Phua et al., 2012
PLA PLA/carbon nanotubes	Soil	Square-shaped films incubated at 15 cm depth	180	7 4	Norazlina et al., 2019
PBS/PBAT PBS/PBAT/organoclay	River water	Films:25 mm×25mm×0.03 mm; incubated in 100 mL river water	20	4 1	Moustafa et al., 2017

Material	Type of environment	Experimental conditions	Experimental period (days)	Weight loss (%)	Reference
Alginate Alginate/cellulose nanocrystals	Soil	Films (30 mm×30 mm) incubated at 6 cm depth	35	35 35	Doh et al., 2020
Alginate Alginate/cellulose nanocrystals	Lake water	Films (3 cm×3 cm) incubated in 500 mL lake water	35	30 25	Doh et al., 2020
Starch-based bags	Soil	Films (150 mm×150 mm) incubated at 10 cm depth; 25 ℃	90	37	Accinelli et al., 2012
Starch-based bags	Fresh water from the lagoon	Films (150 mm×150 mm) incubated in 5 L of freshwater on an orbital shaker, 25 ℃	90	1.6	Accinelli et al., 2012
Starch-based bags	Sea water	Films (150 mm×150 mm) incubated in 5 L of freshwater on an orbital shaker, 25 ℃	90	1.7	Accinelli et al., 2012

PBAT: poly (butylene adipate-co-terephthalate); PBS: polybutylene succinate; PLA: polylactic acid; PHB: poly (3-hydroxybutyrate); RH: relative humidity; GS: grapeseed oil

6.6. Summary

The biodegradability of PHB, PHB/5GS, and PHB/5GS/0.7MgO films fabricated via the solution casting route was evaluated in natural soil and river water environments. The results of the characterization of the PHB-based films, in terms of their molecular weight, structural, chemical, morphological, optical, and colorimetric properties both before and after degradation in soil and river water revealed the biodegradation mechanism involved. The efficiency and rate of weight loss of the PHB-based films were higher in soil compared to river water. The PHB-based films showed complete (100 %) weight loss in soil in 25 days, and their weight loss in river water was 20-26 % in 125 days. XRD analysis showed that the percentage crystallinity of all three types of PHB-based films increased with an increase in degradation time in soil and river water, confirming that the amorphous regions were degraded faster than the crystalline portions in the polymer film. FESEM analysis confirmed morphological changes in these PHB-based films, including the emergence of surface irregularities and the formation of pores during their degradation. During their biodegradation, the opacity, as well as the yellow color of the PHB-based films, increased along with their degradation time in soil and river water. In addition, a reduction in average molecular weight and carbonyl index values, along with an increase in the number of chain scissions per unit mass, was observed for the various PHB-based films during their biodegradation. Based on this study, it can be deduced that the degradation of PHB-based films occurs through random chain scission and cleavage of carbonyl bonds in the molecular chains. Furthermore, the degradation proceeded via the formation of lower molecular weight compounds, such as oligomers and monomers, which are easily assimilated by the microorganisms present.

Chapter 7

Overall conclusions and Future perspectives

Overall conclusions and Future perspectives

This chapter summarizes the inferences drawn from the works carried out in this thesis. In addition, some valuable suggestions for future research that can be conducted in the relevant area are presented in this chapter.

7.1. Conclusions

The primary objective of this thesis is to develop an active and eco-friendly food packaging material based on the biopolymer, poly (3-hydroxybutyrate) (PHB). To address the limitations of PHB in food packaging applications, combinational loading of essential oil and MgO nanoparticles (MgO NPs) was employed. In this work, the development of the PHB-based active packaging material involved three main steps. In the first step, MgO NPs were synthesized via five different chemical synthesis routes: precipitation (PT), sonication-precipitation (SPT), microwave combustion (MWC), conventional combustion (CC), and solvothermal (ST) processes. The properties of MgO NPs obtained from these synthesis routes were evaluated to identify the best route that yields optimal characteristics for their reinforcement in PHB-based films. In the second step, PHB-based films were prepared by incorporating varying concentrations (1-10 wt%) of essential oils, viz., grapeseed oil (GS), bergamot oil (BG), and ginger oil (GG), through the solution casting route. The best essential oil and its optimal loading rate for the maximum enhancement in the flexibility of PHB were determined in this step by comprehensive characterization of PHB/essential oil composite films. In the third step, PHB-based films loaded with essential oil (best oil and optimum loading rate) and MgO NPs (best route and varying loading rate) were prepared by a sonication-assisted solution casting route. Subsequently, the resulting PHB/essential oil/MgO nanocomposite films were characterized for their structural, optical, tensile, thermal, gas barrier, water contact angle, antioxidant, and antimicrobial properties to identify the optimal composition. The

performance of PHB-based nanocomposite films of optimal composition was evaluated for the storage of fresh produce, viz., white button mushrooms and cherry tomatoes. Lastly, the biodegradability of PHB-based nanocomposite films was assessed in natural soil and river water environments. The key findings from this research are presented below:

- MWC yielded MgO NPs with the most favorable characteristics for reinforcement in food packaging materials, including a higher specific surface area (67.32 m^2/g), smaller particle size (5-35 nm), and superior antimicrobial and antioxidant activities compared to other synthesis routes (PT, SPT, CC, and ST).
- The tensile strength (TS) and elongation at break (EB) of pristine PHB films are 20.48±0.51 MPa and 0.51±0.04 %, respectively. The best improvement (30-fold) in the EB of PHB is obtained with a 5 wt% loading of GS, but at the expense of a 1.3-fold reduction in TS. The PHB/5GS films exhibited 53.1±4.7 % antioxidant activity and inhibited the growth of *E. coli* by 19.7±0.9 % and *S. aureus* by 61.5±3.4 %.
- In comparison with pristine PHB films, the PHB-based films loaded with 5 wt% GS and 0.7 wt% MgO NPs (PHB/5GS/0.7MgO) demonstrated 1.4-fold higher TS and 30-fold higher EB, along with 79 and 90 % reduction in water vapor and oxygen transmission, respectively. In addition, PHB/5GS/0.7MgO films showed good UV-blocking properties, 65.25±0.98 % antioxidant activity, and completely inhibited the growth of *S. aureus* and *E. coli*. Above 0.7 wt% reinforcement of MgO NPs in the PHB-based films, a decrement in thermal, tensile, and gas barrier properties was noticed due to the formation of agglomerates at the higher concentration of the nanofiller.
- The PHB/5GS/0.7MgO films demonstrated beneficial effects on maintaining the physicochemical as well as organoleptic attributes of white button mushrooms and cherry tomatoes, extending their shelf-life to 6 and 21 days, respectively, at ambient room conditions.

- The migration of MgO NPs from the PHB/5GS/0.7MgO nanocomposite films to white button mushrooms and cherry tomatoes was found to be negligible, indicating these PHB-based films are safe for packaging fresh produce.
- The developed PHB-based active packaging material (PHB/5GS/0.7MgO) showed complete (100 %) weight loss in soil in 25 days and 20 % weight loss in river water in 120 days.
- The biodegradation of PHB-based films in soil and river water environments proceeded via chain scission and cleavage of carbonyl bonds in the molecular chains, leading to the formation of oligomers and monomers that were readily assimilated by the microorganisms.
- The PHB-based active food packaging material (PHB/5GS/0.7MgO) developed in this study contributes to the Sustainable Development Goals, which defined sustainable development as "***Development that meets the needs of people without compromising the ability of future generations to meet their own needs.***" Herein, the utilization of PHB, a biopolymer derived from renewable resources, reduces reliance on non-renewable fossil fuels and promotes the sustainable use of natural resources for food packaging. By demonstrating 100 % weight loss in soil within 25 days, the PHB/5GS/0.7MgO films contribute to environmental sustainability by minimizing pollution and reducing the accumulation of non-biodegradable waste. Furthermore, the antioxidant and antibacterial properties of this material aid in extending the shelf-life of food products packaged in it, thereby minimizing food waste and promoting sustainable consumption of food. Therefore, it can be summarized that the PHB-based food packaging material developed in this study embodies the principles of sustainable development by addressing environmental and social considerations to meet the needs of both current and future generations.

7.2. Recommendations for future work

- In the present work, a laboratory-scale sonication-assisted solution casting method was employed for fabricating PHB-based nanocomposite films. Future research endeavors can explore advanced production techniques, such as 3D printing, which could not only enable large-scale manufacturing of these nanocomposite films but also facilitate the production of various forms of packaging products, including boxes and bottles.
- Conventionally, mushrooms are packaged in rigid PS or PET trays sealed with stretchable materials such as PVC. The focus of the current study was restricted to the substitution of the non-renewable and non-biodegradable PVC films utilized in mushroom packaging with an active PHB/5GS/0.7MgO composite. Hence, future research should aim to substitute PS or PET trays with environmentally friendly materials, thus further advancing the sustainability of mushroom packaging.
- Given the outstanding gas barrier, antimicrobial, and antioxidant properties of the environmentally-friendly PHB/5GS/0.7MgO packaging material developed in this study, its application in the storage of other food products, including cut fruits and meat, can be explored.
- The biodegradability of the PHB-based nanocomposite films can be tested in seawater to comprehend their impact on marine ecosystems.

Bibliography

Bibliography

Abdelwahab, M., Salahuddin, N., Gaber, M. and Mousa, M., 2018. Poly (3-hydroxybutyrate)/polyethylene glycol-NiO nanocomposite for NOR delivery: antibacterial activity and cytotoxic effect against cancer cell lines. Int. J. Biol. Macromol., 114, 717-727. doi: 10.1016/j.ijbiomac.2018.03.050

Accinelli, C., Saccà, M.L., Mencarelli, M. and Vicari, A., 2012. Deterioration of bioplastic carrier bags in the environment and assessment of a new recycling alternative. Chemosphere, 89 (2), 136-143. doi: 10.1016/j.chemosphere.2012.05.028

Adorna, J.A., Aleman, C.K.A., Gonzaga, I.L.E., Pangasinan, J.N., Sisican, K.M.D., Dang, V.D., Doong, R.A., Ventura, R.L.G., and Ventura, J.R.S., 2020. Effect of lauric acid on the thermal and mechanical properties of polyhydroxybutyrate (PHB)/starch composite biofilms. Int. J. Polym. Sci., 7947019, 1-11. doi:10.1155/2020/7947019

Ahipathy, M.V. and Puttaiah, E.T., 2006. Ecological characteristics of Vrishabhavathy river in Bangalore (India), Environ. Geol., 49 (8), 1217-1222. doi: 10.1007/s00254-005-0166-0

Ahmad, K. and Mobin, S.M., 2019. High surface area 3D-MgO flowers as the modifier for the working electrode for efficient detection of 4-chlorophenol. Nanoscale Adv., 1 (2), 719-727. doi:10.1039/c8na00007g

Ahmed, J., Mulla, M.Z. and Arfat, Y.A., 2016. Thermo-mechanical, structural characterization and antibacterial performance of solvent casted polylactide/cinnamon oil composite films. Food Control, 69,196-204. doi:10.1016/j.foodcont.2016.05.013

Ahsan, W.A., Hussain, A., Lin, C. and Nguyen, M.K., 2023. Biodegradation of different types of bioplastics through composting-a recent trend in green recycling. Catalysts, 13 (2), 294. doi: 10.3390/catal13020294

Aksay, S., 2019. Effects of Al dopant on XRD, FT-IR and UV-vis properties of MgO films. Physica B: Condens. Matter, 570, 280-284. doi: 10.1016/j.physb.2019.06.020

Akhter, R., Masoodi, F.A., Wani, T.A. and Rather, S.A., 2019. Functional characterization of biopolymer based composite film: incorporation of natural essential oils and

antimicrobial agents. Int. J. Biol. Macromol., 137, 1245-1255. doi:10.1016/j.ijbiomac.2019.06.214

Akin, O., and Tihminlioglu, F., 2018. Effects of organo-modified clay addition and temperature on the water vapor barrier properties of polyhydroxybutyrate homo and copolymer nanocomposite films for packaging applications. J. Polym. Environ., 26 (3), 1121-1132. doi:10.1007/s10924-017-1017-2

Alavi, M.A. and Morsali, A., 2010. Syntheses and characterization of $Mg(OH)_2$ and MgO nanostructures by ultrasonic method. Ultrason. Sonochem., 17 (2), 441-446. doi: 10.1016/j.ultsonch.2009.08.013

Albuquerque, R.M., Meira, H.M., Silva, I.D., Silva, C.J.G., Almeida, F.C.G., Amorim, J.D., Vinhas, G.M., Costa, A.F.S., and Sarubbo, L.A., 2021. Production of a bacterial cellulose/poly (3-hydroxybutyrate) blend activated with clove essential oil for food packaging. Polym. Polym. Compos., 29 (4), 259-270. doi:10.1177%2f0967391120912098

Albright, V.C. and Chai, Y., 2021. Knowledge gaps in polymer biodegradation research, Environ. Sci. Technol., 55, 11476-11488. doi: 10.1021/acs.est.1c00994

Alghamdi, H.M., Abutalib, M.M., Mannaa, M.A., Nur, O., Abdelrazek, E.M. and Rajeh, A., 2022. Modification and development of high bioactivities and environmentally safe polymer nanocomposites doped by Ni/ZnO nanohybrid for food packaging applications. J. Mater. Res. Technol., 19, 3421-3432. doi: 10.1016/j.jmrt.2022.06.077

Al Hosni, A.S., Pittman, J.K. and Robson, G.D., 2019. Microbial degradation of four biodegradable polymers in soil and compost demonstrating polycaprolactone as an ideal compostable plastic. Waste Manag., 97, 105-114. doi: 10.1016/j.wasman.2019.07.042

Alizadeh-Sani, M., Moghaddas Kia, E., Ghasempour, Z. and Ehsani, A., 2021. Preparation of active nanocomposite film consisting of sodium caseinate, ZnO nanoparticles and rosemary essential oil for food packaging applications. J. Polym. Environ., 29, 588-598. doi: 10.1007/s10924-020-01906-5

Ali, M.Y., Sina, A.A.I., Khandker, S.S., Neesa, L., Tanvir, E.M., Kabir, A., Khalil M.I., and Gan S.H., 2021. Nutritional composition and bioactive compounds in tomatoes and their impact on human health and disease: a review. Foods, 10 (1), 45. doi: 10.3390/foods10010045

Altamimi, M.A., Hussain, A., Alshehri, S., Imam, S.S. and Alnemer, U.A., 2021. Development and evaluations of transdermally delivered luteolin loaded cationic nanoemulsion: in vitro and ex vivo evaluations. Pharmaceutics, 13 (8), 1218. doi:10.3390/pharmaceutics13081218

Amani, T., Haghighi, M. and Rahmanivahid, B., 2019. Microwave-assisted combustion design of magnetic Mg-Fe spinel for MgO-based nanocatalyst used in biodiesel production: Influence of heating-approach and fuel ratio. J. Ind. Eng. Chem., 80, 43-52. doi:10.1016/j.jiec.2019.07.029

Amorati, R., Foti, M.C. and Valgimigli, L., 2013. Antioxidant activity of essential oils. J. Agric. Food Chem., 61 (46), 10835-10847. doi:10.1021/jf403496k

Anbukarasu, P., Sauvageau, D. and Elias, A., 2015. Tuning the properties of polyhydroxybutyrate films using acetic acid via solvent casting. Sci. Rep., 5 (1), 1-14. doi:10.1038/srep17884

Ankush, K., Pugazhenthi, G., Mohit, K. and Vasanth, D., 2022. Experimental study on fabrication, biocompatibility and mechanical characterization of polyhydroxybutyrate-ball clay bionanocomposites for bone tissue engineering. Int. J. Biol. Macromol., 209, 1995-2008. doi: 10.1016/j.ijbiomac.2022.04.178

Ansari, A., Ali, A. and Asif, M., 2018. Microwave-assisted MgO NP catalyzed one-pot multicomponent synthesis of polysubstituted steroidal pyridines. New J. Chem., 42 (1), 184-197. doi:10.1039/c7nj03742b

Arfat, Y.A., Ahmed, J., Ejaz, M. and Mullah, M., 2018. Polylactide/graphene oxide nanosheets/clove essential oil composite films for potential food packaging applications. Int. J. Biol. Macromol., 107, 194-203. doi: 10.1016/j.ijbiomac.2017.08.156

Arfat, Y.A., Ahmed, J., Al Hazza, A., Jacob, H. and Joseph, A., 2017. Comparative effects of untreated and 3-methacryloxypropyltrimethoxysilane treated ZnO nanoparticle reinforcement on properties of polylactide-based nanocomposite films. Int. J. Biol. Macromol., 101, 1041-1050. doi: 10.1016/j.ijbiomac.2017.03.176

Aragüez, L., Colombo, A., Borneo, R. and Aguirre, A., 2020. Active packaging from triticale flour films for prolonging storage life of cherry tomato. Food Packag. Shelf Life, 25, 100520. doi: 10.1016/j.fpsl.2020.100520

Arrieta, M.P., Fortunati, E., Dominici, F., Rayón, E., López, J. and Kenny, J.M., 2014. PLA-PHB/cellulose based films: mechanical, barrier and disintegration properties. Polym. Degrad. Stab., 107, 139-149. doi: 10.1016/j.polymdegradstab.2014.05.010

Arumugam, S., Kandasamy, J., Thiyaku, T. and Saxena, P., 2022. Effect of low concentration of SiO_2 nanoparticles on grape seed essential oil/PBAT composite films for sustainable food packaging application. Sustain., 14 (13), 8073. doi: 10.3390/su14138073

Atarés, L. and Chiralt, A., 2016. Essential oils as additives in biodegradable films and coatings for active food packaging. Trends in Food Sci. Technol., 48, 51-62. doi: 10.1016/j.tifs.2015.12.001

Ayana, B., Suin, S. and Khatua, B.B., 2014. Highly exfoliated eco-friendly thermoplastic starch (TPS)/poly (lactic acid) (PLA)/clay nanocomposites using unmodified nanoclay. Carbohydr. Polym., 110, 430-439. doi: 10.1016/j.carbpol.2014.04.024

Baek, N., Kim, Y.T., Marcy, J.E., Duncan, S.E., and O'Keefe, S.F., 2018. Physical properties of nanocomposite polylactic acid films prepared with oleic acid modified titanium dioxide. Food Packag., 17, 30-38. doi: 10.1016/j.fpsl.2018.05.004

Balaguer, M.P., Borne, M., Chalier, P., Gontard, N., Morel, M.H., Peyron, S., Gavara, R. and Hernandez-Munoz, P., 2013. Retention and release of cinnamaldehyde from wheat protein matrices. Biomacromolecules, 14 (5), 1493-1502. doi:10.1021/bm400158t

Bail, S., Stuebiger, G., Krist, S., Unterweger, H. and Buchbauer, G., 2008. Characterisation of various grape seed oils by volatile compounds, triacylglycerol composition, total phenols and antioxidant capacity. Food Chem., 108 (3), 1122-1132. doi:10.1016/j.foodchem.2007.11.063

Balakrishnan, G., Velavan, R., Batoo, K.M. and Raslan, E.H., 2020. Microstructure, optical and photocatalytic properties of MgO nanoparticles. Results Phys., 16, 103013. doi:10.1016/j.rinp.2020.103013

Barragán, D.H., Pelacho, A.M. and Martin-Closas, L., 2016. Degradation of agricultural biodegradable plastics in the soil under laboratory conditions. Soil Res., 54, (2), 216-224. doi: 10.1071/sr15034

Baltieri, R.C., Innocentini Mei, L.H. and Bartoli, J., 2003, July. Study of the influence of plasticizers on the thermal and mechanical properties of poly (3-hydroxybutyrate) compounds. Macromol. Symp., 197, 33-44. doi:10.1002/masy.200350704

Bhat, V.G., Narasagoudr, S.S., Masti, S.P., Chougale, R.B., Vantamuri, A.B. and Kasai, D., 2022. Development and evaluation of Moringa extract incorporated chitosan/guar gum/poly (vinyl alcohol) active films for food packaging applications. Int. J. Biol. Macromol., 200, 50-60. doi:10.1016/j.ijbiomac.2021.12.116

Bhattacharya, P., Dey, A. and Neogi, S., 2021. An insight into the mechanism of antibacterial activity by magnesium oxide nanoparticles. J. Mater. Chem. B, 9 (26), 5329-5339. doi:10.1039/d1tb00875g

Bikiaris, D.N., 2013. Nanocomposites of aliphatic polyesters: An overview of the effect of different nanofillers on enzymatic hydrolysis and biodegradation of polyesters. Polym. Degrad. Stab., 98 (9), 1908-1928. doi: 10.1016/j.polymdegradstab.2013.05.016

Bindhu, M.R., Umadevi, M., Micheal, M.K., Arasu, M.V. and Al-Dhabi, N.A., 2016. Structural, morphological and optical properties of MgO nanoparticles for antibacterial applications. Mater. Lett., 166, 19-22. doi: 10.1016/j.matlet.2015.12.020

Bonilla, J., Poloni, T., Lourenço, R.V. and Sobral, P.J., 2018. Antioxidant potential of eugenol and ginger essential oils with gelatin/chitosan films. Food biosci., 23, 107-114. doi: 10.1016/j.fbio.2018.03.007

Bonemann, D.H., Luckow, A.C.B., Pereira, C.C., de Souza, A.O., Cadore, S., Nunes, A.M., Vieira, M.A. and Ribeiro, A.S., 2021. Determination of total concentration and bioaccessible fraction of metals in tomatoes and their derivatives by MIP OES. J. Food Compos. Anal., 96, 103716. doi: 10.1016/j.jfca.2020.103716

Boonsiriwit, A., Xiao, Y., Joung, J., Kim, M., Singh, S. and Lee, Y.S., 2020. Alkaline halloysite nanotubes/low density polyethylene nanocomposite films with increased ethylene absorption capacity: applications in cherry tomato packaging. Food Packag. Shelf Life, 25, 100533. doi: 10.1016/j.fpsl.2020.100533

Boro, U., Priyadarsini, A. and Moholkar, V.S., 2022. Synthesis and characterization of poly (lactic acid)/clove essential oil/alkali-treated halloysite nanotubes composite films for food packaging applications. Int. J. Biol. Macromol., 216, 927-939. doi: 10.1016/j.ijbiomac.2022.07.209

Briassoulis, D., Mistriotis, A., Mortier, N. and Tosin, M., 2020. A horizontal test method for biodegradation in soil of bio-based and conventional plastics and lubricants. J. Clean. Prod., 242, 118392. doi: 10.1016/j.jclepro.2019.118392

British plastic federation, 2019. Oil consumption.

https://www.bpf.co.uk/press/Oil_Consumption (last accessed 19 January 2020).

Buendía, L., Soto, S., Ros, M., Antolinos, V., Navarro, L., Sánchez, M.J., Martínez, G.B. and López, A., 2019. Innovative cardboard active packaging with a coating including encapsulated essential oils to extend cherry tomato shelf life. LWT, 116, 108584. doi: 10.1016/j.lwt.2019.108584

Çakmak, H., Özselek, Y., Turan, O.Y., Fıratlıgil, E. and Karbancioğlu-Güler, F., 2020. Whey protein isolate edible films incorporated with essential oils: antimicrobial activity and barrier properties. Polym. Degrad. Stab., 179, 109285. doi: 10.1016/j.polymdegradstab.2020.109285

Canbay, H.S. and Bardakci, B., 2011. Determination of fatty acid, C, H, N and trace element composition in grape seed by GC/MS, FTIR, elemental analyzer and ICP/OES. Süleyman Demirel Univ. Fac. Arts J. Sci., 6 (2), 140-148.

Cantwell, M., Nie, X. and Hong, G., 2009. Impact of storage conditions on grape tomato quality. In 6th ISHS postharvest symposium, 1-8.

Cazón, P., Antoniewska, A., Rutkowska, J. and Vázquez, M., 2021. Evaluation of easy-removing antioxidant films of chitosan with *Melaleuca alternifolia* essential oil. Int. J. Biol. Macromol., 186, 365-376. doi:10.1016/j.ijbiomac.2021.07.035

Chaiwarit, T., Ruksiriwanich, W., Jantanasakulwong, K. and Jantrawut, P., 2018. Use of orange oil loaded pectin films as antibacterial material for food packaging. Polymers, 10 (10), 1144. doi:10.3390/polym10101144

Chakraborty, S., Kumar, M., Suresh, K., and Pugazhenthi, G., 2014. Influence of organically modified NiAl layered double hydroxide (LDH) loading on the rheological properties of poly (methyl methacrylate) (PMMA)/LDH blend solution. Powder Technol., 256, 196-203. doi: 10.1016/j.powtec.2014.02.035

Chakravartula, S.S.N., Lourenço, R.V., Balestra, F., Bittante, A.M.Q.B., Do Amaral Sobral, P.J., and Dalla Rosa, M., 2020. Influence of pitanga (*Eugenia uniflora L.*) leaf extract and/or natamycin on properties of cassava starch/chitosan active films. Food Packag., 24, 100498. doi: 10.1016/j.fpsl.2020.100498

Cheng, M., Wang, J., Zhang, R., Kong, R., Lu, W., and Wang, X., 2019. Characterization and application of the microencapsulated carvacrol/sodium alginate films as food packaging materials. Int. J. Biol. Macromol., 141, 259-267. doi: 10.1016/j.ijbiomac.2019.08.215

Chernozem, R.V., Pariy, I.O., Pryadko, A., Bonartsev, A.P., Voinova, V.V., Zhuikov, V.A., Makhina, T.K., Bonartseva, G.A., Shaitan, K.V., Shvartsman, V.V., and Lupascu, D.C., 2022. A comprehensive study of the structure and piezoelectric response of biodegradable polyhydroxybutyrate-based films for tissue engineering applications. Polym. J., 54, 1225-1236. doi:10.1038/s41428-022-00662-8

Chinthala, M., Balakrishnan, A., Venkataraman, P., Manaswini Gowtham, V. and Polagani, R.K., 2021. Synthesis and applications of nano-MgO and composites for medicine, energy, and environmental remediation: a review. Environ. Chem. Lett., 19 (6), 4415-4454. doi:10.1007/s10311-021-01299-4

Chi, H., Song, S., Luo, M., Zhang, C., Li, W., Li, L., and Qin, Y., 2019. Effect of PLA nanocomposite films containing bergamot essential oil, TiO_2 nanoparticles, and Ag nanoparticles on shelf life of mangoes. Sci. Hortic., 249, 192-198. doi: 10.1016/j.scienta.2019.01.059

Claro, P.I.C., Neto, A.R.S., Bibbo, A.C.C., Mattoso, L.H.C., Bastos, M.S.R., and Marconcini, J.M., 2016. Biodegradable blends with potential use in packaging: a comparison of

PLA/chitosan and PLA/cellulose acetate films. J. Polym. Environ., 24 (4), 363-371. doi:10.1007/s10924-016-0785-4

Cui, R., Jiang, K., Yuan, M., Cao, J., Li, L., Tang, Z. and Qin, Y., 2020. Antimicrobial film based on polylactic acid and carbon nanotube for controlled cinnamaldehyde release. J. Mater. Res. Technol., 9 (5), 10130-10138. doi: 10.1016/j.jmrt.2020.07.016

Da Roz, A.L., Zambon, M.D., Curvelo, A.A., and Carvalho, A.J., 2011. Thermoplastic starch modified during melt processing with organic acids: the effect of molar mass on thermal and mechanical properties. Ind. Crops Prod., 33 (1), 152-157. doi: 10.1016/j.indcrop.2010.09.015

D'Aquino, S., Mistriotis, A., Briassoulis, D., Di Lorenzo, M.L., Malinconico, M. and Palma, A., 2016. Influence of modified atmosphere packaging on postharvest quality of cherry tomatoes held at 20 C. Postharvest Biol. Technol., 115, 103-112. doi: 10.1016/j.postharvbio.2015.12.014

Dairi, N., Ferfera-Harrar, H., Ramos, M., and Garrigos, M.C., 2019. Cellulose acetate/AgNPs-organoclay and/or thymol nano-biocomposite films with combined antimicrobial/antioxidant properties for active food packaging use. Int. J. Biol. Macromol., 121, 508-523. doi: 10.1016/j.ijbiomac.2018.10.042

Dawadi, E., Magar, P.B., Bhandari, S., Subedi, S., Shrestha, S. and Shrestha, J., 2022. Nutritional and post-harvest quality preservation of mushrooms: a review. Heliyon, 8 (12), e12093. doi: 10.1016/j.heliyon.2022.e12093

De Silva, R.T., Mantilaka, M.M.M.G.P.G., Ratnayake, S.P., Amaratunga, G.A.J., and De Silva, K.N., 2017. Nano-MgO reinforced chitosan nanocomposites for high performance packaging applications with improved mechanical, thermal and barrier properties. Carbohydr. Polym., 157, 739-747. doi: 10.1016/j.carbpol.2016.10.038

Dhar, P., Tarafder, D., Kumar, A. and Katiyar, V., 2015. Effect of cellulose nanocrystal polymorphs on mechanical, barrier and thermal properties of poly (lactic acid) based bionanocomposites. RSC Adv., 5 (74), 60426-60440. doi:10.1039/c5ra06840a

Díez-Pascual, A.M. and Díez-Vicente, A.L., 2014. ZnO-reinforced poly (3-hydroxybutyrate-co-3-hydroxyvalerate) bionanocomposites with antimicrobial function for food packaging. ACS Appl. Mater. Interfaces, 6 (12), 9822-9834. doi: 10.1021/am502261e

Ding, Y.D., Song, G., Zhu, X., Chen, R. and Liao, Q., 2015. Synthesizing MgO with a high specific surface for carbon dioxide adsorption. RSC Adv., 5 (39), 30929-30935. doi:10.1039/c4ra15127e

Díez-Pascual, A.M. and Díez-Vicente, A.L., 2014. Poly (3-hydroxybutyrate)/ZnO bionanocomposites with improved mechanical, barrier and antibacterial properties. Int. J. Mol. Sci., 15 (6) (2014), 10950-10973. doi: 10.3390/ijms150610950

Doh, H., Dunno, K.D. and Whiteside, W.S., 2020. Cellulose nanocrystal effects on the biodegradability with alginate and crude seaweed extract nanocomposite films. Food Biosci., 38, 100795. doi: 10.1016/j.fbio.2020.100795

Dotto, G.L. and Pinto, L.A.A., 2017. General considerations about Chitosan. in: Dotto, G. L., Campana-Filho, S. P., Pinto L. A. A. (Eds.) Materials and its applications. Bentham Science Publishers, Sharjah, 3-33

Ebrahimi, S. and Yarmand, B., 2019. Morphology engineering and growth mechanism of ZnS nanostructures synthesized by solvothermal process. J. Nanopart. Res., 21 (12), 1-12. doi:10.1007/s11051-019-4714-z

El-Shaer, A., Abdelfatah, M., Mahmoud, K.R., Momay, S. and Eraky, M.R., 2020. Correlation between photoluminescence and positron annihilation lifetime spectroscopy to characterize defects in calcined MgO nanoparticles as a first step to explain antibacterial activity. J. Alloys Compd., 817, 152799. doi: 10.1016/j.jallcom.2019.152799

El-Sawy, N.M., Raafat, A.I., Badawy, N.A. and Mohamed, A.M., 2020. Radiation development of pH-responsive (xanthan-acrylic acid)/MgO nanocomposite hydrogels for controlled delivery of methotrexate anticancer drug. Int. J. Biol. Macromol., 142, 254-264. doi: 10.1016/j.ijbiomac.2019.09.097

Emadian, S.M., Onay, T.T. and Demirel, B., 2017. Biodegradation of bioplastics in natural environments. Waste Manag., 59, 526-536. doi: 10.1016/j.wasman.2016.10.006

Engel, J.B., Luchese, C.L. and Tessaro, I.C., 2022. Making the reuse of agro-industrial wastes a reality for starch-based packaging sector: a storage case study of carrot cake and cherry tomatoes. Int. J. Biol. Macromol., 206, 740-749. doi: 10.1016/j.ijbiomac.2022.03.074

Ercan, I., Kaygili, O., Ates, T., Gunduz, B., Bulut, N., Koytepe, S. and Ozcan, I., 2018. The effects of urea content on the structural, thermal and morphological properties of MgO nanopowders. Ceram. Int., 44 (12), 14523-14527. doi: 10.1016/j.ceramint.2018.05.068

Esmaeili, E., Khodadadi, A. and Mortazavi, Y., 2009. Microwave-induced combustion process variables for MgO nanoparticle synthesis using polyethylene glycol and sorbitol. J. Eur. Ceram. Soc., 29 (6), 1061-1068. doi: 10.1016/j.jeurceramsoc.2008.07.051

European Bioplastics, 2023. Market. https://www.european-bioplastics.org/bioplastics-market-development-update-2023-2/ (last accessed 20 May 2024)

European Commission, 2007. Corrigendum to Commission Directive 2007/19/EC of 30 March 2007 amending directive 2002/72/EC relating to plastic materials and articles intended to come into contact with food and council directive 85/572/EEC laying down the list of simulants to be used. Off. J. Eur. Union, 50-69. https://eurlex.europa.eu/LexUriServ/LexUriServ.do?uri=OJ:L:2007:097:0050:0069:EN:PDF (last accessed 20 May 2024)

Fagundes, C., Moraes, K., Pérez-Gago, M.B., Palou, L., Maraschin, M. and Monteiro, A.R., 2015. Effect of active modified atmosphere and cold storage on the postharvest quality of cherry tomatoes. Postharvest Biol. Technol., 109, 73-81. doi: 10.1016/j.postharvbio.2015.05.017

FDA, 2002. Guidance for industry: Preparation of food contact notifications (administrative). https://www.fda.gov/regulatory-information/search-fda-guidance-documents/guidance-industry-preparation-food-contact-notifications-administrative (last accessed 7 February 2022)

Ferreira, R.R., Farina, M.C., Maia, A. and Torin, R.F., 2023. PLA films containing montmorillonite nanoclay-citronella essential oil hybrids for potential active film formulation. Macromol, 3 (2), 200-210. doi:10.3390/macromol3020012

Fernández-Menéndez, T., García-López, D., Argüelles, A., Fernández, A. and Viña, J., 2020. Industrially produced PET nanocomposites with enhaced properties for food packaging applications. Polym. Test., 90, 106729. doi: 10.1016/j.polymertesting.2020.106729

Foletto, E.L., Battiston, S., Simoes, J.M., Bassaco, M.M., Pereira, L.S.F., de Moraes Flores, E.M. and Müller, E.I., 2012. Synthesis of $ZnAl_2O_4$ nanoparticles by different routes and the effect of its pore size on the photocatalytic process. Microporous and Mesoporous Mater., 163, 29-33. doi: 10.1016/j.micromeso.2012.06.039

Fukushima, K., Tabuani, D., Abbate, C., Arena, M. and Ferreri, L., 2010. Effect of sepiolite on the biodegradation of poly (lactic acid) and polycaprolactone. Polym. Degrad. Stab., 95 (10), 2049-2056. doi: 10.1016/j.polymdegradstab.2010.07.004

Garavaglia, J., Markoski, M.M., Oliveira, A. and Marcadenti, A., 2016. Grape seed oil compounds: Biological and chemical actions for health. Nutr. Metab. Insights, 9, 59-64. doi:10.4137/nmi. s32910

Garcia-Garcia, D., Carbonell-Verdu, A., Arrieta, M.P., López-Martínez, J. and Samper, M.D., 2020. Improvement of PLA film ductility by plasticization with epoxidized karanja oil. Polym. Degrad. Stab., 179, 109259. doi:10.1016/j.polymdegradstab.2020.109259

García-García, I., Taboada-Rodríguez, A., López-Gomez, A. and Marín-Iniesta, F., 2013. Active packaging of cardboard to extend the shelf life of tomatoes. Food Bioprocess Technol., 6, 754-761. doi: 10.1007/s11947-011-0759-4

Garrido-Miranda, K.A., Rivas, B.L., Pérez-Rivera, M.A., Sanfuentes, E.A. and Peña-Farfal, C., 2018. Antioxidant and antifungal effects of eugenol incorporated in bionanocomposites of poly (3-hydroxybutyrate)-thermoplastic starch. LWT, 98, 260-267. doi:10.1016/j.lwt.2018.08.046

Gasti, T., Dixit, S., Hiremani, V.D., Chougale, R.B., Masti, S.P., Vootla, S.K. and Mudigoudra, B.S., 2022. Chitosan/pullulan based films incorporated with clove essential oil loaded chitosan-ZnO hybrid nanoparticles for active food packaging. Carbohydr. Polym., 277, 118866. doi: 10.1016/j.carbpol.2021.118866

Geng, C., Liu, X., Ma, J., Ban, H., Bian, H. and Huang, G., 2023. High strength, controlled release of curcumin-loaded ZIF-8/chitosan/zein film with excellence gas barrier and

antibacterial activity for litchi preservation. Carbohydr. Polym., 306, 120612. doi: 10.1016/j.carbpol.2023.120612

Geyer, R., Jambeck, J.R. and Law, K.L., 2017. Production, use, and fate of all plastics ever made. Sci. Adv., 3 (7), 1700782. doi:10.1126/sciadv.1700782

Gharezi, M., Joshi, N. and Sadeghian, E., 2012. Effect of postharvest treatment on stored cherry tomatoes. J. Nutr. Food Sci., 2 (8), 1-10. doi: 10.4172/2155-9600.1000157

Gholami, R., Aghili Nategh, N. and Rabbani, H., 2023. Evaluation the effects of temperature and packaging conditions on the quality of button mushroom during storage using e-nose system. J. Food Sci. Technol, 60 (4), 1355-1366. doi: 10.1007/s13197-023-05682-7

Gholami, R., Ahmadi, E. and Farris, S., 2017. Shelf life extension of white mushrooms (*Agaricus bisporus*) by low temperatures conditioning, modified atmosphere, and nanocomposite packaging material. Food Packag. Shelf Life, 14, 88-95. doi: 10.1016/j.fpsl.2017.09.001

Giannoglou, M., Xanthou, Z.M., Chanioti, S., Stergiou, P., Christopoulos, M., Dimitrakellis, P., Efthimiadou, A., Gogolides, E., and Katsaros, G., 2021. Effect of cold atmospheric plasma and pulsed electromagnetic fields on strawberry quality and shelf-life. Innov. Food Sci. Emerg. Technol., 68, 102631. doi: 10.1016/j.ifset.2021.102631

Giaquinto, C.D.M., Souza, G.K.M.D., Caetano, V.F. and Vinhas, G.M., 2017. Evaluation of the mechanical and thermal properties of PHB/canola oil films. Polímeros, 27, 201-207. doi:10.1590/0104-1428.10716

Global market insights, By materials (paper & cardboard, rigid plastics, metal, flexible plastics, glass, wood, textiles), by product (bottles & cans, containers & jars, bags, pouches, & wraps, closures & lids, boxes & crates, drums & ibcs), by end-use & forecast, 2024-2032. https://www.gminsights.com/industry-analysis/packaging-materials-market, 2024 (last accessed 22 April 2024)

Gómez-Estaca, J., Lopez-de-Dicastillo, C., Hernandez-Munoz, P., Catala, R. and Gavara, R., 2014. Advances in antioxidant active food packaging. Trends Food Sci. Technol., 35 (1), 42-51. doi: 10.1016/j.tifs.2013.10.008

Gupta, K., Kumari, S.V.G. and Pugazhenthi, G., 2023. Synergistic influence of multi-walled carbon nanotubes and graphene nanoparticles on the structural, thermal and mechanical characteristics of poly (3-hydroxybutyrate) films. Mater. Today: Proc., In press. doi: 10.1016/j.matpr.2023.07.292

Guillaume, C., Schwab, I., Gastaldi, E. and Gontard, N., 2010. Biobased packaging for improving preservation of fresh common mushrooms (*Agaricus bisporus L.*). Innov. Food Sci. Emerg. Technol., 11 (4), 690-696. doi: 10.1016/j.ifset.2010.05.007

Hadia, N.M.A. and Mohamed, H.A.H., 2015. Characteristics and optical properties of MgO nanowires synthesized by solvothermal method. Mater. Sci. Semicond. Process., 29, 238-244. doi: 10.1016/j.mssp.2014.03.049

Haghighi, H., Biard, S., Bigi, F., De Leo, R., Bedin, E., Pfeifer, F., Siesler, H.W., Licciardello, F. and Pulvirenti, A., 2019. Comprehensive characterization of active chitosan-gelatin blend films enriched with different essential oils. Food Hydrocoll., 95, 33-42. doi.org: 10.1016/j.foodhyd.2019.04.019

Han, Y., Yang, T. and Chen, Y., 2020. A perspective on morphology controlled synthesis of powder by tuning chemical diffusion and reaction. Adv. Powder Tech., 31 (3), 922-925. doi: 10.1016/j.apt.2019.12.008

Han, L., Qin, Y., Liu, D., Chen, H., Li, H. and Yuan, M., 2015. Evaluation of biodegradable film packaging to improve the shelf-life of *Boletus edulis* wild edible mushrooms. Innov. Food Sci. Emerg. Technol., 29, 288-294. doi: 10.1016/j.ifset.2015.04.008

Halder, R. and Bandyopadhyay, S., 2017. Synthesis and optical properties of anion deficient nano MgO. J. Alloys Compd., 693, 534-542. doi: 10.1016/j.jallcom.2016.09.164

Haghighi, H., Licciardello, F., Fava, P., Siesler, H.W., Pulvirenti, A., 2020. Recent advances on chitosan-based films for sustainable food packaging applications. Food Packag., 26, 100551. doi: 10.1016/j.fpsl.2020.100551

Hassiotis, C.N. and Lazari, D.M., 2010. Decomposition process in the mediterranean region. chemical compounds and essential oil degradation from *Myrtus communis*. Int. Biodeterior. Biodegrad., 64 (5), 356-362. doi:10.1016/j.ibiod.2010.02.007

Heo, Y.J. and Park, S.J., 2017. Facile synthesis of MgO-modified carbon adsorbents with microwave-assisted methods: effect of MgO particles and porosities on CO_2 capture. Sci. Rep., 7 (1), 1-9. doi:10.1038/s41598-017-06091-5

Heydari-Majd, M., Ghanbarzadeh, B., Shahidi-Noghabi, M., Najafi, M.A. and Hosseini, M., 2019. A new active nanocomposite film based on PLA/ZnO nanoparticle/essential oils for the preservation of refrigerated *Otolithes* ruber fillets. Food Packag. Shelf Life, 19, 94-103, doi: 10.1016/j.fpsl.2018.12.002

Ilyas, R.A., Sapuan, S.M., Megashah, L.N., Ibrahim, R., Atikah, M.S.N., Ainun, Z.M.A., Aung, M.M., SaifulAzry, S.O.A., Lee, C.H., 2021. Regulations for food packaging materials. in: Sapuan, S. M., Ilyas, R. A. (Eds.), Bio-based packaging: material, environmental and economic aspects. 467-494

Ismail, R.A., Mousa, A.M. and Shaker, S.S., 2020. Preparation of visible-enhanced PbI_2/MgO/Si heterojunction photodetector. Optik, 202, 163585. doi: 10.1016/j.ijleo.2019.163585

Ismail, R.A., Mousa, A.M. and Shaker, S.S., 2019. Pulsed laser deposition of nanostructured MgO film: effect of laser fluence on the structural and optical properties. Mater. Res. Express, 6 (7), 075007. doi:10.1088/2053-1591/ab1208

Ismail, R.A., Sulaiman, G.M., Abdulrahman, S.A. and Marzoog, T.R., 2015. Antibacterial activity of magnetic iron oxide nanoparticles synthesized by laser ablation in liquid. Mater. Sci. Eng. C, 53, 286-297. doi: 10.1016/j.msec.2015.04.047

Iwata, T. and Doi, Y., 1999. Crystal structure and biodegradation of aliphatic polyester crystals. Macromol. Chem. Phys., 200 (1999) 2429-2442

Jafri, M., Jha, A., Bunkar, D.S. and Ram, R.C., 2013. Quality retention of oyster mushrooms (*Pleurotus florida*) by a combination of chemical treatments and modified atmosphere packaging. Postharvest Biol. Technol., 76, 112-118. doi: 10.1016/j.postharvbio.2012.10.002

Jain, N., Marwaha, N., Verma, R., Gupta, B.K. and Srivastava, A.K., 2016. Facile synthesis of defect-induced highly-luminescent pristine MgO nanostructures for promising solid-state lighting applications. RSC Adv., 6 (6), 4960-4968. doi:10.1039/c5ra21150f

Jamali, M. and Tehrani, F.S., 2020. Effect of synthesis route on the structural and morphological properties of WO_3 nanostructures. Mater. Sci. Semicond. Process., 107, 104829. doi: 10.1016/j.mssp.2019.104829

Jebel, F.S., Almasi, H., 2016. Morphological, physical, antimicrobial and release properties of ZnO nanoparticles-loaded bacterial cellulose films. Carbohydr. Polym., 149, 8-19. doi: 10.1016/j.carbpol.2016.04.089

Jiang, J., Gong, L., Dong, Q., Kang, Y., Osako, K. and Li, L., 2020. Characterization of PLA-P3, 4HB active film incorporated with essential oil: application in peach preservation. Food Chem., 313, 126134. doi: 10.1016/j.foodchem.2019.126134

Jin, X.Z., Yu, X., Yang, C., Qi, X.D., Lei, Y.Z. and Wang, Y., 2019. Crystallization and hydrolytic degradation behaviors of poly (l-lactide) induced by carbon nanofibers with different surface modifications. Polym. Degrad. Stab., 170, 109014. doi: 10.1016/j.polymdegradstab.2019.109014

Joung, J., Boonsiriwit, A., Kim, M. and Lee, Y.S., 2021. Application of ethylene scavenging nanocomposite film prepared by loading potassium permanganate-impregnated halloysite nanotubes into low-density polyethylene as active packaging material for fresh produce. LWT, 145, 111309. doi: 10.1016/j.lwt.2021.111309

Kadoya, R., Soga, H., Matsuda, M., Sato, M. and Taguchi, S., 2023. Bacterial population changes during the degradation process of a lactate (LA)-enriched biodegradable polymer in river water: LA-cluster preferable bacterial consortium. Polymers, 15 (20), 4111. doi: 10.3390/polym15204111

Kaewklin, P., Siripatrawan, U., Suwanagul, A. and Lee, Y.S., 2018 Active packaging from chitosan-titanium dioxide nanocomposite film for prolonging storage life of tomato fruit. Int. J. Biol. Macromol., 112, 523-529. doi: 10.1016/j.ijbiomac.2018.01.124

Kang, J. and Yun, S.I., 2022. Chitosan-reinforced PHB hydrogel and aerogel monoliths fabricated by phase separation with the solvent-exchange method. Carbohydr. Polym., 284, 119184. doi: 10.1016/j.carbpol.2022.119184

Karthik, K., Dhanuskodi, S., Gobinath, C., Prabukumar, S. and Sivaramakrishnan, S., 2019. Fabrication of MgO nanostructures and its efficient photocatalytic, antibacterial and

anticancer performance. J. Photochem. Photobiol. B, 190, 8-20. doi: 10.1016/j.jphotobiol.2018.11.001

Keshavarz, T. and Roy, I., 2010. Polyhydroxyalkanoates: Bioplastics with a green agenda. Curr. Opin. Microbiol., 13 (3), 321-326. doi: 10.1016/j.mib.2010.02.006

Keller, P.E., Kouzes, R.T., 2017. Water vapor permeation in plastics (No. PNNL-26070). Pacific Northwest National Lab (PNNL), Richland, WA (United States). https://www.pnnl.gov/main/publications/external/technical_reports/pnnl-26070.pdf (last accessed 21 May 2024)

Khah, M.D., Ghanbarzadeh, B., Nezhad, L.R. and Ostadrahimi, A., 2021. Effects of virgin olive oil and grape seed oil on physicochemical and antimicrobial properties of pectin-gelatin blend emulsified films. Int. J. Biol. Macromol., 171, 262-274. doi: 10.1016/j.ijbiomac.2021.01.020

Khalid, M., Mujahid, M., Amin, S., Rawat, R.S., Nusair, A. and Deen, G.R., 2013. Effect of surfactant and heat treatment on morphology, surface area and crystallinity in hydroxyapatite nanocrystals. Ceram. Int., 39 (1), 39-50. doi: 10.1016/j.ceramint.2012.05.090

Kim, I., Viswanathan, K., Kasi, G., Sadeghi, K., Thanakkasaranee, S. and Seo, J., 2019. Poly (lactic acid)/ZnO bionanocomposite films with positively charged ZnO as potential antimicrobial food packaging materials. Polymers, 11 (9), 1427. doi:10.3390/polym11091427

Kim, S.H., Ahn, S.H. and Hirai, T., 2003. Crystallization kinetics and nucleation activity of silica nanoparticle-filled poly (ethylene 2, 6-naphthalate). Polymer, 44 (19), 5625-5634. doi: 10.1016/S0032-3861(03)00623-2

Kowalska, H., Marzec, A., Domian, E., Kowalska, J., Ciurzynska, A. and Galus, S., 2021. Edible coatings as osmotic dehydration pretreatment in nutrient-enhanced fruit or vegetable snacks development: a review. Compr. Rev. Food Sci. Food Saf., 20 (6), 5641-5674. doi:10.1111/1541-4337.12837

Krishnamoorthy, K., Manivannan, G., Kim, S.J., Jeyasubramanian, K. and Premanathan, M., 2012. Antibacterial activity of MgO nanoparticles based on lipid peroxidation by oxygen vacancy. J. Nanopart. Res., 14 (9), 1-10. doi:10.1007/s11051-012-1063-6

Kumari, S.V.G., Manikandan, N.A., Pakshirajan, K. and Pugazhenthi, G., 2020. Sustained drug release and bactericidal activity of a novel, highly biocompatible and biodegradable polymer nanocomposite loaded with norfloxacin for potential use in antibacterial therapy. J. Drug Deliv. Sci. Technol., 59, 101900. doi: 10.1016/j.jddst.2020.101900

Kumar, N., Kaur, P., Devgan, K. and Attkan, A.K., 2020. Shelf life prolongation of cherry tomato using magnesium hydroxide reinforced bio-nanocomposite and conventional plastic films. J. Food Process. Preserv., 44 (4), 1-11. doi: 10.1111/jfpp.14379

Kumar, N., Kaur, P. and Bhatia, S., 2017. Advances in bio-nanocomposite materials for food packaging: a review. Nutr. Food Sci., 7 (4), 591-606. doi:10.1108/nfs-11-2016-0176

Kurusu, R.S., Siliki, C.A., David, E., Demarquette, N.R., Gauthier, C. and Chenal, J.M., 2015. Incorporation of plasticizers in sugarcane-based poly (3-hydroxybutyrate) (PHB): changes in microstructure and properties through ageing and annealing. Ind. Crops Prod., 72, 166-174. doi: 10.1016/j.indcrop.2014.12.040

Lee, J., Park, H.J., Moon, M., Lee, J.S., Min, K., 2021. Recent progress and challenges in microbial polyhydroxybutyrate (PHB) production from CO_2 as a sustainable feedstock: a state-of-the-art review. Bioresour. Technol., 339, 125616. doi: 10.1016/j.biortech.2021.125616

Lencova, S., Zdenkova, K., Demnerova, K. and Stiborova, H., 2022. Antibacterial and antibiofilm effect of natural substances and their mixtures over *Listeria monocytogenes*, *Staphylococcus aureus* and *Escherichia coli*. LWT, 154, 112777. doi: 10.1016/j.lwt.2021.112777

Leng, J., Mukhopadhyay, S., Sokorai, K., Ukuku, D.O., Fan, X., Olanya, M. and Juneja, V., 2020. Inactivation of *Salmonella* in cherry tomato stem scars and quality preservation by pulsed light treatment and antimicrobial wash. Food Control, 110 (2020), 107005. doi: 10.1016/j.foodcont.2019.107005

Li, W., Zheng, K., Chen, H., Feng, S., Wang, W. and Qin, C., 2019. Influence of nano titanium dioxide and clove oil on chitosan-starch film characteristics. Polymers, 11 (9), 1418. doi:10.3390/polym11091418

Li, X., Xiao, W., He, G., Zheng, W., Yu, N. and Tan, M., 2012. Pore size and surface area control of MgO nanostructures using a surfactant-templated hydrothermal process: high adsorption capability to azo dyes. Colloids Surf. A: Physicochem. Eng. Asp., 408, 79-86. doi: 10.1016/j.colsurfa.2012.05.034

Liu, W., Zhang, M. and Bhandari, B., 2020. Nanotechnology-a shelf life extension strategy for fruits and vegetables. Crit. Rev. Food Sci. Nutr., 60 (10), 1706-1721. doi: 10.1080/10408398.2019.1589415

Liu, J., Liu, S., Zhang, X., Kan, J. and Jin, C., 2019. Effect of gallic acid grafted chitosan film packaging on the postharvest quality of white button mushroom (*Agaricus bisporus*). Postharvest Biol. Technol., 147 (2019), 39-47. doi: 10.1016/j.postharvbio.2018.09.004

Liu, Y., Wang, S., Lan, W. and Qin, W., 2017. Fabrication and testing of PVA/chitosan bilayer films for strawberry packaging. Coatings, 7 (8), 1-16. doi: 10.3390/coatings7080109

Lv, S., Zhang, Y., Gu, J. and Tan, H., 2018. Physicochemical evolutions of starch/poly (lactic acid) composite biodegraded in real soil. J. Environ. Manag., 228, 223-231. doi: 10.1016/j.jenvman.2018.09.033

Lyn, F.H., Adilah, Z.M., Nor-Khaizura, M.A.R., Jamilah, B. and Hanani, Z.N., 2020. Application of modified atmosphere and active packaging for oyster mushroom (*Pleurotus ostreatus*). Food Packag. Shelf Life, 23, 100451, doi: 10.1016/j.fpsl.2019.100451

Mageshwari, K., Mali, S.S., Sathyamoorthy, R. and Patil, P.S., 2013. Template-free synthesis of MgO nanoparticles for effective photocatalytic applications. Powder technol., 249, 456-462. doi: 10.1016/j.powtec.2013.09.016

Majhi, A., Pugazhenthi, G. and Shukla, A., 2010. Comparative study of ultrasound stimulation and conventional heating methods on the preparation of nanosized γ-Al_2O_3. Ind. Eng. Chem. Res., 49 (10), 4710-4719. doi:10.1021/ie901857q

Mallikarjuna, S.E., Ranjini, A., Haware, D.J., Vijayalakshmi, M.R., Shashirekha, M.N. and Rajarathnam, S., 2013. Mineral composition of four edible mushrooms. J. Chem., 2013, 805284, doi: 10.1155/2013/805284

Malu, S.P., Obochi, G.O., Tawo, E.N. and Nyong, B.E., 2009. Antibacterial activity and medicinal properties of ginger (*Zingiber officinale*). Glob. J. Pure Applied Sci., 15 (3-4). doi:10.4314/gjpas. v15i3-4.48561

Manikandan, N.A., Pakshirajan, K., Pugazhenthi, G., 2021. Techno-economic assessment of a sustainable and cost-effective bioprocess for large scale production of polyhydroxybutyrate. Chemosphere, 284, 131371. doi: 10.1016/j.chemosphere.2021.131371

Manikandan, N.A., Pakshirajan, K., Pugazhenthi, G., 2020. Preparation and characterization of environmentally safe and highly biodegradable microbial polyhydroxybutyrate (PHB) based graphene nanocomposites for potential food packaging applications. Int. J. Biol. Macromol., 154, 866-877. doi: 10.1016/j.ijbiomac.2020.03.084

Martucci, J.F. and Ruseckaite, R.A., 2015. Biodegradation behavior of three-layer sheets based on gelatin and poly (lactic acid) buried under indoor soil conditions. Polym. Degrad. Stab., 116, 36-44. doi: 10.1016/j.polymdegradstab.2015.03.005

Maran, J.P., Sivakumar, V., Thirugnanasambandham, K. and Sridhar, R., 2014. Degradation behavior of biocomposites based on cassava starch buried under indoor soil conditions. Carbohydr. Polym., 101 (1), 20-28. doi: 10.1016/j.carbpol.2013.08.080

Martin, O. and Averous, L., 2001. Poly (lactic acid): plasticization and properties of biodegradable multiphase systems. Polymer, 42 (14), 6209-6219. doi:10.1016/s0032-3861(01)00086-6

Mangaraj, S., Yadav, A., Bal, L.M., Dash, S.K. and Mahanti, N.K., 2019. Application of biodegradable polymers in food packaging industry: a comprehensive review. J. Packag. Technol. Res., 3 (1), 77-96. doi:10.1007/s41783-018-0049-y

Mao, S., Ren, Y., Wei, C., Chen, S., Ye, X. and Jinhu, T., 2023. Development of novel EGCG/Fe loaded sodium alginate-based packaging films with antibacterial and slow-release properties. Food Hydrocoll., 145, 109032. doi: 10.1016/j.foodhyd.2023.109032

Majid, I., Nayik, G.A., Dar, S.M., Nanda, V., 2018. Novel food packaging technologies: Innovations and future prospective. J. Saudi Soc. Agric. Sci., 17 (4), 454-462. doi: 10.1016/j.jssas.2016.11.003

Maureira, J., Olate-Moya, F., Bastías, R., Farias, S., Alvarez, R., Rosales-Cuello, N. and Palza, H., 2023. Multifunctional poly (3-hydroxybutyrate) composites with MoS_2 for food packaging applications. Eur. Polym. J., 188 (2023), 111914. doi: 10.1016/j.eurpolymj.2023.111914

Meijer, L.J., Van Emmerik, T., Van Der Ent, R., Schmidt, C. and Lebreton, L., 2021. More than 1000 rivers account for 80 % of global riverine plastic emissions into the ocean, Sci. Adv., 7 (18), eaaz5803. doi: 10.1126/sciadv. aaz5803

Merlo, T.C., Contreras-Castillo, C.J., Saldana, E., Barancelli, G.V., Dargelio, M.D.B., Yoshida, C.M.P., Junior, E.E.R., Massarioli, A., Venturini, A.C., 2019. Incorporation of pink pepper residue extract into chitosan film combined with a modified atmosphere packaging: effects on the shelf life of salmon fillets. Food Res. Int., 125, 108633. doi: 10.1016/j.foodres.2019.108633

Meshkani, F. and Rezaei, M., 2009. Facile synthesis of nanocrystalline magnesium oxide with high surface area. Powder Tech., 196 (1), 85-88. doi: 10.1016/j.powtec.2009.07.010

Mirabolghasemi, S.M., Najafi, M., Azizi, A. and Haji Bagherian, M., 2021. Physico-mechanical properties of polylactic acid bio-nanocomposites filled by hybrid nanoparticles. Polym. Polym. Compos., 29 (9), S1510-S1519. doi: 10.1177/09673911211060132

Mittal, M., Ahuja, S., Yadav, A. and Aggarwal, N.K., 2023. Development of poly (hydroxybutyrate) film incorporated with nano silica and clove essential oil intended for active packaging of brown bread. Int. J. Biol. Macromol., 233, 123512. doi: 10.1016/j.ijbiomac.2023.123512

Miteluț, A.C., Tanase, E.E., Popa, V.I., Popa, M.E., 2015. Sustainable alternative for food packaging: chitosan biopolymer-a review. AgroLife Sci. J., 4 (2), 52-61

Miksusanti, M., Herlina, H. and Masril, K.M.K., 2013. Antibacterial and antioxidant of uwi (*Dioscorea alata L*) starch edible film incorporated with ginger essential oil. Int. J. Biosci. Biochem. Bioinform., 3 (4), 354-356. doi:10.7763/ijbbb. 2013.v3.230

Moeini, A., Germann, N., Malinconico, M. and Santagata, G., 2021. Formulation of secondary compounds as additives of biopolymer-based food packaging: a review. Trends Food Sci. Technol., 114, 342-354. doi: 10.1016/j.tifs.2021.05.040

Mohan, C.C., Harini, K., Karthikeyan, S., Sudharsan, K. and Sukumar, M., 2018. Effect of film constituents and different processing conditions on the properties of starch based thermoplastic films. Int. J. Biol. Macromol., 120, 2007-2016. doi:10.1016/j.ijbiomac.2018.09.161

Mohebbi, M., Ansarifar, E., Hasanpour, N. and Amiryousefi, M.R., 2012. Suitability of aloe vera and gum tragacanth as edible coatings for extending the shelf life of button mushroom. Food Bioprocess Technol., 5 (8), 3193-3202. doi: 10.1007/s11947-011-0709-1

Mollamahale, Y.B., Liu, Z., Zhen, Y., Tian, Z.Q., Hosseini, D., Chen, L. and Shen, P.K., 2017. Simple fabrication of porous NiO nanoflowers: growth mechanism, shape evolution and their application into Li-ion batteries. Int. J. Hydrogen Energy, 42 (10), 7202-7211. doi: 10.1016/j.ijhydene.2016.05.193

Moharir, R.V. and Kumar, S., 2019. Challenges associated with plastic waste disposal and allied microbial routes for its effective degradation: a comprehensive review. J. Clean. Prod., 208, 65-76. doi: 10.1016/j.jclepro.2018.10.059

Moustafa, H., Galliard, H., Vidal, L. and Dufresne, A., 2017. Facile modification of organoclay and its effect on the compatibility and properties of novel biodegradable PBE/PBAT nanocomposites. Eur. Polym. J., 87, 188-199. doi: 10.1016/j.eurpolymj.2016.12.009

Munda, S., Dutta, S., Haldar, S. and Lal, M., 2018. Chemical analysis and therapeutic uses of ginger (*Zingiber officinale Rosc.)* essential oil: a review. J. Essent. Oil Bear. Plants, 21 (4), 994-1002. doi:10.1080/0972060x.2018.1524794

Nath, B.K., Chaliha, C., Bhuyan, B., Kalita, E., Baruah, D.C. and Bhagabati, A.K., 2018. GIS mapping-based impact assessment of groundwater contamination by arsenic and other heavy metal contaminants in the Brahmaputra river valley: a water quality assessment study. J. Clean. Prod., 201, 1001-1011. doi: 10.1016/j.jclepro.2018.08.084

Narayanan, M., Loganathan, S., Valapa, R.B., Thomas, S. and Varghese, T.O., 2017. UV protective poly (lactic acid)/rosin films for sustainable packaging. Int. J. Biol. Macromol., 99, 37-45. doi: 10.1016/j.ijbiomac.2017.01.152

Naser, A.Z., Deiab, I., Darras, B.M., 2021. Poly (lacticacid)(PLA) and polyhydroxyalkanoates (PHAs), green alternatives to petroleum-based plastics: a review. RSC Adv., 11 (28), 17151-17196. doi:10.1039/d1ra02390j

Nasiri, M., Barzegar, M., Sahari, M.A. and Niakousari, M., 2018. Application of Tragacanth gum impregnated with *Satureja khuzistanica* essential oil as a natural coating for enhancement of postharvest quality and shelf life of button mushroom (*Agaricus bisporus*). Int. J. Biol. Macromol., 106, 218-226. doi: 10.1016/j.ijbiomac.2017.08.003

Nazzaro, F., Fratianni, F., De Martino, L., Coppola, R. and De Feo, V., 2013. Effect of essential oils on pathogenic bacteria. Pharmaceuticals, 6 (12), 1451-1474. doi:10.3390/ph6121451

Nilsen-Nygaard, J., Fernandez, E.N., Radusin, T., Rotabakk, B.T., Sarfraz, J., Sharmin, N., Sivertsvik, M., Sone, I., Pettersen, M.K., 2021. Current status of biobased and biodegradable food packaging materials: impact on food quality and effect of innovative processing technologies. Compr. Rev. Food Sci. and Food Saf., 20 (2), 1333-1380. doi:10.1111/1541-4337.12715

Norazlina, H., Hadi, A.A., Qurni, A.U., Amri, M., Mashelmie, S. and Kamal, Y., 2019. Effects of multi-walled carbon nanotubes (MWCNTs) on the degradation behavior of plasticized PLA nanocomposites. Polym. Bull., 76 (3), 1453-1469. doi: 10.1007/s00289-018-2454-3

Nowak, B., Pająk, J., Drozd-Bratkowicz, M. and Rymarz, G., 2011. Microorganisms participating in the biodegradation of modified polyethylene films in different soils under laboratory conditions. Int. Biodeterior. Biodegrad., 65 (6), 757-767. doi: 10.1016/j.ibiod.2011.04.007

Olawuyi, I.F. and Lee, W.Y., 2022. Development and characterization of biocomposite films based on polysaccharides derived from okra plant waste for food packaging application. Polymers, 14 (22), 4884. doi: 10.3390/polym14224884

Oliveira, P.R., Mendoza, P.X., da Silva Crespo, J., da Silva Daitx, T. and Carli, L.N., 2024. Biodegradation study of poly (hydroxybutyrate-co-hydroxyvalerate)/halloysite/oregano essential oil compositions in simulated soil conditions. Int. J. Biol. Macromol., 133768. doi:10.1016/j.ijbiomac.2024.133768

Ortega-Toro, R., Bonilla, J., Talens, P. and Chiralt, A., 2017. Future of starch-based materials in food packaging. In: Villar, M. A., Barbosa, S. E., Garcia, M. A., Castillo, L. A., Lopez, O. V. (Eds.), Starch-Based Materials in Food Packaging. Academic press, 257-312

Othman, S.H., 2014. Bio-nanocomposite materials for food packaging applications: types of biopolymer and nano-sized filler. Agric. Agric. Sci. Procedia, 2, 296-303. doi: 10.1016/j.aaspro.2014.11.042

Ouraipryvan, P., Sreethawong, T. and Chavadej, S., 2009. Synthesis of crystalline MgO nanoparticle with mesoporous-assembled structure via a surfactant-modified sol-gel process. Mater. Lett., 63 (21), 1862-1865. doi: 10.1016/j.matlet.2009.05.068

Pachiyappan, J., Gnanasundaram, N. and Rao, G.L., 2020. Preparation and characterization of ZnO, MgO and ZnO-MgO hybrid nanomaterials using green chemistry approach. Results Mater., 7, 100104. doi: 10.1016/j.rinma.2020.100104

Palai, B., Mohanty, S. and Nayak, S.K., 2021. A comparison on biodegradation behaviour of polylactic acid (PLA) based blown films by incorporating thermoplasticized starch (TPS) and poly (butylene succinate-co-adipate) (PBSA) biopolymer in soil. J. Polym. Environ., 29 (9), 2772-2788. doi: 10.1007/s10924-021-02055-z

Palsikowski, P.A., Kuchnier, C.N., Pinheiro, I.F. and Morales, A.R., 2018. Biodegradation in soil of PLA/PBAT blends compatibilized with chain extender. J. Polym. Environ., 26 (1), 330-341. doi: 10.1007/s10924-017-0951-3

Pandey, S., Sharma, K. and Gundabala, V., 2022. Antimicrobial bio-inspired active packaging materials for shelf life and safety development: a review. Food Biosci., 48, 101730. doi: 10.1016/j.fbio.2022.101730

Pan, R., Wu, Y., Wang, Q. and Hong, Y., 2009. Preparation and catalytic properties of platinum dioxide nanoparticles: a comparison between conventional heating and microwave-assisted method. Chem. Eng. J., 153 (1-3), 206-210. doi: 10.1016/j.cej.2009.06.009

Parsafar, B., Ahmadi, M., Khaniki, G.J.J., Shariatifar, N. and Foroushani, A.R., 2023. The impact of fruit and vegetable waste on economic loss estimation. J. Environ. Sci. Manag., 9 (4), 871-884. doi: 10.22035/gjesm.2023.04.14

Paulsen, E., Lema, P., Martínez-Romero, D. and García-Viguera, C., 2022. Use of PLA/PBAT stretch-cling film as an ecofriendly alternative for individual wrapping of broccoli heads. Sci. Hortic., 304, 111260. doi: 10.1016/j.scienta.2022.111260

Pawar, P.A., Purwar, A.H., 2013. Biodegradable polymers in food packaging. Am. J. Eng. Res., 2 (5), 151-164. doi: 10.1016/j.tifs.2008.07.003

Peelman, N., Ragaert, P., De Meulenaer, B., Adons, D., Peeters, R., Cardon, L., Van Impe, F., Devlieghere, F., 2013. Application of bioplastics for food packaging. Trends Food Sci. Technol., 32 (2), 128-141. doi: 10.1016/j.tifs.2013.06.003

Perera, K.Y., Sharma, S., Duffy, B., Pathania, S., Jaiswal, A.K. and Jaiswal, S., 2022. An active biodegradable layer-by-layer film based on chitosan-alginate-TiO_2 for the enhanced shelf life of tomatoes. Food Packag. Shelf Life, 34, 100971. doi: 10.1016/j.fpsl.2022.100971

Phua, Y.J., Lau, N.S., Sudesh, K., Chow, W.S. and Ishak, Z.M., 2012. Biodegradability studies of poly (butylene succinate)/organo-montmorillonite nanocomposites under controlled compost soil conditions: effects of clay loading and compatibiliser. Polym. Degrad. Stab., 97 (8), 1345-1354. doi: 10.1016/j.polymdegradstab.2012.05.024

Pischedda, A., Tosin, M. and Degli-Innocenti, F., 2019. Biodegradation of plastics in soil: the effect of temperature. Polym. Degrad. Stab., 170, 109017. doi: 10.1016/j.polymdegradstab.2019.109017

Pilarska, A.A., Klapiszewski, L. and Jesionowski, T., 2017. Recent development in the synthesis, modification and application of $Mg(OH)_2$ and MgO: a review. Powder Technol., 319, 373-407. doi: 10.1016/j.powtec.2017.07.009

Plantic Technologies Limited., 2007. Products.

http://www.plantic.com.au/case%20studies/plantic_cadbury_cs.pdf. (last accessed 27 January 2022)

Plastic Oceans Foundation, 2018. A plastic ocean educational supplement. https://plasticoceans.org/wp-content/uploads/2018/01/plastic-oceans_educational-supplement_vjan2108.pdf. (last accessed 24 January 2022)

Pleșoianu, A.M. and Nour, V., 2022. Effect of some polysaccharide-based edible coatings on fresh white button mushroom (*Agaricus bisporus*) quality during cold storage. Agric., 12 (9), 1491. doi: 10.3390/agriculture12091491

Podder, S., Chanda, D., Mukhopadhyay, A.K., De, A., Das, B., Samanta, A., Hardy, J.G. and Ghosh, C.K., 2018. Effect of morphology and concentration on crossover between antioxidant and pro-oxidant activity of MgO nanostructures. Inorg. Chem., 57 (20), 12727-12739. doi: 10.1021/acs.inorgchem.8b01938

Pola, C.C., Medeiros, E.A., Pereira, O.L., Souza, V.G., Otoni, C.G., Camilloto, G.P. and Soares, N.F., 2016. Cellulose acetate active films incorporated with oregano (*Origanum vulgare*) essential oil and organophilic montmorillonite clay control the growth of phytopathogenic fungi. Food Packag. Shelf Life, 9, 69-78. doi: 10.1016/j.fpsl.2016.07.001

Postiglione, G., Natale, G., Griffini, G., Levi, M. and Turri, S., 2015. Conductive 3D microstructures by direct 3D printing of polymer/carbon nanotube nanocomposites via liquid deposition modeling. Compos. Part A: Appl. Science and Manuf., 76, 110-114. doi: 10.1016/j.compositesa.2015.05.014

Pollution control board Assam, NWMP Data for the month of march, 2023. https://pcbassam.org/wqd%20under%20NWMP/NWMP%20Data%20-%20March'2023.pdf. (last accessed 13 May 2024)

Pradhan, S., Borah, A.J., Poddar, M.K., Dikshit, P.K., Rohidas, L. and Moholkar, V.S., 2017. Microbial production, ultrasound-assisted extraction and characterization of biopolymer polyhydroxybutyrate (PHB) from terrestrial (*P. hysterophorus*) and aquatic (*E. crassipes*) invasive weeds. Bioresour. Technol., 242, 304-310. doi: 10.1016/j.biortech.2017.03.117

Purnima, M., Paul, T., Pakshirajan, K. and Pugazhenthi, G., 2023. Onshore oilfield produced water treatment by hybrid microfiltration-biological process using kaolin based ceramic membrane and oleaginous *Rhodococcus Opacus*. Chem. Eng. J., 453, 1385-8947. doi: 10.1016/j.cej.2022.139850

Qian, Z.J., Zhang, J., Xu, W.R. and Zhang, Y.C., 2022. Development of active packaging films based on liquefied shrimp shell chitin and polyvinyl alcohol containing β-cyclodextrin/cinnamaldehyde inclusion. Int. J. Biol. Macromol., 214 (2022), 67-76. doi: 10.1016/j.ijbiomac.2022.06.052

Qin, Y., Li, W., Liu, D., Yuan, M. and Li, L., 2017. Development of active packaging film made from poly (lactic acid) incorporated essential oil. Prog. Org. Coat., 103, 76-82. doi: 10.1016/j.porgcoat.2016.10.017

Qubbaj, T. and Daraghmah, F.S., 2023. Postharvest guar gum coating modulates fruit ripening, storage life, and quality of tomato fruits kept in ambient or cold storage conditions. J. Agric. Sci. Technol., 25 (4), 963-974. doi:10.22034/jast.25.4.14

Qu, T., Li, B., Huang, X., Li, X., Ding, Y., Chen, J. and Tang, X., 2020. Effect of peppermint oil on the storage quality of white button mushrooms (*Agaricus bisporus*). Food Bioprocess Technol., 13 (3), 404-418. doi: 10.1007/s11947-019-02385-w

Rapisarda, M., Mistretta, M.C., Scopelliti, M., Leanza, M., La Mantia, F.P. and Rizzarelli, P., 2022. Influence of calcium carbonate nanoparticles on the soil burial degradation of Polybutyleneadipate-co-butylenetherephthalate films. Nanomater., 12 (13), 2275. doi: 10.3390/nano12132275

Rao, K.G., Ashok, C.H., Rao, K.V. and Chakra, C.S., 2014. Structural properties of MgO nanoparticles: synthesized by co-precipitation technique. Int. J. Sc. Res., 3 (12), 43-46.

Rech, C.R., Brabes, K.C., Silva, B.E., Martines, M.A., Silveira, T.F., Alberton, J., Amadeu, C.A., Caon, T., Arruda, E.J. and Martelli, S.M., 2021. Antimicrobial and physical-mechanical properties of polyhydroxybutyrate edible films containing essential oil mixtures. J. Polym. Environ., 29, 1202-1211. doi:10.1007/s10924-020-01943-0

Rahman, A., Jahanara, I. and Jolly, Y.N., 2021. Assessment of physicochemical properties of water and their seasonal variation in an urban river in Bangladesh. Water Sci. Eng., 14 (2), 139-148. doi: 10.1016/j.wse.2021.06.006

Rajendran, V., Deepa, B. and Mekala, R., 2018. Studies on structural, morphological, optical and antibacterial activity of Pure and Cu-doped MgO nanoparticles synthesized by co-precipitation method. Mater. Today Proc., 5 (2), 8796-8803. doi: 10.1016/j.matpr.2017.12.308

Requena, R., Vargas, M. and Chiralt, A., 2017. Release kinetics of carvacrol and eugenol from poly (hydroxybutyrate-co-hydroxyvalerate) (PHBV) films for food packaging applications. Eur. Polym. J., 92, 185-193. doi:10.1016/j.eurpolymj.2017.05.008

Revathi, V. and Karthik, K., 2018. Microwave assisted CdO-ZnO-MgO nanocomposite and its photocatalytic and antibacterial studies. J. Mater. Sci.: Mater. Electron., 29 (21), 18519-18530. doi:10.1007/s10854-018-9968-1

Riahi, Z., Hong, S.J., Rhim, J.W., Shin, G.H. and Kim, J.T., 2023. High-performance multifunctional gelatin-based films engineered with metal-organic frameworks for active food packaging applications. Food Hydrocoll., 144, 108984. doi: 10.1016/j.foodhyd.2023.108984

Rizwana, H., Bokahri, N.A., Alsahli, S.A., Al Showiman, A.S., Alzahrani, R.M. and Aldehaish, H.A., 2021. Postharvest disease management of *Alternaria* spots on tomato fruit by *Annona muricata* fruit extracts. Saudi J. Biol. Sci., 28 (4), 2236-2244. doi: 10.1016/j.sjbs.2021.01.014

Roebroek, C.T., Harrigan, S., Van Emmerik, T.H., Baugh, C., Eilander, D., Prudhomme, C. and Pappenberger, F., 2021. Plastic in global rivers: are floods making it worse? Environ. Res. Lett, 16 (2), 025003. doi:10.1088/1748-9326/abd5df

Rouhani, P., Taghavinia, N. and Rouhani, S., 2010. Rapid growth of hydroxyapatite nanoparticles using ultrasonic irradiation. Ultrason. Sonochem., 17 (5), 853-856. doi: 10.1016/j.ultsonch.2010.01.010

Roy, S., Priyadarshi, R., Ezati, P. and Rhim, J.W., 2021a. Curcumin and its uses in active and smart food packaging applications-a comprehensive review. Food Chem., 375, 131885. doi: 10.1016/j.foodchem.2021.131885

Roy, S. and Rhim, J.W., 2021b. Carrageenan/agar-based functional film integrated with zinc sulfide nanoparticles and pickering emulsion of tea tree essential oil for active packaging applications. Int. J. Biol. Macromol., 193, 2038-2046. doi: 10.1016/j.ijbiomac.2021.11.035

Salomez, M., George, M., Fabre, P., Touchaleaume, F., Cesar, G., Lajarrige, A. and Gastaldi, E., 2019. A comparative study of degradation mechanisms of PHBV and PBSA under laboratory-scale composting conditions. Polym. Degrad. Stab., 167, 102-113. doi: 10.1016/j.polymdegradstab.2019.06.025

Salari, M., Khiabani, M.S., Mokarram, R.R., Ghanbarzadeh, B., Kafil, H.S., 2018. Development and evaluation of chitosan based active nanocomposite films containing bacterial cellulose nanocrystals and silver nanoparticles. Food Hydrocoll., 84, 414-423. doi: 10.1016/j.foodhyd.2018.05.037

Salaberria, A.M., Labidi, J., Fernandes, S.C., 2014. Chitin nanocrystals and nanofibers as nano-sized fillers into thermoplastic starch-based biocomposites processed by melt-mixing. Chem. Eng. J., 256, 356-364. doi: 10.1016/j.cej.2014.07.009

Sangeeta, M., Karthik, K.V., Ravishankar, R., Anantharaju, K.S., Nagabhushana, H., Jeetendra, K., Vidya, Y.S. and Renuka, L., 2017. Synthesis of ZnO, MgO and ZnO/MgO by solution combustion method: characterization and photocatalytic studies. Mater. Today: Proc., 4 (11), 11791-11798. doi: 10.1016/j.matpr.2017.09.096

Saratale, R.G., Saratale, G.D., Cho, S.K., Kim, D.S., Ghodake, G.S., Kadam, A., Kumar, G., Bharagava, R.N., Banu, R., Shin, H.S., 2019. Pretreatment of kenaf (*hibiscus cannabinus l.*) biomass feedstock for polyhydroxybutyrate (PHB) production and characterization. Bioresour. Technol., 282, 75-80. doi: 10.1016/j.biortech.2019.02.083

Sarasa, J., Gracia, J.M. and Javierre, C., 2009. Study of the biodisintegration of a bioplastic material waste. Bioresour. Technol., 100 (15), 3764-3768. doi: 10.1016/j.biortech.2008.11.049

Selvam, N.C.S., Kumar, R.T., Kennedy, L.J. and Vijaya, J.J., 2011. Comparative study of microwave and conventional methods for the preparation and optical properties of novel MgO-micro and nano-structures. J. Alloys Compd., 509 (41), 9809-9815. doi: 10.1016/j.jallcom.2011.08.032

Sganzerla, W.G., Ribeiro, C.P.P., Uliana, N.R., Rodrigues, M.B.C., da Rosa, C.G., Ferrareze, J.P., de Lima Veeck, A.P. and Nunes, M.R., 2021. Bioactive and pH-sensitive films based on carboxymethyl cellulose and blackberry (*Morus nigra L.*) anthocyanin-rich extract: a perspective coating material to improve the shelf life of cherry tomato (*Solanum lycopersicum L. var. cerasiforme*). Biocatal. Agric. Biotechnol., 33, 101989. doi: 10.1016/j.bcab.2021.101989

Shaghaleh, H., Xu, X., Wang, S., 2018. Current progress in production of biopolymeric materials based on cellulose, cellulose nanofibers, and cellulose derivatives. RSC Adv., 8 (2), 825-842. doi:10.1039/c7ra11157f

Sheikh, M., Asghari, M. and Afsari, M., 2018. Effect of tiny amount of zinc oxide on morphological and thermal properties of nanocomposite PEBA thin films. Alex. Eng. J., 57 (4), 3661-3669. doi: 10.1016/j.aej.2018.01.016

Sharma, S., Perera, K.Y., Pradhan, D., Duffy, B., Jaiswal, A.K. and Jaiswal, S., 2022. Active packaging film based on poly lactide-poly (butylene adipate-co-terephthalate) blends incorporated with tannic acid and gallic acid for the prolonged shelf life of cherry tomato. Coatings, 12 (12), 1902. doi:10.3390/coatings12121902

Sharma, S., Barkauskaite, S., Jaiswal, A.K. and Jaiswal, S., 2021. Essential oils as additives in active food packaging. Food Chem., 343, 128403. doi: 10.1016/j.foodchem.2020.128403

Shankar, S. and Rhim, J.W., 2018. Preparation of sulfur nanoparticle-incorporated antimicrobial chitosan films. Food Hydrocoll., 82, 116-123. doi: 10.1016/j.foodhyd.2018.03.054

Silva, F.M., Pinto, R.J., Barros-Timmons, A.M. and Freire, C.S., 2023. Tung oil-based coatings towards sustainable paper packaging materials. Prog. Org. Coatings, 178, 107476. doi: 10.1016/j.porgcoat.2023.107476

Siripireddy, B. and Mandal, B.K., 2017. Facile green synthesis of zinc oxide nanoparticles by Eucalyptus globulus and their photocatalytic and antioxidant activity. Adv. Powder Tech., 28 (3), 785-797. doi: 10.1016/j.apt.2016.11.026

Sooch, B.S. and Mann, M.K., 2021. Nanoreinforced biodegradable gelatin based active food packaging film for the enhancement of shelf life of tomatoes (*Solanum lycopersicum L.*). Food Control, 130, 108322. doi: 10.1016/j.foodcont.2021.108322

Srivastava, V., Sharma, Y.C. and Sillanpaa, M., 2015. Green synthesis of magnesium oxide nanoflower and its application for the removal of divalent metallic species from synthetic wastewater. Ceram. Int., 41 (5), 6702-6709. doi: 10.1016/j.ceramint.2015.01.112

Sridewi, N., Bhubalan, K. and Sudesh, K., 2006. Degradation of commercially important polyhydroxyalkanoates in tropical mangrove ecosystem. Polym. Degrad. Stab., 91 (12), 2931-2940. doi: 10.1016/j.polymdegradstab.2006.08.027

Suzuki, M., Tachibana, Y. and Kasuya, K.I., 2021. Biodegradability of poly (3-hydroxyalkanoate) and poly (ε-caprolactone) via biological carbon cycles in marine environments. Polym. J., 53 (1), 47-66. doi: 10.1038/s41428-020-00396-5

Swaroop, C., Shukla, M., 2019. Development of blown polylactic acid-MgO nanocomposite films for food packaging. Compos. Part A: Appl. Sci. Manuf., 124, 105482. doi: 10.1016/j.compositesa.2019.105482

Swaroop, C. and Shukla, M., 2018. Nano-magnesium oxide reinforced polylactic acid biofilms for food packaging applications. Int. J. Biol. Macromol., 113, 729-736. doi: 10.1016/j.ijbiomac.2018.02.156

Syahirah, W.N., Azami, N.A., Huong, K.H. and Amirul, A.A., 2021. Preparation, characterization and biodegradation of blend films of poly (3-hydroxybutyrate-co-3-hydroxyvalerate) with natural biopolymers. Polym. Bull., 78, 3973-3993. doi: 10.1007/s00289-020-03286-1

Syafri, E., Kasim, A., Asben, A., Senthamaraikannan, P., Sanjay, M.R., 2020. Studies on ramie cellulose microfibrils reinforced cassava starch composite: influence of microfibrils loading. J. Nat. Fibers, 17 (1), 122-131. doi:10.1080/15440478.2018.1470057

Tan, Y.M., Lim, S.H., Tay, B.Y., Lee, M.W. and Thian, E.S., 2015. Functional chitosan-based grapefruit seed extract composite films for applications in food packaging technology. Mater. Res. Bull., 69, 142-146. doi: 10.1016/j.materresbull.2014.11.041

Talan, A., Pokhrel, S., Tyagi, R.D., Drogui, P., 2022. Biorefinery strategies for microbial bioplastics production: Sustainable pathway towards circular bioeconomy. Bioresour. Technol. Rep., 17, 100875. doi: 10.1016/j.biteb.2021.100875

Talukdar, M., Nath, O. and Deb, P., 2021. Enhancing barrier properties of biodegradable film by reinforcing with 2D heterostructure. Appl. Surf. Sci., 541, 148464. doi: 10.1016/j.apsusc.2020.148464

Tavares, L. and Noreña, C.P.Z., 2020. Encapsulation of ginger essential oil using complex coacervation method: coacervate formation, rheological property, and physicochemical characterization. Food and Bioprocess Technol., 13, 1405-1420. doi:10.1007/s11947-020-02480-3

Tawakkal, I.S., Cran, M.J., Miltz, J., Bigger, S.W., 2014. A review of poly (lactic acid) -based materials for antimicrobial packaging. J. Food Sci., 79 (8), R1477-R1490. doi:10.1111/1750-3841.12534

Thakur, R.R., Shahi, N.C., Mangaraj, S., Lohani, U.C. and Chand, K., 2021. Development of an organic coating powder and optimization of process parameters for shelf life enhancement of button mushrooms (*Agaricus bisporus*). J. Food Process. Preserv., 45 (3), e15036. doi: 10.1111/jfpp.15306

Tournas, V.H., 2005. Spoilage of vegetable crops by bacteria and fungi and related health hazards. Crit. Rev. Microbiol., 31 (1), 33-44. doi: 10.1080/10408410590886024

Trombetta, D., Saija, A., Bisignano, G., Arena, S., Caruso, S., Mazzanti, G., Uccella, N. and Castelli, F., 2002. Study on the mechanisms of the antibacterial action of some plant α, β-unsaturated aldehydes. Lett. Appl. Microbiol., 35 (4), 285-290. doi:10.1046/j.1472-765x.2002. 01190.x

Tzortzakis, N., Chrysargyris, A., 2017. Postharvest ozone application for the preservation of fruits and vegetables. Food Rev. Int, 33 (3), 270-315. doi:10.1080/87559129.2016.1175015

Vahid, B.R. and Haghighi, M., 2016. Urea-nitrate combustion synthesis of MgO/$MgAl_2O_4$ nanocatalyst used in biodiesel production from sunflower oil: Influence of fuel ratio on catalytic properties and performance. Energy Convers. Manag., 126, 362-372. doi: 10.1016/j.enconman.2016.07.050

Valapa, R., Hussain, S., Krishnan Iyer, P., Pugazhenthi, G., Katiyar, V., 2016a. Non-isothermal crystallization kinetics of sucrose palmitate reinforced poly (lactic acid) bionanocomposites. Polym. Bull., 73 (1), 21-38. doi:10.1007/s00289-015-1468-3

Valapa, R.V., Pugazhenthi, G. and Katiyar, V., 2016b. Hydrolytic degradation behaviour of sucrose palmitate reinforced poly (lactic acid) nanocomposites. Int. J. Biol. Macromol., 89, 70-80. doi: 10.1016/j.ijbiomac.2016.04.040

Valapa, R.B., Pugazhenthi, G. and Katiyar, V., 2015. Effect of graphene content on the properties of poly (lactic acid) nanocomposites. RSC Adv., 5 (36), 28410-28423. doi:10.1039/c4ra15669b

Varghese, S.A., Siengchin, S. and Parameswaranpillai, J., 2020. Essential oils as antimicrobial agents in biopolymer-based food packaging-a comprehensive review. Food Biosci., 38, 100785. doi: 10.1016/j.fbio.2020.100785

Vasile, C., Pamfil, D., Râpă, M., Darie-Niţă, R.N., Mitelut, A.C., Popa, E.E., Popescu, P.A., Draghici, M.C. and Popa, M.E., 2018. Study of the soil burial degradation of some PLA/CS biocomposites. Compos. Part B Eng., 142, 251-262. doi: 10.1016/j.compositesb.2018.01.026

Vaizogullar, A.I., 2018. Needle-like La-doped MgO photocatalyst: synthesis, characterization and photodegradation of flumequine antibiotic under UV irradiation. J. Electron. Mater., 47 (11), 6751-6758. doi:10.1007/s11664-018-6591-0

Vandewijngaarden, J., Wauters, R., Murariu, M., Dubois, P., Carleer, R., Yperman, J., D'Haen, J., Ruttens, B., Schreurs, S., Lepot, N. and Peeters, R., 2016. Poly (3-hydroxybutyrate-co-3-hydroxyhexanoate)/organomodified montmorillonite nanocomposites for potential food packaging applications. J. Polym. Environ., 24 (2), 104-118. doi:10.1007/s10924-016-0751-1

Veldurthi, S., Shin, C.H., Joo, O.S. and Jung, K.D., 2012. Synthesis of mesoporous MgO single crystals without templates. Microporous and Mesoporous Mater., 152, 31-36. doi: 10.1016/j.micromeso.2011.11.044

Verma, R., Naik, K.K., Gangwar, J. and Srivastava, A.K., 2014. Morphology, mechanism and optical properties of nanometer-sized MgO synthesized via facile wet chemical method. Mater. Chem. Phys., 148 (3), 1064-1070. doi: 10.1016/j.matchemphys.2014.09.018

Vianna, T.C., Marinho, C.O., Júnior, L.M., Ibrahim, S.A. and Vieira, R.P., 2021. Essential oils as additives in active starch-based food packaging films: a review. Int. J. Biol. Macromol., 182, 1803-1819. doi:10.1016/j.ijbiomac.2021.05.170

Wang, K., Lim, P.N., Tong, S.Y. and San Thian, E., 2019. Development of grapefruit seed extract-loaded poly (ε-caprolactone)/chitosan films for antimicrobial food packaging. Food Packag. Shelf Life, 22, 100396. doi: 10.1016/j.fpsl.2019.100396

Wang, H., Qian, J., Ding, F., 2018. Emerging chitosan-based films for food packaging applications. J. Agric. Food chem., 66 (2), 395-413. doi: 10.1021/acs.jafc.7b04528

Wang, K., Henry, R.J., Gilbert, R.G., 2014. Causal relations among starch biosynthesis, structure, and properties. Springer Sci. Rev., 2 (1), 15-33. doi:10.1007/s40362-014-0016-0

Werner, B.G., Koontz, J.L., Goddard, J.M., 2017. Hurdles to commercial translation of next generation active food packaging technologies. Curr. Opin. Food Sci., 16, 40-48. doi: 10.1016/j.cofs.2017.07.007

Wong, C.W., Chan, Y.S., Jeevanandam, J., Pal, K., Bechelany, M., Abd Elkodous, M. and El-Sayyad, G.S., 2020. Response surface methodology optimization of mono-dispersed MgO nanoparticles fabricated by ultrasonic-assisted sol-gel method for outstanding antimicrobial and antibiofilm activities. J. Clust. Sci., 31 (2), 367-389. doi:10.1007/s10876-019-01651-3

World Economic Forum, 2018. The world's plastic problem in numbers. https://www.weforum.org/agenda/2018/08/the-world-of-plastics-in-numbers. (last accessed 8 August 2020)

Xiong, C., Wang, W., Tan, F., Luo, F., Chen, J. and Qiao, X., 2015. Investigation on the efficiency and mechanism of Cd (II) and Pb (II) removal from aqueous solutions using MgO nanoparticles. J. Hazard. Mater., 299, 664-674. doi: 10.1016/j.jhazmat.2015.08.008

Yahyaoui, M., Gordobil, O., Díaz, R.H., Abderrabba, M. and Labidi, J., 2016. Development of novel antimicrobial films based on poly (lactic acid) and essential oils. React. Funct. Polym., 109, 1-8. doi:10.1016/j.reactfunctpolym.2016.09.001

Youssef, A. M., El-Sayed, S. M., 2018. Bionanocomposites materials for food packaging applications: Concepts and future outlook. Carbohydr. Polym., 193, 19-27. doi: 10.1016/j.carbpol.2018.03.088

Yousefi, S., Ghasemi, B., Tajally, M. and Asghari, A., 2017. Optical properties of MgO and $Mg(OH)_2$ nanostructures synthesized by a chemical precipitation method using impure brine. J. Alloys Compd., 711, 521-529. doi: 10.1016/j.jallcom.2017.04.036

Yu, F., Shi, H., Wang, K., Li, H. and Peng, L., 2022. Preparation of robust and fully bio-based modified paper via mussel-inspired layer-by-layer assembly of chitosan and carboxymethyl cellulose for food packaging. Int. J. Biol. Macromol., 222, 1238-1249. doi: 10.1016/j.ijbiomac.2022.09.243

Yu, Z., Wang, W., Kong, F., Lin, M., Mustapha, A., 2019. Cellulose nanofibril/silver nanoparticle composite as an active food packaging system and its toxicity to human colon cells. Int. J. Biol. Macromol., 129, 887-894. doi: 10.1016/j.ijbiomac.2019.02.084

Yun, J., Fan, X., Li, X., Jin, T.Z., Jia, X. and Mattheis, J.P., 2015. Natural surface coating to inactivate *Salmonella enterica serovar Typhimurium* and maintain quality of cherry tomatoes. Int. J. Food Microbiol., 193, 59-67. doi: 10.1016/j.ijfoodmicro.2014.10.013

Yu, H.Y., Qin, Z.Y., Sun, B., Yang, X.G. and Yao, J.M., 2014. Reinforcement of transparent poly (3-hydroxybutyrate-co-3-hydroxyvalerate) by incorporation of functionalized carbon nanotubes as a novel bionanocomposite for food packaging. Compos. Sci. Technol., 94, 96-104. doi: 10.1016/j.compscitech.2014.01.018

Zabidi, N. A. Nazri, F., Tawakkal, I.S.M.A., Basri, M.S.M., Basha, R.K. and Othman, S.H., 2022. Characterization of active and pH-sensitive poly (lactic

acid)(PLA)/nanofibrillated cellulose (NFC) films containing essential oils and anthocyanin for food packaging application. Int. J. Biol. Macromol., 212, 220-231. doi: 10.1016/j.ijbiomac.2022.05.116

Zaccone, M., Patel, M.K., De Brauwer, L., Nair, R., Montalbano, M.L., Monti, M. and Oksman, K., 2022. Influence of chitin nanocrystals on the crystallinity and mechanical properties of poly (hydroxybutyrate) biopolymer. Polymers, 14 (3), 562. doi:10.3390/polym14030562

Zamir, S.S., Fathi, B., Ajji, A., Robert, M. and Elkoun, S., 2022. Biodegradation of modified starch/poly lactic acid nanocomposite in soil. Polym. Degrad. Stab., 199, 109902. doi: 10.1016/j.polymdegradstab.2022.109902

Zare M, Namratha K, Ilyas S, Sultana A, Hezam A, Surmeneva MA, Surmenev RA, Nayan MB, Ramakrishna S, Mathur S, Byrappa K., 2022. Emerging trends for ZnO nanoparticles and their applications in food packaging. ACS Food Sci. Technol., 2 (5) 763-781. doi:10.1021/acsfoodscitech.2c00043

Zeng, C., Tan, P. and Liu, Z., 2020. Effect of exogenous ARA treatment for improving postharvest quality in cherry tomato (*Solanum lycopersicum L.*) fruits. Sci. Hortic., 261, 108959. doi: 10.1016/j.scienta.2019.108959

Zhang, S., He, Z., Xu, F., Cheng, Y., Waterhouse, G.I., Sun-Waterhouse, D. and Wu, P., 2022. Enhancing the performance of konjac glucomannan films through incorporating zein-pectin nanoparticle-stabilized oregano essential oil pickering emulsions. Food Hydrocoll., 124, 107222. doi: 10.1016/j.foodhyd.2021.107222

Zhao, X., Cornish, K. and Vodovotz, Y., 2020. Narrowing the gap for bioplastic use in food packaging: an update. Environ. Sci. Technol., 54 (8), 4712-4732. doi: 10.1021/acs.est.9b03755

Zheng, H., Tang, H., Yang, C., Chen, J., Wang, L., Dong, Q., Shi, W., Li, L. and Liu, Y., 2022. Evaluation of the slow-release polylactic acid/polyhydroxyalkanoates active film containing oregano essential oil on the quality and flavor of chilled pufferfish (*Takifugu Obscurus*) fillets. Food Chem., 385, 132693. doi: 10.1016/j.foodchem.2022.13269

Zou, Z., Luo, C., Luo, B., Wen, W., Liu, M. and Zhou, C., 2016. Synergistic reinforcing and toughening of poly (L-lactide) composites with surface-modified MgO and chitin whiskers. Compos. Sci. Technol., 133, 128-135. doi: 10.1016/j.compscitech.2016.07.025

List of publications

Publications in international journals

From thesis:

1. **Satti Venu Gopala Kumari,** Kannan Pakshirajan and G. Pugazhenthi, Recent advances and future prospects of cellulose, starch, chitosan, polylactic acid and polyhydroxyalkanoates for sustainable food packaging applications, ***International Journal of Biological Macromolecules,*** 221 (2022) 163-182. https://doi.org/10.1016/j.ijbiomac.2022.08.203
2. **Satti Venu Gopala Kumari**, Kannan Pakshirajan and G. Pugazhenthi, Synthesis and characterization of MgO nanostructures: a comparative study on the effect of preparation route. ***Materials Chemistry and Physics***, 294 (2023) 127036. https://doi.org/10.1016/j.matchemphys.2022.127036
3. **Satti Venu Gopala Kumari**, Kannan Pakshirajan and G. Pugazhenthi, Facile fabrication of novel antimicrobial and antioxidant poly (3-hydroxybutyrate)/essential oil composites for potential use in active food packaging applications, ***International Journal of Biological Macromolecules***, 252 (2023) 126566. https://doi.org/10.1016/j.ijbiomac.2023.126566
4. **Satti Venu Gopala Kumari**, Kannan Pakshirajan and G. Pugazhenthi, Development and characterization of active poly (3-hydroxybutyrate) based composites with grapeseed oil and MgO nanoparticles for shelf-life extension of white button mushrooms *(Agaricus bisporus),* ***International Journal of Biological Macromolecules***, 260 (2023) 129521. https://doi.org/10.1016/j.ijbiomac.2024.129521
5. **Satti Venu Gopala Kumari**, Kannan Pakshirajan and G. Pugazhenthi, Application of active and environment-friendly poly (3-hydroxybutyrate)/grapeseed oil/MgO nanocomposite packaging for prolonging the shelf-life of cherry tomatoes *(Solanum lycopersicum L. var. cerasiforme),* ***Sustainable Chemistry and Pharmacy***, 41 (2024) 101681. https://doi.org/10.1016/j.scp.2024.101681
6. **Satti Venu Gopala Kumari,** Kannan Pakshirajan and G. Pugazhenthi, Key insights into mechanism and kinetics of biodegradation of poly (3-hydroxybutyrate)-based

nanocomposite films in natural soil and river water environments, ***Bioresource Technology***, 409 (2024), 131238. https://doi.org/10.1016/j.biortech.2024.131238

From other works:

1. **Satti Venu Gopala Kumari**, Arul Manikandan, Kannan Pakshirajan, and G. Pugazhenthi, Sustained drug release and bactericidal activity of a novel, highly biocompatible and biodegradable polymer nanocomposite loaded with norfloxacin for potential use in antibacterial therapy. ***Journal of Drug Delivery Science and Technology***, 59 (2020) 101900. https://doi.org/10.1016/j.jddst.2020.101900
2. **Satti Venu Gopala Kumari**, Shiv Prakash Anil Gupta, Kannan Pakshirajan and G. Pugazhenthi, Facile fabrication and characterization of novel polyvinyl alcohol/polyethylene glycol/aluminum nitride nanocomposites, ***Polymer Engineering & Science***, 63 (11) (2023), 3855-3864. https://doi.org/10.1002/pen.26491
3. Khushboo Gupta, **Satti Venu Gopala Kumari**, and G. Pugazhenthi, Synergistic influence of multi-walled carbon nanotubes and graphene nanoparticles on the structural, thermal and mechanical characteristics of poly (3-hydroxybutyrate) films. ***Materials Today: Proceedings***, (In press). https://doi.org/10.1016/j.matpr.2023.07.292
4. Rinki Singh, **Satti Venu Gopala Kumari**, Kannan Pakshirajan and G. Pugazhenthi, Optimizing the synthesis conditions of CaAl-Layered Double Hydroxide (LDH) and poly (3-hydroxybutyrate)/CaAl-LDH nanocomposite for potential use in antibacterial drug delivery, ***Polymer Engineering & Science***, (In press). https://doi.org/10.1002/pen.26972

Book Chapter:

1. **Satti Venu Gopala Kumari,** Kannan Pakshirajan and G. Pugazhenthi, Freshness indicator in intelligent food packaging system, ***In: smart food packaging: innovations and technology applications,*** John Wiley & Sons (In press).

<u>Presentation in international/national conferences</u>

1. **Satti Venu Gopala Kumari**, Kannan Pakshirajan, and G. Pugazhenthi, Synthesis of nanoflakes-assembled MgO nanoflowers by facile template-free solvothermal method and evaluation of their structural, optical, and antimicrobial characteristics. International online Conference on Material Science and Technology (ICMT-2021), 12-14 November 2021, Mahatma Gandhi University, Kottayam, Kerala, India.

2. **Satti Venu Gopala Kumari,** Kannan Pakshirajan, and G. Pugazhenthi, A comparative study on structural and antibacterial properties of MgO nanostructures synthesized via microwave and conventional combustion methods, International Online Conference on Nano Materials (ICN-2022), 12-14 August 2022, International and Inter University Centre for Nanoscience and Nanotechnology, Kerala, India.
3. **Satti Venu Gopala Kumari,** Kannan Pakshirajan, and G. Pugazhenthi, Development of novel flexible antimicrobial films of poly (3-hydroxybutyrate)/grapeseed oil for potential food packaging applications, International Conference on Sustainable Approaches in Food Engineering and Technology (SAFEty-2022), 19-20 October 2022, Tezpur University, Assam, India.
4. **Satti Venu Gopala Kumari,** Kannan Pakshirajan, and G. Pugazhenthi, Facile fabrication of antimicrobial and antioxidant poly (3-hydroxybutyrate)/ginger oil composites for active food packaging applications, 4th International Conference on Materials, Manufacturing and Modelling (ICMMM-2023), 24-26 March, 2023, Vellore Institute of Technology, Vellore, India.
5. **Satti Venu Gopala Kumari,** Kannan Pakshirajan, and G. Pugazhenthi, Application of active and environmentally safe poly (3-hydroxybutyrate)/grapeseed oil/MgO nanocomposite packaging for prolonging the shelf-life of white button mushrooms, International Conference on Advances in Interdisciplinary Nanoscience (ICANIS-2024), 10-12 January 2024, Government College for Women, Thiruvananthapuram, Kerala, India.
6. **Satti Venu Gopala Kumari,** Kannan Pakshirajan, and G. Pugazhenthi, Synergistic effects of grapeseed oil and MgO nanoparticles loading on physicochemical, antimicrobial, and antioxidant properties of poly (3-hydroxybutyrate) for active food packaging applications, The 14th International Conference on Advanced Materials Research (ICAMR-2024), 25-27 January 2024, Phuket, Thailand.
7. **Satti Venu Gopala Kumari,** Kowthalam Vishnu Vardhan, Kannan Pakshirajan, and G. Pugazhenthi, Development of polylactic acid/poly(3-hydroxybutyrate) blend films via solution casting route and their characterization, 1st International Conference on Trends in Chemical, Energy and Environmental Engineering (ChemEEE-2024), 19-21 February 2024, Indian Institute of Petroleum and Energy (IIPE), Visakhapatnam, Andhra Pradesh, India.

Awards received in international /national conferences

1. **First prize** for best oral presentation, ICMT 2021, Kottayam, Kerala, India.
2. **Second prize** for best oral presentation, SAFEty 2022, Tezpur, Assam, India.
3. **First prize** for best oral presentation, ICAMR 2024, Phuket, Thailand.
4. **First prize** for best oral presentation, ChemEEE 2024, Visakhapatnam, India.